"The boundaries between hydrology and meteorology has become more diffuse and the 'hydrometeorological' fraternity has grown in size and influence"

— Cluckie and Collier, 1991

Hydrological Modelling With Weather Radar Data in Urban Drainage Systems

J. Yuan B.Sc

January 1994

HYDROLOGICAL MODELLING WITH WEATHER RADAR DATA IN URBAN DRAINAGE SYSTEMS

By

Jianming Yuan B.Sc

January, 1994

This thesis is submitted for the degree of

Doctor of Philosophy of the University of Salford

Water Resources Research Group

Telford Institute of Environmental Systems

University of Salford

U. K.

To My Mum, Wife & Daughter

CONTENTS

LIST OF FIGURES

LIST OF TABLES

LIST OF SYMBOLS

a	A constant in the Z-R relation
A	Parameter of the A-Law compressor
$A_1(t)$	Dynamic storage factor of a dynamic linear reservoir
A′	Catchment area (km^2)
AF	Assessment Factor
ADC	Analogue-to-Digital Conversion
Arch	Inverse hyperbolic cosine
Arsh	Inverse hyperbolic sine
α	CPTF PR parameter (stability factor) or GW PDF parameter
b	A constant in the Z-R relation
B	Back-shifting operator, B=1- ∇
β	β-Law parameter, or PR parameter (stability factor)
c	The speed of light, or parameter of the X-Law compressor
C	A numerical factor known as the radar constant
CAPPI	Constant Altitude Plan-Position Indicator
CIR	Confident Interpolation Radius
C_k	Autocovariance coefficients
CPTF	Conceptually Parametrised Transfer Function
CSO	Combined Sewer Overflow
χ	Data resolution of model input
χ^2	Chi-square
d	Radar aerial diameter or distance or flow depth
dB	Decibel=$10\log_{10}(\bullet)$
D	Rainfall or flow event duration
δ	Time increment or quantum

$\partial(B)$	Transfer function
δ_i	Constants, i=1, 2, 3,$\cdots$s
ς_i	Constants, i=1, 2, 3,$\cdots$r
Δ	CPTF PR parameter (lag time=$\Delta-1$)
∇	differential operator: $\nabla R_t=R_t-R_{t-1}$
e	$\approx$ 2.7182818
E[]	Mean of a data population
$E(\varepsilon^2)$	Mean quantisation noise power
ε	A numerical constant
f	Wave frequency,
$f(\omega)$	Spectral density function
FF	Fitness Factor
ϕ	Maximum diameter of rainfall droplet
Φ	Total fitness
GA	Genetic Algorithm
GMT	Greenwich Mean Time
GW PDF	Generalised Weibull Probability Density Function
G_r	The gain of the receiving antenna in the direction of the target
G_t	The gain of the transmitting antenna in the direction of the target
$\gamma(t)$	The autocovariance function
Γ	Gamma function
h(t), H(t)	Pulse response function
HOLTID	Half of the Lag-to-Inflection Duration
η	CPTF PR parameter (the percentage runoff factor)
φ	Numerical constant
k	One way attenuation coefficient (dB/km), or parameter of the A-Law
k_p	One way attenuation coefficient due to precipitation
$\|K\|^2$	= 0.93 for water and 0.197 for ice

L	Quantisation levels
LIR	Local Interpolation Radius
L_t	A numerical factor to account for losses in the transmitting system
L_r	A similar factor for the receiving system
LT	Lead Time of forecast
L_{mt}	Numerical factors allowing the propagating medium to have loss
L_{mr}	Numerical factors allowing the propagating medium to have loss
L_p	A numerical factor to represent the polarisation effects
λ	Wavelength
ℓ	Mean length of interior stream links
m	Numerical constant
M	CPTF model order
MSL	Mean Sea Level
MDS	Minimum Detectable Signal
MDR	Minimum Detectable Rainfall
μ	Parameter of the μ-Law compressor
n	CPTF PR parameter or GW PDF parameter
n_0	Manning roughness coefficient
N	Numerical constant
N_c	Total number of chords used to approximate a compressor
NCTF	Non-Conceptual Transfer Function
NRA	National River Authority
NWW	North West Water Ltd.
p(s)	Probability density function of variable *s*
P	Radar signal power
PDF	Probability Density Function
PPI	Radar Plan-Position Indicator
P_r	Radar signal power
PR	Pulse Response (function)

$\overline{P}_r$	Mean returned power
P_t	The transmitter power in watts
π	≈ 3.1415926
$Q(t), Q_t$	Continuous and discrete flow time series
θ	PR parameter (stability factor)
Θ_u	Parameters of the Advanced CPTF model
r_t	Radar range from the antenna to target
r	Radar range from target to antenna or the TF model order
R	Rainfall intensities
RAI	Relative Attenuation Index of X-band radar to C-band radar
RHI	Radar Range-Height Indicator
R_0	Rainfall derived from Z_0 (mm/h)
R_d	Rainfall derived from Z_d (mm/h)
R_a	Rainfall derived from Z_a (mm/h)
R_r	MDR derived from Z_r (mm/h)
RR	Reduction rate of the CSO volume
R_{max}	Maximum rainfall (mm/h)
$R(t), R_t$	Continuous and discrete rainfall time series
RTC	Real-Time Control
ρ	Percentage runoff over a unit area
s	Order of the Advanced CPTF model
s_0	Channel bed slope
$s(t), s_t$	Analogue continuous and discrete time series
S	Storage volume (m^3)
SNR	Signal-to-Noise Ratio
σ	The backscattering cross section
σ_s^2	Mean signal power or the mean of the squared signal magnitude
t	Time ordinates
T	Return period

T_{90}	The time when the accumulation of a PR has just reached 90%
T_{95}	The time when the accumulation of a PR has just reached 95%
TF	Transfer Function
τ	CPTF PR parameter (Static storage factor) or GW PDF parameter
$\tau_0, \tau_1, \tau_2, \tau_3$	PR parameters of the dynamic linear reservoir (Static storage factor)
u	Time ordinates
UDS	Urban Drainage System
UH	Uhit Hydrograph
IUH	Instantaneous Unit Hydrograph
U_i	Time to Inflection
U_p	Time to peak
ϑ	Basin magnitude
v	Velocity of of flow translation
w	Width of the box pipe cross section
WASSP	Wallingford Storm Sewer Procedure (WALLRUS, Revised WASSP)
W_k	A set of weights
WRc	Water Research Centre (UK)
ω	Frequency=$2\pi f$
ω_N	Nyquist frequency
Ξ	PR parameter space
y(s)	Compressed version of signal s
ψ	Temporal sampling interval
Z	Radar reflectivity (mm^6/mm^3 or dB)
Z_0	Detectable minimum reflectivity in absence of attenuation (dB)
Z_d	Detectable minimum reflectivity in presence of attenuation (dB)
Z_a	Detectable minimum reflectivity in absence of precipitation (dB)
Z_r	Detectable minimum reflectivity in presence of precipitation (dB)
Z_p	Total attenuation due to precipitation (dB)
ζ_u	Parameters of the Advanced CPTF model

ACKNOWLEDGEMENTS

Without the generous support, guidance and warm encouragement from my supervisor, Professor Ian D. Cluckie, it would not have been possible for this research to be completed. I am indebted to him for everything relevant to this thesis.

I also want to express my thanks to Dr. Dawei Han, a sincere friend, who has consistently and patiently offered me invaluable advice during the course of the research leading to the preparation of this thesis.

I should like to acknowledge the support and assistance of Mr. John Tyson, Ms. Pippa Davis, Mr. George Szunko, Mr. Brain Morrow (North West Water Ltd.) and Mr. Will Britain (Blackpool Council) in carrying out this research.

Finally, it is a great pleasure to thank all of my colleague in the Water Resources Research Group (WRRg), the Telford Institute of Environmental System (TIES) at the University of Salford, especially, Barney Austin, Brehim Abes, Johnson Cox, Richard Griffith, Frank Lin, Richard Norreys, Kevin Tilford, (Miss) Sandra Towers, Adrian Wild, Owen Wedgwood, David Viner and Limin Zhang, who have provided a great deal of time in discussions. Some of the ideas described and elaborated in this thesis only became clear and concrete as a consequence of these fruitful discussions.

ABSTRACT

The management of large scale strategic urban combined drainage systems is becoming increasingly dependent upon weather radar systems which can provide quantitative precipitation information to improve the overall efficiency of a system's operational performance. Thus, there has been an increasing requirement for a more detailed knowledge of the radar rainfall data accuracy and the development of a mathematical rainfall-runoff model that can be used to analyse and control a system in real-time.

Within this context, several important factors including signal attenuation, temporal and spatial data resolutions and rainfall quantisation schemes that determine the accuracy of radar rainfall estimates were examined in this thesis. In order to facilitate real-time flow simulation and forecast, a Conceptually Parametrised Transfer Function (CPTF) model has been developed based on Dynamic Linear Reservoir theory. The model is structurally simple and operationally reliable. It can be easily identified and robustly updated following a pulse response-to-CPTF procedure in which Genetic Algorithms play a key role. Using the model, the accuracy of areal rainfall estimates obtained by the Hameldon Hill radar has been assessed, firstly by comparing the radar rainfall estimates with 'ground truth', and then by comparing the simulated hydrographs with the actual flow observations. Finally, a case study was conducted using radar rainfall data to highlight the potential benefit of real-time control for the strategic urban drainage system in the Fylde Coast. The major achievements documented in this thesis are: **1)** A rule for determination of an appropriate input data resolution for hydrological models; **2)** A general probability density function for describing the sampled radar rainfall intensities; **3)** An efficient quantising law (β-Law) and an associated adaptive rainfall quantisation scheme; **4)** Three general conceptual pulse-response functions developed based on Dynamic Linear Reservoir theory; **5)** CPTF model; and **6)** A case study on the potential benefit of real-time control in the Fylde urban drainage system.

CHAPTER 1

INTRODUCTION AND SYNOPSIS

Over the last 50 years, weather radars have been developed and used to provide valuable precipitation information mainly for meteorological studies and forecasts. However, in recent years, radar rainfall data has been increasingly applied to solve hydrological problems.

In the UK, the symposium on 'Weather radar and Flood Forecasting' held at the University of Lancaster in September 1985 marked the completion of the highly successful North West Radar Project, in which the first unmanned weather radar station in the United Kingdom was established and operated to give radar data in real-time for both meteorological and hydrological applications (Collinge and Kirby, 1987). Since then considerable potential for quantitative radar rainfall data to be used for real-time control (RTC) of urban drainage systems (UDSs) has been recognised by the regional water utilities which has stimulated research into the Radar Hydrology of predominately urban areas.

In recognising that weather radar can offer hydrological science a ground-based remote sensor of the precipitation process, the first International Symposium on 'Hydrological Applications of Weather Radar' was held at the University of Salford during August 1989 (Cluckie and Collier, 1991). Of the 57 papers presented more than 35% reported the achievements in the hydrological utilisation of radar rainfall information. Quantitative application of radar rainfall data for UDS management has increasingly

become an international practice in many places around the world, such as in the U.K. (Forshaw and Walters, 1990; Green, 1989; Yuan and Cluckie, 1992, Yuan and Cluckie 1993), France (Blanchet, Brunelle and Guillon, 1992; Blanchet, Guillon, et. al. 1993), Germany (Semke, 1989; Verworn, 1989; Jäke and Einfalt, 1992), Sweden (Andersson, T and B. Andersson, 1992) and Russia (Ermolin, 1992).

This thesis attempts to 1) address a number of problems related to the accuracy and hydrological utilisation of weather radar rainfall data (particularly the Hameldon Hill radar rainfall data), and 2) develop a real-time simulation and forecasting model suitable for analysis and control of a UDS.

1.1 Objectives

A. To investigate the sensitivity of UDS simulation errors to the temporal and spatial resolutions of radar rainfall data

Rainfall as an important input data source to the UDS models is usually a time-space series discretised at equal time and space intervals which are referred to as the data resolution. Data resolution determines to which extent a continuous rainfall process can be depicted. The present UK radar rainfall products employ 5-minute as the highest temporal resolution and 2-km as the highest spatial resolution. Are these resolutions adequate for quantitative urban hydrological applications? Is it possible to reduce these resolutions in order to cut the data management and application costs? A study on the sensitivity of UDS simulation errors to the temporal and spatial resolutions of radar rainfall data is required.

B. *To develop an adaptive quantisation procedure for data processing, transmission and archive purposes*

At the present time, a logarithmic quantisation scheme is used in the current UK procedure for analogue-to-digital conversion (ADC), data transmission and archive tasks. However, this has been recognised as being inefficient and may be replaced by a numerically more efficient scheme which is able to achieve a higher quantisation accuracy.

C. *To develop a hybrid model suitable for real-time flow simulation and forecasting purposes*

Real-time applications for UDS control require an appropriate adaptive model able to simulate and forecast the system status. Since under RTC the system's physical parameters, and hence the Impulse Response (IR) or Pulse Response (PR) varies with time, the model has to be:

- *Simple in structure with few data requirements*
- *Flexible to a wide range of catchment conditions*
- *Unconditionally stable and physically realisable*
- *Robust in case of data error*
- *Resilient to missing data*
- *Rapid in execution*
- *Simple in calibration and upgrading*

Though there have been a great number of mathematical models available to

hydrologists, few of them have all of the required properties suitable for the intended purpose. Chatfield (1984) has pointed out that: 'complex models often give forecasts which are no better than simple models and in general, the more frequent and greater the number of forecasts required, the more desirable it is to use a simple approach'. Therefore, it is necessary to develop a hybrid model with the required properties.

D. To assess the accuracy of radar rainfall estimates of Hameldon Hill radar

Hameldon Hill radar rainfall products have two types of correction applied on-site in real-time (Collier, 1986). The first type is a calibration which varies with rainfall type and locality, optimised within a range of about 100 km from the radar and derived from observations from a few interrogatable gauges (domain-correction procedure), and the second type is a long-range correction, mainly effective beyond 100 km, independent of rainfall type and direction from the radar, which is intended to compensate for the loss of radar sensitivity due to the beam not detecting rain producing clouds as a result of the curvature of the earth and other effects (Hitch and Hems, 1987).

Observations obtained at an economically small number of calibration raingauge sites (i.e. 4) are used as 'ground truth' for assessing the radar rainfall data accuracy in the domain-correction procedure. The ratio of radar rainfall measurement to a gauge measurement is defined as the assessment factor (when used for data correction purposes, it is called the calibration or adjustment factor). The objective of the corrections is to modify the radar rainfall surface using the gauge observed surface. Since the assessment factor varies significantly and systematically (not randomly) with rainfall types, the objective determination of rainfall type is made by a simple parametric representation of the temporal variability of the assessment factor. The relationship between rainfall type and the assessment factor is identified using a harmonic analysis of the variations of the running hourly mean assessment factors over

periods of one hour and the hourly mean assessment factor (Collier, Larke and May 1983).

The domain-correction procedure using a small number of raingauge and the harmonic analysis technique was found useful. With this correction technique the accuracy of radar rainfall estimates has been improved to some extent as compared to the ground raingauge observations. Since there are substantial smoothing effects as rainfall moves through the various phases in its passage to a flood risk zone and current research suggests that for this reason the accuracy requirements could be quite low (Cluckie, 1987), this study is intended to further assess the accuracy of radar rainfall estimates within the urban hydrological context based on not only the 'ground truth' but also the simulated and observed urban drainage flows.

E. To investigate the potential benefits of RTC for the Fylde drainage system using radar rainfall data

In order to comply with the EC Bathing Water Directive (Council of the European Communities, 1976), the Fylde coast has been included in a number of bathing beaches where cleaning up is required. Installation of a RTC system within the Fylde catchment is one of the options for improvement of the bathing water quality. To assist the planning and design of the control system, an investigation on the potential benefits of real-time control for the Fylde system is required, which will be carried out using radar rainfall data.

To achieve the above objectives, WASSP was used as a primary simulation tool for its ability to accept distributed rainfall input and the other advantages in the detailed representation of the urban drainage system.

1.2 WASSP

WASSP is the abbreviation of Wallingford Storm Sewer Package, developed by a national working party (DoE, 1981) for use in the analysis and design of urban sewerage and drainage networks. The package consists of six modules designed to suit different purposes.

The simulation program used throughout this thesis is WASSP-SIM, one of the six modules. This program is capable of modelling time dependent flow with or without surface flooding and/or surcharging in existing or design stage sewer networks. It can use built-in rainfall data or can accept user defined rainfall event data. Overflow structures, flow bifurcations (treated as overflow), online and off-line storage tanks, pumping stations and outfall flaps are supported. The operation of the outfall flaps may be controlled by the application of tidal hydrographs. The program may accept either lumped or distributed rainfall as inputs. Inflow hydrographs may be applied to any part of the network.

In order to use the program, the user is required to prepare two types of data files, one is the so-called Program Control Data (PCD) file and another is the Sewer System Data (SSD) file. The detailed record format and related specifications on the preparation of the data files may be found in the second volume of the WASSP reports.

1.3 Synopsis

In common with other countries, increasing attention in the UK is now being focussed on the role of weather radars in hydrology, particularly on the quantitative utilisation of radar rainfall data as input to UDS hydrological models. In this thesis some of the problems regarding to the accuracy and application of radar rainfall data were examined, and to facilitate the real-time flow simulation and forecast, a conceptually parametrised transfer function (CPTF) model was developed.

Chapter 2 gives a brief review of the basic principles and technical terms relating to weather radar technology. The scope is confined to those areas which are helpful to the readers in understanding the related contents presented in this thesis. Rainfall data adjustment using raingauge measurements is demonstrated by the procedure developed for the Hameldon Hill radar which provided the majority of the rainfall data used in this thesis. The importance of radar wavelength to the rainfall measurements and the suitability of X-band radars is briefly discussed at the end of this chapter.

The minimum detectable rainfall (MDR) is used as an objective index to quantify the suitability of X-band radar systems. Providing that the target rainfall intensity is not below the MDR, the rainfall is detectable and can be corrected to a comparable accuracy of that would have been observed by a co-located C-band radar system. Since at shorter ranges (<20 km) within a moderate rainfall field, the MDR is smaller than the intervening rainfall, rainfalls within the range are detectable everywhere. Consequently, X-band radars may be used to sense small to moderate rainfalls within a 15-20km range.

Chapter 3 investigates the significance of temporal and spatial resolution of radar rainfall data on the accuracy of sewer flow simulations through a case study. The problem was addressed in respect to the storm and system characteristics.

It was found that using a lower temporal resolution than 5-minutes (i.e 10 minutes, or 15 minutes) is possible. Using a spatial resolution lower than 2-km (i.e. 5-km, or lumped) is not recommended. The studied system has a comparatively fast response (i.e. time-to-peak is less than 1 hour).

Chapter 4 develops a more efficient quantisation scheme than the existing schemes used in the UK. The new scheme is devised using the inverse parabolic cosine as its compressor and may be applied in either static or adaptive mode.

The compressor is able to cope with a wider dynamic range of rainfall intensities with relatively less quantising errors than many of the existing compressors. With the adaptive quantisation, more accurate rainfall data can be obtained than using the static quantisation schemes. The adaptively quantised 3-bit data can be used to replace the statically quantised 8-bit data for urban hydrological applications.

It was also noticed that the distribution of rainfall intensity in Northwestern England follows the Weibull process and the true occurrence frequency of the quantised rainfall intensities is magnified by a factor being approximately equal to the quantum.

Chapter 5 introduces a Conceptually Parametrised Transfer Function (CPTF) model which has two forms: Naive and Advanced. The former is a linear filter type and the latter is a Markov process. The Naive CPTF model is suitable for parameter-adaptive applications whereas the Advanced CPTF model is ready for state updating. The CPTF model was developed based on Dynamic Linear Reservoir Theory and by hybridising the advantages of the conceptual instantaneous unit hydrograph (IUH) model with the Non-Conceptual Transfer Function (NCTF) model.

Chapter 6 details the method for identification of a CPTF model. Essentially, it is a two-step procedure. The PR parameters identified at the first step guarantees a physically realisable PR function to be established, from which a Naive CPTF model can be derived and the model parameters estimated at the second step enable a CPTF model of the Markov Process type (i.e. Advanced CPTF) to be constructed. A new procedure utilising the Genetic Algorithms plays an important part in the model identification.

Chapter 7 explains how to convert a static Non-conceptual Transfer Function (NCTF) model or Unit Hydrograph (UH) model into a CPTF model. The aim is twofold: 1) to reduce the labour required for identification of the CPTF models when existing NCTF or UH models are available, and 2) to improve the performance of the

existing models. The basic idea is to convert the PR function defined by the non-conceptual parameters into a conceptually parametrised PR function.

Chapter 8 presents a preliminary assessment of the CPTF model, which was made by 1) comparing the CPTF model with the NCTF model and UH model, 2) examining the performance of CPTF model in simulation of actual flow observations and 3) demonstrating the performance of CPTF model in urban drainage flow predictions.

The performance of the CPTF model in an adaptive simulation mode is quite satisfactory. However, in a prediction mode, it is mainly dependent on two factors: the system's lag-to-inflection duration and the variability of its PR. The former determines the maximum forecasting lead time and the latter governs the system's predictability.

Chapter 9 summarises a case study on the Hameldon Hill radar rainfall data accuracy using the CPTF model. It is assumed that radar rainfall data is for use in the urban hydrology context. The problem is addressed by (1) comparing the single-site rainfall data with the observations of a densely scattered (1 gauge/13km^2) telemetry raingauge network which is located at a range of about 20 km from the radar and (2) comparing the simulated hydrographs with the urban drainage flow observations. In the first case, raingauge rainfall is taken as the 'ground truth' upon which the accuracy of radar rainfall data is assessed and in the second case, the observed hydrograph, which was continuously monitored over a period of 18 days by an ultrasonic telemetry system, serves as the ultimate criteria indicating the accuracy of radar rainfall data.

When compared with the 'ground truth', Hameldon Hill radar overestimated the rainfall at a range shorter than 20 km and underestimated the rainfall beyond the 20-km range within the studied rainfall field. However, applying the lumped radar rainfall to the CPTF model yielded a more accurate reproduction of the observed hydrograph than using the raingauge rainfall data in the same model. This proved that even using a densely scattered raingauge network it is difficult to portray the actual rainfall field and

hence derive satisfactory areal rainfall estimates.

Chapter 10 investigates the potential benefits of RTC using radar rainfall for the Fylde drainage system. The major objectives of the current rehabilitation projects of the Fylde system are to protect the bathing water for coastal communities and ensure the discharges of storm water do not prejudice compliance with the requirements of the EC Bathing Water Directive. To indicate the viability of real-time control using radar rainfall data in the Fylde system, an investigation on the potential benefits was carried out. This is an essential prerequisite in the on-going development of radar based RTC procedure in the region.

The results indicated that RTC is viable in terms of operational improvements and reduction of the urban drainage impacts on the environment and radar rainfall data has an important role to play in the RTC of UDSs.

Chapter 11 summarises the main findings and conclusions. Potential areas for further study and options for the way forward to develop a RTC system have been recommended.

CHAPTER 2

MEASURING RAINFALL BY RADAR

The formation and evolution of rainfall in the atmosphere is the most variable subprocess within the hydrological cycle. In general, real-time hydrological models appear to be most sensitive to the spatial and temporal distributions of rainfall. Therefore, improvement in the rainfall measurements plays a key role for satisfactory flow simulation and prediction in real-time. Weather radars, by their nature, can sense the distribution patterns in both time and space at a higher resolution than the raingauges. When properly calibrated, they can provide reasonable estimates of precipitation.

The purpose of this chapter is to give a brief review of the basic principles and technical limitations of the weather radar technology to Radar hydrology. The scope is confined to those areas helpful for understanding the relevant issues addressed in this thesis. Rainfall data adjustment using raingauge measurements will be demonstrated by the procedure developed for the Hameldon Hill radar which provided the majority of the rainfall data used in this thesis. The importance of radar wavelength to the rainfall measurements and the suitability of X-band radar will be briefly discussed at the end of the chapter.

2.1 Weather Radar

Radar, (RAdio Detecting And Ranging), has been used for the study of weather systems since its development during the second world war. Differing from the military and other type of radars, weather radar is used to observe, study and provide precipitation information. Over the last 40 years, a rapid and steady growth in the use of weather radars has been witnessed in many places over the world, especially, in European countries. The spread of weather radars is driven by the increasing awareness of the benefits of weather radars in contributing to the solution of meteorological and hydrological problems.

The basic components of a weather radar system are the magnetron (or klystron), electromagnetic wave transmitter, receiver and antenna. The magnetron is an oscillator tube which produces high-power pulses (about 100 kW) at random phases (Collier, 1989). Figure 2.1 illustrates the principle of weather radar in detection of precipitation, which shows: 1) An electromagnetic pulse generated by the magnetron is emitted through the transmitter and the automatic transmit-receive (T/R) switch in sequence, then 2) propagated at a speed of 300,000 km/second (i.e. the speed of light) towards the desired direction under the guidance of antenna; 3) when the beam is blocked part of the emitted energy carried by the echo returns to the antenna and pass through the T/R switch again where the backscattered pulse is directed to the receiver; 4) the receiver seperates the returned signal from the noisy background then passes it to the data processing, displaying and archive system which usually is a computer system. The T/R switch is employed to prevent the receiver from being damaged by the emitted outgoing high-power and ensures the backscattered signal is transmitted to the receiver rather than the transmitter.

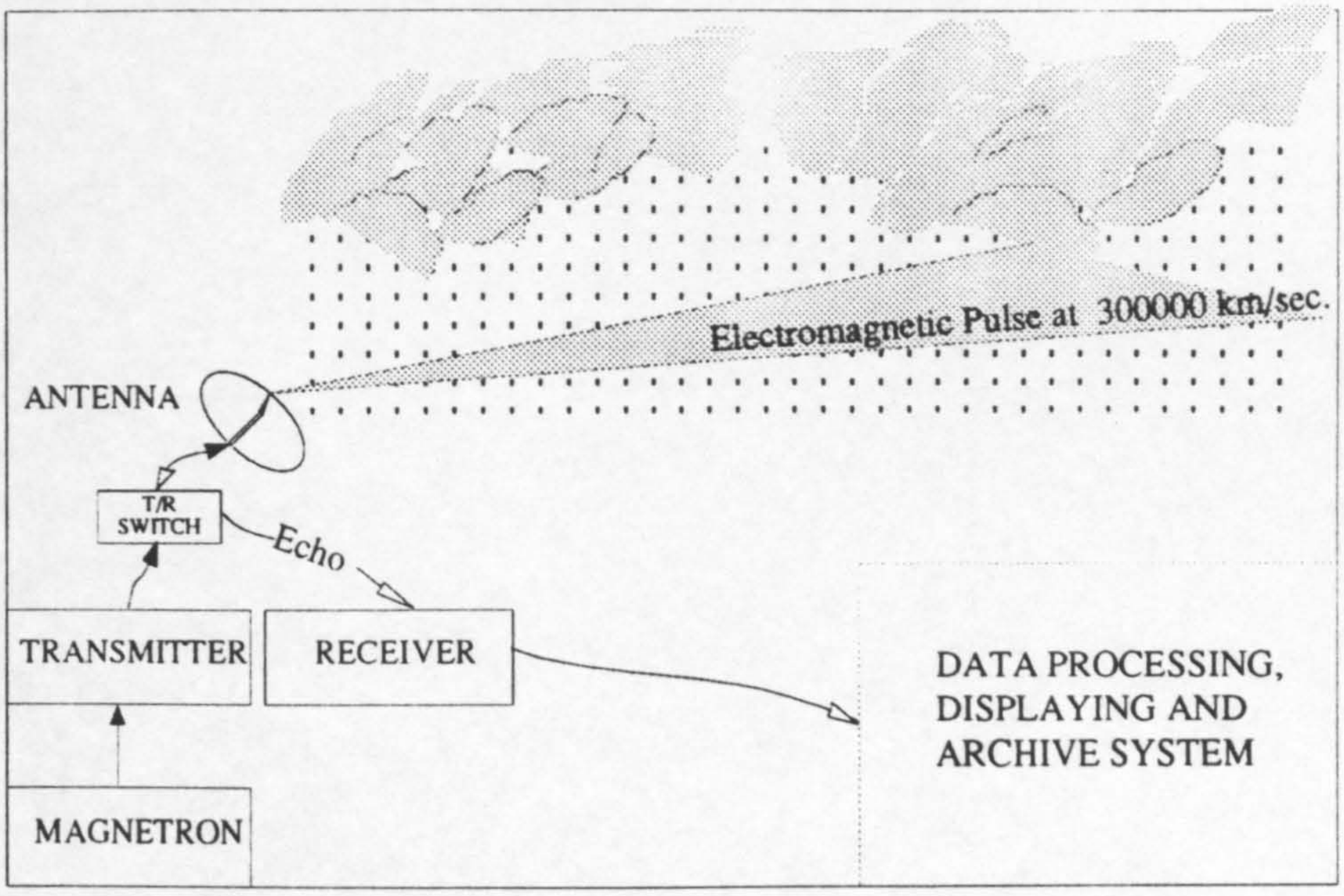

Fig. 2.1 Basic components of a weather radar system

A very important feature of the radar receiver is its Minimum Detectable Signal (MDS) level, the smallest signal which may be recognised above the system noise level. MDS is a fundamental quality index of the radar system. Therefore, the radar receiver is usually designed to have as low MDS as possible. Note MDS is only a measure of the system noise level and is not dependent on the range between radar and the target , attenuation and other factors. Because of the wide range of powers to be dealt with in a radar system (e.g. 10^{-13} to 10^{6} Watts), commonly, the signal power, P, is expressed in decibels, dB, which is defined as:

$$P_{dB}=10\log_{10}(P/P_0) \tag{2.1}$$

In radar technology, however it is usual using dBm to measure the relative strength of P to a base power P_0:

$$P_{dBm}=10\log_{10}(P/P_0) \tag{2.2}$$

Where P_0 is taken to be a milliwatt.

Logarithmic receivers are often used in radar systems to increase the system dynamic range which can be as much as 80 dB for the modern civil radars (Tilford, 1992). The continuous analogue signals are converted to digital form by the receiver. This is called data quantisation and will be further discussed in detail in Chapter 4.

The data processing system works out the position of the detected object by taking account of 1) the travelling time of the returned signal since it was emitted, 2) the scanning beam height and 3) the bearing of the beam. When the target is displayed on a horizontal plane the plane is called a **Plan-Position Indicator** (PPI) and the data is called PPI data. From a PPI the range and bearing of the detected target can be immediately read, however, the height of the target is not known. Fortunately, the height of the precipitation is often less important than its plan position. Otherwise, a **Range-Height Indicator** (RHI) should be used at the same time. RHI displays a vertical profile.

Figure 2.2 illustrates the PPI and RHI. The concentric circles on the PPI plane indicates the ranges from the radar. Any point on the PPI plane in the figure is projected from the scanning cone. If the PPI data are projected by a number of scanning cones of different elevation angles then the plane becomes Constant Altitude Plan Position Indicator (CAPPI) (Marshall, 1957) and the data is called CAPPI data in consequence. The RHI is shown as the vertical plane (W-E-R-R′) in the figure.The detectability of a radar with a given power is determined essentially by the strength of returned signal and the MDS level of the radar receiver. One of the important factors determining the strength of returned signal power is the wave length. see Eq.(2.4) and Eq.(2.5).

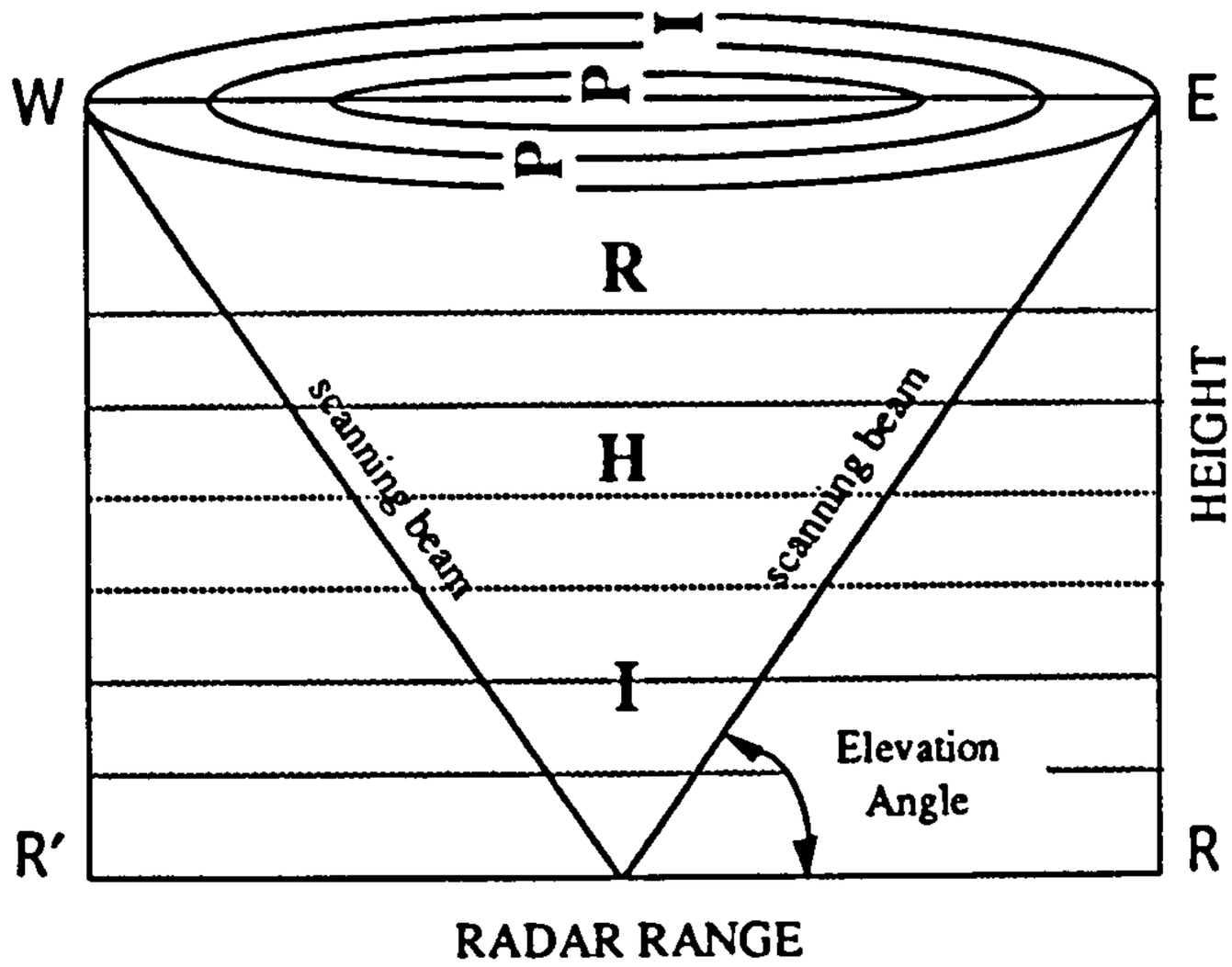

Fig. 2.2 PPI and RHI

According to the wavelength, radars have been practically classified as K-band, X-band, C-band, S-band and L-band radars. Table 2.1 shows the relationship between the band categories and the wavelengths. Since the travelling speed, c, of the magnetic wave is 300,000 km/sec, the wave frequency, f, can be calculated using the wavelength, λ by $f = c/\lambda$.

Table 2.1 Wavelengths and the associated weather radar categories

WAVELENGTH (cm)	BAND	COSTS	SENSITIVITY	ATTENUATION
0.8	K	*Low*	*High*	*High*
3.2	X	↓	↑	↑
5.6	C	↓	↑	↑
10	S	↓	↑	↑
20	L	*High*	*Low*	*Low*

Radars of different categories have different advantages and disadvantages. K band

radars are very sensitive (i.e. able to detect very small particles , e.g. cloud droplets). However its signal attenuation is significant and it is unable to efficiently detect rainfall at a far range. In contrast, the attenuation effect for L-band radars is very minor. However, they are not sufficiently sensitive to detect rainfall but can detect hails. In general radars with shorter wavelength are cheaper, more sensitive and prone to attenuation than those with longer wavelengths. For this reason, X-band, C-band and S-band radars are usually chosen for meteorological application purposes.

2.2 Electromagnetic Wave Polarisation

When an electromagnetic wave pulse is radiated from an antenna, it propagates in space as a time-varying electric field and magnetic field which are respectively described by the electric field density **E** and magnetic field density **H**. As the total energy carried by the electromagnetic wave is shared by the two fields, a decrease in the vector **E** will induce an increase in the vector **H**, so that the total energy can be conserved at any spatial point.

The relationship between the electric field density vector **E** and the magnetic field density **H** as well as the direction of wave propagation is shown in Figure 2.3, which indicates that the electric field is sinusoidally varying (i.e. oscillating) within the horizontal plane and the magnetic field is varying within the vertical plane, and both are perpendicular to the direction of propagation.

The plane containing the electric field is conventionally referred to as the 'plane of polarisation' (Battan, 1973). To specify the orientation of an electromagnetic wave in space, it is necessary to specify the orientation of the vector **E**. The polarisation of electromagnetic wave is determined by the polarisation of antenna since the plane of polarisation is parallel to the orientation of the dipole or the short side of a rectangular waveguide if either of these types of antennas is employed.

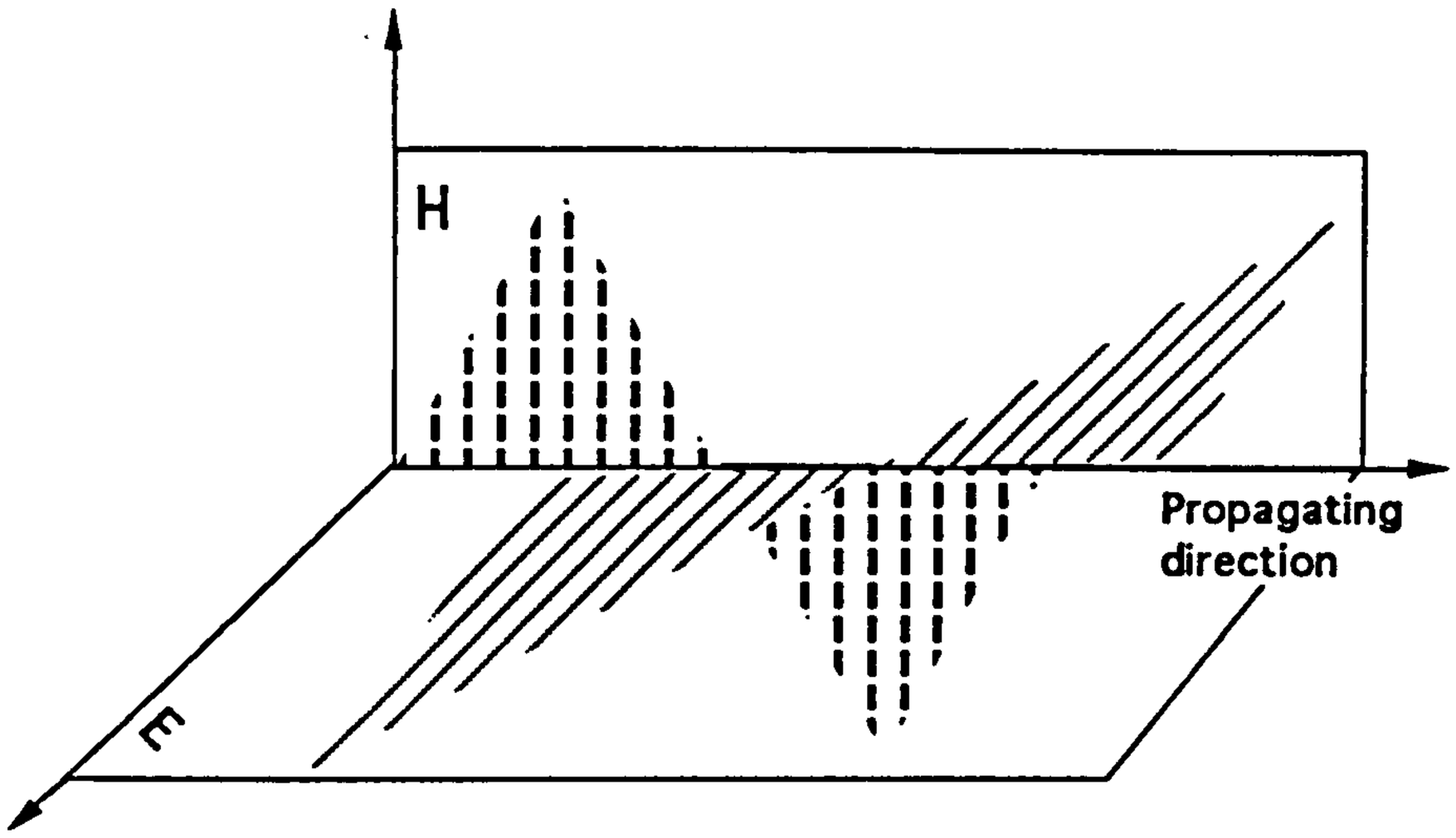

Fig. 2.3 Relations between the vectors E, H and the propagation direction

For example, if a dipole antenna is placed in a direction parallel to the earth's surface, then the 'plane of polarisation' will be parallel to the ground. In this case, the electromagnetic wave (radar) polarisation is called horizontal polarisation. If the antenna is vertically placed then the 'plane of polarisation' will be perpendicular to the earth's surface and the polarisation is called the vertical polarisation. If the angle of the vector **E** in the plane of polarisation does not vary with time then the polarisation is linear polarisation otherwise, circular or ellipse polarisation depending on whether the magnitude of the vector **E** is a constant or variable. In the case of circular polarisation, the vector **E** will rotate in the plane of polarisation around the direction of propagation. Most of the weather radar sets now used are linearly polarised, that is the vector **E** does not rotate in space.

To receive a signal, the receiving antenna has to be polarised in the same manner as the transmitting antenna, otherwise the power carried by the electromagnetic wave can not be entirely intercepted by the receiving system or in extreme no signal will enter into the receiving antenna. This is called the polarisation loss. Given a target rainfall different polarisation will yield different reflectivity values.

2.3 From Analogue Signal to Rainfall Intensity

Unlike a ground raingauge, the radar received signal is not the actual rainfall intensity but in analogue form (i.e. power). To obtain the required rainfall intensities, a relationship between the analogue signals and rainfall intensities needs to be derived. As indicated by Ruck, et. al. (1970), the radar received power, P_r may be written as a function of the radar transmitting, receiving systems, and the two-way propagation paths between radar and target:

$$P_r = A \cdot B \cdot \sigma \cdot C \cdot D \cdot E \qquad (2.3)$$

Where, $A = P_t \cdot G_t / L_t$, is the contribution of the transmitting system;

$B = 1/(4 \cdot \pi \cdot r_t^2 \cdot L_{mt})$, is the factor of the outgoing propagating medium;

σ is the backscattering cross section;

$C = 1/(4 \cdot \pi \cdot r^2 \cdot L_{mr})$, is the factor of the returning propagating medium;

$D = G_r \cdot \lambda^2/(4 \cdot \pi \cdot L_r)$, accounts for the receiving system;

$E = 1/L_p$, reflects the polarisation effects.

The parameters are defined as:

P_t is the transmitter power in watts;

G_t is the gain of the transmitting antenna in the direction of the target

G_r is the gain of the receiving antenna in the direction of the target

L_t is a numerical factor to account for losses in the transmitting system;

L_r is a similar factor for the receiving system;

L_{mt}, L_{mr} are numerical factors allowing the propagating medium to have loss;

r_t , r is the one-way range between the receiving or transmitting antenna and the target;

λ is the radar wave length and

L_p is a numerical factor to represent the polarisation effects

The returned power is proportional to the cross section of the target, σ, which is defined by Ruck et al as 'given the target echo at a receiving system, the cross section of target is the area which would intercept sufficient power from the transmitted field to produce the given echo by isotropic radiation'. In the precipitation case, the cross section of target is a function of the radar wave length and the diameter of rainfall droplet. If the ratio of the maximum diameter (ϕ) of rainfall droplet to the radar wave length is very small (i.e. ≤ 0.13) the droplet is said to be within the Rayleigh Region. Within the Rayleigh Region,

$$\sigma = \pi^5 \cdot |K|^2 \cdot \phi^6 \lambda^{-4} \tag{2.4}$$

where $|K|^2 = 0.93$ for water and 0.197 for ice. The relationship between σ and the average returned power is:

$$\bar{P}_r = \frac{C\lambda^4 \sum_{Vol} \sigma}{\pi^5 r^2} = \frac{C|K|^2 \sum_{Vol} \phi^6}{r^2} \tag{2.5}$$

where C is a numerical factor known as the radar constant (Battan, 1973). The method for calculation of the mean signal power can be found from Marshall and Hitschfeld (1953) or Wallace (1953) or Battan (1973). Replacing the sum of all droplets in a unit pulse volume, $\sum \phi^6$, by a new parameter Z called radar reflectivity (mm^6/m^3), Eq.(2.5) is simplified into:

$$\bar{P}_r = \frac{C|K|^2 Z}{r^2} \tag{2.6}$$

Eq.(2.6) is the well-known radar equation. It has been developed under a number of assumptions which may be found from Crozier (1986) and Collier (1989). Note Eq.(2.6) is only valid for the rainfall droplets scattering within the Rayleigh Region.

However, this may not be the case in practice and the shape of the rainfall droplets may not be spheroids. Hence, the measured reflectivity is only an effective reflectivity (Atlas et al., 1964). Empirically the reflectivity (mm^6/m^3) is related to rainfall intensity by:

$$Z = aR^b \tag{2.7}$$

Where a, b are constants and R is the rainfall intensity in mm/h. If Z is in dB then Eq.(2.7) becomes: $Z = 10\log_{10}(aR^b)$. A very popular value for the constant *a* is taken to be 200 and *b*, 1.6 as suggested by Marshall and Palmer (1948). However, it is recognised that the constants may vary with time, rainfall type and radar locality although *b* does not vary as much as *a*. A number of Z-R relations may be found from Joss *et. al.*, (1970) and Battan, (1973). Since there are many factors in addition to the uncertainty in the Z-R relation, which cause the measuring errors, correction of the radar rainfall estimates is usually necessary.

2.4 Corrections for the Hameldon Radar Rainfall Data

Hameldon Hill radar is a C-band radar, equipped with an on-site computer transmitting PPI data primarily obtained from a surface beam every 5 minutes.

Figure 2.4 shows the location of the radar.

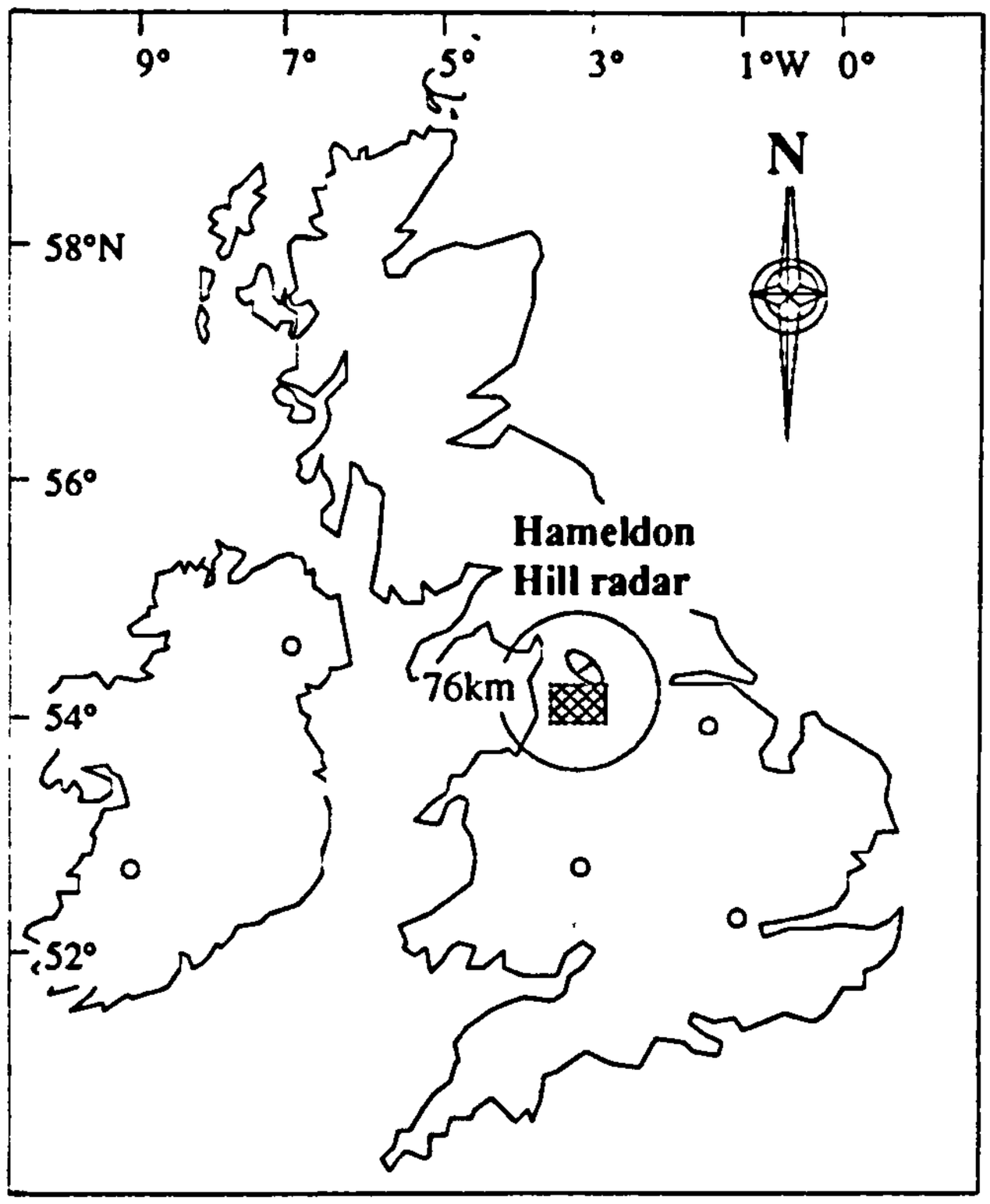

Fig. 2.4 Location of Hameldon Hill radar

The beam width is 1.0 degree. The 'surface beam' consists mainly of data from the lowest elevation (0.5 degree in the vertical profile) beam but filled with the data from one higher elevation (1.5 degree) beam at shorter ranges (≤ 24km) in order to minimise the effect of ground reflections (ground 'clutter'). Two types of rainfall data having different spatial resolutions are available. The 2-km rainfall data covers a range of 76km and the 5-km data extends to 210km. Table 2.2 gives more detailed information.

The PPI data are quantised initially in polar coordinates by the radar receiver, and then transmitted to the radar site computer system which performs a number of tasks including:

Table 2.2 Information on the Hameldon Hill radar

Radar site (Hameldon Hill,			**National Grid**		**Latitude**		**Longitude**
Burnley, Lancashare)			3811E, 4287N		53° 45′ N		2° 17′ W
Radar grid center			3800E, 4250N		53° 43′ N		2° 18′ W
Top left hand corner	(5km grid)		1700E, 6350N		55° 33′ N		5° 39′ W
Bottom right hand corner	(5km grid)		5900E, 2150N		51° 48′ N		0° 45′ E
Top left hand corner	(2km grid)		3040E, 5010N		54° 24′ N		3° 29′ W
Bottom right hand corner	(2km grid)		4560E, 3490N		53° 02′ N		1° 10′ W
Radar Type		45 C	BEAM INFORMATION	Beam	Elevation Angle	Occulted (Yes/No)	Infill (Yes/No)
Scanner height-OD	(Metres)	405		0	0.5°	Y	Y
Beam width	(Degrees)	1		1	1.5°	N	Y
Rotation rate	(Revs/Min.)	1.2		2	2.5°	N	N
Frequency	(Mz)	5640		3	4.0°	N	N
Antenna		Parabolic dish					
Diameter		3.7m					
Gain		43 dB					
Polarization		Vertical					
Elevation		-2° to 9°					
Transmitter		Peak power: 250 kW					
Pulse width		2m					
Receiver		Logarithmic					
Noise factor (Threshold)		8.5 dB or less					

1) Ground clutter removal;
2) Beam occultation corrections;
3) Conversion of the quantised analogue signal into rainfall intensities
4) Additional software correction for range beyond 100 km;
5) Empirical two-way attenuation correction;
6) Conversion to Cartesian coordinates (2-km and 5-km grids);
7) Gauge adjustment using domain maps;
8) Construction of a nominal surface precipitation field;
9) Conversion to the 8-bit float notation and data packing

Beam infilling is one of the techniques used in the ground clutter removal, which replaces the data derived from the lowest beam by that from a higher beam at shorter

ranges near the radar site. Figure 2.5 shows the infill area.

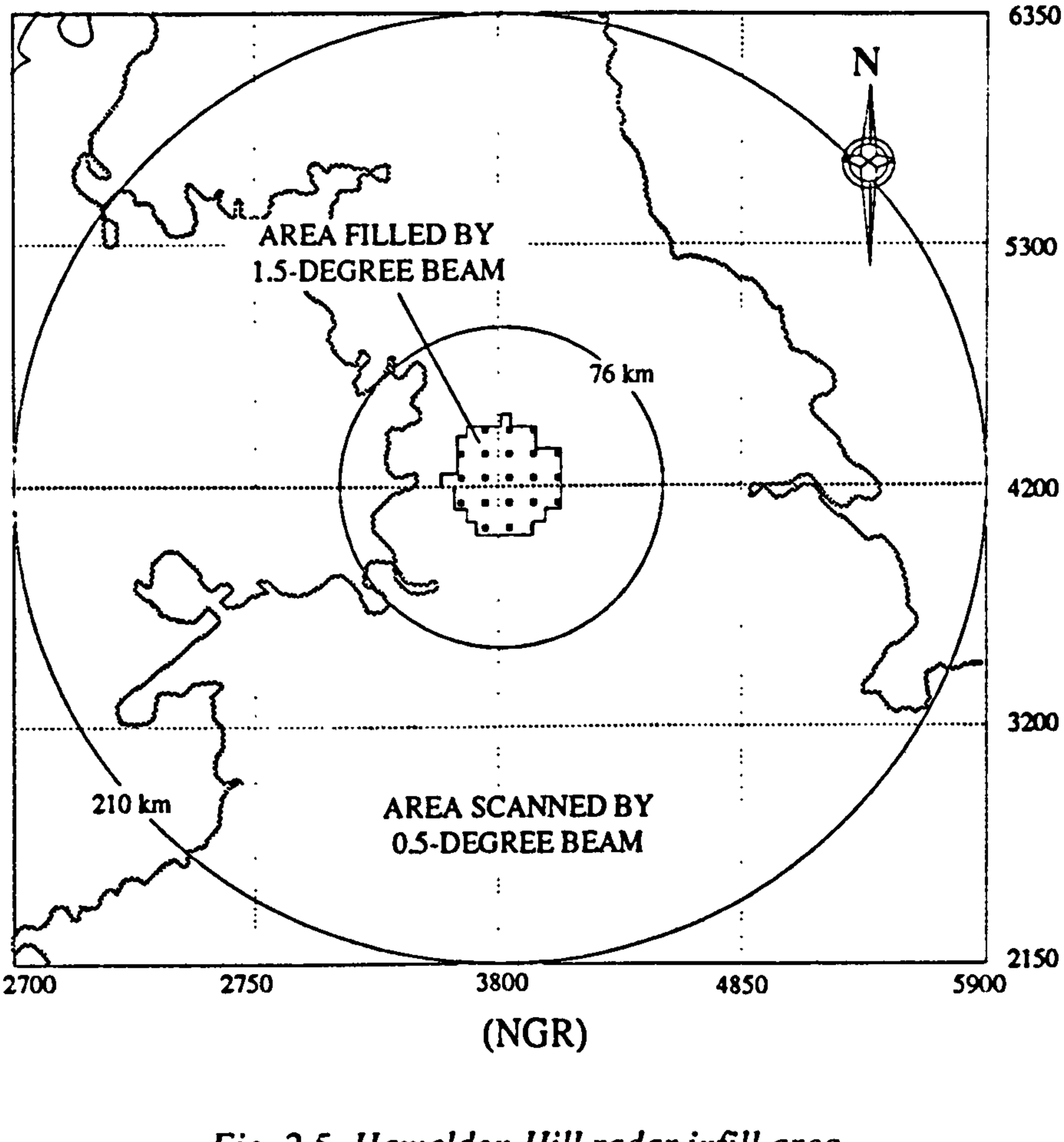

Fig. 2.5 Hameldon Hill radar infill area

The shaded area within the 210km range is filled by data from the 1.5-degree beam and for rest of the grids within the range are filled by data from the 0.5-degree surface beam.

The range and beam attenuation corrections are for compensation of the uneven loss of the radar signal strength along the radar beam. Beam attenuation may be caused by range and energy absorption/scattering due to atmospheric gases, liquids and solids and radome wetting. Table 2.3 shows a summary of the beam attenuation due to range and atmospheric mediums.

Table 2.3 Attenuation caused by absorption and scattering
(source: Tilford, 1992)

MEDIUM	WAVELENGTH (cm)	ATTENUATION (one-way dB/km)	ATTENUATION (two-way at 100 km)
OXYGEN[1]	ALL[2]	0.008 - 0.01	1.6 - 2.0
WATER VAPOUR	3	0.01[3]	2.0
	10	0.0002	0.04
CLOUD[4] (water droplets)	3	0.1	20
	10	0.01	2.0
CLOUD[5] (ice crystals)	3	0.004	0.8
	10	0.0008	0.16

PRECIPTATION (mm/h)	TWO-WAY ATTENUATION (dB/km)		
	10 cm	5 cm	3 cm
0.5	0.0003	0.002	0.006
1.0	0.0006	0.004	0.014
5.0	0.003	0.030	0.122
10.0	0.006	0.066	0.302
50.0	0.03	0.430	2.500
100.0	0.06	0.962	6.160

[1] at sea level pressure
[2] nearly constant for wavelengths in the range from 3 to 10 cm
by the 0.5 cm line of oxygen at a temperature of 20 C° and a pressure of 1 atm.;
[3] Assuming 7.5 g/m^3
[4] Assuming a water vapour content of 1 g/m^3 , high for most clouds
[5] Assuming an ice crystal content of 1 g/m^3

Range attenuation is simply accommodated by the range parameter, r, in the radar equation, Eq.(2.6), for the scattering of electromagnetic pulses by an extended target. The received signal power is inversely proportional to the square of r. More detailed information on the radar signal attenuation may be found in Hitschfeld and Bordan (1954), Battan (1973) and Joss and Waldvogel (1989).

Note, any correction made for compensation of attenuation is subjected to the MDS level. For signals below the MDS are unable to be recovered by whatever means. Consequently, S-band radars have found application in tropical areas where intense

rainfall is relatively common whilst C-band radars are generally regarded as suitable for use in the areas of temperate latitudes. With the increasing awareness of the potential benefits of weather radars for urban drainage system controls, low cost X-band and C-band radars have attracted great interest. For this reason, a comparison between the X-band and C-band radar estimates of precipitation is presented in Section 2.5.

The correction technique using domain maps was developed during the course of the North West Radar Project (Collier, 1989). The comparisons between radar and raingauge measurements revealed that the assessment factors varied over a great range, especially during shower cases. However, it was found that the assessment factor can be correlated to the orographic features and storm types within the radar coverage. This lead to the development of a calibration procedure using raingauge and domain maps which are defined by taking two factors into account, i) rainfall types and ii) orographic features (Collier, Larke and May 1983, Collier, 1989).

The likely radar rainfall type may be frontal, shower, Welsh shadow and bright-band. The assessment factors of different rainfall types have different variabilities. In frontal and bright-band cases, the variation of AF is often slow, and more rapid in showers When rain is falling within strong southwesterly winds, the Welsh shadow occurs because the Hameldon Hill radar is located to the east of the Welsh hills. In this case, radar overestimates the rainfall over the shadowed area and the variation of AF is small. Based on the variabilities of the assessment factor rainfall type can be determined. The determination of the variabilities of the assessment factor is facilitated by the harmonic analysis. Two harmonics with a period of 30 and 60 minutes respectively are used every 15 minutes to construct the time-series average assessment factors over the previous one-hour period. The average assessment factors are calculated using the observations from four calibration rainfall gauges every 15 minutes. If the complex wave of the two harmonics accounts for most of the total variance in the time-series assessment factor then the variability of the assessment

factors in the series is regarded as rapid otherwise, slow. The ratio of the power of the complex wave to the total variance is referred to as the temporal variability factor of the average assessment factors, which is subsequently estimated at every 15 minutes. To distinguish the frontal, shower, Welsh shadow and bright-band type storms from each other, the mean of the average assessment factors over the hour is estimated. For convenience, it is referred to as mean assessment factor. Using the mean assessment factor and the temporal variability factor the rainfall type for each 15 minutes (a time step) is designated by looking up a diagram indicating the relationship between the rainfall types, the mean assessment factor and the temporal variability factor. This diagram may be found from Collier (1989), which was produced using archived data over a 5-month period (300 hours) during September 1980-January 1981.

Having recognised the rainfall type, different adjustment factors may be applied to radar measurements. In cases when the assessment factor is outside of a range from 0.1 to 10, either 0.1 or 10 will be forced to apply. These limits have also been used to minimise the occurrence of large sudden changes in assessment factors. Which assessment factor should be applied to a grid cell for the rainfall type is dependent on the orographical feature of the cell. According to the orographical features within the radar coverage, cells with similar rainfall-orography interaction features during a type of rainfall were incorporated into a domain. All of the domains make up a domain map. Different domain maps have been identified respectively for the frontal, shower, Welsh shadow and bright-band rainfalls. Figure 2.6 illustrates the old domain maps used for different rainfall types and the adjustment algorithm for the Hameldon Hill radar, the revised domain maps can be found from the FAAG report (Banks, et al, 1984), in which the combined Domains were used respectively for Bright-Band/Shower, Welsh Shadow/Frontal type rainfalls.

According to Collier et. al (1983), the adjusted rainfall data using raingauge data are more accurate than those without adjustment and also more accurate than those adjusted only using a single average assessment factor.

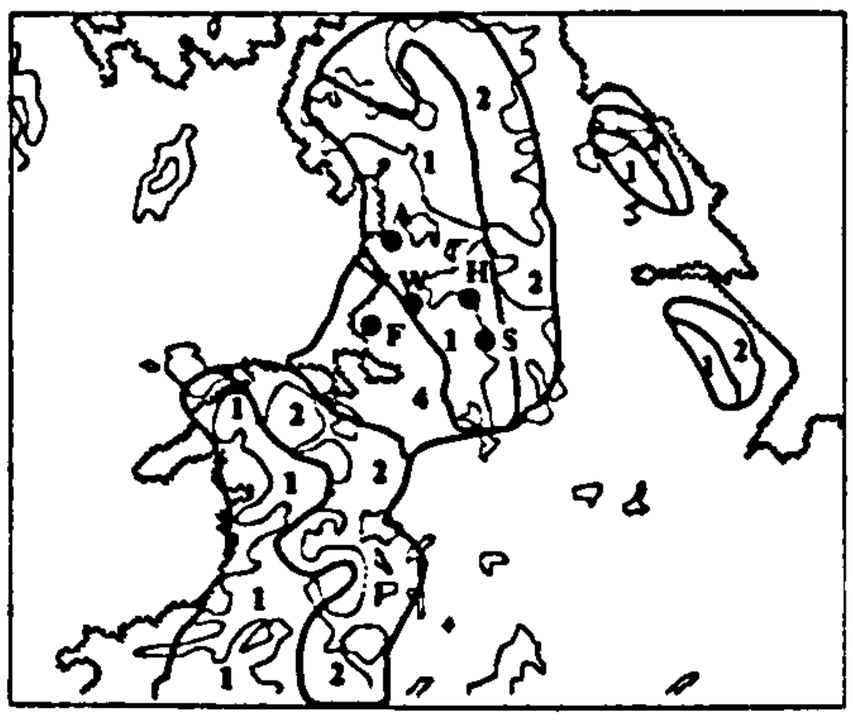

FRONTAL

Domain-1 Use average adjustment factors from gauges A, W, H and S
Domain-2 Use $Z=180R^{1.6}$
Domain-4 Use adjustment factor from gauge F
Elsewhere use $Z=200R^{1.6}$

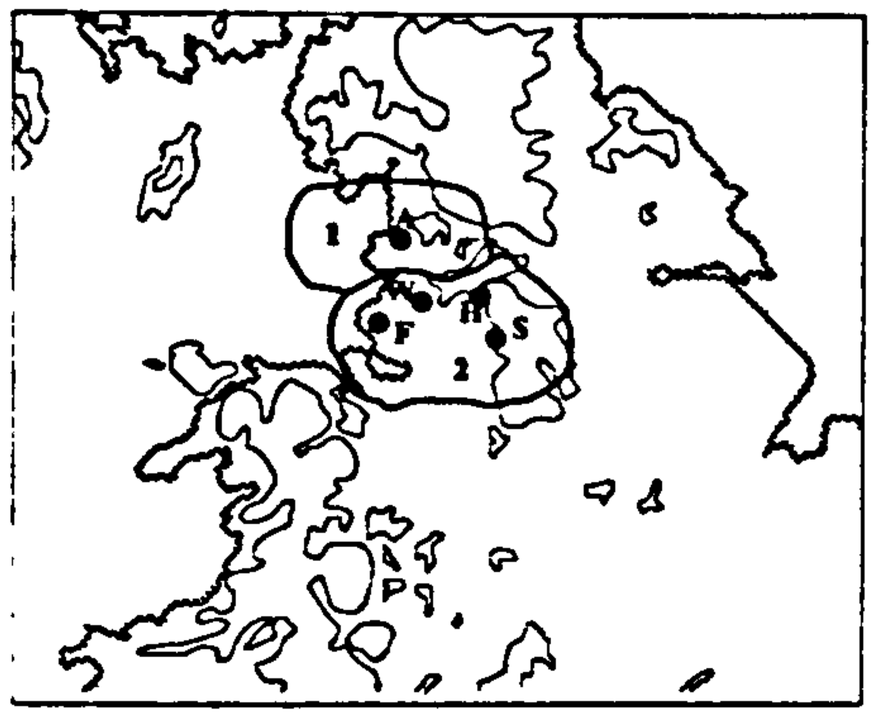

SHOWERS

Apply adjustment factor from gauge A in Domain-1, and average adjustment factors from gauges W, H and S in Domain-2

Elsewhere use $Z=300R^{1.6}$

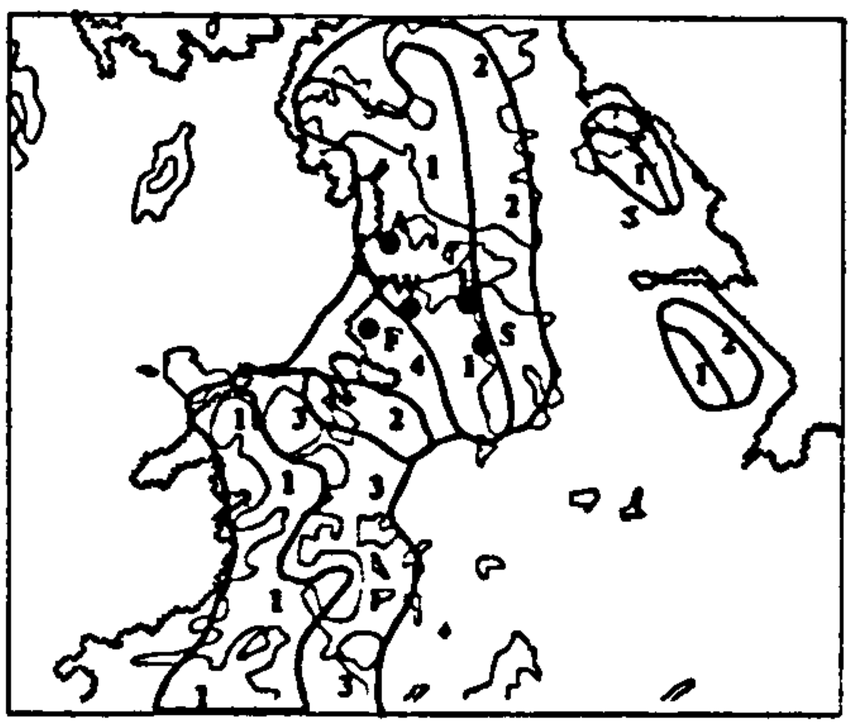

WELSH SHADOW

Domain-1 Use average adjustment factors from gauges A and W
Domain-2 Use average adjustment factors from gauges H and S
Domain-3 Use $Z=180R^{1.6}$
Domain-4 Use adjustment factor from gauge F
Elsewhere use $Z=200R^{1.6}$

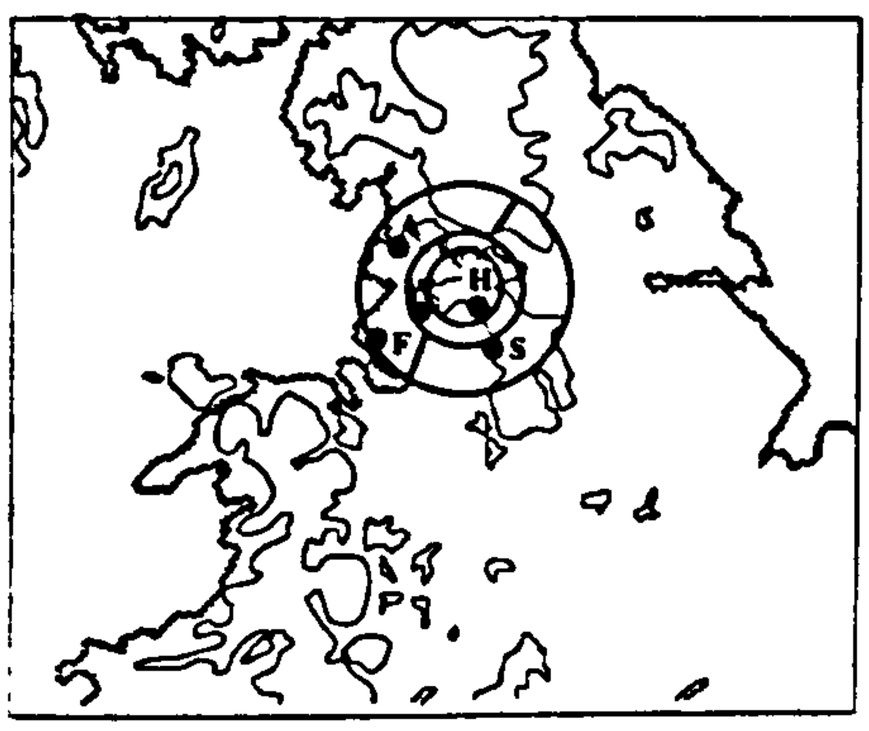

BRIGHT-BAND

Apply individual adjustment factors from gauges A, W, H and S in appropriate sectors.

Elsewhere use $Z=200R^{1.6}$

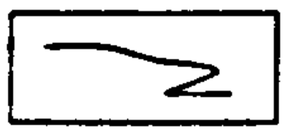

200m contour MSL

Fig. 2.6 Domain maps for the Hameldon Hill radar (source: Collier, 1989)

2.5 Comparing X-band Radar with C-band Radar

X-band radars are cheaper to buy and have many advantages when compared with the radars of longer wavelengths. The performance of a weather radar may be considered under the headings of sensitivity, resolution and precision of rainfall measurement (Ulaby et. al, 1981, Smith, 1986). The sensitivity of an X-band radar is significantly greater than a C-band radar due to greater scattering at the shorter wavelength (inversely proportional to the fourth power of the wavelength). Moreover, using X-band radar is able to produce rainfall data with higher resolution, however, it is more prone to attenuation in high intensity rainfall. This effect has been studied by Hitschfeld and Bordan (1954). They found that a mere 8 mm/h rainfall extending over 10 miles would cause a 5 dB attenuation which may result in serious errors in the measurements of rainfall for X-band radar,whereas for C-band radar, 30 mm/h extending over the same distance may have a similar effect. Figure 2.7 shows the reproduced results.

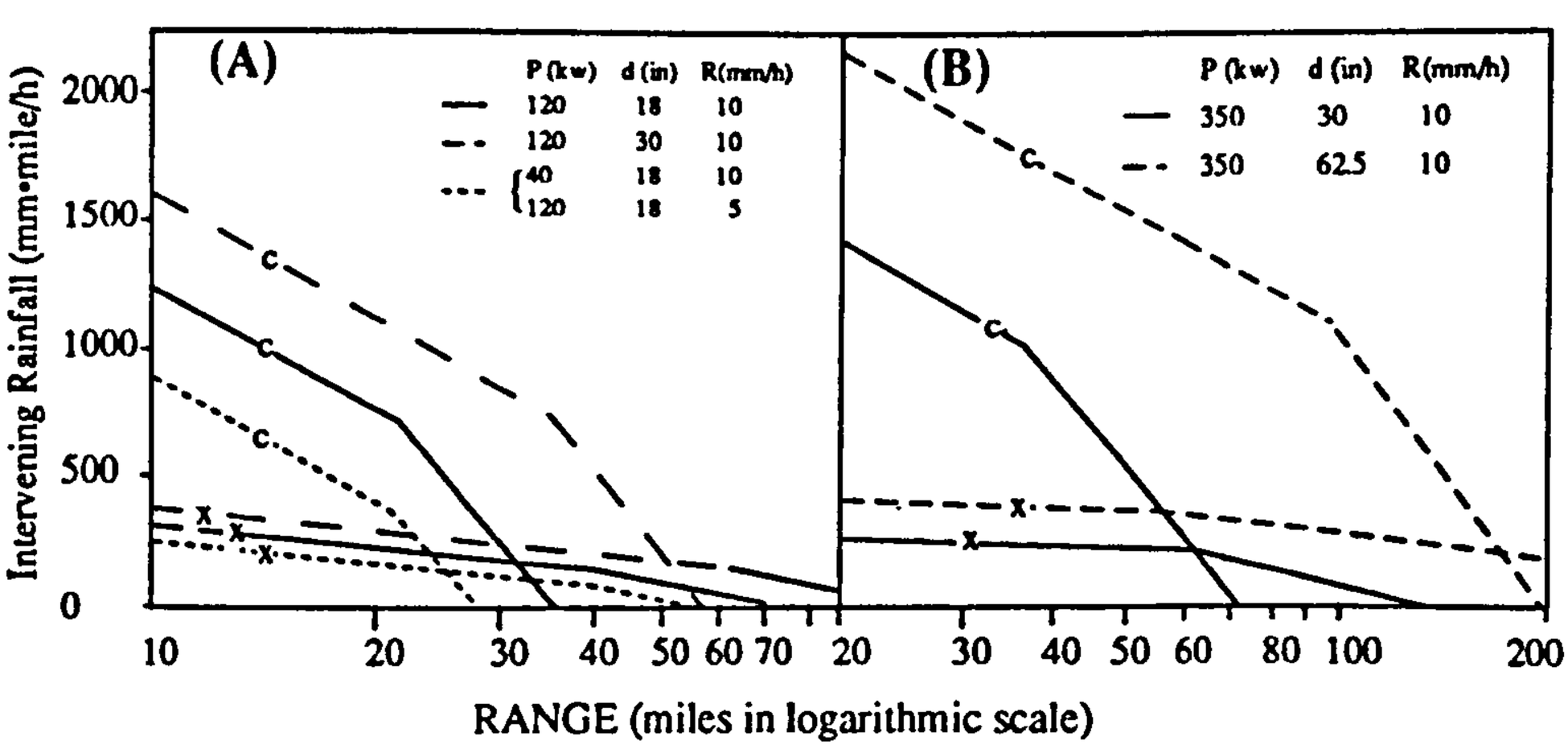

Fig. 2.7 Relations of the intervening rainfall and detectable rainfall at different ranges for a radar with (A) low-power, small aerial size; and (B) high power and larger aerials. (Source: Hitschfeld and Bordan 1954)

In the figure, the quantity of intervening rainfall through which a shower of a given intensity, R, may be detected is plotted against the range. The target rainfall was rather arbitrarily assumed to be a 3-mile by 3-mile box. Diagram (A) refers to low-power, P kW and small aerial diameter, d inch. Sensitivity at 3-cm wavelength is seen to vary rapidly with the amount of intervening rainfall. This rapid variation itself may lead to uncertainty in interpretation of signals. 500 mm·mile/h is shown as enough to render X-band radar practically useless. The diagram (B) shows the results produced using a higher power and larger aerials.

Furthermore, M. R. Duncan, *et. al.* (1991) studied the same problem. They compared the simulated X-band and C-band radar rainfall accumulations with the initial observations made by a S-band radar and concluded that significant signal attenuation below the MDS of the receiver is a source of error for X-band wavelengths for which no correction scheme exists; and there should be little confidence in the rainfall estimates provided by X-band radars beyond a radius where the attenuation causes the signal strength to approach the MDS.

For the above reasons, in the present urban meteorological/hydrological radar development, the acute interest in obtaining high precision data tends to urge the desirable wavelength upwards in order to minimise the combined effects of attenuation and minimum detectable rainfall. However, on the other hand, the requirements on the high data resolution and low cost have driven the hydrologists into a dilemma. Therefore, it may be useful to make a further comment on the suitability of X-band radars through a comparison made with the C-band radar measurements and to clarify a number of concepts such as minimum detectable signal and minimum detectable rainfall by taking the advantages of the existing results.

2.5.1 Relative Attenuation

Similar to the definition of assessment factor which indicates the relative difference in the radar and raingauge measurements, a ratio of X-band radar measurements to that from a 'co-located' C-band radar can be used as an index to indicate the relative difference between the data obtained from the two radar types. Assuming that the difference is dominantly caused by the attenuation factors, this index can be used to quantify the relative attenuation level of X-band radar to C-band radar. Thus, it may be referred to as relative attenuation index (RAI). The variability of RAI is a function of radar range and intervening rainfall intensity, which may be investigated using the Marshall-Palmer Z-R relation. Assuming that the reflectivity at a range of r (km) detected in absence of signal attenuation is Z_o dB and the attenuation causes a drop from Z_o to Z_d dB due to atmospheric gases, clouds, and precipitation, Delrieu, Creutin and Andrieu (1989) have utilised:

$$Z_o = Z_d + 2\int_0^r k\,dr \tag{2.8}$$

Where k is the one-way attenuation coefficient (dB/km). The attenuation caused by atmospheric gases is substantially constant with time for a given range and can be taken into account in the range correction. The effect of clouds is normally slight (Duncan, *et. al.*, 1991). Without considering these two attenuation factors, Eq.(2.8) becomes:

$$Z_o = Z_d + 2\int_0^r k_p\,dr \tag{2.9}$$

Where k_p is the one-way attenuation coefficient due to precipitation (dB/km). The relationship between k_p and the intervening rainfall has been established by Gunn and East (1954), which can be expressed as $k_p(i) = \alpha' R_i^{\beta'}$ in general, where, $k_p(i)$ is the

one-way attenuation coefficient at a radar grid *i* in dB/km, R_i is the intervening rainfall intensity in mm/h of the grid and, α' and β' are experimental constants which are assumed to be the same for any grid.

Replacing the terms in Eq.(2.9) with the Z-R relationship and the rainfall-attenuation relation, we obtain:

$$R_o = R_d + \frac{2}{b}\int_0^r \alpha' R_r^{\beta'} dr \qquad (2.10)$$

Where R_o and R_d are in dB. For the spatially discrete rainfall field Eq.(2.10) can be rewritten as:

$$R_o = R_d + \frac{2}{b}\sum_{i=1}^{N-1} \alpha' R_i^{\beta'} \Delta r \qquad (2.11)$$

Where Δr is the bin size (km) in the direction of *r* and $N=r/\Delta r$. When X-band and C-band radar is used respectively to detect the same storm the detected rainfall R_d in Eq.(2.11) should be respectively replaced by R_x and R_c in dB, and correspondingly α' and β' by α'_x and β'_x, or by α'_c and β'_c. Thus,

$$R_0 = R_x + \frac{2}{b}\sum_{i=1}^{N-1} \alpha'_x R_i^{\beta'_x} \Delta r \qquad (2.12)$$

or

$$R_0 = R_c + \frac{2}{b}\sum_{i=1}^{N-1} \alpha'_c R_i^{\beta'_c} \Delta r \qquad (2.13)$$

Where α'_x takes the value of 0.0074; α'_c, 0.0022; β'_x, 1.31 and β'_c, 1.17 (Gunn and East, 1954). Using Eq.(2.12) and Eq.(2.13) the ratio of R_x over R_c (i.e. RAI) can be

calculated as:

$$RAI = \frac{2\Delta r}{b} \sum_{i=1}^{N-1} \left(\alpha_c' R_i^{\beta_c'} - \alpha_x' R_i^{\beta_x'} \right) \qquad (2.14)$$

Where RAI is in dB. If RAI is equal to 0 dB then the attenuation level of the X-band radar is at the same level as the C-band radar. Theoretically, RAI is less than 0 dB because the attenuation of X-band radar is greater than the C-band radar. Figure 2.8 illustrates how the RAI varies as a function of radar range (r) and the uniformly distributed intervening rainfalls (R_i) for *b* taking a value 1.6 (under Marshall-Palmer condition) and Δ=1.

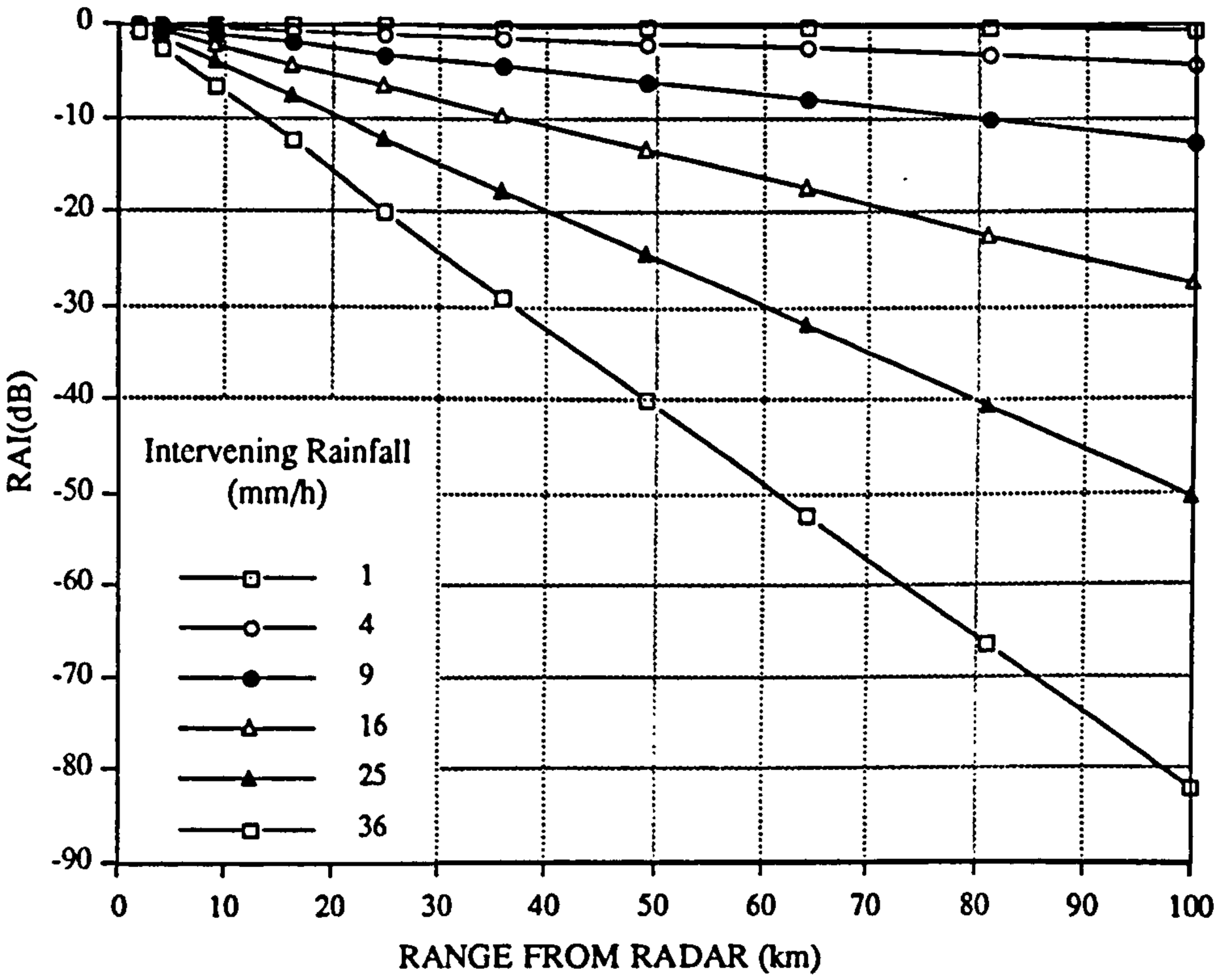

Fig.2.8 RAI as a function of range and the intervening rainfall intensity along the radar beam

It is evident in the figure that 1) the RAI (dB) decreases proportionally with an increase in the radar range; 2) the signal attenuation effect is significant at the further ranges or within very intense rainfall fields; Even the detecting range is limited to 20 km (i.e. about the size of a medium urban catchment), the RAI can be as much as -15 dB within a intervening rainfall field of 36 mm/h (i.e. the X-band radar observations are only about 3.2% of the amount detected by the C-band radar). This RAI value is regarded as relatively significant; However 3) due to the existence of the relationship among the RAI, intervening rainfall and the radar range, it is possible to correct the X-band radar measurements to the level of equivalent C-band radar measurements, providing that the target rainfall intensities are not below the Minimum Detectable Rainfall of the X-band radar.

2.5.2 Minimum Detectable Rainfall

Minimum Detectable Rainfall (MDR) in this analysis refers to the minimum rainfall intensity being able to be detected by a weather radar system with a given transmitting power in the presence of signal attenuation due to precipitation. It is determined by the noise level (or MDS) of the radar receiver, range from radar, rainfall type (i.e. Z-R relation) and the amount of intervening precipitation within the radar beam (i.e. the major attenuation factor). The MDR is a major limitation to the suitability of X-band radars in hydrology since it determines the possibility of attenuation compensation and hence the applicable range.

Assuming that Z_a (dB) is the detected minimum reflectivity at a range, *r*, in absence of attenuation due to precipitation, the actual reflectivity strength, Z_r (dB), being detectable at this range when attenuation is presented due to precipitation, may be calculated as:

$$Z_r \approx Z_a + Z_p \tag{2.15}$$

Where Z_p is the total attenuation due to precipitation (dB). It is reasonably assumed that other attenuation factors can be easily compensated. According to Gunn and East (1954), if the grid bin size Δr is 1km then for X-band radars,

$$Z_p \approx \sum_{i=1}^{r-1} 0.0148 R_i^{1.31} \quad \text{(dB)} \tag{2.16}$$

Incorporating this formula and the Z-R relation into Eq.(2.15), we get:

$$\frac{R_r}{R_a} = 10^{\frac{1}{10b}\sum_{i=1}^{r-1} 0.0148 R_i^{1.31}} \tag{2.17}$$

Where R_a is the rainfall intensity (mm/h) derived from Z_a;

R_r is the rainfall intensity (mm/h) derived from Z_r and

R_i is the intervening rainfall intensity (mm/h)

The left-hand side of Eq.(2.17) is referred to as the minimum detectable rainfall factor (for short, MDRF), which indicates the MDR of X-band radar as a proportion of the R_a. Figure 2.9 shows the MDRF varying with radar range and the intervening rainfall intensity for different rainfall types. A number of conclusions may be drawn from the figure subjected to the assumption made on the spatial rainfall distribution: 1) unlike MDS, MDR is not constant for a given radar. It increases as the radar range or/and intervening rainfall increases; 2) for different rainfall types, the variabilities of MDR are different; Therefore, 3) the feasibility for compensation of the attenuation in X-band radar measurements are dependent on the three factors: radar range, intervening rainfall and rainfall type; 4) assuming R_a is equal to 0.15 mm/h (i.e Z_a is about 10~15 dB under Marshall-Palmer condition, Note, Z_a may be close but not equal to MDS) then the MDR at a radar range can be calculated as 0.15 times the MDRF of that range. If the product is less than the intervening rainfall intensity R_i then everywhere within the range is detectable. For example, within a convective rainfall field (i.e. b=1.37, Jones, 1956) of 36 mm/h, the MDRF at the 20km range is approximately 200. Thus,

the MDR at the range is equal to 0.15×200=30 mm/h, which is less than the intervening rainfall. Therefore, the rainfall is detectable at anywhere within the 20km range.

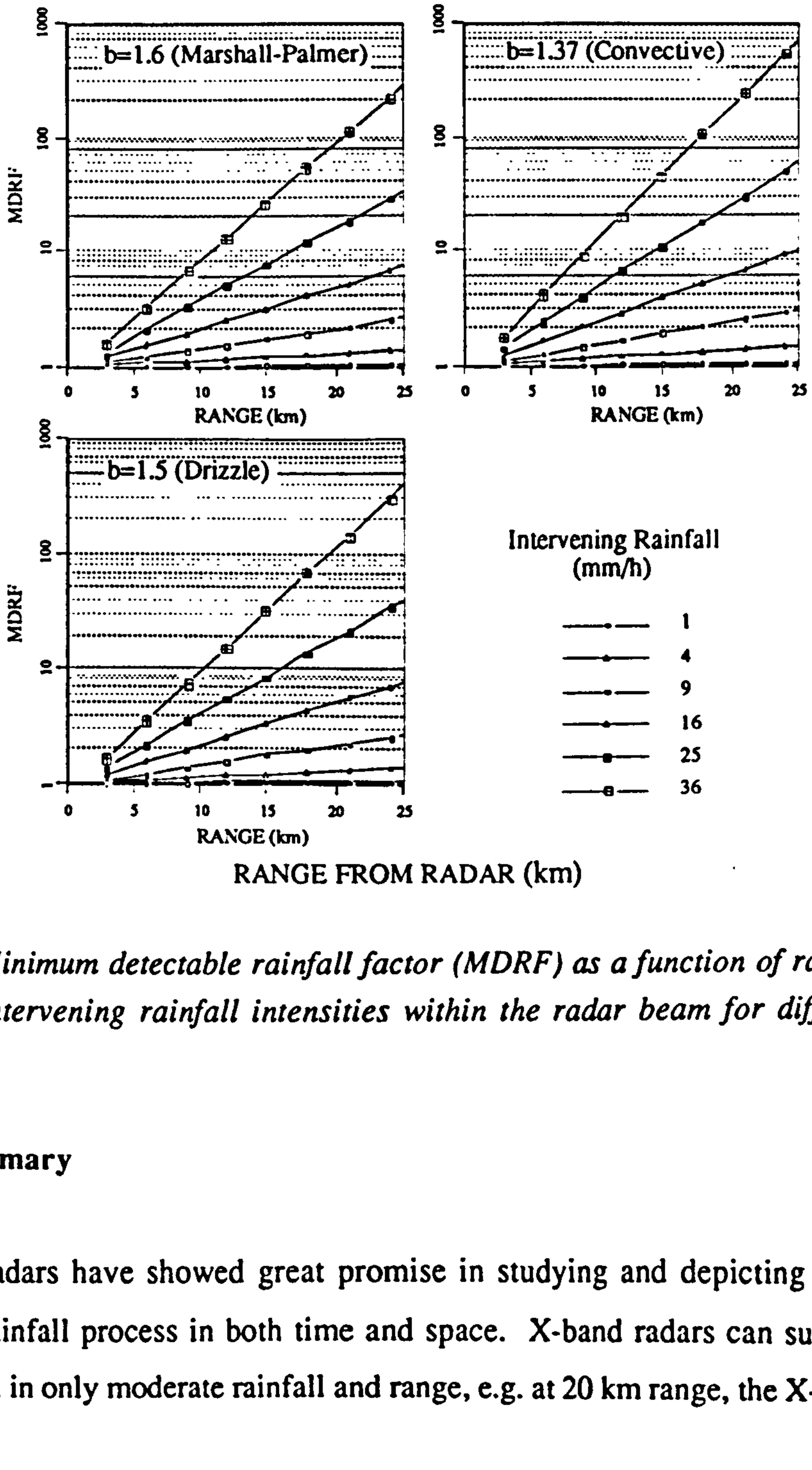

Fig.2.9 Minimum detectable rainfall factor (MDRF) as a function of radar range and the intervening rainfall intensities within the radar beam for different Z-R relations

2.6 Summary

Weather radars have showed great promise in studying and depicting the highly variable rainfall process in both time and space. X-band radars can suffer severe attenuation in only moderate rainfall and range, e.g. at 20 km range, the X-band radar

measurements can be 30 times less than that from a 'co-located' C-band radar within a uniformly distributed rainfall field of 36 mm/h. However, the minimum detectable rainfall threshold is a function of radar range, intervening rainfall intensity, rainfall type and the radar constant. Providing that the target rainfall intensity at a range is not below the MDR of an X-band radar at that range then it is able to be detected by the radar, and the measurements obtained may be adjusted to a comparable accuracy level as that would have been achieved by a 'co-located' C-band radar. This is of course assuming that the attenuation was identifiable through references to some ground truth!

Noticing the fact that the detectable target rainfalls are only a small proportion of the intervening rainfall intensities which are distributed evenly within a range of 20 km, a general conclusion may be drawn that X-band radars may be applicable within a range of 15-20 km unless the distribution of the rainfall field is considerably uneven or the target rainfalls are significantly less intense than the intervening rainfall. However, the choice of wavelength is clearly a compromise significantly influenced by cost. The general robust estimation of rainfall in real-time is preferable by utilising 5-cm (C-band) radars or above for operational purposes.

Hameldon Hill radar produces quantitative precipitation estimates operationally in real-time, which may be used to improve the UDS management in the Northwest region of England. However, due to the large sources of error present in the data, a number of aspects in relation to the quantitative application of the rainfall information in the urban hydrological context needs to be investigated and the following work targets those aspects considered to be priority items.

CHAPTER 3

RADAR RAINFALL DATA RESOLUTION

Radar rainfall data are sampled discrete series in time and averaged discrete series in space. Granger and Newbold (1977) defined the sampled series as instantaneously recorded series. Since discrete series can also be obtained by averaging a number of data points over a larger time or space interval, therefore, in broad terms, data resolution is a general designation of the sampling and averaging intervals. Without confusion, data resolution may be referred to by the corresponding sampling or averaging interval, for instance, 5-minute resolution, 2-km resolution and so on.

If a data series is obtained by sampling, then it is called sampled discrete series otherwise, if it is obtained by averaging a number of data points or the accumulation over a time interval then it is called averaged discrete series. The averaged series tends to be smoother than the sampled series of the same resolution. Temporal and spatial resolutions are important factors which determine the accuracy of quantitative radar rainfall data. This chapter attempts to highlight the resolutions that are suitable for urban hydrological applications.

3.1 Data Acquisition

The rainfall data used in this analysis were observed by the Hameldon Hill radar. Three storms occurring on 23 May, 18 August and 1 September in 1988 over the

Bolton catchment were used in the following analysis. The storms are described in Table 3.1 and the basic resolution of the data is 5 minutes in time and 2 km in space. From these resolutions coarser resolutions can be derived.

Table 3.1 Three analysed storms

DATE	RAINFALL TYPE	DURATION (Min.)	ACCUMULATED DEPTH (mm)
23 May, 88	Frontal	600	7.3
18 Aug., 88	Frontal	800	16.2
01 Sep., 88	Frontal	560	2.6

It was a Monday on 23rd May. During the night much of the UK stayed clear. However, in the morning the skies above the British Isles were dominated by a low pressure system slowly moving towards the east. Over Northwestern England, Wales and Northern Ireland there was a lot of cloud which turned into rainfall in the afternoon and evening. There was some heavy rain. The accumulated rainfall depth measured by the Hameldon Hill radar was 7.3 mm over the Bolton catchment.

On 18th August, Northwestern England, Wales and Northern Ireland had a mostly cloudy night with some outbreaks of rain. Lengthy and heavy spells of rain moved Northeast during the night. The accumulated rainfall depth over the catchment was 16.2 mm

Rain already across Southern England and Northern Ireland by the day of 1st September and extended Northeastwards over night to reach the central lowlands of Scotland by dawn. The rain was accompanied by a gale force Southeasterly wind. The accumulated rainfall was 2.6 mm on average over the catchment.

The Bolton catchment and the telemetered raingauge network within the catchment are

shown in Figure 3.1 and the catchment location is indicated by the shaded square at the bottom left-hand corner, which is about 20 km to the South West of the radar.

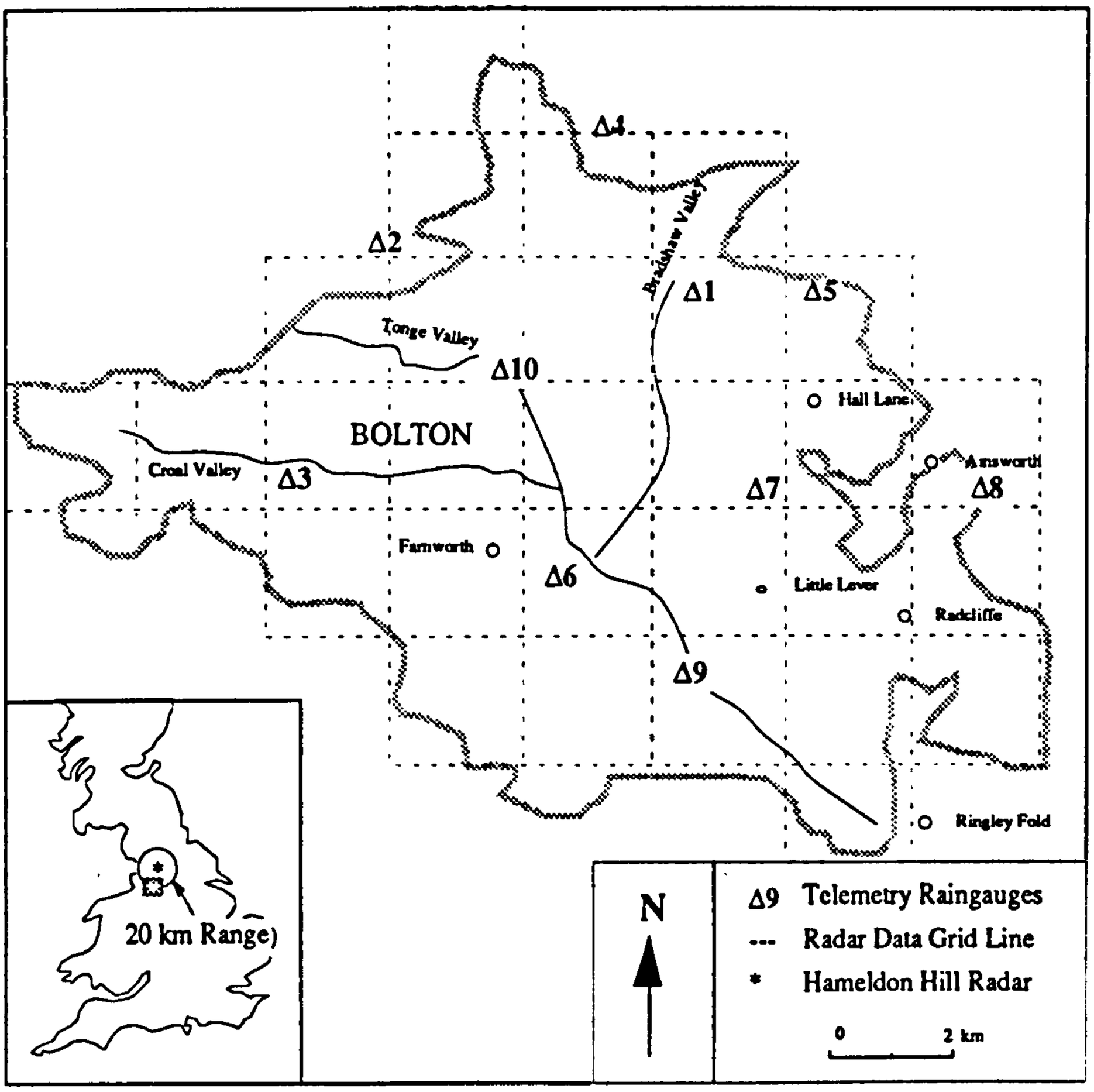

Fig. 3.1 Location of the Bolton catchment and Hameldon Hill radar

3.2 Temporal Resolution

Radar rainfall data are discrete time-space series. Each data point in the series is obtained at equal time intervals, which consists of analogue signals representing the strength of the return (i.e. reflectivity). This process is called data sampling. Sampling is a major data discretising approach, and therefore deserves a more detailed description.

3.2.1 Temporal Data Sampling

In sampling a continuous time series, the main question is how to choose a proper sampling interval ψ. Theoretically, radar signals can be sampled at any temporal resolution. However, it is expensive and unnecessary to make the sampling interval very small providing that the information content contributed by the various data frequencies being higher than the Nyquist frequency is zero or negligible.

Consider the following example. Suppose that rainfall readings were taken every day at noon (i.e. sampling interval is 1 day). It is clear that these observations would tell little about the rainfall variations within a day. In order to get information about variations within a day, we must use a shorter sampling interval and make more observations per day. The inverse of ψ is called sampling frequency. Generally, if a sampling interval has been chosen then after sampling, all the variances in the continuous series contributed by the frequencies higher than $1/(2\psi)$ cycles per unit time will be lost, in other words, the highest frequency embedded in the discrete data series is $1/(2\psi)$ cycles per unit time or π/ψ radians per unit time. This frequency is called the Nyquist frequency (ω_N). Note the Nyquist frequency is two times slower than the sampling frequency. For instance, in the given example, the sampling frequency is 1 cycle/day whereas the ω_N is equal to 1/2 cycle/day or 1 cycle per two days. If viewed from the angle of sampling interval rather than frequency, because no data variations can be recognised within the sampling interval, all variations with a period being less than or equal to the sampling interval are lost after sampling. However, if the power contributed by the frequencies higher than ω_N is negligible then the sampled series can be treated as being no different to the continuous series regardless of how large the sampling interval ψ is.

Providing that the frequency ω_N is known or can be estimated then the determination

of ψ is quite straightforward according to the definition of ω_N. However, if there is no advance knowledge about the maximum frequency available then spectral analysis has to be conducted on the tentatively sampled data.

For a continuous rainfall process R(t), the power spectral density function $f(\omega)$, which is also called power, is defined for all of the positive frequencies, ω as (Chatfield, 1984):

$$f(\omega) = 2/\pi \int \gamma(t)\, e^{-i\,\omega\, t}\, dt \qquad (0 < t < \infty) \tag{3.1}$$

Where $\gamma(t) = \int f(\omega)\cos(\omega t)d\omega$ $(0 < \omega < \infty)$, is the autocovariance function of R(t).

The spectral density function, $f(\omega)$ varies with the frequency ω, and indicates how the power is distributed in respect to frequency, or the information strength contributed by each frequency

It is difficult to directly estimate $f(\omega)$ from Eq.(3.1). A common practice is to estimate $f(\omega)$ from its smoothed discrete expression (Koopmans, 1974):

$$f(\omega) = \frac{\Psi}{\pi}\left\{C_0 + 2\sum_{k=1}^{M-1} W_k C_k \cos(\omega k)\right\} \tag{3.2}$$

for each frequency:

$$\omega = \frac{\pi i}{\psi M} \quad \text{for } i = 0, 1, 2, \cdots, M \tag{3.3}$$

and

$$C_k = \frac{1}{N}\sum_{t=1}^{N-k}[R(t)R(t+k)] \tag{3.4}$$

Where $f(\omega)$ is the power spectral density function;

ω is the frequency (radians per unit time);

W_k is a set of weights called the lag window;

M is called the truncation point (< the number of sampled data N);

C_k is the autocovariance coefficients of the process and

N is the data number of R(t).

There is no general rule for choosing a truncation point, M. In this analysis, M was chosen as $2N^{1/2}$ (Chatfield, 1984).

The Parzen window (Chatfield, 1984):

$$W_k = \begin{cases} 1-6\left(\frac{k}{M}\right)^2+6\left(\frac{k}{M}\right)^3 & 0 \le \frac{k}{M} \le \frac{1}{2} \\ 2\left(1-\frac{k}{M}\right)^3 & \frac{1}{2} \le \frac{k}{M} \le 1 \end{cases} \tag{3.5}$$

was used to calculate the smoothing weights. A plot of $f(\omega)$ versus frequency ω is called the power spectrum. If the resulting estimate of $f(\omega)$ approaches zero at a point between zero and the Nyquist frequency, then the sampling interval is almost certainly small enough nevertheless a larger sampling interval may be also feasible. Otherwise, a smaller interval should be tried. To illustrate the frequency content of the radar rainfall data, Figure 3.2, Figure 3.3 and Figure 3.4 show the time series rainfalls sampled at different frequencies (i.e. 12, 6, 4, 2 cycles/hour) and the spectrums of the data sampled at the frequency of 12 cycles/hour of the three events (Table 3.1).

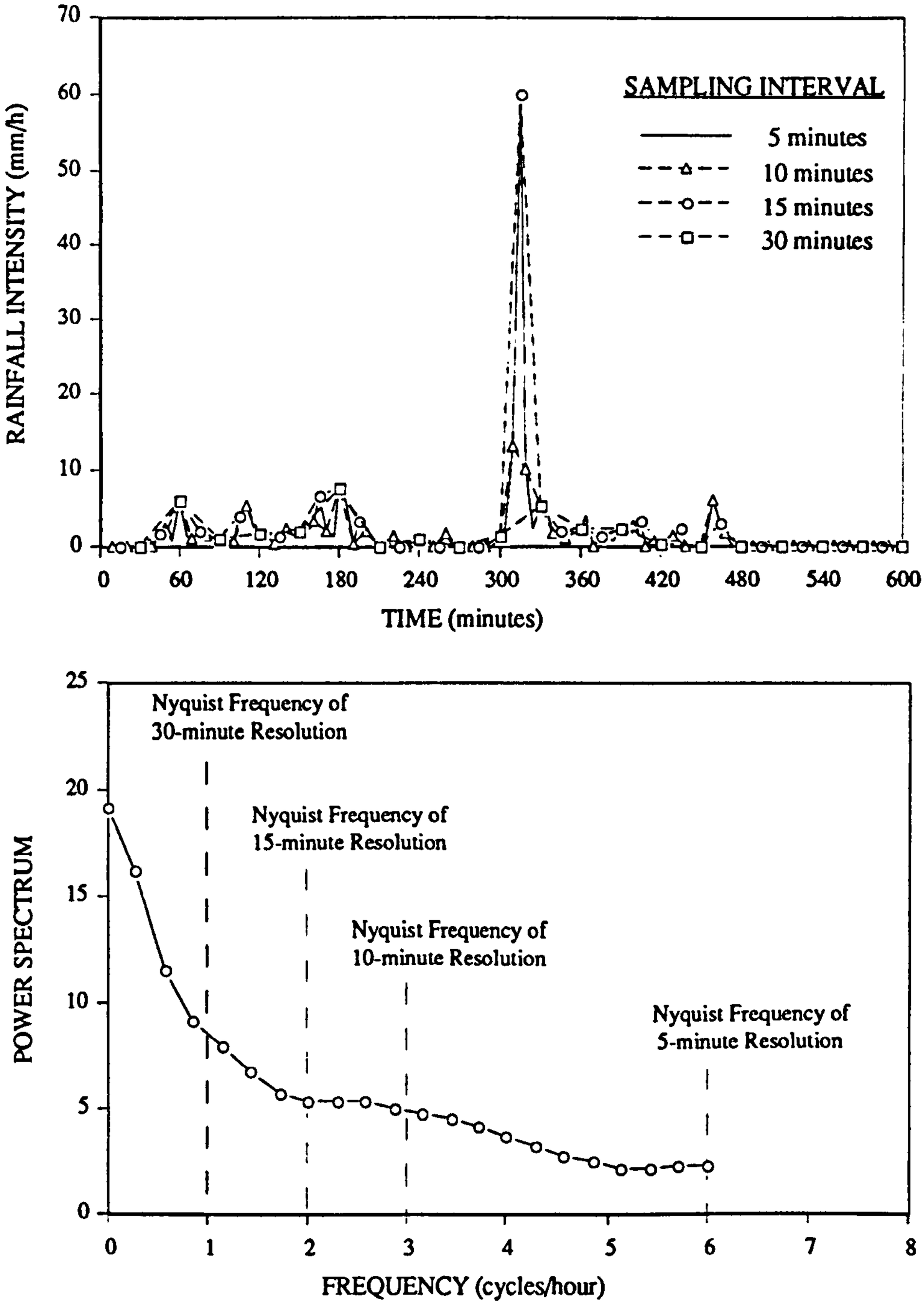

Fig. 3.2 Time series rainfalls sampled at different time intervals and the Power Spectrum of the 5-minute data for storm on 23/05/88

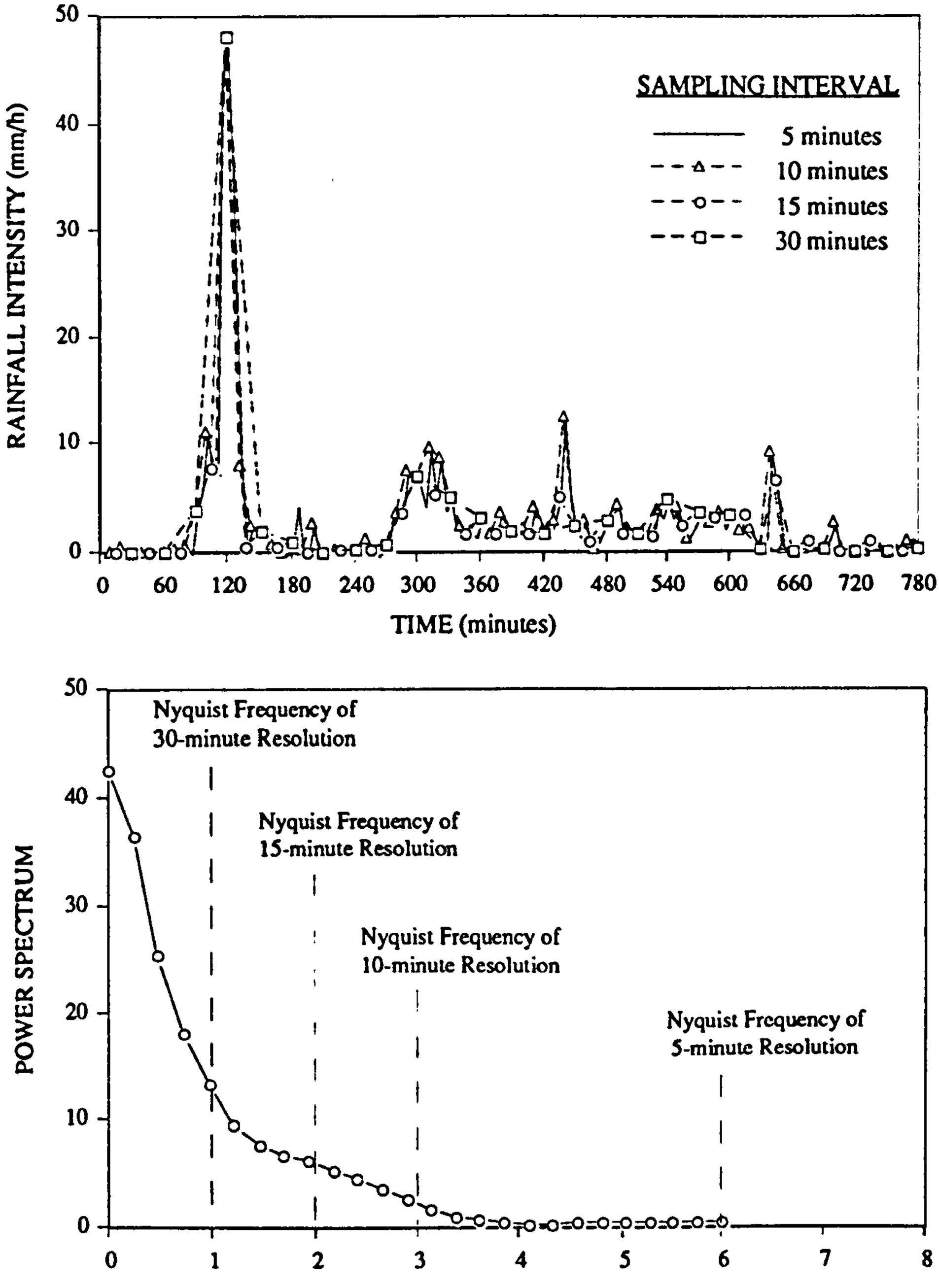

Fig. 3.3 Time series rainfalls sampled at different time intervals and the Power Spectrum of of the 5-minute data for storm on 18/08/88

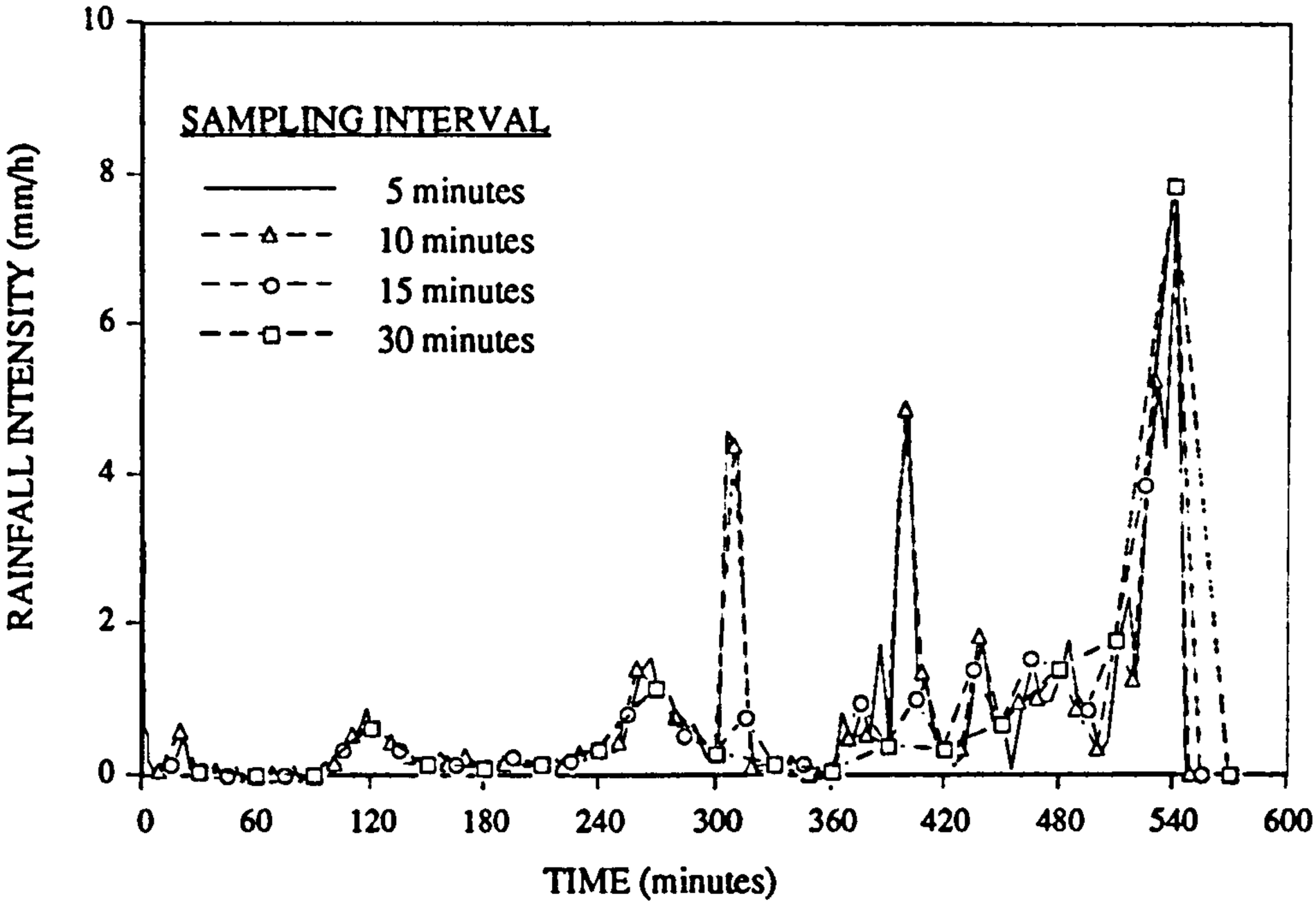

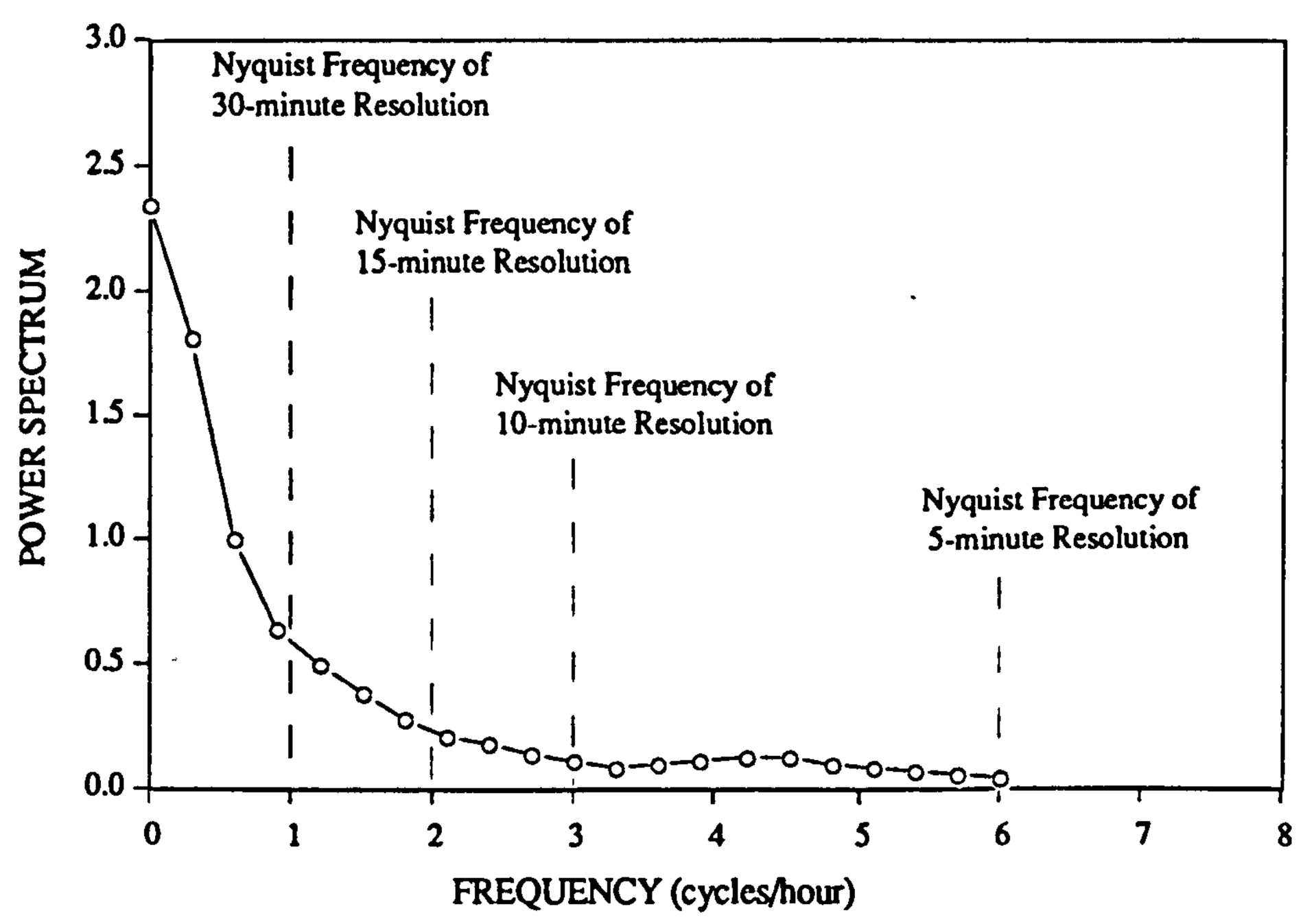

Fig. 3.4 Time series rainfalls sampled at different time intervals and the Power Spectrum of of the 5-minute data for storm on 01/09/88

In the figures, frequency values were shown in cycles/hour. All the powers contributed by the frequencies higher than the Nyquist frequency were lost. For example, in Figure 3.4, the power contributed by the frequency, 1 cycle/hour, is about 0.6. The powers (i.e. < 0.6) contributed by the frequencies higher than 1 cycle/hour and lower than 6 cycles/hour are not negligible, therefore in the data with a 30-minute resolution some information content has been lost comparing with that in the data with a 5-minute resolution or a sampling frequency of 12 cycles/hour.

It can be recognised from the figures that: (1) the loss of frequency increases as the data resolution decreases in general. However, the increment is highly variable among the different events and different data resolutions. For instance, for event 01/09/88, even using a 10-minute sampling interval will not cause significant loss of information when compared with the 5-minute resolution. This is because the power values at the Nyquist frequencies for the two sampling intervals are almost the same, see Figure 3.4. If observing the hyetographs it becomes more apparent that the 10-minute data has captured almost all of the major peaks within the 5-minutes data series. (2) Only a small proportion of the frequencies were lost in the data sampled at 5-minute time interval.

The results revealed that 5-minute sampling interval is generally satisfactory. However, the feasibility of a sampling interval is dependent on the rainfall intensity variability during an event and should be a matter subjected to the actual application objectives. Due to the 'low pass' filtering effects of the hydrological systems on the rainfall variations (Cluckie, 1987), a lower resolution than 5 minutes is likely applicable, especially when the reduction of data resolution is undertaken by averaging the data points over a longer duration rather than by re-sampling at a larger time interval. This will be proved by the following analysis.

3.2.2 Potential Impacts on UDS Simulations

The minimum sampling or averaging interval determines the highest data resolution and hence determines the maximum information content of the data, however, the higher data resolution, the higher costs due to the additional data processing and archiving. Therefore, an investigation of the sensitivity of UDS simulation accuracy to the temporal resolution is necessary in order to examine the possibility of using a lower resolution whilst maintaining an acceptable accuracy.

The investigation was carried out by comparing the hydrographs simulated using the rainfall data at different resolutions. To obtain the hydrographs, Bolton drainage system was used. The major branches of the drainage system are sketched in Figure 3.5

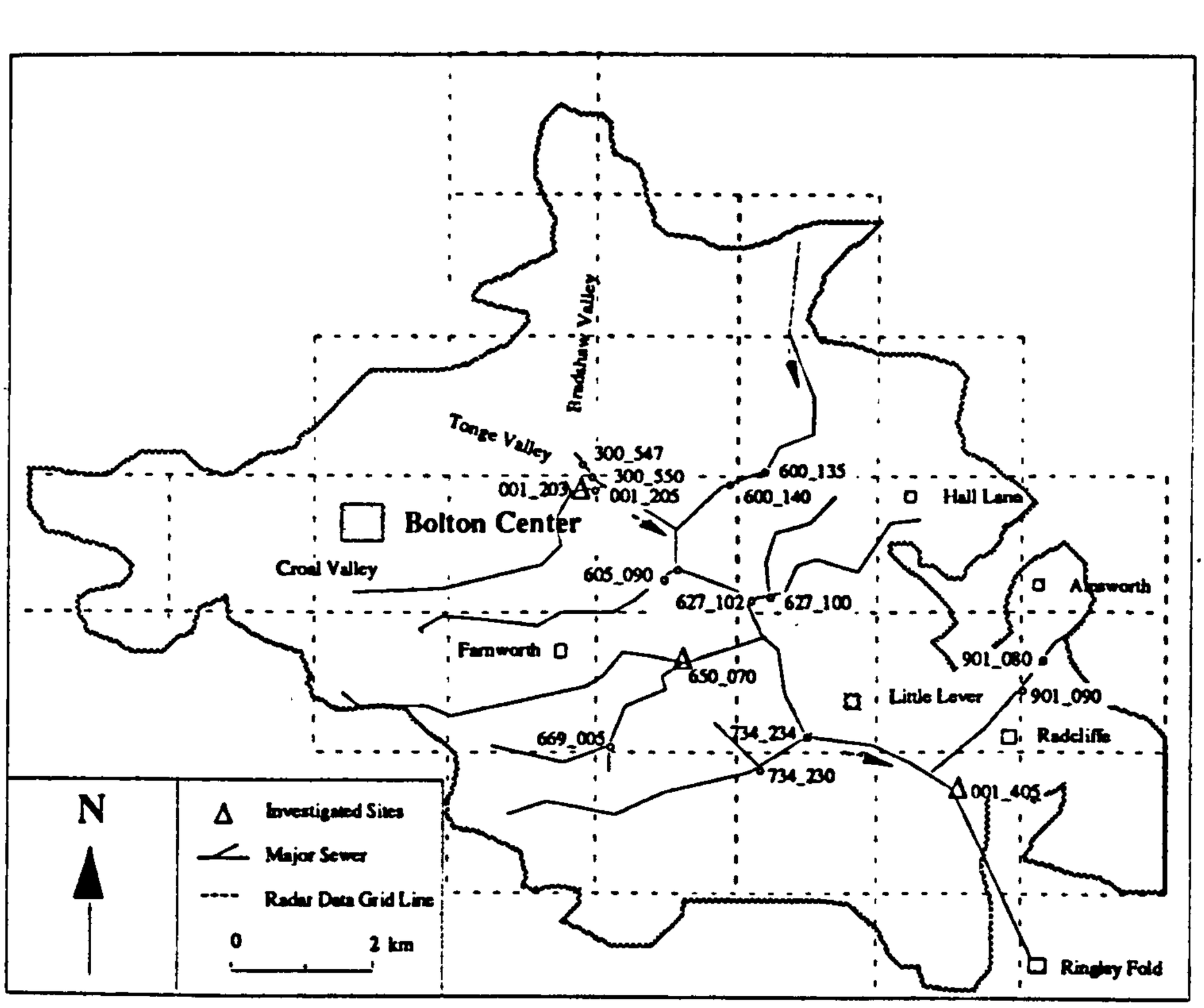

Fig. 3.5 Sketch of the Bolton drainage system showing the major sewers

The catchment is approximately 120 km^2 in size. It encompasses the North and East of the Bolton centre and includes three river valleys: Croal, Tonge and Bradshaw. The area is predominantly residential with associated schools, shopping and commercial development. Several light industry sites are also located within the catchment which is essentially drained by a combined sewer system to Ringley Fold where a treatment works is located.

As it is impractical and unnecessary to check the impacts of temporal data resolution on the hydrograph simulations for every pipe, three key locations were investigated: 001_203, located at the upstream of the trunk sewer, 001_405, downstream of the trunk sewer with a significant storage capacity attached and 650_070, the outlet of a small subsystem.. At each of the three locations, 9 hydrographs were produced using WASSP and the three events given in Table 3.1 for three temporal resolutions (i.e. 5 minutes, 10 minutes and 15 minutes). The 10-minute and 15-minute resolutions were derived by averaging the 5-minute data (with a 2km spatial resolution) over every 10 minutes and 15 minutes respectively.

A simple index called assessment ratio (AR) is adopted to compare two hydrographs, which is defined as the ratio of the two hydrographs at each time point. For example, the AR for comparing the hydrograph yielded from the rainfall of 10-minute resolution (F10) with that from rainfall of 5-minute resolution (F5) is calculated as: AR=F10/F5 for each time point. In cases of F5 is equal to zero, such points were not considered, in other words, only those points having non-zero values were compared. This analysis intended to find out how AR varies 1) with time and pipe location during an event; 2) with event at a pipe location. The results are shown in the figures from Figure 3.6 to Figure 3.8, where the AR values are plotted against time. Each figure shows the comparisons made for one pipe location.

From the figures it is seen that, 1) with the reduction of temporal resolution, the spreading of AR values appeared to be wider and wider; 2) during an event, the AR

values varied with time and the variation is subjected to pipe locations. At pipe location 001_203 (upstream of the trunk sewer), the variation of AR for the event 23/05/88 is between 0.95 to 1.15%, for the event 18/08/88, 0.93 to 1.17 and for the event 01/09/88, 0.97 to 1.03. At pipe location 001_405 (downstream of the trunk sewer), the variation range was reduced about 10% for all of the events. However, at the pipe location 650_070 (the outlet of a small subsystem), significantly larger AR values were clearly recognised.

Recall the results shown in Figure 3.2, Figure 3.3 and Figure 3.4. It is easy to show that the frequency components of an event are dominant factors that determine the magnitude of the AR values throughout the event for a given pipe location. However, the attenuation capability of the drainage system due to storage is also a major factor. These two factors act on the simulation errors in a contradictory way. In general, a reduction in data resolution will result in a loss of the higher frequencies and potentially evoke higher simulation errors whereas the attenuation effect of the drainage system will effectively suppress the error magnitudes. This is the reason that the simulation outcomes shown in the left column of each figure were very close in terms of operational applications. The results suggested that it is feasible to use a lower temporal resolution than 5 minutes providing that a UDS has sufficient attenuation capability or the storm to be used contains no high frequency components. A rule will be given in chapter 8, which attempts to clarify the strategy to adopt in choosing a suitable sampling interval on basis of the UDS's pulse-response characteristics.

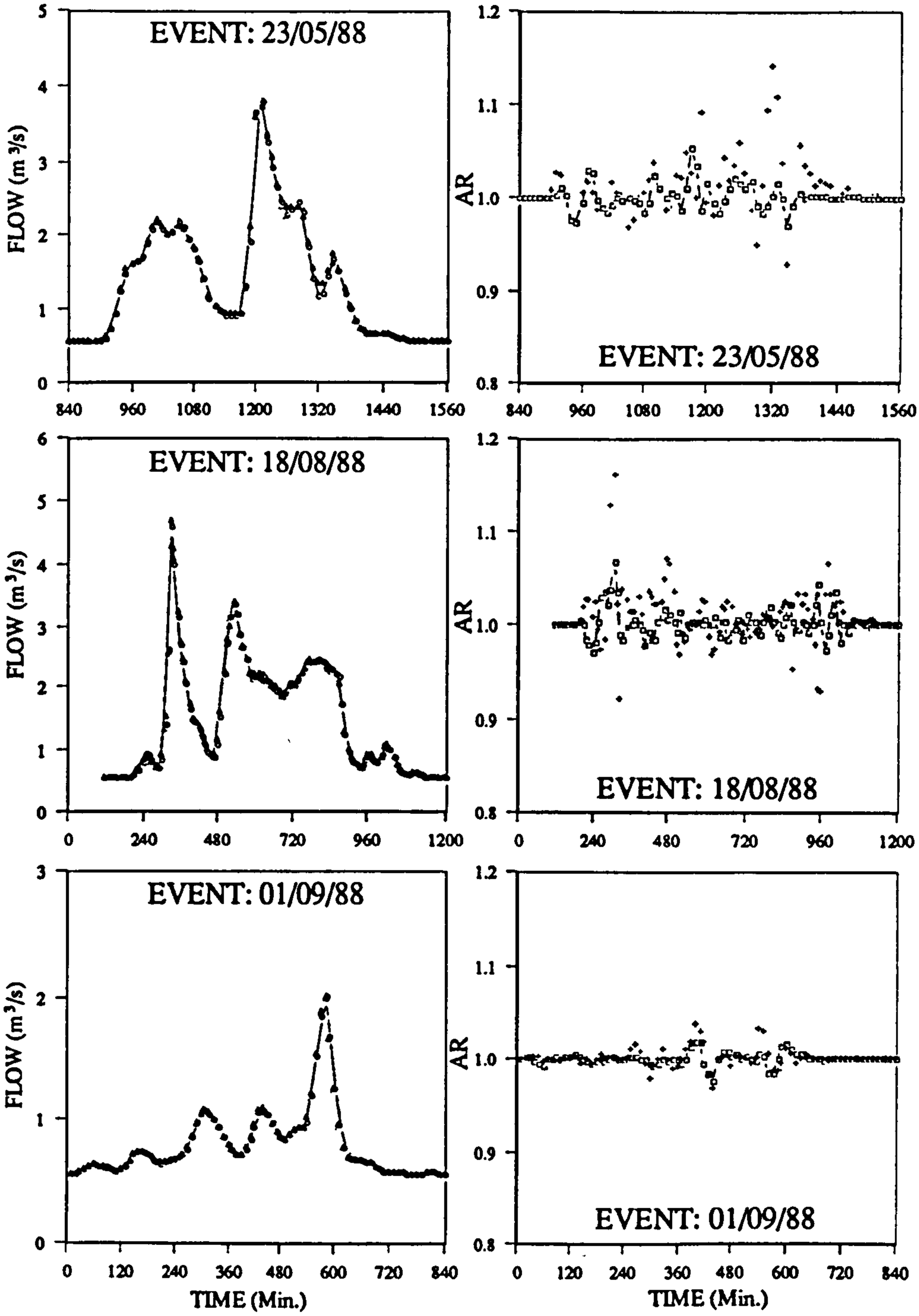

Fig. 3.6 Comparisons of the continuation flow hydrographs at pipe location 001_203

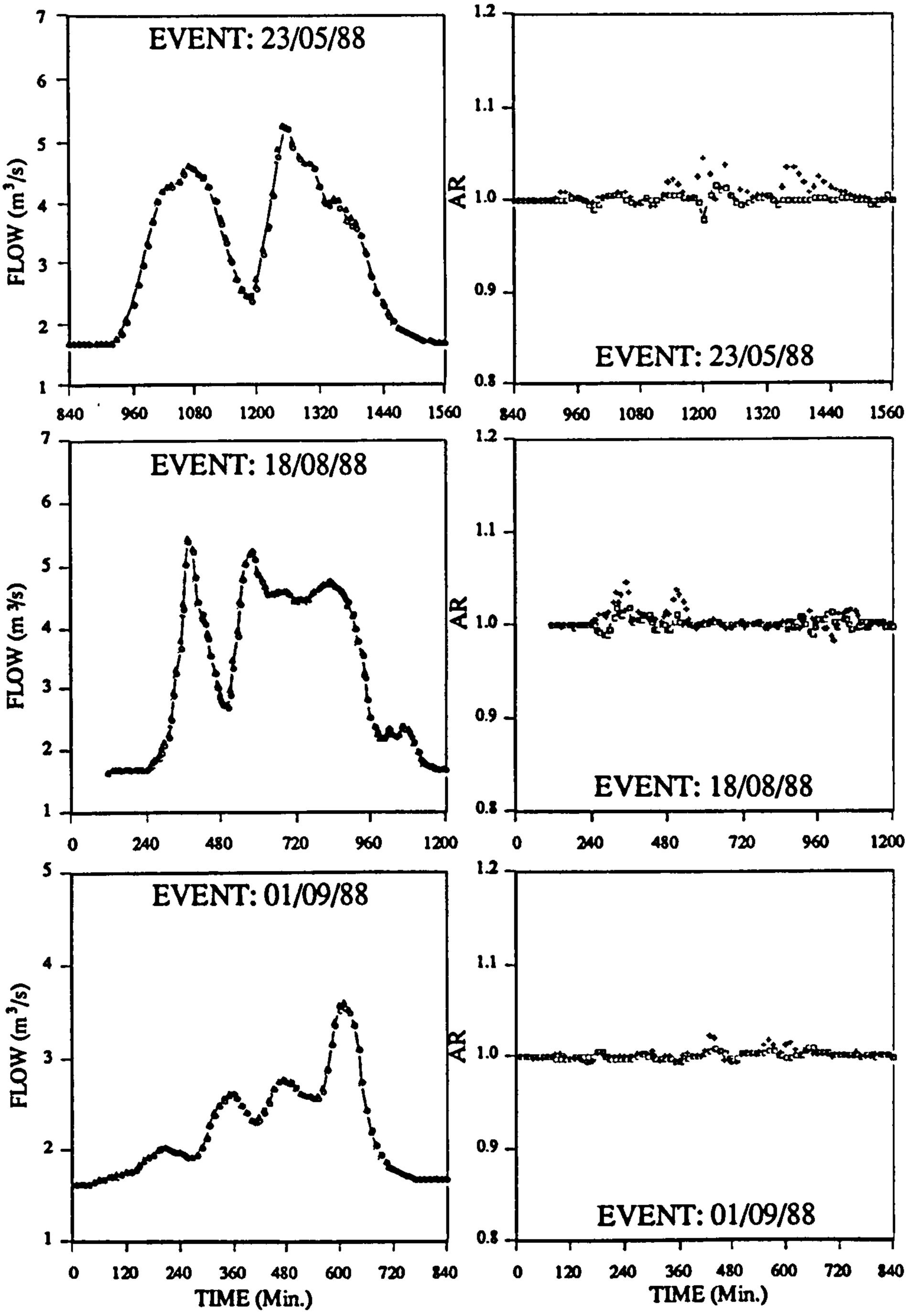

Fig. 3.7 Comparisons of the continuation flow hydrographs at pipe location 001_405

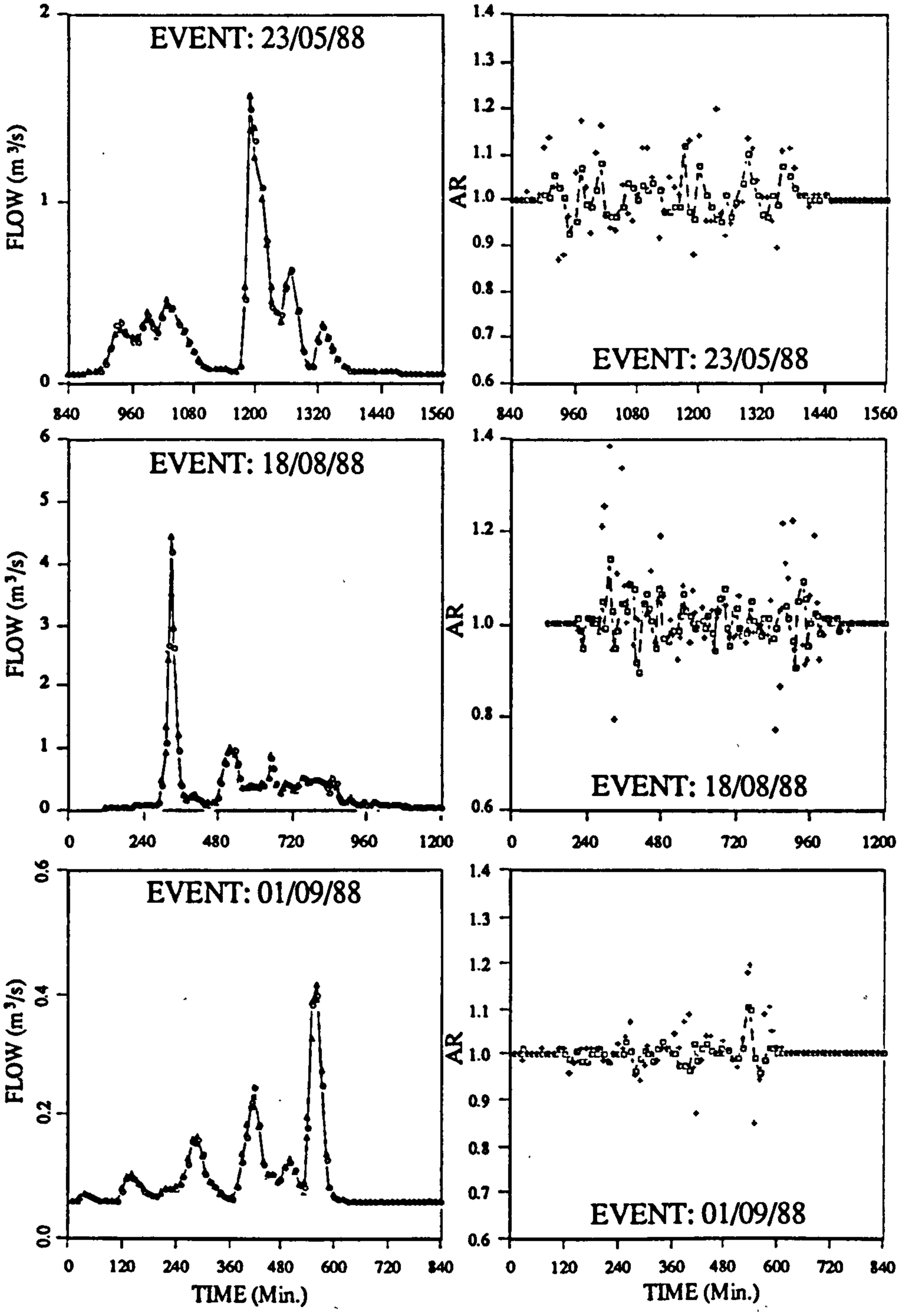

Fig. 3.8 Comparisons of the continuation52 flow hydrographs at pipe location 650_070

3.3 Spatial Resolution

Spatial resolution is also an important issue, which determines the accuracy of radar rainfall data. Similar to the previous analysis on the radar rainfall temporal resolution, the potential impacts of spatial resolution on UDS simulation accuracy is investigated in this section.

3.3.1 Spatial Data Discretising

The initial radar signals are scanned and received continuously in space. The PPI data are discretised by averaging the surface rainfalls over every grid defined by the polar coordinate system. The discrete data are in turn converted into the Cartesian coordinates. Therefore, the spatial data resolution is defined as the side length of the square grid of the Cartesian system. Two spatial data resolutions are available in the U.K. The 2-km data covers a range up to 76km and the 5-km data extends to a further range of 210 km. These two types of data are used in the following analysis.

3.3.2 Potential Impacts on UDS Simulations

The rainfall data used in this analysis were obtained from the same events as shown in Table 3.1. To demonstrate the impacts of spatial data resolution on the urban drainage system simulation, lumped rainfall data were also used in addition to the 2-km and 5-km data. The lumped data were derived by averaging the 2-km data.

WASSP model was again used to generate the simulated hydrographs for the three pipe locations in the Bolton UDS as indicated in Figure 3.5. The simulated hydrographs were shown in Figure 3.9, Figure 3.10 and Figure 3.11, which indicate that the spatial resolution had a significant impact on the accuracy of the simulations.

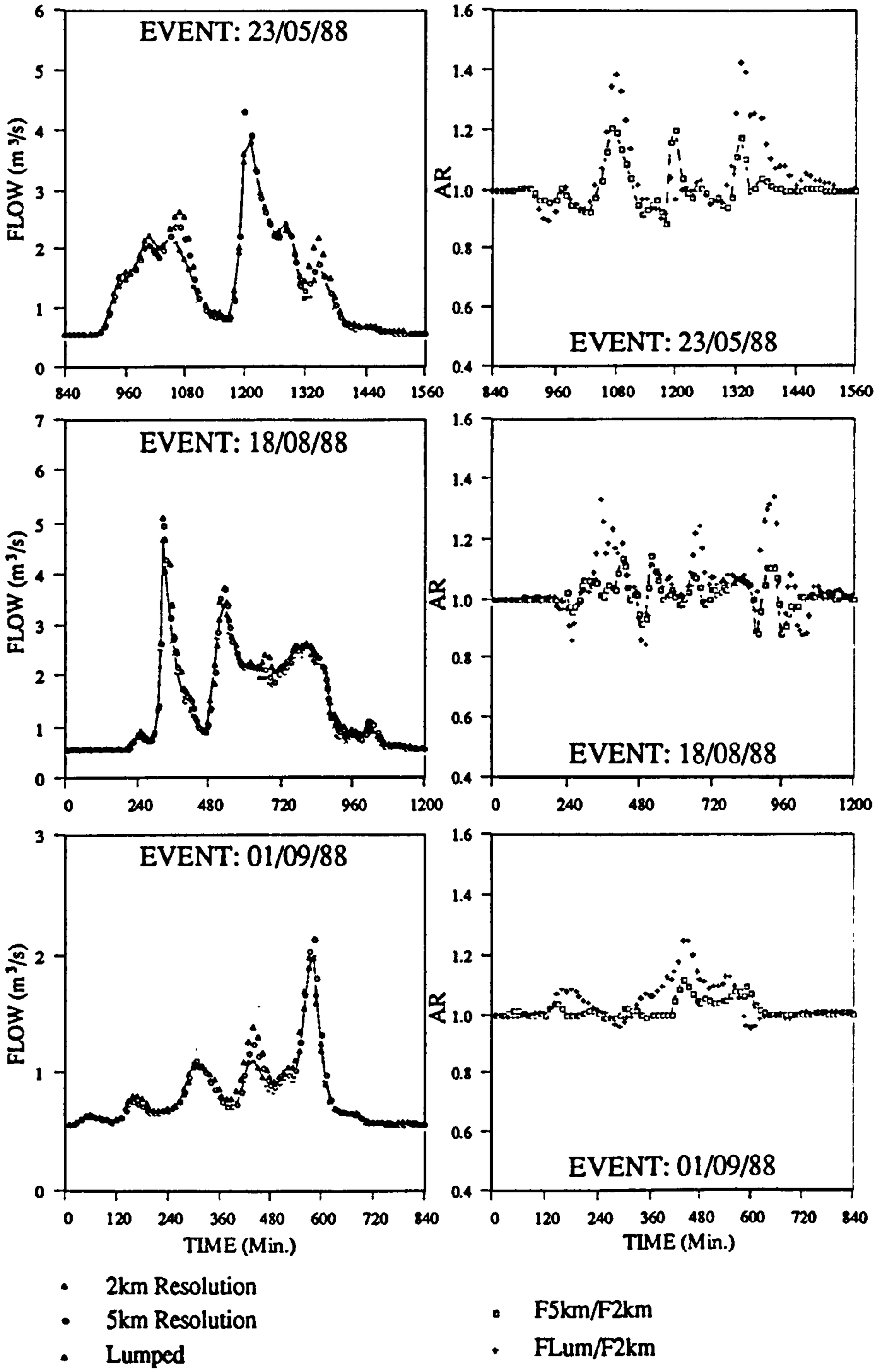

Fig. 3.9 Comparisons of the continuation flow hydrographs at pipe location 001_203

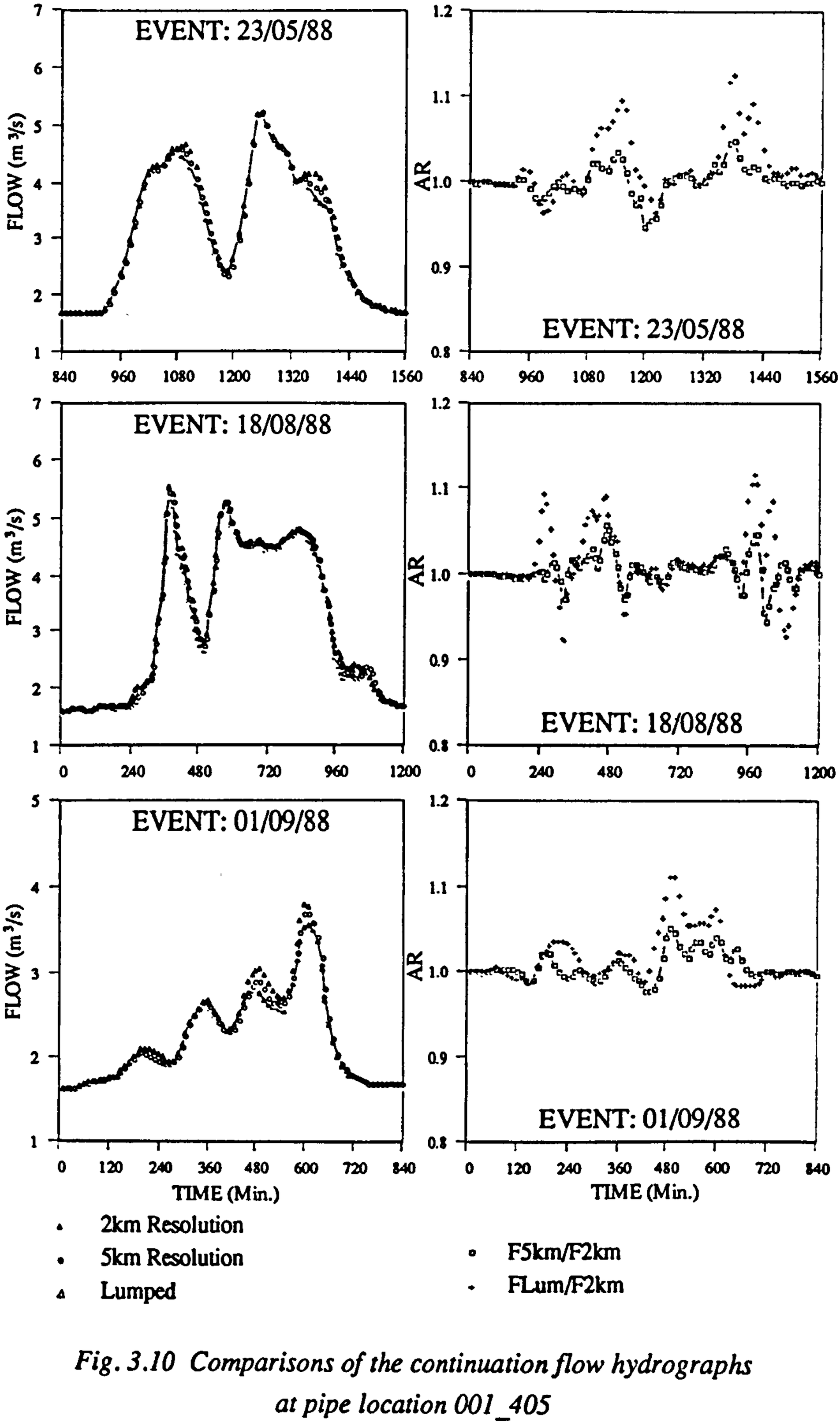

Fig. 3.10 Comparisons of the continuation flow hydrographs at pipe location 001_405

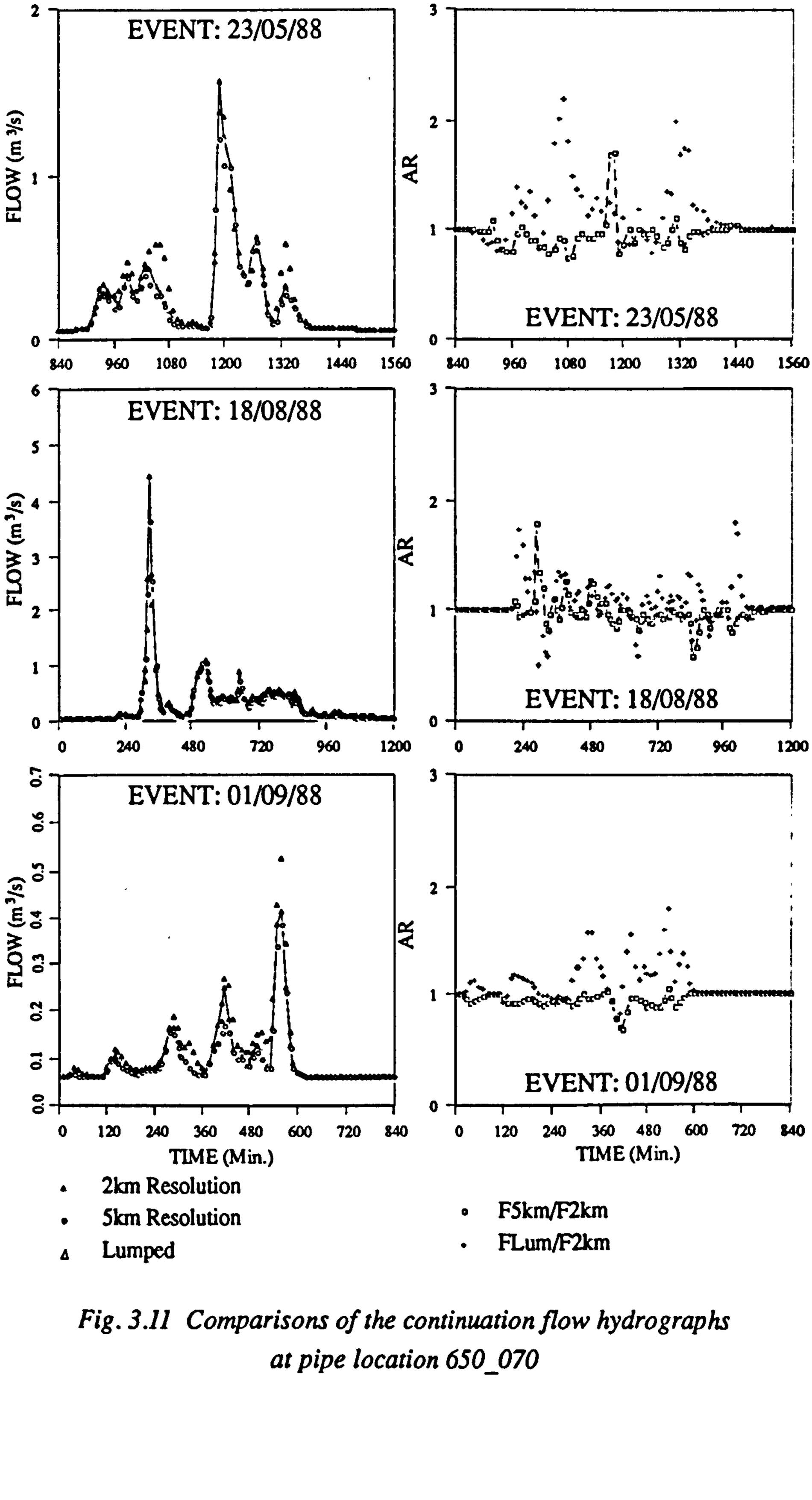

Fig. 3.11 Comparisons of the continuation flow hydrographs at pipe location 650_070

At pipe location 001_203 (upstream of the trunk sewer) the variation of AR for the event 23/05/88 is between 0.95 to 1.42%, for the event 18/08/88, 0.90 to 1.38 and for the event 01/09/88, 0.97 to 1.25. At pipe location 001_405 (downstream of the trunk sewer), the variation range was reduced about 15% for all of the events, however, at the pipe location 560_070 (the outlet of a small subsystem), increased about 20%. Therefore, a similar conclusion to the temporal resolution issue can be drawn from the results. That is, the impacts of spatial resolution is dependent on the storm characteristics and the pipe locations and the simulation errors increased with the reduction of spatial data resolution.

3.4 Summary

Radar rainfall data are discrete series in both time and space. The impacts of data resolution on the urban drainage system simulation accuracy are determined by the storm and system characteristics. A reduction in data resolution will result in a removal of the higher frequency components contained in the rainfall data and potentially evoke higher simulation errors whereas the attenuation effect of the drainage system will result in a suppression of the error magnitudes.

Using a lower temporal resolution than 5 minutes (i.e 10 minutes, or 15 minutes) is feasible, at least for those systems having a similar response characteristics to the Bolton system. A more general rule on the determination of a temporal resolution suitable for use with a model will be derived in Chapter 8.

The use of a lower spatial resolution than 2-km (i.e. 5 km) is not recommended for distributed urban hydrological applications. With the development of very high resolution (i.e. 250m spatial and 2 minutes temporal) C-band hydrological radars, it will be possible to complete the study outlined in this thesis in relation to higher resolution data.

CHAPTER 4

DATA QUANTISATION

Data quantisation is the process whereby the magnitude of a sampled analogue signal is digitised into one of the prescribed quantisation levels. Unlike the temporal and spatial data discretising process, data quantisation always results in an irretrievable loss of information. This is called the quantisation noise or quantisation error. It is impossible to restore the original analogue signal from its quantised version. However, as radar rainfall data is processed by digital computer, quantisation is inevitable for the practical application of the data in their discrete form.

Various quantisation schemes have been available, which can be broadly classified into three categories: linear, nonlinear and adaptive (see Cattermole, 1969, Schwarts, 1980 and Han, 1991). If a scheme can yield a smaller quantisation error than another scheme whilst using the same or even fewer quantisation levels, then the scheme is regarded as more efficient. The existing schemes used in the UK have been recognised as inefficient. Therefore, a better scheme is proposed in this chapter following a brief discussion on data quantisation theory.

4.1 The Principle of Data Quantisation

4.1.1 Analogue-to-Digital Conversion (ADC)

There is actually no need to transmit all possible data amplitudes because the receiving

systems (such as data displaying monitors, natural water courses or drainage systems) are not able to distinguish very fine variations in rainfall data amplitude. This ultimate limitation in identifying among all possible amplitudes thus makes data quantisation possible. The sampled analogue data may be quantised, or both sampled and quantised simultaneously, see Figure 4.1.

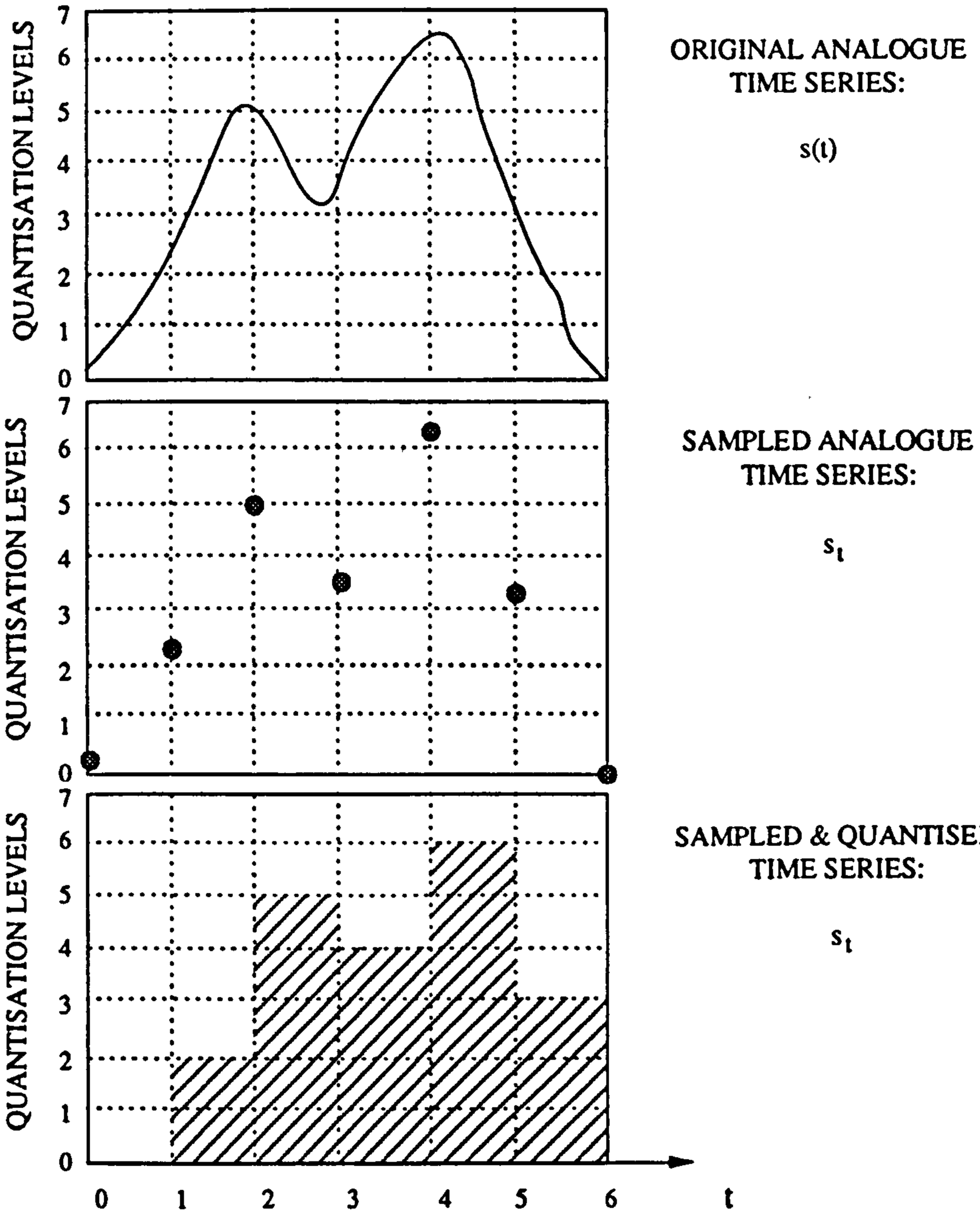

Fig. 4.1 Quantising process of an analogue time series

(Source from Schwarts, 1980)

In the figure, s(t) stands for an analogue continuous time series. The data were sampled at unit time intervals and in turn the sampled analogue signal was quantised or rounded to its nearest quantisation level. The maximum signal amplitude has been broken into 8 levels (i.e. 0, 1, 2, 3, 4, 5, 6, 7) which requires 3 binary digits (bits) to represent them, i.e. using codes: 000, 001, 010,011, 100, 101, 110 and 111. This implies that such a quantiser can only quantise signals up to 7.5 units if the increment between two adjacent levels (i.e. quantum) is 1.0 unit. Otherwise the quantisation will result in unpredictable error. Under this circumstance, the quantiser is said to be over-saturated.

Obviously, the quantising process introduces some error in the eventual reproduction of the signal. The demodulated data will differ somewhat from the original signal, as has been noticed in the figure. This quantisation noise of course can be reduced by increasing the number of quantisation levels. However, there is a tradeoff between the number of quantisation levels used and the transmission time, the more levels, the greater the number of binary digits required for coding and it therefore takes a longer time to be transmitted with a constant transmission speed. So, it is expected that an ideal quantisation scheme should use only a small number of quantisation levels whereas at the same time produce minimal noise.

The noise performance is usually quantified by a signal-to-noise ratio (SNR) which is defined as the ratio of mean signal power to the mean noise power:

$$SNR = \frac{\sigma_s^2}{E(\varepsilon^2)} \qquad (4.1)$$

Where σ_s^2 is the mean signal power or the mean of the squared signal magnitude;

$E(\varepsilon^2)$ is the mean quantisation noise power.

Although the level separation or quantum in Figure 4.1 is shown as uniform, it is often

tapered in practice in order to avoid over-saturation and reduce the system noise. In particular, the spacing of levels is decreased at low amplitude levels. This is called nonlinear quantisation which is done by a technique called data compression.

4.1.2 Nonlinear Data Quantisation

In the linear quantisation, a known maximum signal amplitude has been tacitly assumed and the quantisation levels were chosen to be equally spaced to cover the total signal amplitude. For rainfall data, however, the peak value may be unknown. Therefore, to cover the likely range of rainfall intensity, a nonlinear quantisation scheme has to be used, which can maintain a constant SNR over a wider dynamic range of rainfall intensities and consequently avoid penalising the lower rainfall intensities or encouraging over-saturation by the higher intensities.

A nonlinear quantisation scheme constitutes two steps: 1) uses a nonlinear compressor to compress the data and 2) represents the compressed data by the nearest quantisation level which is uniformly spaced. At the recipients the data are then expanded following an inverse procedure to the compression. This is equivalent to tapering the spacing of quantisation levels. The formula used for data compressing is called the compressor.

The μ-Law is an important compressor which is defined as:

$$\mu\text{-Law:} \qquad y(s) = \frac{\ln(1+\mu s)}{\ln(1+\mu)} \tag{4.2}$$

where s is the normalised signal amplitude to be compressed;

y(s) is the compressed version of signal s, and is linearly quantised and

μ is a parameter which governs the properties of the compressor.

It has a higher SNR value over a wider signal power range than the other alternative compressors, such as A-Law, Inverse Hyperbolic Sine (C-Law) and Hyperbolic (M-Law):

$$\text{A-Law:} \qquad y(s) = \begin{cases} \dfrac{1+\ln(As)}{1+\ln A} & \dfrac{1}{A} \le s \le 1 \\ \dfrac{As}{1+\ln A} & 0 \le s \le \dfrac{1}{A} \end{cases} \tag{4.3}$$

$$\text{C-Law:} \qquad y(s) = \frac{\text{Arsh}(cs)}{\text{Arsh}(c)} \tag{4.4}$$

$$\text{M-Law:} \qquad y(s) = \frac{(1+m)s}{1+ms} \tag{4.5}$$

Where A, c and m are positive parameters. Note that all the compressors have the characteristics that the signal s to be compressed is normalised (i.e. $0 \le s \le 1$). The μ-Law compressor was described in the paper by B. Smith (1957) and was regarded as the most important one in Cattermole (1969). The A-Law compressor was first published by Cattermole (1962). The C-Law compressor was proposed in 1963 by Kaneko and Sekimoto, and the M-Law compressor was derived by B. D. Smith (1953). Any of the compressors enables an extension of the signal range to be accomplished.

4.1.3 Existing Nonlinear Quantisation Schemes

The present rainfall quantisation schemes adopted by the UK Meteorological Office consist of two types: 3-bit (8 level) and 8-bit (208 levels), see Table 4.1 and Table 4.2. The three-bit scheme makes use of the whole 3 bits to represent the data and the 8-bit scheme uses 208 levels of the total 256 available levels (the remaining levels are utilised for data transmission purposes) and the rainfall intensities are represented by

integers held in float notation in which the two high order bits of a byte (i.e. 8 bits) are the exponent and the other 6 bits are the mantissa and the value is interpreted as 2 to the power of twice the exponent multiplied by the mantissa. This allows numbers up to 4032, [i.e. $2^{2\times3}\times(2^6-1)$] to be held in 8 bits. This data compressing scheme is equivalent to that utilising a logarithmic compressor, i.e. the A-Law. The 3-bit scheme was derived based on the 8-bit scheme.

Table 4.1 Existing 3-bit rainfall data quantisation (Source: Banks, 1984)

QUANTISING LEVEL	ORIGINAL (mm/h)			3 - BIT REPRESENTATION (mm/h)
1	0	⇒	0.125	0.00
2	0.125	⇒	1	0.56
3	1	⇒	4	2.50
4	4	⇒	8	6.00
5	8	⇒	16	12.00
6	16	⇒	32	24.00
7	32	⇒	126	79.00
8	126	⇒	∞	319.00

Table 4.2 Existing 8-bit rainfall data quantisation (Source: Banks, 1984)

SEGMENT No.	INTEGER: *n*	INCREAMENT OF *n*	Conversion of *n* to Rainfall (mm/h)	RAINFALL (mm/hr)
1	0 ⇒ 63	1	$\frac{n}{32}$	0.0 ⇒ 1.96875
2	64 ⇒ 252	4		2.0 ⇒ 7.87500
3	256 ⇒ 1008	16		8.0 ⇒ 31.50000
4	1024 ⇒ 4032	64		32.0 ⇒ 126.00000

While it may have certain advantages using the float notation, however, the logarithmic compressing with A-Law is not efficient in terms of preserving the information content of the signal and may be replaced by an alternative compressor.

4.2 A more Efficient Compressing Law

There are three basic problems associated with the data compression and nonlinear quantisation: (1) determination of a nonlinear compressor; (2) properties of the compressor and (3) the effect of compression on the data accuracy.

Let y = y(s) (s>0) be the desired compressor, and the normalised signal s and its compressed version y range between 0 and 1, as shown in Figure 4.2.

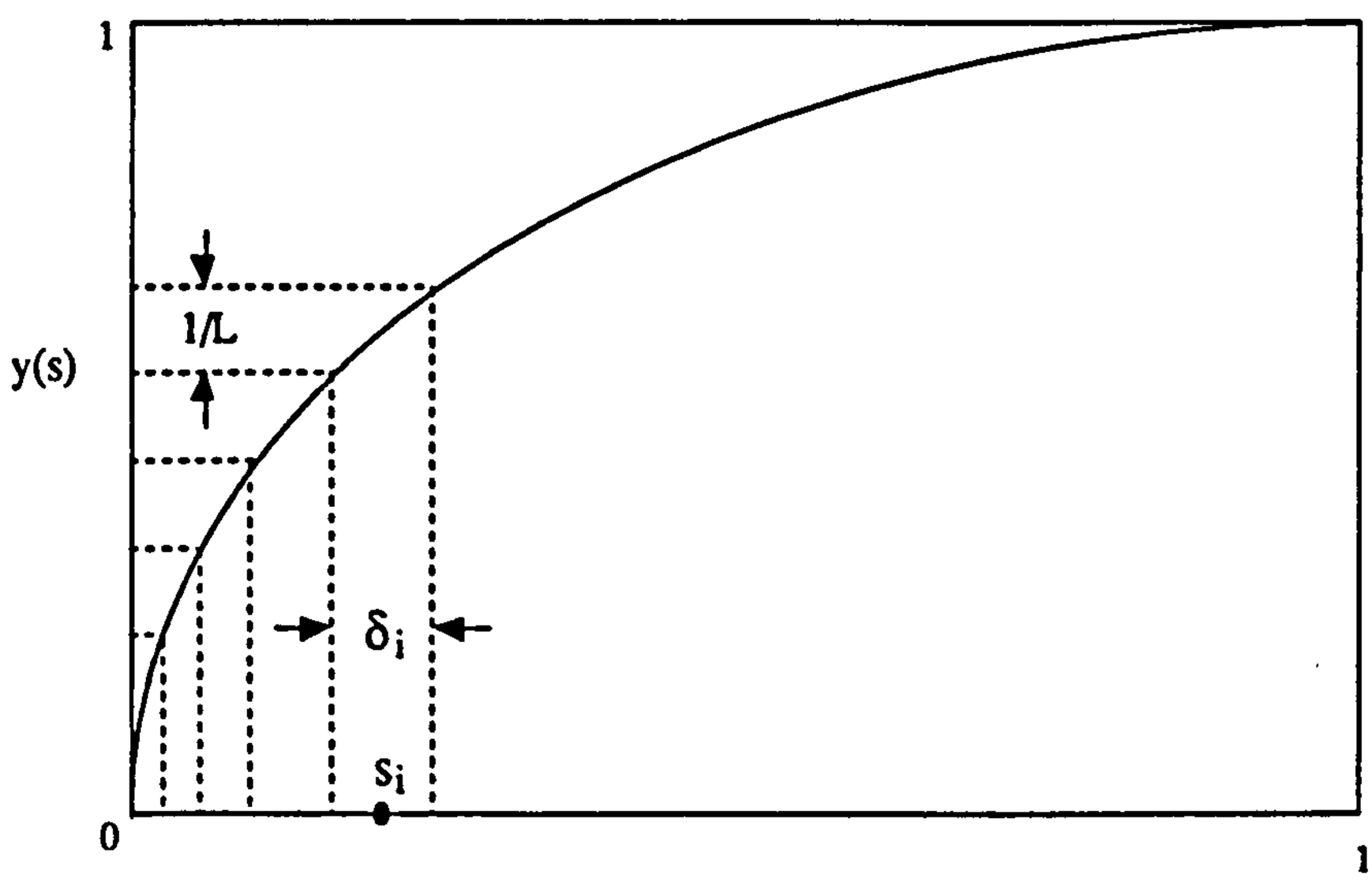

Fig. 4.2 Compressor determination

The whole range of y is sliced into L levels. Any interval 1/L uniformly spaced on the y axis projects into a nonuniform spacing δ_i (i = 1, 2, ···, L) on the s axis. Considering a particular interval centred at a point s_i as shown in the figure, it is apparent that for a sufficiently small δ_i the slope, $y'(s_i)$, of the curve at the point s_i is approximately equal to $(1/L)/\delta_i$ or

$$\delta_i = \frac{1/L}{y'(s_i)} \tag{4.6}$$

All values of s in the range δ_i will, after quantisation, be rounded to one value and represented by the quantisation level y_i. Consequently, the mean-squared quantisation error due to these values can be found by appropriately averaging over δ_i.

Assuming that the occurrence of the signal to be quantised is random with a known probability density function (PDF), p(s), the variation about s_i is then, by definition, given by

$$\begin{aligned} E(\varepsilon_i^2) &= \int_{s_i-\delta_i/2}^{s_i+\delta_i/2} (s-s_i)^2 p(s)ds \\ &= p(s_i)\frac{\delta_i^3}{12} \end{aligned} \tag{4.7}$$

It is reasonable for p(s) to be assumed as being constant over the integration range if δ_i is very small. Substituting δ_i in Eq.(4.7) by Eq.(4.6), the total mean-squared quantisation noise $E(\varepsilon^2)$ over the whole range of s can be written as:

$$E(\varepsilon^2) = \sum_{i=0}^{L} \frac{1}{12L^2}\frac{p(s_i)}{y'^2(s_i)}\delta_i = \frac{1}{12L^2}\int_0^1 \frac{p(s)}{y'^2(s)}ds \tag{4.8}$$

For uniform quantisation, since $y(s) = s$ and $y'(s_i) = 1$, the total mean squared quantisation noise, $E(\varepsilon^2) = 1/12L^2$ as

$$\int_0^1 p(s)ds = 1$$

Recall the definition of signal-to-noise ratio, we obtain:

$$SNR = \frac{\sigma_s^2}{E(\varepsilon^2)} = \frac{\int_0^1 s^2 p(s)\,ds}{\frac{1}{12L^2}\int_0^1 \frac{p(s)}{y'^2(s)}\,ds} \tag{4.9}$$

Clearly, it is preferable for SNR to be both high and constant within the whole range of signal power, which requires the SNR to be independent of the signal variance, i.e. p(s). Unfortunately, this is practically impossible. What can be achieved is to adopt a good compressor so that the SNR is both high and as independent as possible to the signal statistical characteristics. For a positive constant β, if

$$y'(s) = \frac{\beta}{\sqrt{(\beta s)^2 - 1}} \tag{4.10}$$

then the SNR is almost independent of the statistical characteristics of signal amplitude, especially when β is sufficiently large (say, =500). By solving this differential equation we get

$$y(s) = Arch(\beta s) = \ln\left(\beta s + \sqrt{(\beta s)^2 - 1}\right) \tag{4.11}$$

Where Arch(βs) denotes the inverse hyperbolic cosine. Unfortunately, Eq.(4.11) is not feasible to be directly used as a compressor since its input, *s*, must be greater than or equal to $1/\beta$. To mitigate this shortcoming, the variable *s* at the right hand side is replaced by $s+1/\beta$. Thus Eq.(4.11) becomes:

$$y(s) = Arch(\beta s + 1) = \ln\left(\beta s + 1 + \sqrt{(\beta s + 1)^2 - 1}\right) \tag{4.12}$$

Since *s* is normalised, y(s) need to be normalised so that y = 1 when s = 1. Then,

$$y(s) = \frac{\text{Arch}(\beta s+1)}{\text{Arch}(\beta+1)} = \frac{\ln(\beta s+1+\sqrt{(\beta s+1)^2-1})}{\ln(\beta+1+\sqrt{(\beta+1)^2-1})} \tag{4.13}$$

This is the desired compressor, which may be referred to as β-Law.

4.2.1 Properties of the β-Law

This compressor is defined over a normalised signal range from 0 to 1. It has a steeper slope at the smaller signal values for a given value of the parameter β. This allows more quantising levels to be allocated to the relatively smaller signals. By varying the parameter β, different characteristics of the compressor can be obtained, see Figure 4.3 which indicates that the curvature of the s–y(s) curve increases as the parameter β increases, and when β decreases toward zero, the law approaches to an asymptote, $y = s^{1/2}$.

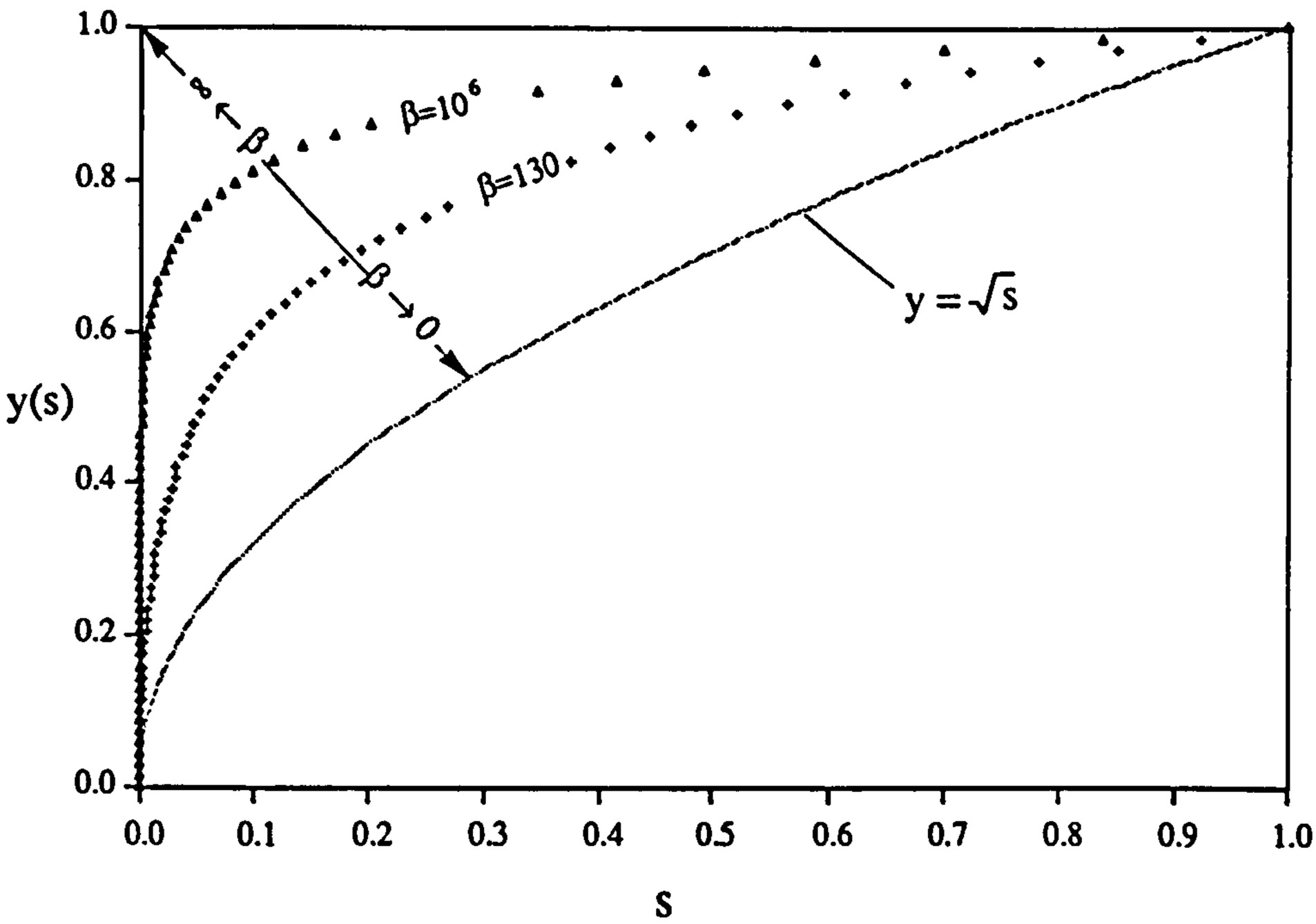

Fig. 4.3 β-Law Compressor

A practical compressor can be devised by choosing a moderate β. This will be discussed later.

Since the slope can be calculated as:

$$y'(s) = \frac{1}{\mathrm{Arch}(1+\beta)} \frac{\beta}{\sqrt{(1+\beta s)^2 - 1}} \tag{4.14}$$

Inserting this in the Eq.(4.9), we get

$$\mathrm{SNR} = \frac{\sigma_s^2}{E(\varepsilon^2)} = \frac{12L^2}{[\mathrm{Arch}(1+\beta)]^2 \left(1 + \frac{2E[s]}{\beta\sigma_s^2}\right)} \tag{4.15}$$

where σ_s^2 and E[s] is the mean signal power and the signal mean respectively:

$$\sigma_s^2 \approx \int_0^1 s^2 p(s)ds \quad \text{and} \quad E[s] \approx \int_0^1 s p(s)ds$$

Note, E[s] is different from E(ε). Eq.(4.15) can be used to analyse the SNR characteristic of the β-Law in respect to different mean signal powers. However, this requires the value of signal mean E[s] or the ratio $E[s]/\sigma_s$ to be estimated initially using the PDF, p(s), of rainfall intensity.

4.2.2 PDF of Rainfall Intensities for the Northwestern England

A probability density function for rainfall intensity can be found by fitting the sample frequency distribution. Finding a general and universally applicable PDF is difficult because it is a problem dependent on geographical and meteorological conditions. An attempt is directed to find a PDF for Northwestern England due to the dedicated

objective of this study and the data availability from Hameldon Hill.

A total number of 2887 time-series rainfalls were used to obtain the intensity data, which were observed by the Hameldon Hill radar during the years from 1986 to 1989 over an area of 76km radius. The total number of data points obtained was 154,436 which were sampled at 5-minute temporal resolution and 2km spatial resolution, and quantised using the existing 8-bit scheme (208 levels). A three-step procedure was followed to find the desired PDF:

1) ***Determination of the number and intervals of rainfall intensity categories.***

Following the existing 8-bit quantising scheme, the whole range of rainfall intensity from 0 to 126 mm/h is sliced into 3 segments each having a different number of rainfall intensity categories. The first segment from 0^+ to 8 mm/h has 80 categories with an incremental step of 0.1 mm/h, the third segment from 8^+ to 32.0 mm/h has 48 categories with an incremental step of 0.5 mm/h and the last segment from 32.0^+ to 126.0 mm/h has 47 categories with an incremental step of 2.0 mm/h, where '$^+$' means the lower bound is exclusive to that segment. The total number of the categories is 175. Note the incremental steps are different.

2) ***Choosing the representative rainfall intensity and calculating the occurrence frequency of each category.***

For the sake of simplicity, the representative point of a category was chosen as the upper bound of that category, for instance, 0.1 for the first category: 0.0^+~0.1, and 0.2 for the second category: 0.1^+~0.2, where '$^+$' means the lower bound is exclusive

to that category. The relative occurrence frequency of each category is calculated as the number of intensity occurrences within the category divided by the total data number (i.e. 154,436).

3) Representation of the result and derivation of the PDF.

The result was interpreted by plotting the occurrence frequency of each category against the representative rainfall intensities as shown in Figure 4.4 .

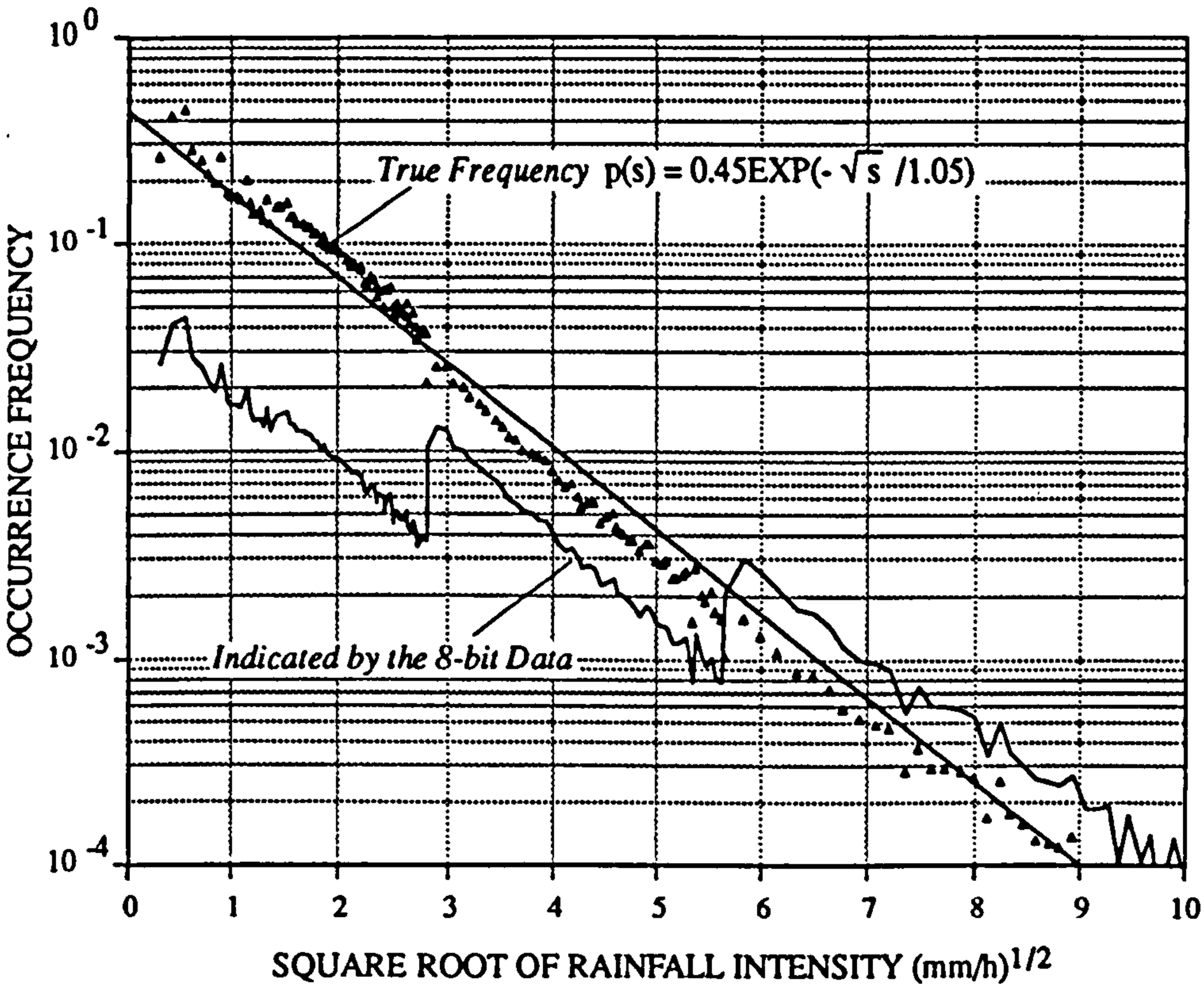

Fig. 4.4 The frequency distribution of rainfall intensity in Northwestern England

The vertical axis in Figure 4.4 shows the relative frequency on a logarithmic scale and the horizontal axis shows the square root of the rainfall intensities. The zigzag curve is

what the 8-bit data indicates, which is abnormal and is resulted from the abrupt change of the quantisation step (quantum). A conclusion that may be drawn from the result is that the true occurrence frequency of a rainfall intensity in the quantised data has been magnified by a factor being approximately equal to the quantum. This is another effect of data quantisation. To estimate the 'true frequency', the frequency values of each category were divided by a factor equal to the category interval (e.g. 0.1 for the first category and 2.0 for the last category). Then, the result was plotted again in Figure 4.4 as the 'true frequency' curve, which indicates that the frequency distribution in the Northwestern England takes a form:

$$p(s) = \frac{1}{2\tau^2} e^{-\sqrt{s}/\tau} \tag{4.16}$$

It is known from Eq.(4.16) that the occurrence of rainfall intensity follows the Weibull process, where τ is a parameter (≈ 1.05) and s is the rainfall intensity in mm/h. A detailed discussion of the Weibull Process has been included in Appendix-I.

$$\text{The ratio: } \frac{2E[s]}{\sigma_s} = \frac{2\Gamma(4)}{\sqrt{\Gamma(6)}} = \frac{2\times3\times2\times1}{\sqrt{5\times4\times3\times2\times1}} = \sqrt{1.2} \tag{4.17}$$

Inserting this value into Eq.(4.15), we get

$$SNR = \frac{\sigma_s^2}{E(\varepsilon^2)} = \frac{12L^2}{[Arch(1+\beta)]^2\left(1+\frac{\sqrt{1.2}}{\beta\sigma_s}\right)} \tag{4.18}$$

This equation enables the SNR characteristic of the β-Law with different signal power σ_s^2 input to be analysed.

4.2.3 Comparing β-Law with Other Compressors

The strong point of the β-Law can be demonstrated by comparing the law with μ-Law, C-Law, A-Law and the Uniform compressors.

The signal-to-noise ratios for the μ-Law is similar to Eq.(4.18):

$$SNR = \frac{\sigma_s^2}{E(\varepsilon^2)} = \frac{12L^2}{[\ln(1+\mu)]^2\left(1+\frac{\sqrt{1.2}}{\mu\sigma_s}+\frac{1}{\mu^2\sigma_s^2}\right)} \tag{4.19}$$

For the C-Law:

$$SNR = \frac{\sigma_s^2}{E(\varepsilon^2)} = \frac{12L^2}{[\mathrm{Arsh}(c)]^2\left(1+\frac{1}{c^2\sigma_s^2}\right)}. \tag{4.20}$$

For the A-Law:

$$SNR = \frac{\sigma_s^2}{E(\varepsilon^2)} = \begin{cases} \dfrac{12L^2}{[1+\ln A]^2} & \dfrac{1}{A} \le s \le 1 \\ \dfrac{12L^2\sigma_s^2A^2}{[1+\ln A]^2} & 0 \le s \le \dfrac{1}{A} \end{cases} \tag{4.21}$$

and for the Uniform compressor it is proportional to the signal power:

$$SNR = \frac{\sigma_s^2}{E(\varepsilon^2)} = 12L^2\sigma_s^2 \tag{4.22}$$

Let the logarithmic part of the denominator in Eq.(4.18) be the same as that in Eq.(4.19) and Eq.(4.21), then parameter β can be related to μ and A by

$$\beta = \frac{\mu^2}{2(1+\mu)} \text{ or } \beta = \frac{(2.72A-1)^2}{5.44A} \tag{4.23}$$

Since a typical value for parameter μ is 255 and for parameter A is 100 (Schwarts, 1980), therefore a typical value for β is taken as 130. Similarly, a typical value for the parameter of the C-law is taken as 132. Using these typical parameter values, the SNR characteristics of each compressor with different signal power levels were compared subjected to the PDF of rainfall intensities and the total number of 208 quantisation levels. The results were given in Figure 4.5.

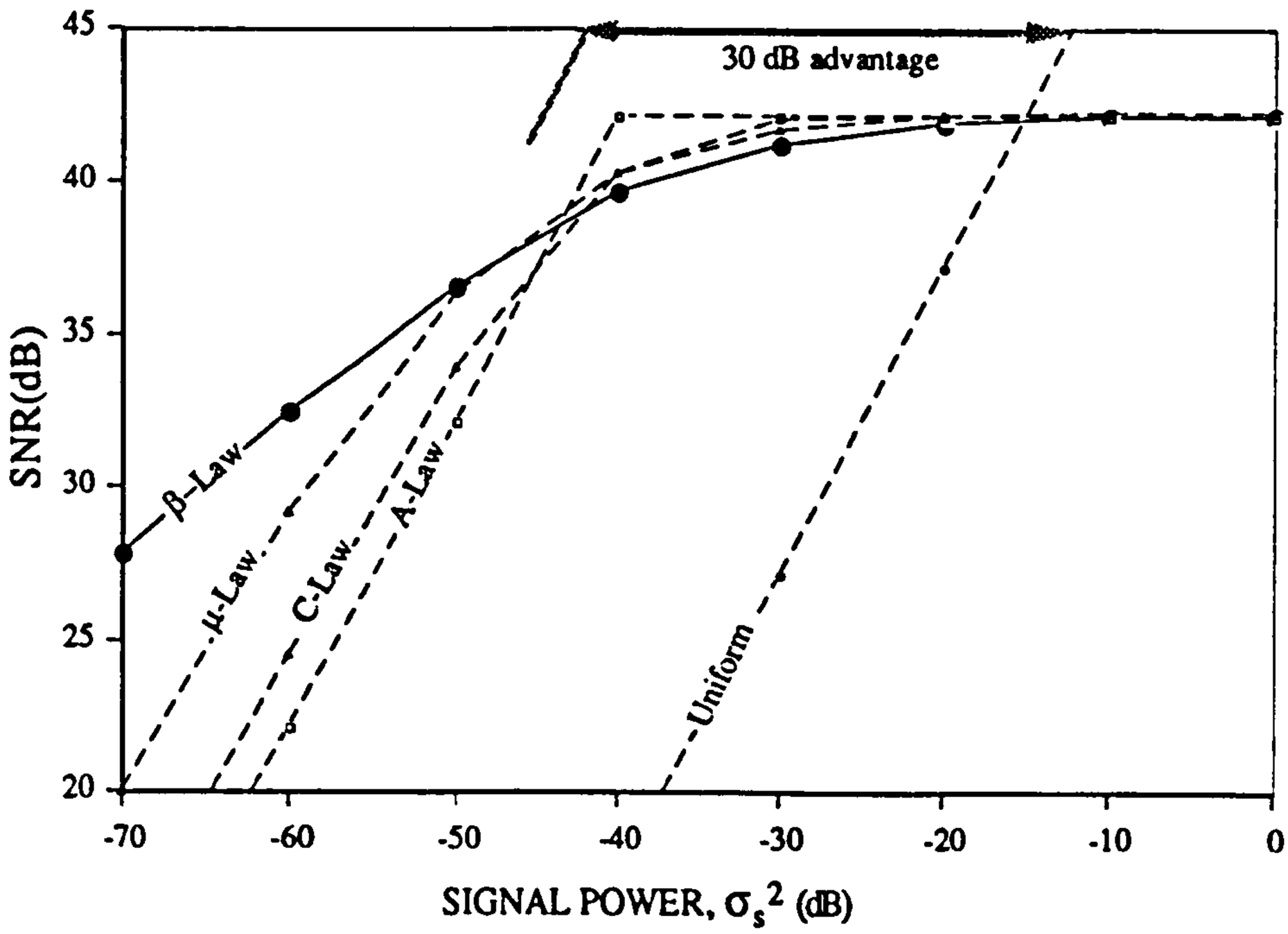

Fig. 4.5 Comparisons between the β-Law, μ-Law, C-Law, A-Law and the Uniform compressors
(Note: Quantisation levels = 208, β=130, C=132, μ= 255, A=100)

Since the signal s has been normalised, both the input signal power and the SNR are shown in decibel (dB) in the figure, which are defined as:

$$\sigma_{dB}^2 = 10\log_{10}(\sigma_s^2) \text{ and } SNR_{dB} = 10\log_{10}(SNR) \tag{4.24}$$

It is evident that the β-Law compressor with its parameter β taking a value 130 achieved a much wider range of uniformity than the μ-Law, C-law, A-law and the Uniform compressors while its maximum SNR value was as high as the μ-Law, C-law and A-law. Besides, if a smaller β value than 130 were used the maximum SNR would rise to a larger value. However, with the increase in the maximum SNR a penalty would be exerted on the SNR uniformity. A larger β would cause a slight decrease in the maximum SNR but would further extend the uniformity of the SNR. When β is approaching to zero, the performance of the β-Law is in the vicinity of $y = s^{1/2}$. Such a compressor greatly favours the quantisation of the frequently occurring weak signals. The four compressing laws, if placed in the order 1) A-Law, 2) C-Law, 3) μ-Law and 4) β-Law, exhibit a progressively increasing range of uniformity (i.e. maintaining higher SNR values over a wider range of signal powers). Comparing to the linear quantisation using the Uniform compressor, a quantisation advantage of more than 30dB can be achieved with the β-Law in terms of the SNR uniformity, whereas using the other logarithmic laws it is usually less than 30 dB, as can be seen in the figure.

4.3 Quantisation Accuracy Using β-Law

The quantisation accuracy using the β-Law compressor is dependent on the number of quantisation levels and the signal power. From Eq.(4.18) it is seen that the SNR in dB can be expressed as

$$SNR_{dB} = 10\log_{10}12 + 20\log_{10}L - 20\log_{10}[Arch(1+\beta)] - 10\log_{10}(1+1.1/\beta/\sigma_s) \tag{4.25}$$

Where L is the total number of quantisation levels and β = 130. With binary coding,

m digits (bits) are required to represent the L levels. Thus $L = 2^m$. With the relation, Eq.(4.25) becomes

$$\begin{aligned} SNR_{dB} &= 10\log_{10}12 + 20m\log_{10}2 - 20\log_{10}[Arch(1+\beta)] \\ &\quad - 10\log_{10}(1+1.1/\beta/\sigma_s) \\ &\approx 6.02m - 10\log_{10}(1+0.0063/\sigma_s)-4.12 \end{aligned} \tag{4.26}$$

The relation between SNR and the mean signal power, σ_s^2, for different number of coding bits, m, is shown in Figure 4.6.

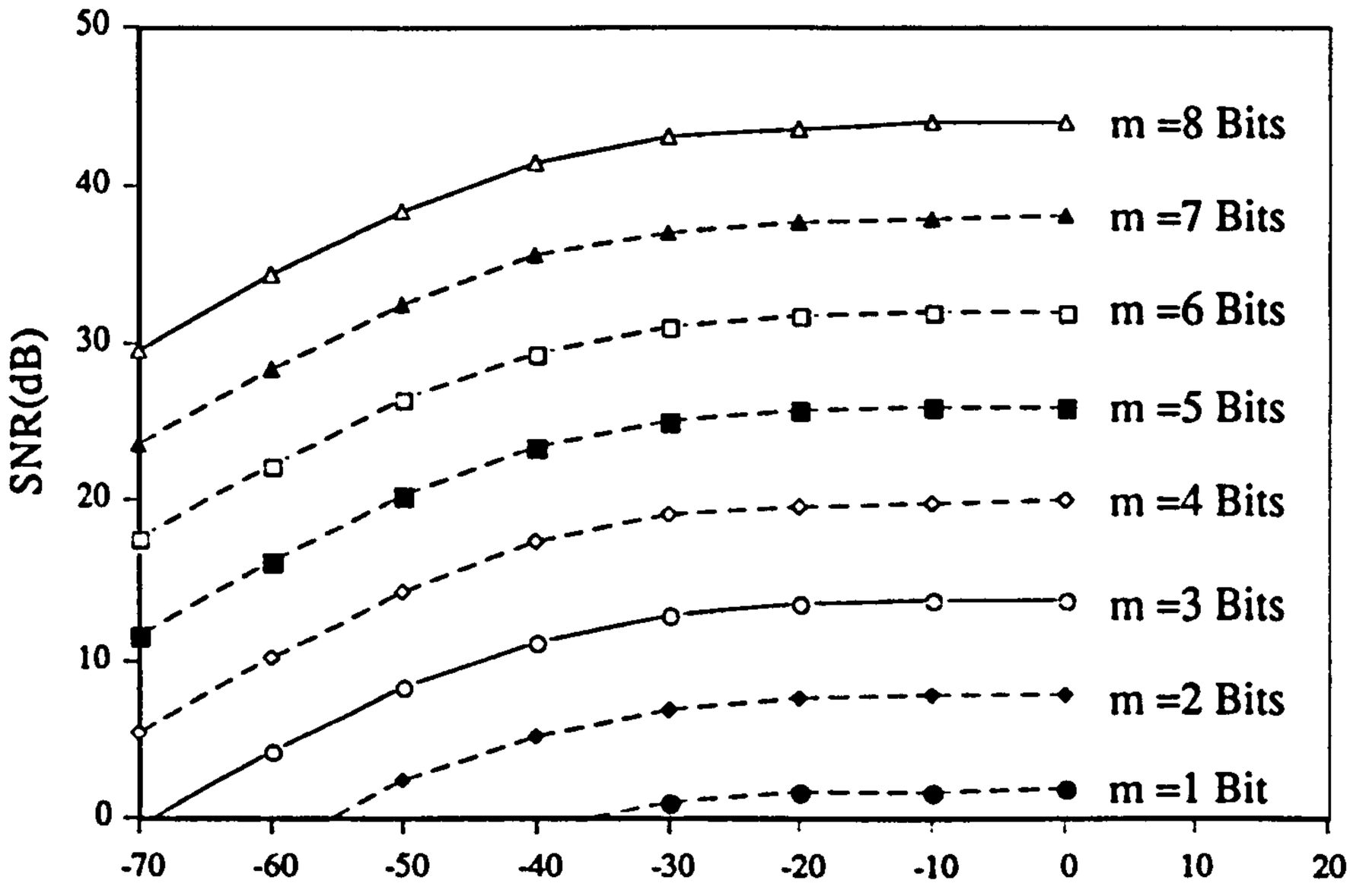

Fig. 4.6 SNR varying with the mean signal power for different number of bits

From the figure it can be seen that 1) the effect of any quantisation level is nearly identical for the mean signal power ranging from -30 to 0 dB; 2) given a mean signal power, the SNR in dB is proportional to the number of coding bits used and an

increment of one bit will result in an increment of approximately 6 dB in the SNR. This means that the optimal number of quantisation levels does not exist. The choice of a suitable number of quantisation levels is often subjected to a benefits to cost ratio. Therefore, it would be ideal if the data quantisation accuracy could be improved without increasing the coding bits.

4.4 New 8-bit Nonlinear Quantisation

The existing 8-bit nonlinear quantisation scheme used in the UK is not efficient in data compressing, which can be improved by adoption of the β-Law compressor while using the same number of coding bits. Theoretically, there are 256 levels for 8-bit quantisation, however only 208 levels (i.e. $y(\bullet) = 0, 1, 2, \cdots, 207$) are used. Some levels have been reserved for data transmission purposes. These levels are not uniformly spaced, which is equivalent to the data compressing with the A-Law, see Figure 4.7.

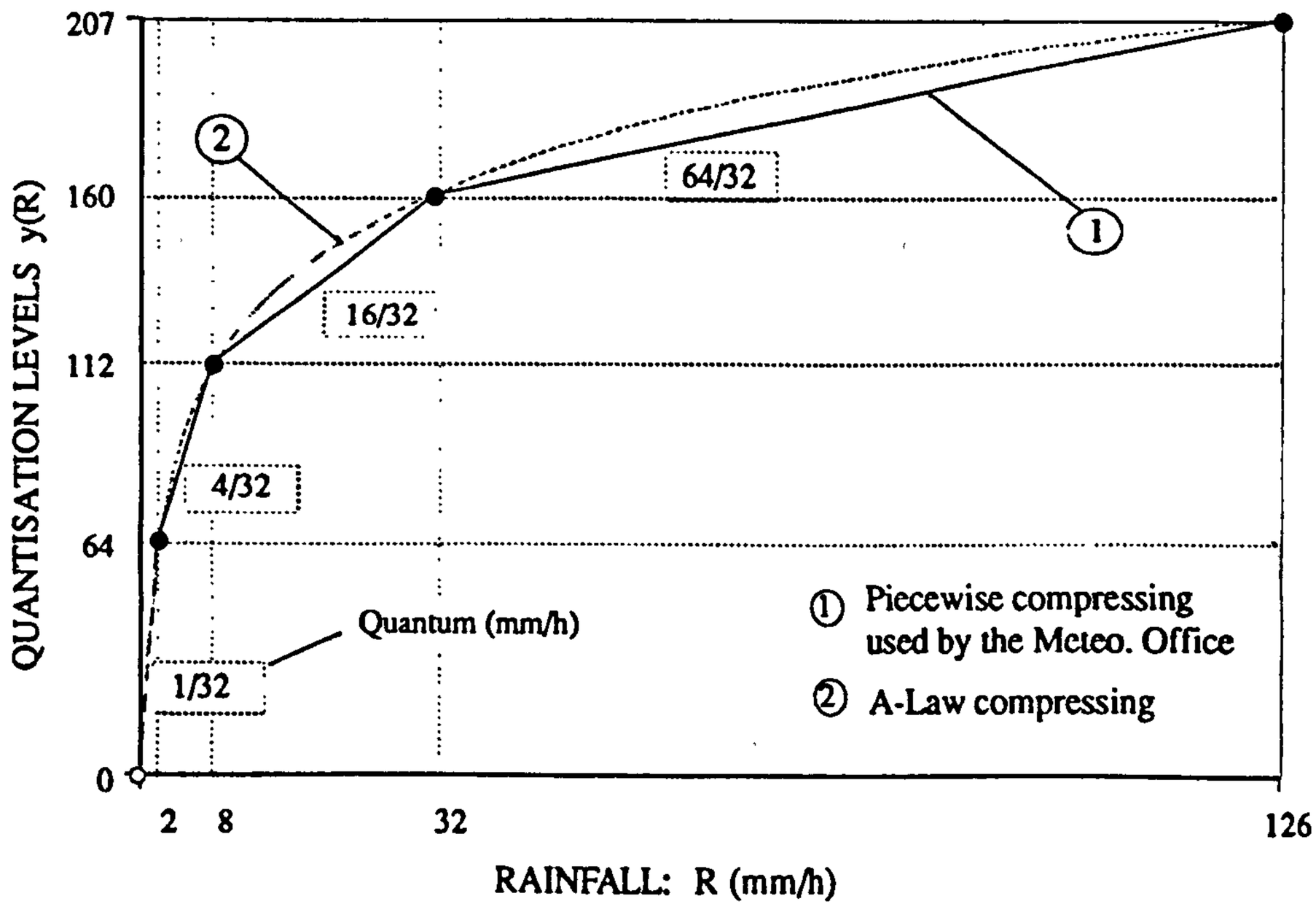

Fig. 4.7 Existing 8-bit quantisation scheme used in the UK

The logarithmic curve shown in the figure was approximated in a piece wise manner using four chords. The first chord has a slope of 32, the second, 32/4, the third, 32/16 and the last, 32/64. Thus the quantum step δ (mm/h) on the R axis can be calculated using δ=ds/dy, where ds/dy is the reciprocal slope of each chord. For example, the first chord has a quantum step 1/32 mm/h. In general, any quantisation level $y(R_i)$ represents a range of rainfall values from $(R_i-\delta/2)$ to $(R_i+\delta/2)$ except for the first level $y(R_0)$ which only represents a value range from R_0 to $(R_0+\delta/2)$, where R_0 (= 0) is the minimum rainfall intensity that may be represented.

In order to understand the efficiency of this quantisation scheme, it is necessary to estimate the quantisation error. For the sake of simplicity only the logarithmic portion of the A-Law compressor is considered. Rewrite the A-Law into the form:

$$y(s)= 1+k\ln s \tag{4.27}$$

where, y(s) and s are normalised,

$$k = 1/(1+\ln A)$$

Let the logarithmic curve over the range from s_{i-1} to s_{i+1} be approximated by a chord a^c. See Figure 4.8. By Eq.(4.8) the mean-squared quantisation error of this chord is:

$$E(\varepsilon^2_{a^c}) = \frac{1}{12L^2}\int_{s_{i-1}}^{s_{i+1}}\left[\frac{ds}{dy}\right]^2 p(s)ds \tag{4.28}$$

Where ds/dy is the reciprocal slope of the chord, $(s_{i+1} - s_{i-1})/(2\Delta y)$. The projection of chord a^c on the y-axis corresponding to that from s_{i-1} to s_{i+1} on the s-axis is $2\Delta y$. From Eq.(4.28) it is not possible to obtain a general conclusion. It would be more meaningful if the upper and lower quantisation error bounds could be found.

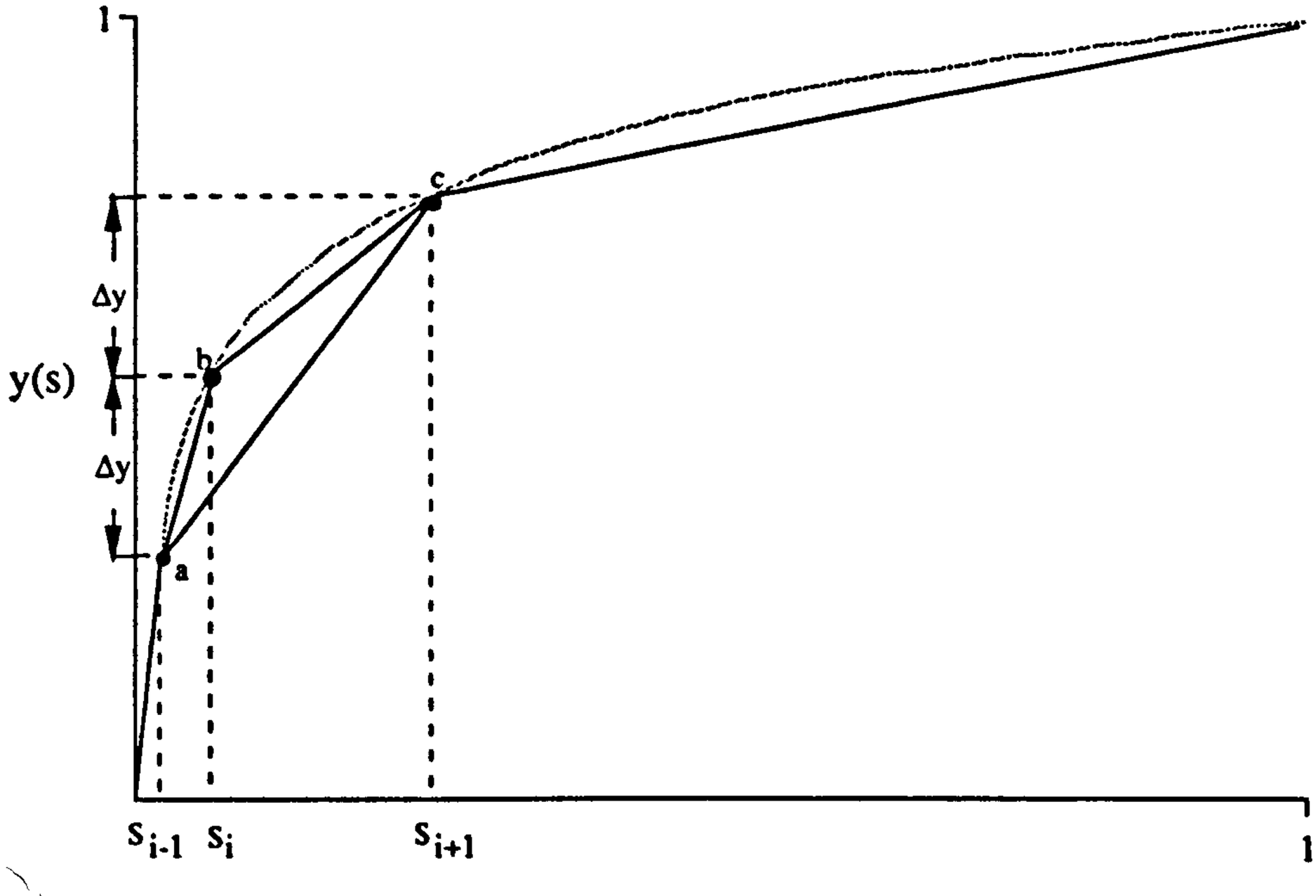

Fig. 4.8 Segmentally approximated A-law

Finding a point s_i between the points s_{i-1} to s_{i+1} such that $s_{i+1} = \varphi s_i$ and $s_i = \varphi s_{i-1}$. This point further separates the logarithmic curve into two segments: a^b and b^c each projects a range Δy on the y-axis. It can be known that $\Delta y = k\ln\varphi$ from Eq.(4.27). The reciprocal slope of the chords is respectively:

$$\left.\frac{ds}{dy}\right|_{a\hat{}b} = \frac{s_i - s_{i-1}}{\Delta y} = \frac{\varphi - 1}{\Delta y \varphi} s_i$$

$$\left.\frac{ds}{dy}\right|_{a\hat{}c} = \frac{s_{i+1} - s_{i-1}}{2\Delta y} = \frac{\varphi^2 - 1}{2\Delta y \varphi} s_i$$

$$\left.\frac{ds}{dy}\right|_{b\hat{}c} = \frac{s_{i+1} - s_i}{\Delta y} = \frac{\varphi - 1}{\Delta y} s_i$$

The reciprocal slope of chord a^c satisfies

$$\frac{\varphi-1}{k\varphi\ln\varphi}s_i \le \left.\frac{ds}{dy}\right|_{a\hat{}c} \le \frac{\varphi-1}{k\ln\varphi}s_i \qquad (4.29)$$

From (4.28) we have:

$$\frac{1}{12L^2}\left[\frac{\varphi-1}{k\varphi\ln\varphi}\right]^2\int_{s_{i-1}}^{s_{i+1}}s^2p(s)ds \le E(\varepsilon^2)\Big|_{a\hat{}c} \le \frac{1}{12L^2}\left[\frac{\varphi-1}{k\ln\varphi}\right]^2\int_{s_{i-1}}^{s_{i+1}}s^2p(s)ds$$

Since for the A-law,

$$E(\varepsilon^2)\Big|_{a\tilde{}c} = \frac{1}{12L^2}\int_{s_{i-1}}^{s_{i+1}}\frac{1}{(dy/ds)^2}p(s)ds = \frac{1}{12k^2L^2}\int_{s_{i-1}}^{s_{i+1}}s^2p(s)ds$$

then,

$$\left[\frac{\varphi-1}{\varphi\ln\varphi}\right]^2 \le \frac{E(\varepsilon^2)\Big|_{seg}}{E(\varepsilon^2)\Big|_{log}} \le \left[\frac{\varphi-1}{\ln\varphi}\right]^2 \qquad (4.30)$$

Where, the subscription a^c and a~c has been replaced respectively by 'seg' for segmented approximation and 'log' for logarithmic quantisation, given that chord a^c was arbitrarily chosen. Eq.(4.30) indicates the lower and upper bounds of the quantisation error for any segment due to a segmentally linear approximation of the A-Law, for convenience, which is referred to as relative error factor. If the total number of chords is N_c, and each chord projects an equal length, $2\Delta y$, on the y-axis, then $2\Delta y$ is equal to $1/N_c$. Recall that $\Delta y = k\ln\varphi$ then φ can be estimated as: $\varphi = e^{1/(2N_c k)}$.

For the equivalent compressor (A-Law) used in the existing 8-bit quantisation scheme, k = 143/(207ln63), therefore, the variation of the relative error factor with the number of chords N_c can be investigated. The result is shown in Figure 4.9.

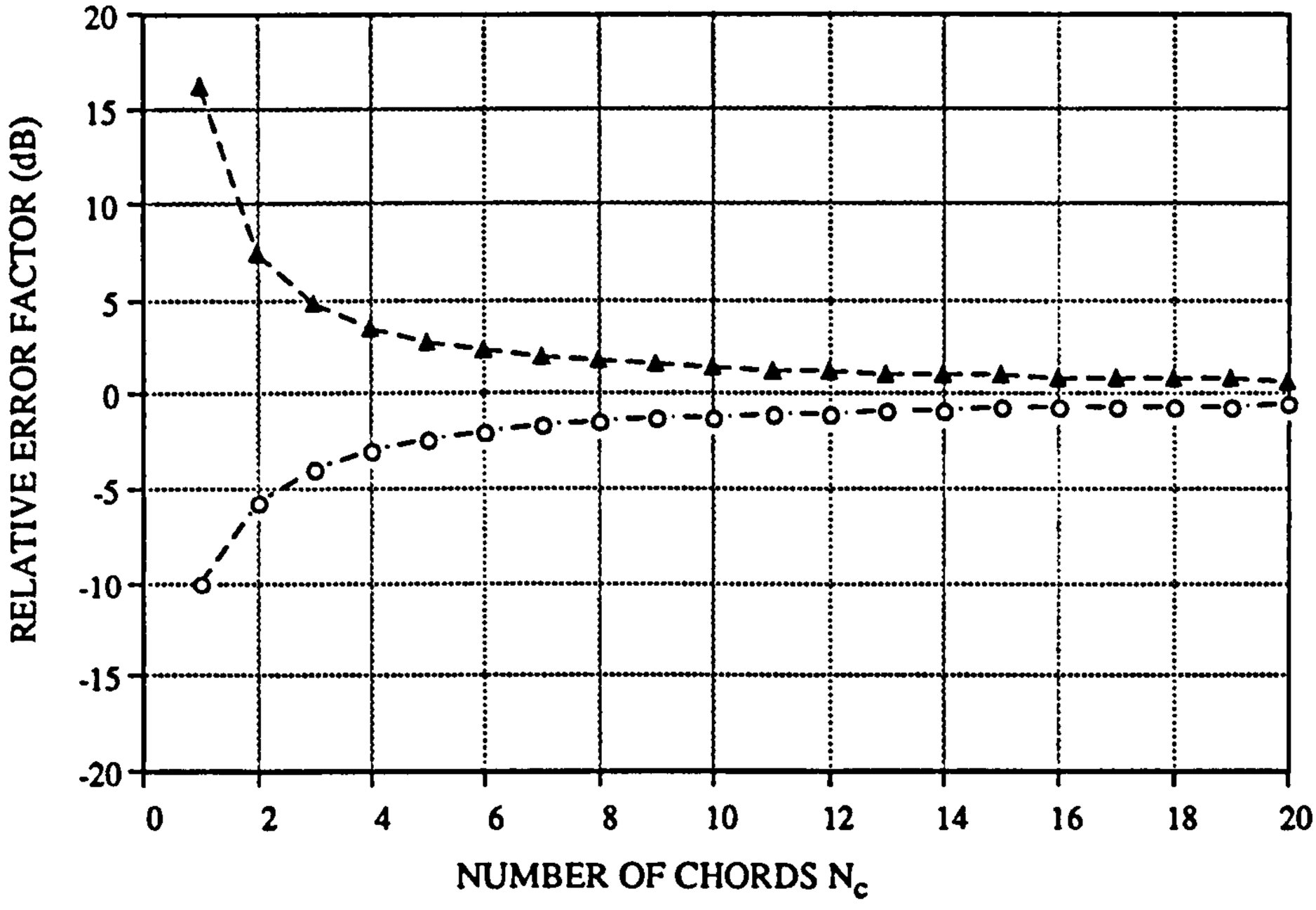

Fig. 4.9 Variation of the relative error factor (dB) with the number of chords

The figure indicates that the relative error factor decreases with the increase in the total number of chords. When only a single chord is used to approximate the logarithmic curve, the relative error factor will take a value within the range from 0.1 (-10 dB) to approximately 41 (16 dB). This means the approximation may result in maximally 10 time less or 41 time higher quantisation error than that using the A-Law depending on different signal statistical characteristics. With a sufficiently large number of chords, the relative error factor approached to 1 (i.e. 0 dB). Only under this circumstance, can the approximation of the nonlinear compressor by the linear chords be treated as satisfactory. The existing 8-bit scheme used 4 chords to approximate the A-Law compressor. As it can be seen from the figure that this number appeared inadequate since the approximation error is significant. It is the inadequate number of chords that resulted in the abrupt change of the quantum from one chord to another. In turn it caused the PDF curve in Figure. 4.4 to appear as a zigzagged shape.

To sum up, the A-Law compressor used in the existing 8-bit scheme is not as efficient as the β-Law compressor as indicated by the SNR–σ_s^2 relationship (Figure. 4.5) and the 4-chord approximation of the nonlinear compressor appeared too coarse. To improve the existing 8-bit scheme, the preference is to approximate the β-Law with more chords, say 207 but without using the float notation technique. This will make the compressing scheme simpler and data expanding easier.

Assuming that the potential variation range of rainfall intensity is from 0 to R_{max} mm/h, and a total number of L levels is used to represent the rainfall intensities within the range, then the new scheme employs Eq.(4.31) to carry out the quantisation.

$$y_i = \frac{(L-1)\,\mathrm{Arch}\left(\frac{\beta R_i}{R_{max}}+1\right)}{\mathrm{Arch}(\beta+1)} \qquad (4.31)$$

Where, y_i is the quantisation level, taking a value of 0, 1, 2,$\cdots$, or L-1 which will be coded in binary form to represent the rainfall intensity of R_i and the parameter β is taken to be 130. Conversely, eversely, the integer, y_i may be translated into a rainfall intensity using the same equation. Obviously, the translated rainfall intensity will deviate somewhat from its original version. This scheme is equivalent to using 207 chords to approximate the β-Law. It can be directly incorporated in the design of an encoder. However, finding an simple and economical way of obtaining a physical realisation goes beyond the scope of this study.

Assuming that R_{max} and L is respectively 126 mm/h and 208 levels (as used by the Meteorological Office, UK), Figure 4.10 shows the new 8-bit quantisation scheme using β-Law. Of the total 208 levels, the rainfall intensity values are shown together with the quantum of each level which varies gradually from 0.0004 to 3.3699 mm/h.

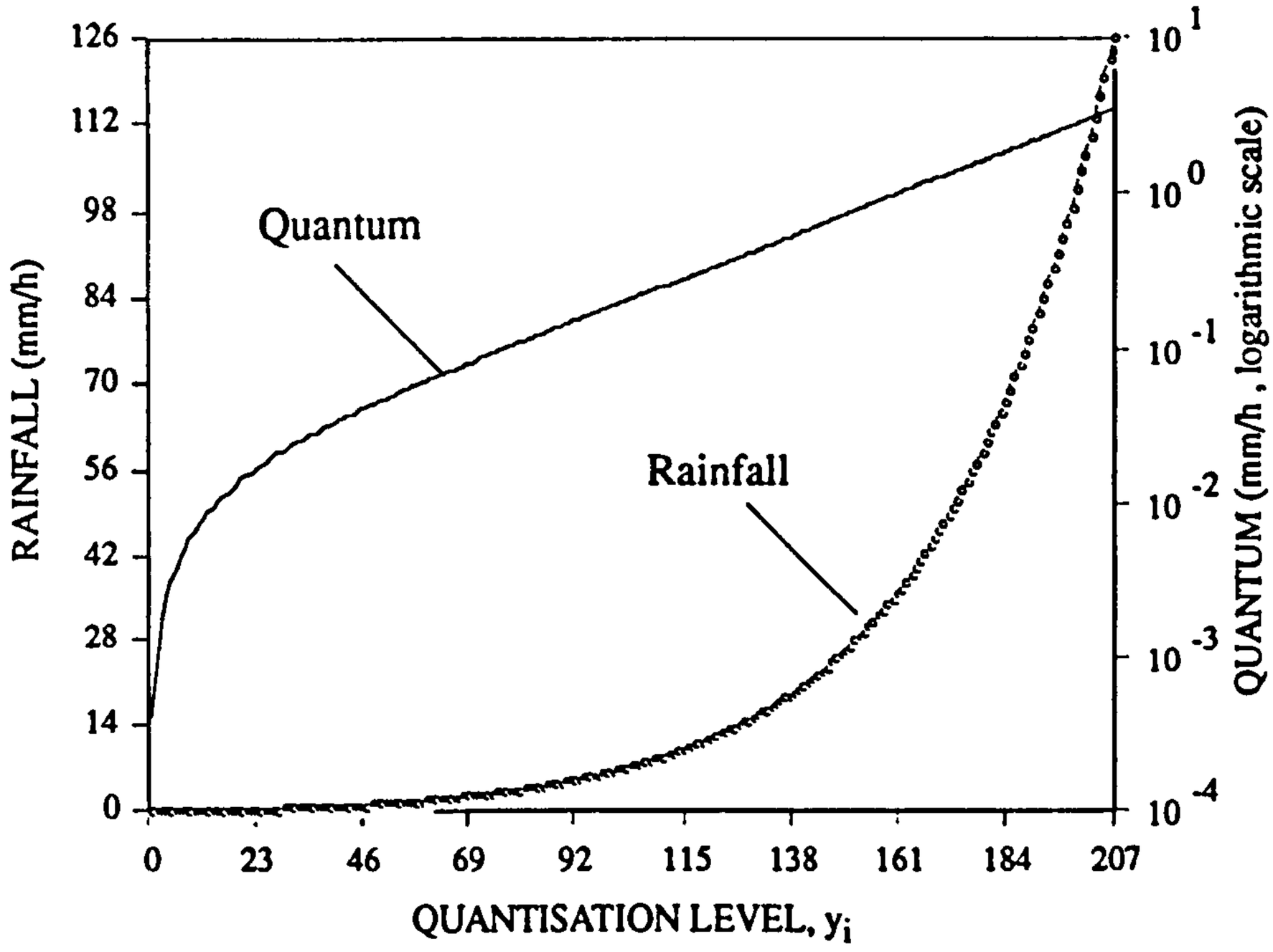

Fig. 4.10 8-bit (208 levels) compressing and expanding using the β-Law

4.5 New 3-bit Nonlinear Quantisation

Based on the new 8-bit quantisation scheme, a 3-bit quantising scheme can be developed following a two-step procedure.

Step-1: division of the total 208 levels in the 8-bit scheme into 16 segments, each having 13 levels. See Figure 4.11.

Step-2: representation of all the rainfall intensities between the two adjacent levels indicated by the circles in the figure by a single level marked by a black dot. i.e. **0**~12, 13~**26**~51, 52~**65**~77, 78~**91**~103, 104~**117**~129, 130~**143**~155, 156~**169**~181, 182~**195**~207. Thus the total 208 levels in the 8-bit scheme reduced to 8 levels in the 3-bit scheme. Substituting the highlighted levels into Eq.(4.31), the

corresponding rainfall intensities can be calculated. For example, the first level of the new 3-bit scheme represents a rainfall intensity of 0 mm/h and the last level represents 88.532 mm/h.

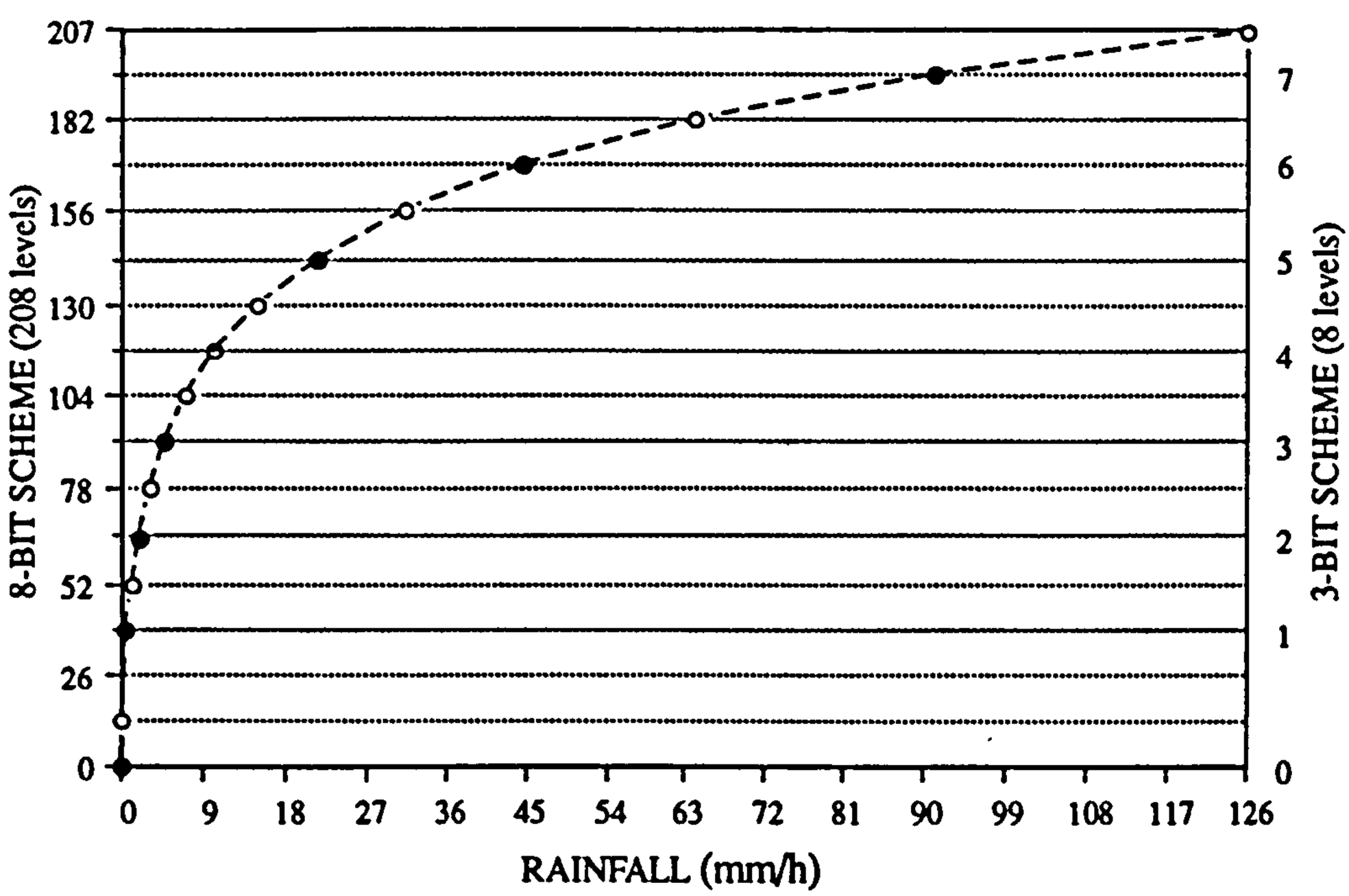

Fig. 4.11 3-bit (8 levels) compressing and expanding using the β-Law

The major difference between the new 3-bit scheme and the existing 3-bit scheme used by the U.K. Meteorological Office will be found mainly in the last two higher levels as can be seen from Figure 4.12. The existing scheme emphasises the possibility of rainfall larger than 126 mm/h whereas the new 3-bit scheme is more concerned with the possible reduction of quantisation error within the specified range from 0 to 126 mm/h.

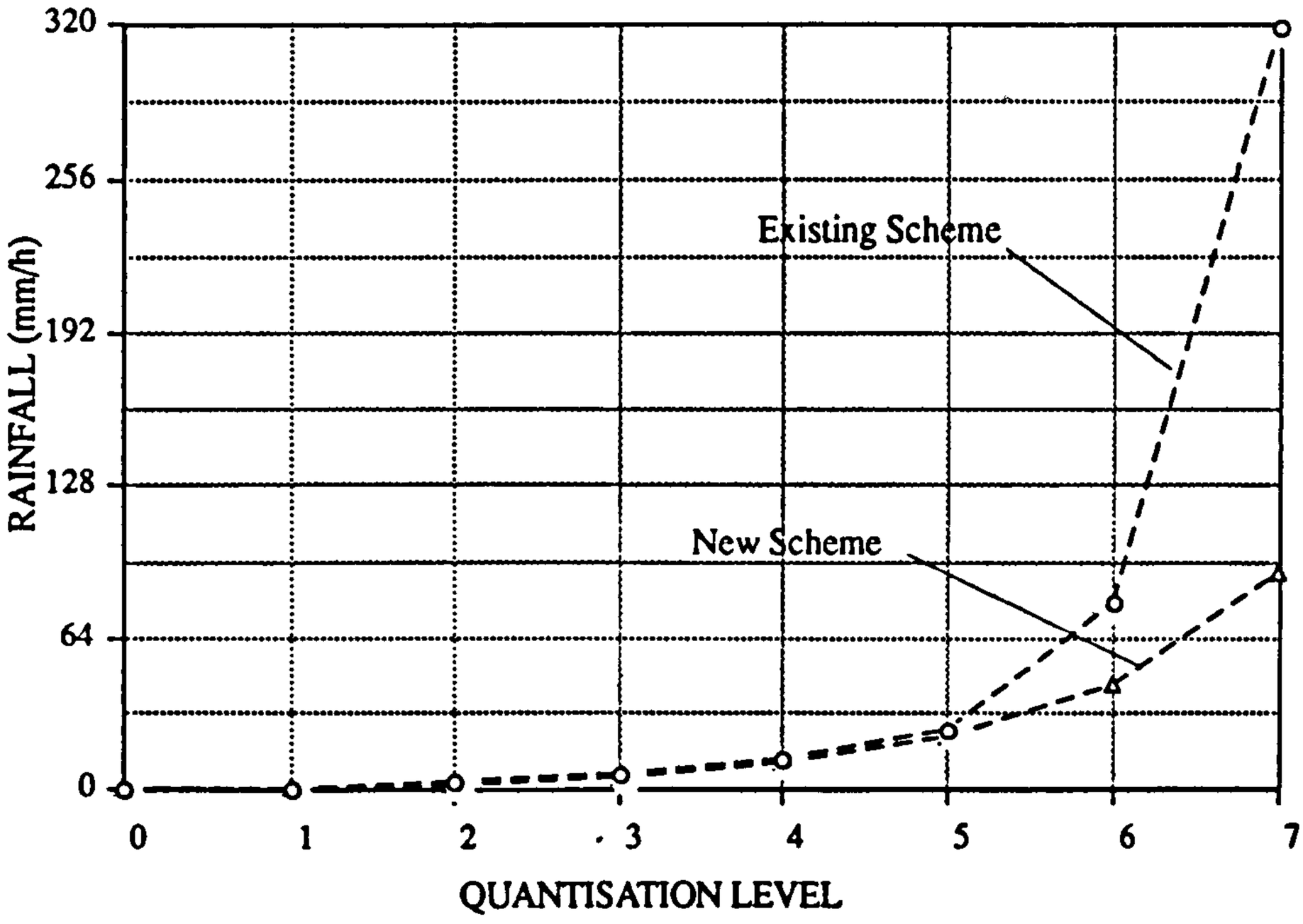

Fig. 4.12 Comparison between the new 3-bit scheme and the existing 3-bit scheme

As for the new 8-bit scheme, it is more precise than the existing scheme. Figure 4.13 shows a comparison between the new 8-bit scheme and the existing 8-bit scheme.

It is important to note that both the existing and the new schemes discussed so far are static. Their efficiencies are subjected to the actual distribution of rainfall intensities occurring over time and space, moreover, what value is chosen to be the potential maximum rainfall intensity, that governs the allocation of the predetermined quantisation levels to the unevenly occurring rainfall intensities, will exert significant impact on the eventual accuracy of the quantisation.

If the value of R_{max} in Eq.(4.31) is not fixed but can vary with the magnitudes of the input rainfall intensities then the quantisation accuracy may be further improved.

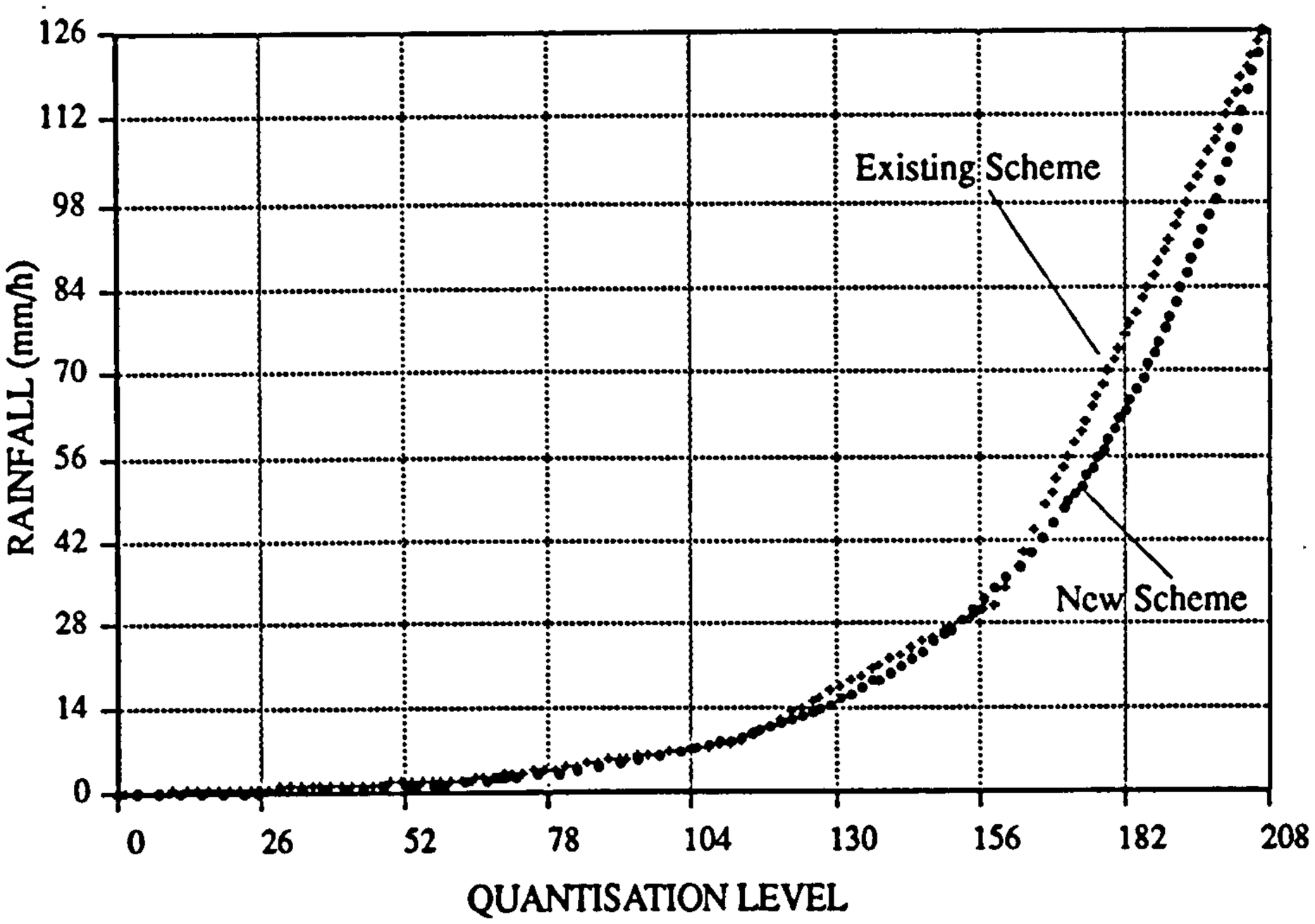

Fig. 4.13 Comparison between the new 8-bit scheme and the existing 8-bit scheme

4.6 A Nonlinear Adaptive Quantisation Scheme

Noticing the fact that radar rainfall data are transferred and processed image by image (or frame by frame), the quantisation error can be further reduced by the application of a nonlinear adaptive quantisation scheme devised using the β-Law.

The scheme is nothing more than giving a clear specification of the maximum rainfall intensity of each frame in the data header, by taking up only an additional 1-byte space. For the 2-km rainfall resolution, the maximum rainfall intensity is the maximum value of a total 76 by 76 (i.e 5776) data numbers and for the 5-km data , of the total 84 by 84 (i.e. 7056) numbers. Thus, the compression and expansion of the data needs to be carried out frame by frame using Eq.(4.31), where R_{max} should be the maximum rainfall intensity of each frame. In this way the quantisation accuracy is only subjected to the statistical characteristic of rainfall intensities within a frame rather than to the

overall PDF. Obviously, those frames having smaller variance will be 'zoomed' more and therefore will represent in more detail the information content than those having wider range of variation.

To demonstrate the efficiency of this adaptive scheme, a preliminary comparison was made between the new adaptive 3-bit scheme and the existing 3-bit scheme which is static using a storm which occurred on 16 June, 1991 over Northwestern England. The closeness of the re-quantised value to the original data is indicated by the root mean square error (mm/h):

$$RMSE = \sqrt{\frac{1}{N}\sum_{i=1}^{N}(R_o - R_q)^2} \qquad (4.32)$$

Where R_o is the rainfall intensity quantised using the existing 8-bit scheme;

R_q is the re-quantised value of R_o using the new or existing 3-bit scheme.

N is the total number of rainfall data of each frame.

The 8-bit (208 levels) outcome from the UK Meteorological Office were used as R_o in the analysis. A three-step procedure was followed to carry out the quantisation:

1) Determine the maximum rainfall intensity of each frame;

2) Requantise the data of every frame using the new adaptive 3-bit scheme and existing 3-bit scheme respectively;

3) Calculate the RMSE values for every frame.

A ratio calculated as the RMSE value of the adaptive scheme divided by that of the static scheme is plotted in Figure 4.14 against the sampling time step (i.e. in the sequence of data frames).

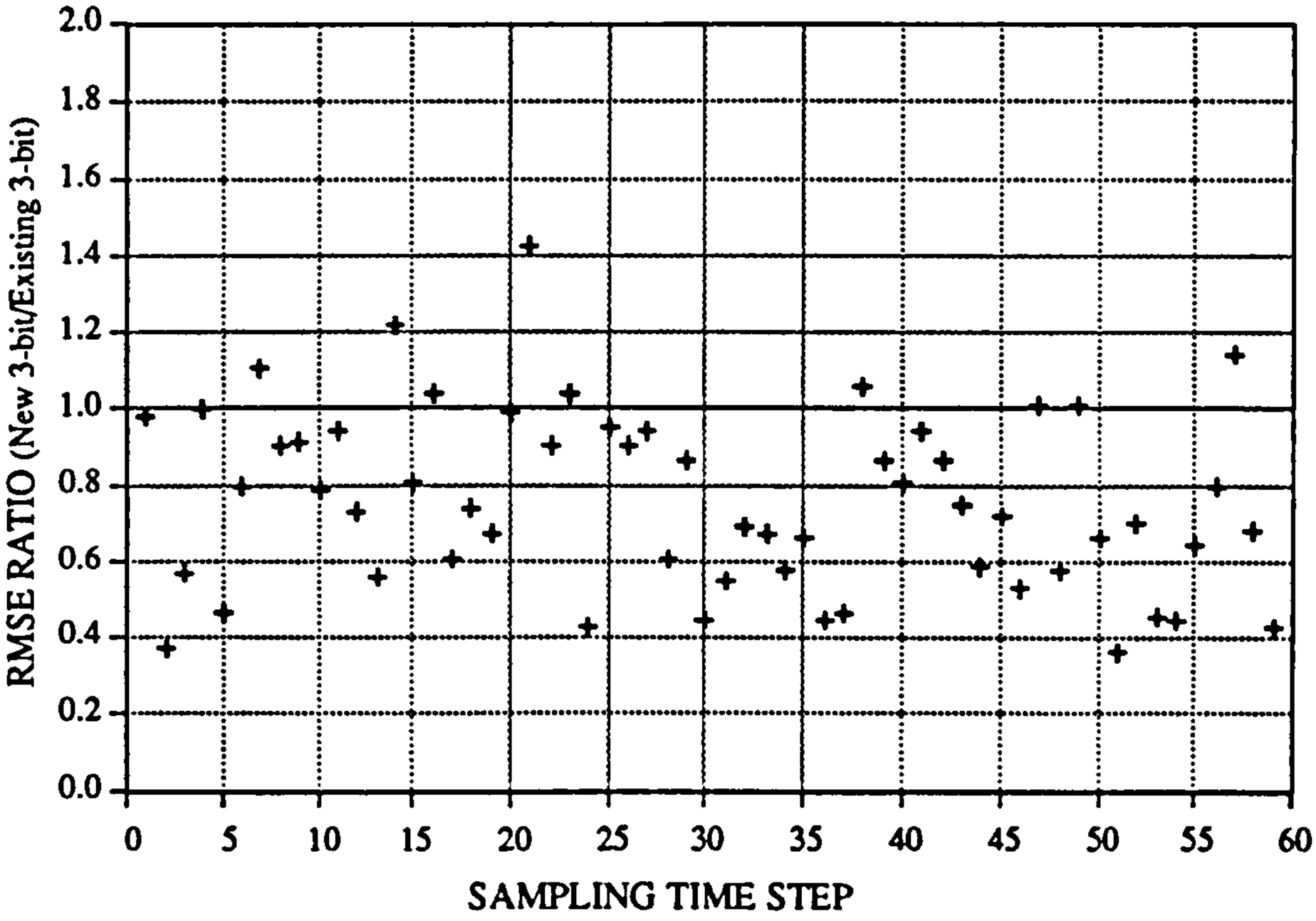

Fig. 4.14 Comparison between the adaptive 3-bit scheme and the existing 3-bit scheme

(Note: Event measured by the Hameldon Hill radar on 14 June, 1991)

It is evident that the adaptive quantisation using the new adaptive 3-bit scheme is more accurate than the existing static 3-bit scheme over approximately 85% of the time steps (i.e. the ratio <1). The quantisation error was significantly reduced. Nevertheless, the other 15% data frames with a higher quantising error than the static existing scheme may be explained by the coincidence of the data structure of the frame with the existing 3-bit quantisation scheme.

4.7 3-bit or 8-bit Data

At the present time, the single-site rainfall data are quantised and archived using the existing 8-bit scheme. Although 8-bit data are more accurate than the 3-bit data, it may not be worth using so many levels when justification is made within the hydrology

context because the low pass filter effect exerted by hydrological systems on the data. Therefore, it is envisaged that 3-bit data may be applicable to hydrological purposes. In addition, using the adaptive quantising scheme may further improve the 3-bit data quality, therefore may be used to replace the 8-bit data. The feasibility will be revealed by the following comparisons made in respect to the rainfall hyetographs and the simulated urban runoff hydrographs. Three storms observed by the Hameldon Hill radar were used in the analysis (see Table 4.3).

Table 4.3 Storm events used in the comparative study

STORMS	Start Time	Stop Time	Duration (Hr.)	Depth (mm)	
				3-bit data	8-bit data
Storm 1	28/10/89 23:35	29/10/89 02:35	3	11.7	10.8
Storm 2	08/11/89 09:55	08/11/89 12:55	3	22.2	20.7
Storm 3	15/06/91 17:00	15/06/91 18:00	1	3.4	3.3

STORM 1: Most places had rain overnight on the day of 28th October, 1989. Central England had a very windy day, with gales. Over Northwestern England it was mostly cloudy with rain at times. **STORM 2:** It was an eventful twenty-four hours! More general rain spread from the southwest to Wales, southern and central England by dawn. During the morning, rain spread to the rest of England. It was a quite windy day. **STORM 3:** Over England there was rain, persistent and heavy in many places. Temperatures were below average everywhere.

Comparisons between 1) the rainfall data quantised using the 3-bit adaptive and existing (static) 8-bit schemes; 2) the simulated hydrographs were shown in the figures from Figure 4.15 to Figure 4.17. The continuation and overflow hydrographs were generated using the WASSP model for the pipe locations at 001_203, 734_230 and 901_080 within the Bolton sewer system (see Figure 3.5).

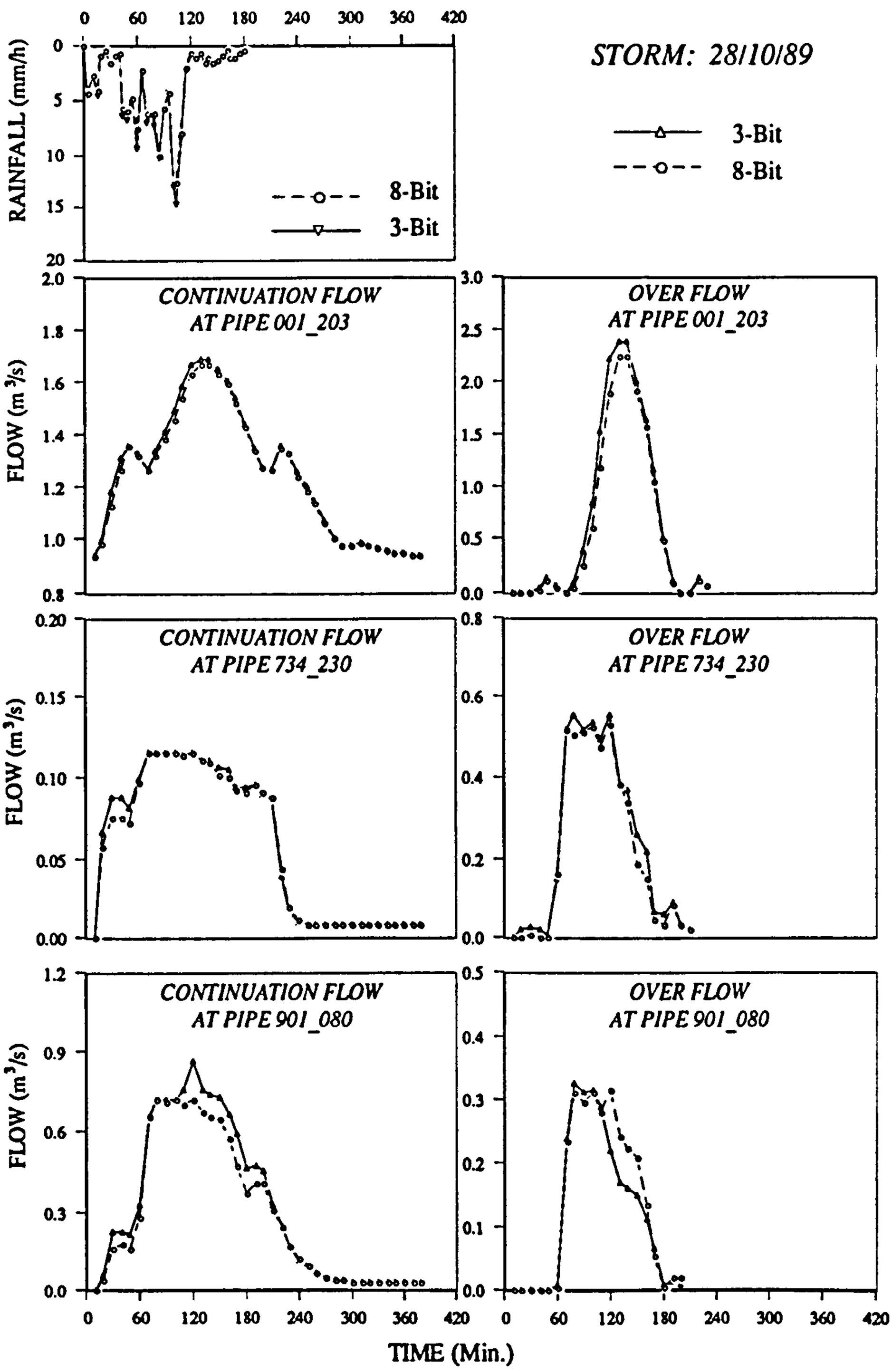

Fig. 4.15 The hyetograph of ***Storm-1*** *and the simulated hydrographs for different pipe locations*

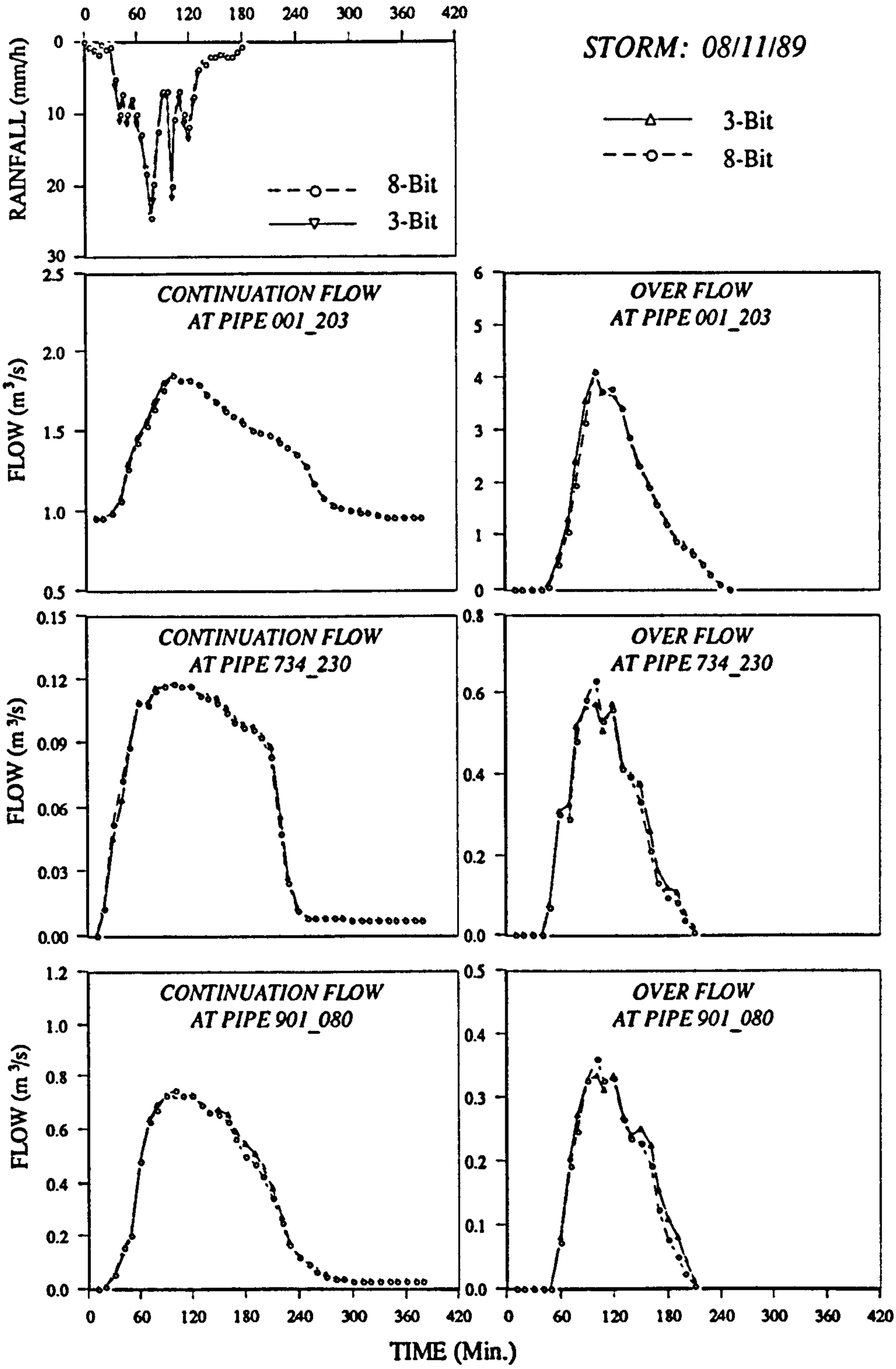

Fig. 4.16 The hyetograph of ***Storm-2*** *and the simulated hydrographs for different pipe locations*

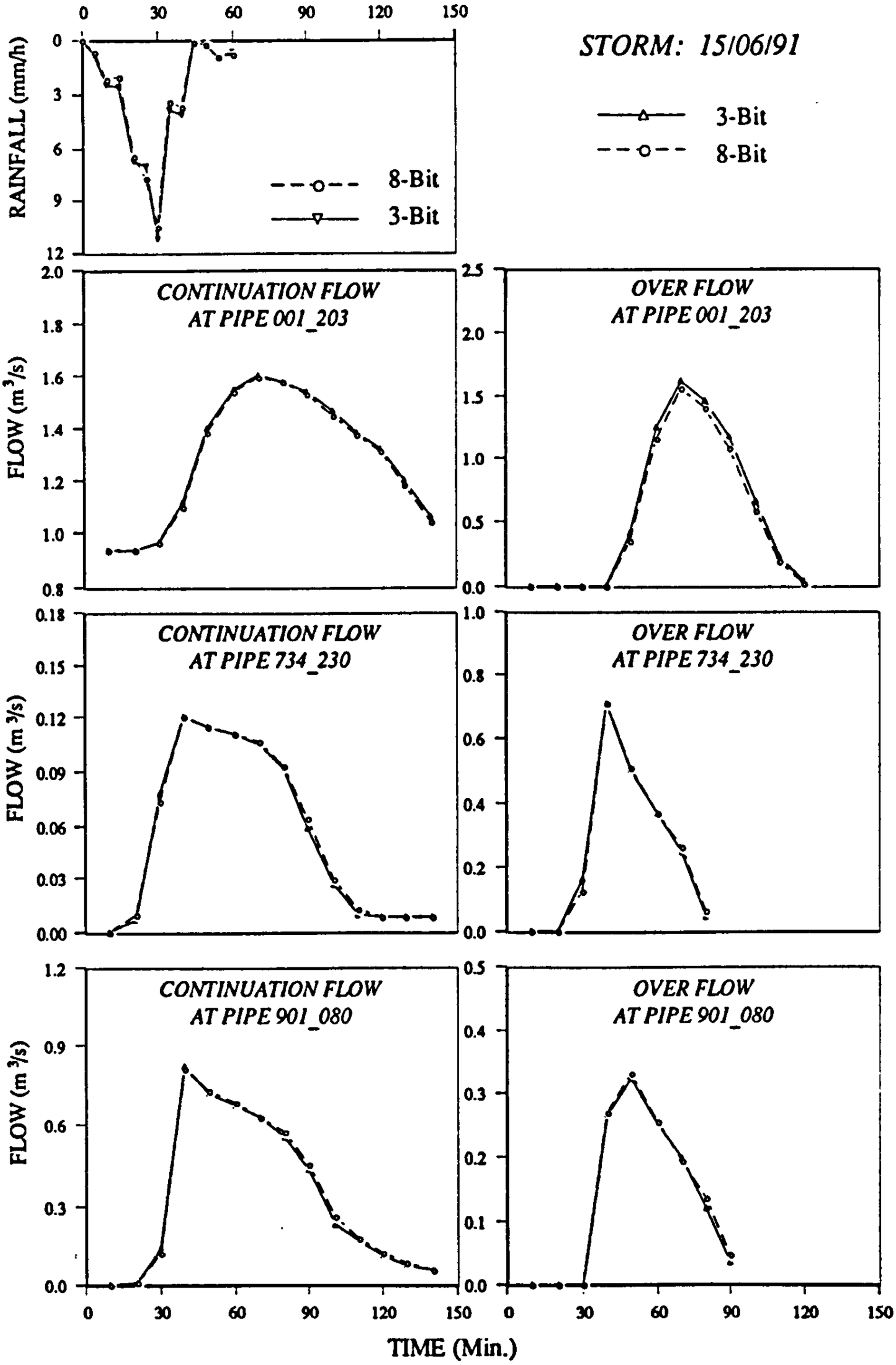

Fig. 4.17 The hyetograph of **Storm-3** *and the simulated hydrographs for different pipe locations*

It can be seen from the figures that the magnitude of difference in the simulated flows varied with storms and pipe locations. However, the difference was not significant. A summary of the comparisons was shown in Figure 4.18. The volumetric ratio is calculated as the flow volume produced using the adaptively quantised 3-bit data over that produced using the 8-bit data for different storms and pipe locations

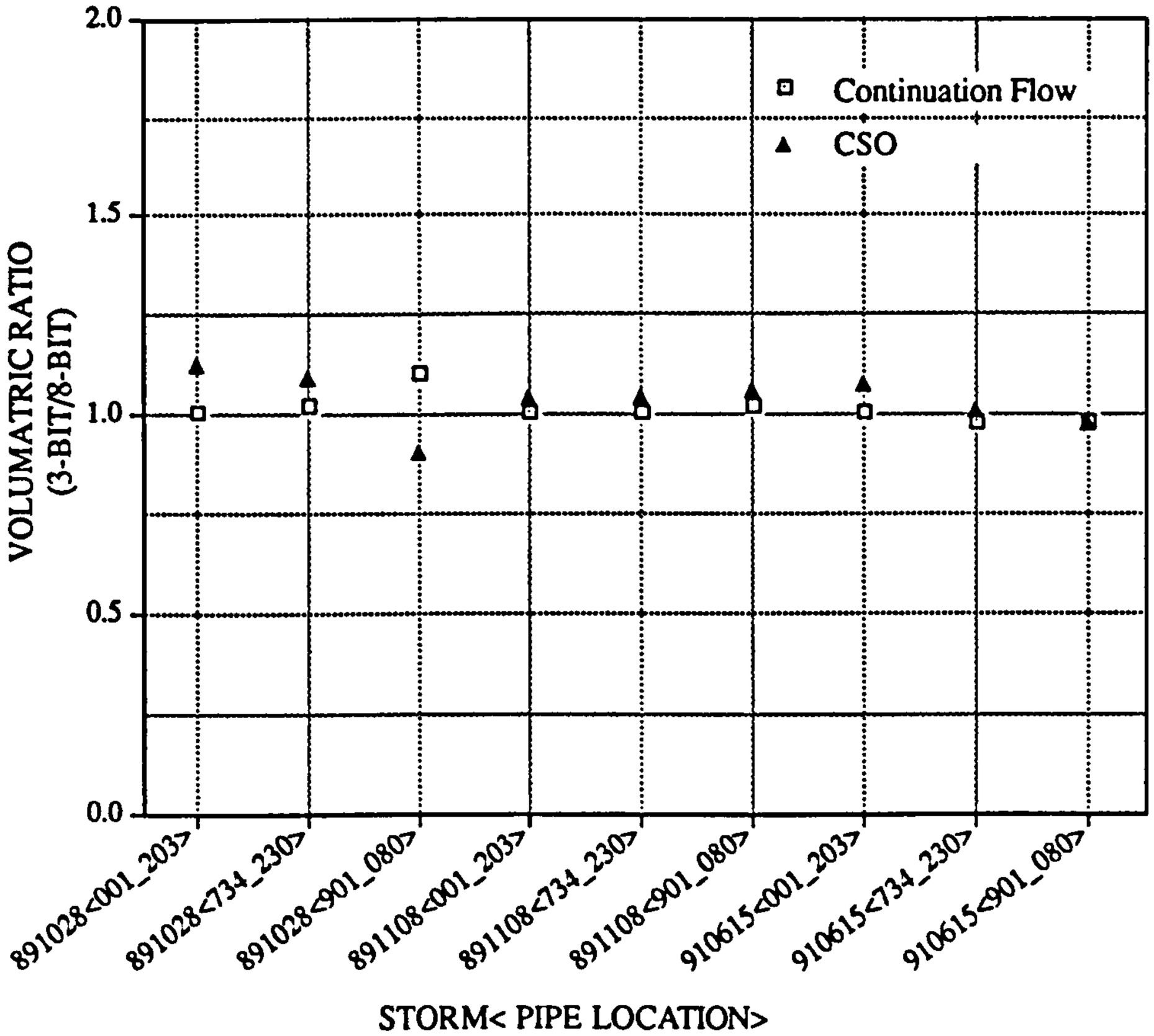

Fig. 4.18 Summary of the comparisons

It is seen that the simulated storm runoff volumes produced using the adaptively quantised 3-bit data and the existing 8-bit data were almost identical. Without loosing the generality, it can be concluded that the use of adaptively quantised 3-bit radar rainfall data is as practicable as the existing quantised 8-bit data in urban hydrological applications.

4.8 Summary

Data quantisation is a very important issue for radar rainfall data quality. The signal-to-noise ratio, SNR, is an objective measure of the efficiency of a compression law. A better compressor has a larger SNR level and less dependency of the input signal magnitude.

The β-Law is able to cope with a wider dynamic range of rainfall intensity with relatively less quantising error than the existing logarithmic compressor used in the UK. The merit of the β-law lies in the better performance at the smaller rainfall intensities.

Using the β-Law an adaptive quantisation scheme was developed. Differing from the static quantisation scheme, the quantum in adaptive quantisation is a function of time. The data are quantised in a image by image manner.

The more quantising levels used, the higher quantising accuracy, however, given the total quantising levels, the accuracy of quantisation is determined by the quantising scheme. The current static quantisation schemes (i.e. 8-level and 207-level) used in the UK are less efficient than the new adaptive quantising schemes proposed in this study. With the adaptive scheme more accurate rainfall data can be obtained. The adaptively quantised 3-bit data is applicable in the urban hydrological context when compared to the statically quantised 8-bit data. This will have considerable influence on the design of the data processing algorithm for the new hydrological radars and will also impact upon any redesign of the National Network of Meteorological Office/NRA radars.

CHAPTER 5

A CONCEPTUALLY PARAMETRISED TRANSFER FUNCTION (CPTF) MODEL

5.1 Real-time Urban Drainage Flow Prediction

Man's influence on the hydrological cycle creates many urban runoff problems, notably, flooding and combined sewer overflows (CSO). While the drainage area surface is dry, the flow conveyed within a combined drainage system comprises only dry weather flow coming from the domestic and industrial foul waters. However, during the wet periods considerable additional load will be contributed by the storm runoff. This additional load once exceeding the available system capacity (a UDS is usually designed to have a capacity equal to 3 times the dry weather flow), flooding or CSO will occur. To minimise the damage to the natural environment, public and private properties, appreciable efforts are required to control the unwanted effects of urban drainage. Real-time flow prediction is one of the effective measures for control, which by definition, means: *using the real-time rainfall and/or flow information to provide flow estimation for a predetermined location and lead time.*

5.1.1 The Role

Real-time flow prediction plays a key role in predictive real-time control of urban drainage systems. The interactions between rainfall and the UDS are complex and must be considered as a whole in order to maximise the control benefit whilst at the

same time achieving an environmentally acceptable solution. This requires a global predictive RTC strategy (see Chapter 10) to be applied, in which real-time flow prediction plays an important part in provision of the necessary first-hand information on the likely system status at a few time steps ahead.

There are variety of measures to fulfil the flow prediction tasks. The major factors influencing the choice of a flow prediction method may include:

- *Availability of data logging and processing facilities;*
- *The quantity and quality of telemetered rainfall and flow data;*
- *System characteristics, e.g. response time;*
- *Technical background of the forecasting personnel and*
- *A model.*

However, mathematical modelling is a most common practice due to its advantages. A fast growing alternative to the traditional analytical method for flow forecasting involves construction of catchment or flow routing models using digital computers. This development reflects the growing rejection by many hydrologists of arbitrary separation of the quick flows and base flow components of total runoff. As Nash and Sutcliffe (1970) observed, if arbitrary hydrograph separation is rejected, the steps by which rainfall is converted to effective rainfall and effective rainfall is converted to runoff can no longer be studied separately but must be treated simultaneously so that a model of the process of conversion of rainfall into runoff must be assumed. The complexity of catchment and of the runoff process itself inevitably mean that even the most rigorous model must involve considerable simplification and approximation. The parameters of the model may be determined from field measurement of hydrologic data or by means of successive optimisation procedures continued until the model behaviour approximates most closely that of the catchment itself, as indicated by

rainfall and runoff data, although care must be taken that the quest for 'curve fitting' does not result in a model that has no inherent physical validity.

5.1.2 Classification of the Existing Models

A vast number of mathematical models have been developed over the past decades. It has been 60 years since Sherman (1932) developed unit hydrograph theory, 40 years since Nash (1957) proposed his two-parameter instantaneous unit hydrograph, 30 years since the development of the Stanford Watershed Model (Crawford, N. H., Lindsay R. K., 1966) and 20 years since the emergence of the physics-based models. The application of transfer function (TF) models to hydrological systems is a relatively recent development. Broadly, models for hydrological system modelling can be classified into two categories: deterministic and stochastic (Shaw, 1983).

A) Deterministic models seek to simulate the physical processes in the catchment involved in the transformation of rainfall to stream flow. Deterministic modelling is an approach to the analysis of the hydrological process whereby the system is treated as a deterministic. This group of models may be subdivided into physics-based and conceptual models.

All models that are based on the conservation of mass and momentum equations in channels, e.g. St. Venant equations (Chow, et. al., 1988), are physics-based models. They are defined in terms of measurable parameters in principle. Conceptual models are developed by representing the actual complex hydrological system as a much simpler analogue model while retaining some of the physical laws (i.e. conservation of mass) and emphasising on the similarities in the most obvious properties of the actual and the analogue systems. The properties are usually represented explicitly by the model parameters which may be measurable.

B) Stochastic models describe the hydrological time series of the several measured

variables such as rainfall, evaporation and stream flow involving distribution in probability. This type of models are also referred to as statistical models or empirical models.

Despite the distinct differences, there is an overlap between the deterministic and stochastic models, which may be collected into the category of black-box models. Black-box models includes the Auto-Regression and Moving Average (ARMA) type of models (Box and Jenkins, 1976) which essentially are developed based on the principle of 'let the data speak for themselves'. They heavily relay on the input-output relationship. Their model parameters do not have explicit physical meanings, consequently are not measurable.

Both the deterministic and stochastic models may be static/dynamic, linear/nonlinear, and lumped/distributed:

- ***Static***, the parameters of model are time-invariant;
- ***Dynamic***, the model parameters are time-variant;
- ***Linear***, the output levels will not change for a same input;
- ***Nonlinear***, the output levels are not constant for a same input;
- ***Lumped***, the model assumes that the represented system is homogeneous in both the interactions with the outside world and its internal properties.
- ***Distributed***, either the interactions or the system's internal properties are considered as heterogeneous.

Figure 5.1 illustrates the above classifications.

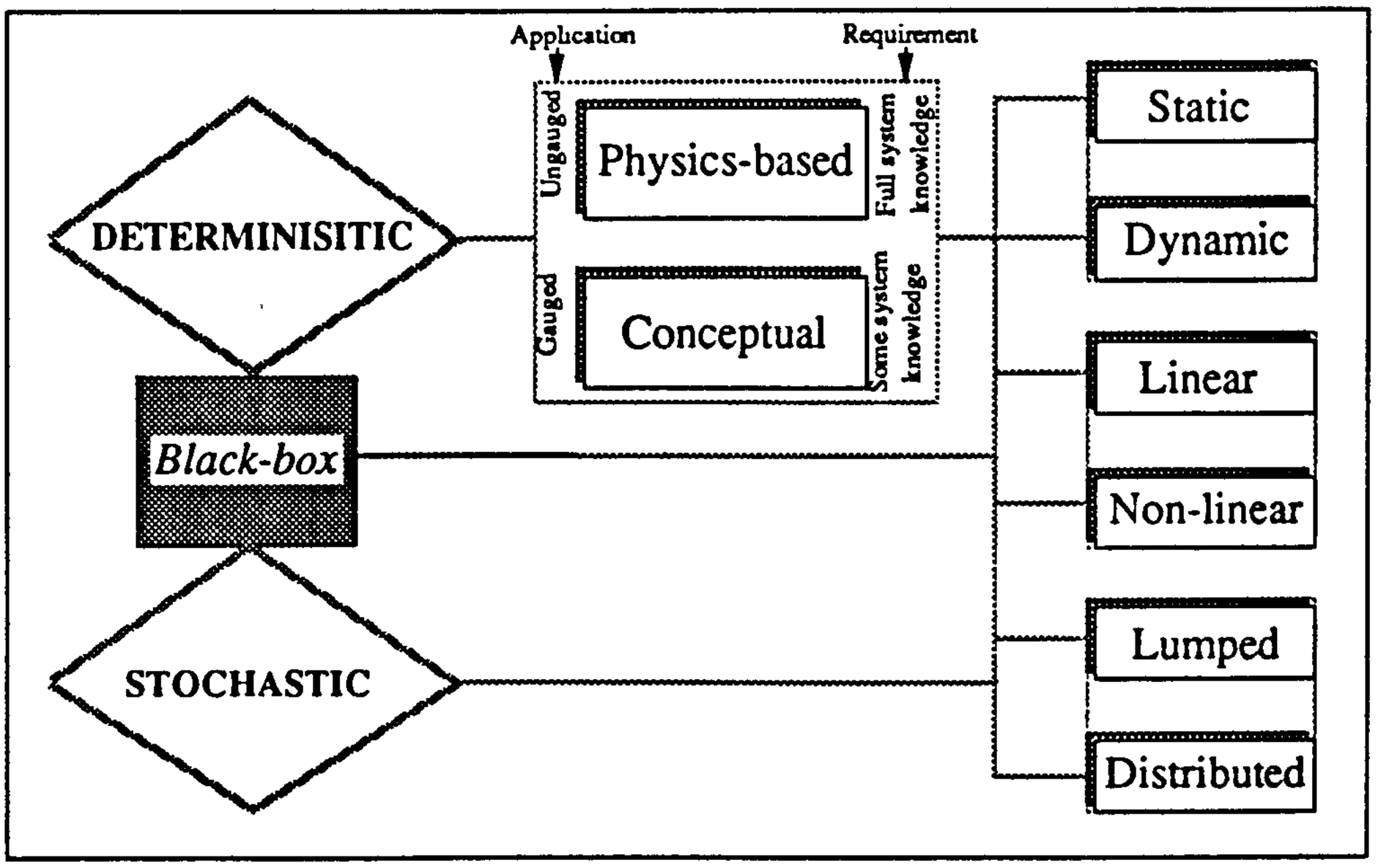

Fig. 5.1 Model Classification

A large number of models developed before 1975 have been well summarised by G. Fleming (1975). The outlines of some more recent models can be found from (Shaw, 1983), (Bedient, 1988) and (Ward and Robinson, 1990). The physically based distribution models that treat the catchment as a spatially variable system are intrinsically better and have significant theoretical advantages that make them more useful. However, these models are both complex and costly. In practice, there are major problems with the representation of the subsurface process and therefore must be treated with caution. In contrast, conceptual models are an appropriate tool for many purposes. Methods of linear analysis provide a unique, though simplified, representation of catchment response and have been extensively used for regional analysis. Concern regarding the predicative capability of black-box models suggests their use in short term prediction. Wheater (1993) suggests that appropriate use of models should seek to take advantage of these strengths and minimise the weakness, for example through hybrid modelling approaches.

5.1.3 Criteria for an Adequate Real-time Model

Successful real-time flow estimation or forecast depends on many interrelated activities. However, an adequate model will certainly benefit the UDS controls. The main objective of real-time forecasting is to detect the future excess of a predetermined threshold with a sufficient lead time to allow the issue of a control instruction. The achievement of this objective is the criteria of an adequate real-time model.

The primary considerations in the development of the CPTF model are those suggested by Dobson (1993):

- *Simple in structure with few data requirements*
- *Flexible to a wide range of catchment conditions*
- *Unconditionally stable and physically realisable*
- *Robust in case of data error*
- *Resilient to missing data*
- *Rapid in execution*
- *Simple in calibration and upgrading*

These considerations are important for ensuring adequate performance of the model. Physically realisable means the pulse-response of the model can be physically observed or have no reason to be unrealisable.

5.2 Development of the CPTF Model

The CPTF model by nature falls in the category of lumped, dynamic, linear and conceptual models though its structure takes the form of a non-conceptual transfer function model. It has three most distinguishable characteristics:

- *Conceptual parameters*
- *Hybrid structure*
- *Physically realisable pulse response*
- *High adaptability*

CPTF model is developed based on Dynamic Linear Reservoir (DLR) theory and attempts to transform radar measured rainfall or telemetered inflow into outflow. To understand its philosophy and structure, two distinctive linear system approaches (i.e. non-conceptual and conceptual) to the modelling of a hydrological system are described.

5.2.1 Non-conceptual Linear System Approach

There are several questions which may be raised in relation to the modelling of UDSs. Should the modelling be based on a literal pipe by pipe approach, that is, a distributed model? In this case each pipe needs to be considered and analysed. On the other hand, can a system be modelled using fewer sensors and using lumped models for their simplicity and minimal data requirements? To avoid trivial argument, in this study, it is assumed that a system can be decomposed into a number of subsystems having relatively uniform characteristics or significance so that each may be feasibly and effectively modelled by a transfer function model.

Under the above assumption, an urban drainage system is defined as a network consisting of interconnected natural and artificial channels which accepts single time-series input and produces single time-series output (i.e. can be represented by a TF model). It should be nonproductive or can be made nonproductive by decomposition. Here nonproductive means no flow is generated within the system but is input from the external world. If only storm runoff or domestic/effluent waste water is conveyed at

any time then the system is called a separated system otherwise, a combined system. In the real world, both of the systems may have either a single input-output relationship or multiple input-output relationships. In order to be modelled by a TF model, it is assumed that the multiple input-output relationships can be simplified into a single input-output relationship by either model clustering and cascading or by spatial lumping of the inputs and outputs as the case shown in Figure 5.2, where the system's inputs have been spatially lumped.

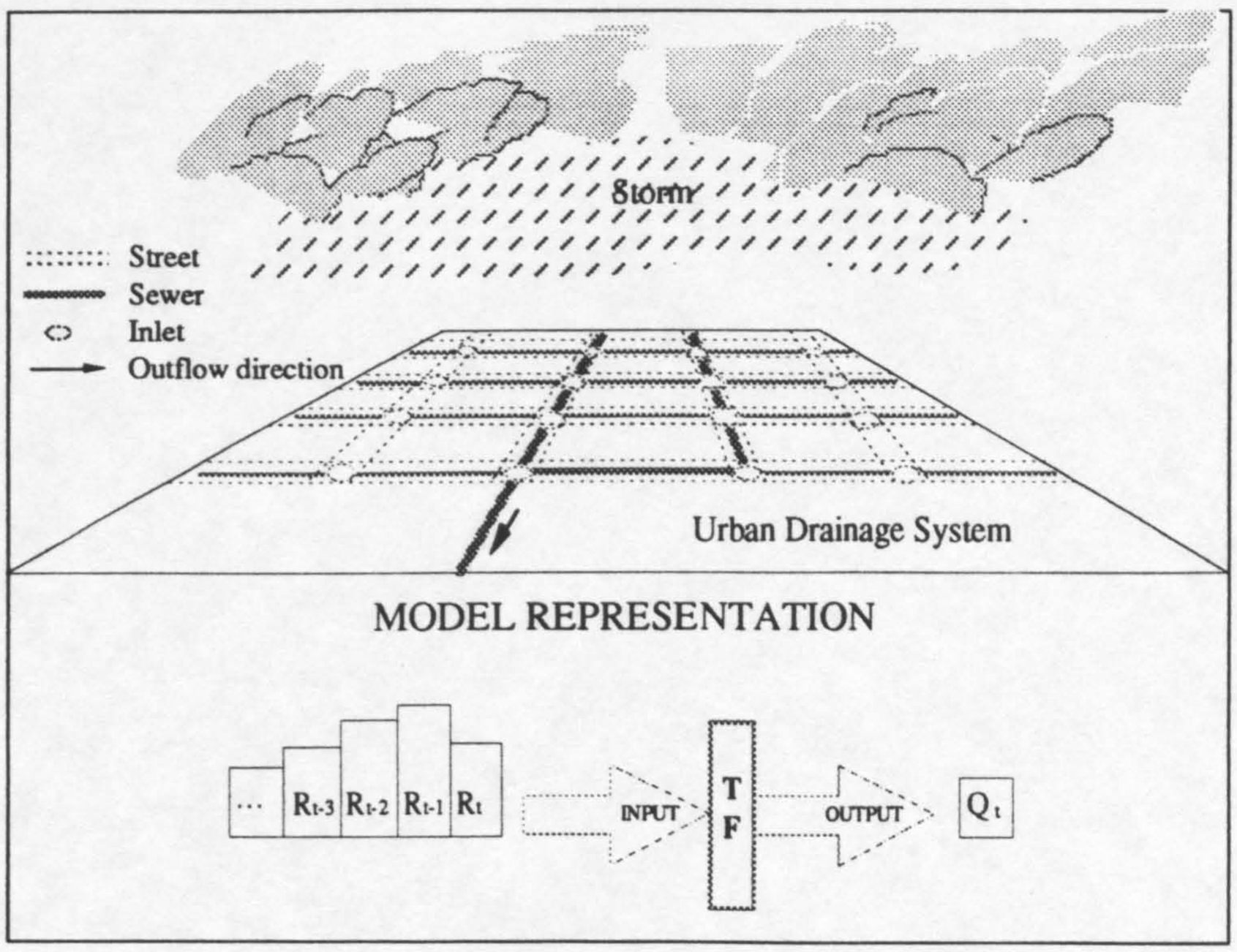

Fig. 5.2 Model representation of a UDS

Urban drainage systems are nonlinear and continuous systems. The continuous observations of inputs and outputs of a system are referred to as continuous realisations of the system. By realisation, it means a sequence of observed data points ordered with respect to time, and not just a single observation. Each sequence is called a time series. Successive observations of a time series are usually expected to be

dependent. Indeed, it is this dependency from one time period to another which makes reliable predictions possible. If a time series is not continuous, it is called a discrete realisation of the system. The order of an observation is denoted by a subscript *t*. For example, R(t) denotes the *t*th observation of a continuous time series and R_t, a discrete time series. The preceding observation is denoted by R(t-1) or R_{t-1} and the next observation as R(t+1) or R_{t+1}. The objective of data discretisation is to enable digital analysis of the system and approximation by an observable discrete linear model that has similar properties to those of the system itself.

O'Donnell (1983) classified a system as linear if its overall behaviour can be described by a linear differential equation:

$$A_n \frac{d^n Q}{dt^n} + A_{n-1} \frac{d^{n-1} Q}{dt^{n-1}} + \cdots + A_1 \frac{dQ}{dt} + Q = R \qquad (5.1)$$

Where R is the system input

Q is the system output

A_i, i =1, 2, ···, n, are coefficients.

If Q or any differential of Q is raised to a power other than one, the system is non-linear. If the coefficients A_i are constants then the linear system is static (i.e. time invariant), otherwise the linear system is said to be dynamic (i.e. time variant). It is easy to understand the concepts of static and dynamic. However, linearity and nonlinearity deserve a further explanation. Linearity can also be described as additivity. If the input level is multiplied by a constant and the output level in response to it is multiplied by the same constant, then the system is linear otherwise it is nonlinear. In hydrological practice, the assumption that a UDS is linear is probably never quite true because the percentage runoff factor varies with time, but it supplies a useful approximation.

Corresponding to the continuous representation in Eq.(5.1), a general discrete linear model form for a pulsed input, is the difference equation:

$$Q_t = \eta \frac{1 + \delta_1 \nabla + \delta_2 \nabla^2 + \cdots + \delta_s \nabla^s}{1 + \varsigma_1 \nabla + \varsigma_2 \nabla^2 + \cdots + \varsigma_r \nabla^r} R_{t-(\Delta-1)} \qquad (5.2)$$

Where Δ-1 is the lag time and η is the steady state gain factor or percentage runoff factor. If η is constant then the system is linear otherwise it is nonlinear. In order to distinguish it from the other transfer function models, especially the CPTF, Eq.(5.2) is referred to as the non-conceptual transfer function model (NCTF) of order (r, s) and may be denoted as NCTF(r, s), NCTF is essentially physics based model. Non-conceptual Linear System Approach utilising the NCTF models to represent the input-output relationships.

5.2.2 Conceptual Linear System Approach

Conceptual modelling bridges the gap between the physics-based and black-box approaches. In essence, the conceptual approach strives for the definition of functional relations between hydrological and geometrical and land use characteristics of a drainage system. The most important stages involved in the modelling approach are model formulation and identification. It frequently happens that, to an adequate approximation, the inertia of the system can be represented by a linear filter of the form:

$$\begin{aligned} Q_t &= \sum_{u=1}^{M} h(u) R_{t-u+1} \\ &= h(1)R_t + h(2)R_{t-1} + h(3)R_{t-2} + \cdots + h(M)R_{t-M+1} \\ &= [h(1) + h(2)\mathbf{B} + h(3)\mathbf{B}^2 + \cdots + h(M)\mathbf{B}^{M-1}]R_t \\ &= \partial(\mathbf{B})R_t \end{aligned} \qquad (5.3)$$

where **B** is a back-shifting operator, for instance, $\mathbf{B}R_t = R_{t-1}$. The function h(u), u=1, 2, 3, ···, M, is called the Pulse Response (PR) of the system (Chow, 1988) and here M is the memory length, physically, it is the maximum number of rainfalls contributing to the outflow of each time step at the system outlet, the larger a system, the longer the memory length. When there is no immediate response, one or more of the initial values of h(u) will be equal to zero. For instance, if h(1) = 0, then the lag time (Δ-1) is 1 time step. The operator function $\partial(\mathbf{B})$ is called the transfer function of the system. Eq.(5.3) is essentially an equivalent form of the model in Eq.(5.2).

The PR function of the system, h(u), can be conceptually parametrised. In the simplest case, assuming that the system behaves like a linear storage reservoir and its storage volume is proportional to its output flow rate (m^3/s):

$$S(t) = \tau Q(t) \tag{5.4}$$

where τ is a constant and governs the storage relaxation speed. It may be called a static storage factor. Mass balance states that the rate of storage change is equal to the difference between R(t) (mm/h) and Q(t):

$$\frac{dS}{dt} = \varepsilon \rho A' R(t) - Q(t) \tag{5.5}$$

where S is the storage volume in m^3;

ρ is the percentage runoff over a unit area;

A' is the catchment area in km^2;

ε is a constant (= 5/18) used to bring the unit of input to m^3/s;

Substitute Eq.(5.4) into Eq.(5.5) we obtain:

$$\frac{dQ}{dt} = \frac{1}{\tau}[\eta R(t) - Q(t)] \tag{5.6}$$

where η is equal to $\varepsilon\rho A$. It is possible to show that the approximate solution of Eq.(5.6) in discrete form with a pulsed input is Eq.(5.3) (Chow, 1988). For this system, the PR function is:

$$h(u) = (\eta/\tau)e^{-u/\tau} \qquad u = 0, 1, 2, 3, \cdots, M \tag{5.7}$$

This PR is denoted as PR-A. It implicitly assumes that the system storage level decays exponentially and asymptotically approaches to zero. This could be never quite true for the drainage system whereby the PR is determined by the system input level and characteristics such as geometric shape, slope, size, roughness, permeability, homogeneity and so on. A more reasonable model is the generalised Nash model:

$$h(u) = \begin{cases} \dfrac{\eta(u-\Delta+1)^{n-1}}{\tau^n \Gamma(n)} e^{-(u-\Delta+1)/\tau}; & u \geq \Delta \\ 0 \qquad\qquad\qquad\qquad\qquad\quad ; & u < \Delta \end{cases} \tag{5.8}$$

where $\Gamma(n) = (n-1)!$ for $n = 1, 2, 3, \cdots$;

η is the steady state gain or percentage runoff factor;

n is the number of linear storage reservoirs;

τ is the static storage factor;

Δ-1 is the lag time.

The Nash model (Nash, 1957) was derived by routing a lumped unit pulse input through *n* number of homogeneous linear reservoirs with Eq.(5.7). It is an analogue to the Gamma PDF in probability theory. For convenience Eq.(5.8) is referred to as

PR-B. Note the accumulation of PR-B from 0 to infinity is equal to η rather than 1. Its time-to-peak is at: $u = (n-1)\tau+\Delta-1$.

Many input-output relationships can be well approximated by PR-B. An example was shown in Figure 5.3, where the simulated PR is seen as a smoothed representation of the observed PR.

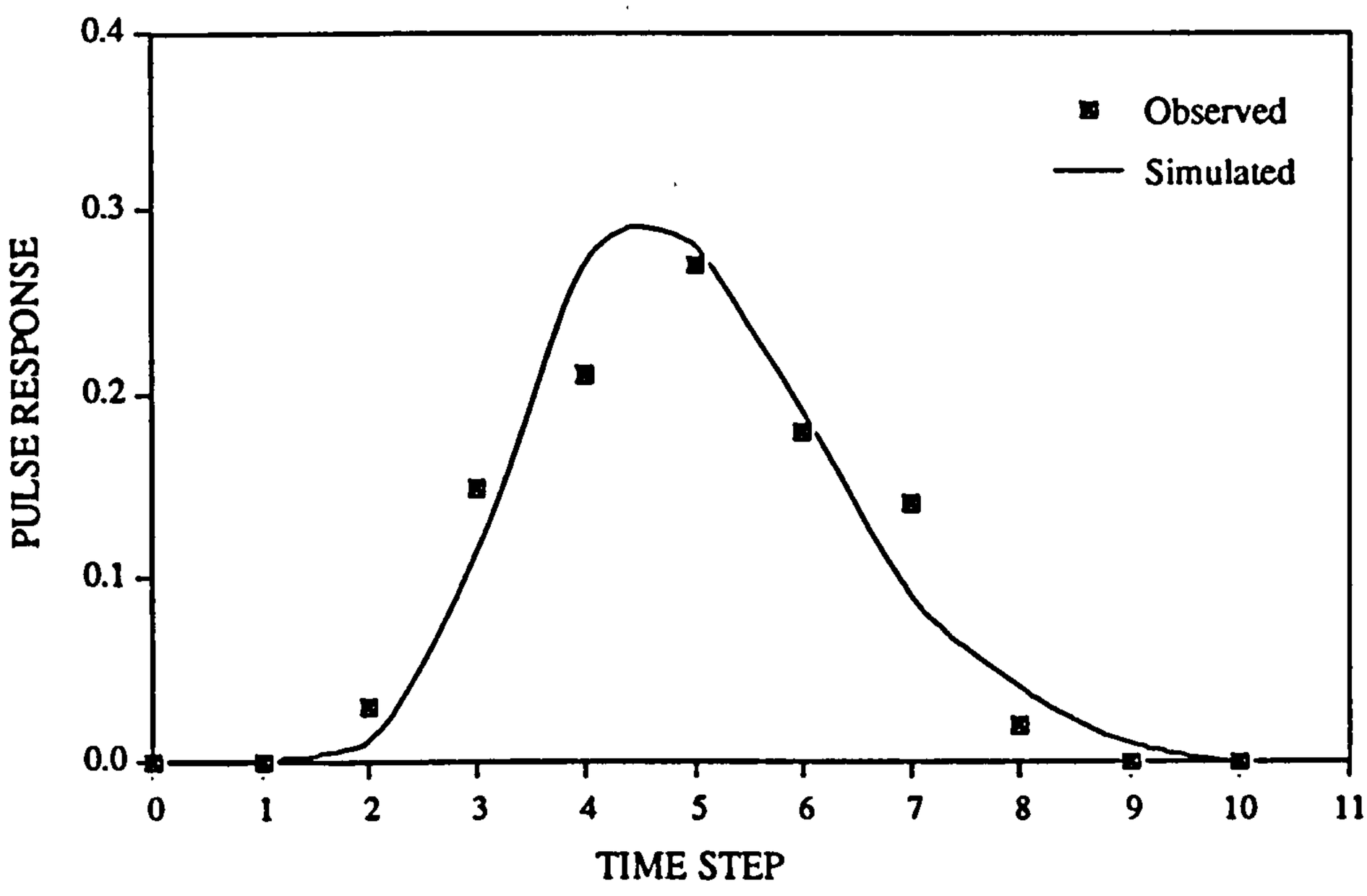

Fig. 5.3 Simulation of an observed PR by PR-B

However, due to the inadequate representation of a linear reservoir by assuming that the storage factor τ is time invariant, many PRs with a dynamic storage factor are unable to be appropriately represented by PR-B. To mitigate against this shortcoming, a hydrological system may be assumed to behave like a dynamic linear reservoir, which is defined as:

$$\frac{dS}{dt} = A_1(t)\frac{dQ}{dt} \tag{5.9}$$

Eq.(5.9) states that, the rate of storage change is proportional to that of the outflow however the proportion factor is a function of time rather than a constant. Where $A_1(t)$ is introduced to portray the dynamic characteristics of the storage decay mainly resulted from the variation of hydraulic gradient, outflow cross-area and system friction coefficient with time. It may be defined as:

$$A_1(t) = \tau t^{1-\alpha} \tag{5.10}$$

Where α is a new dimensionless parameter and its physical meaning will be given later. The relation between $A_1(t)$ and α is shown in Figure 5.4.

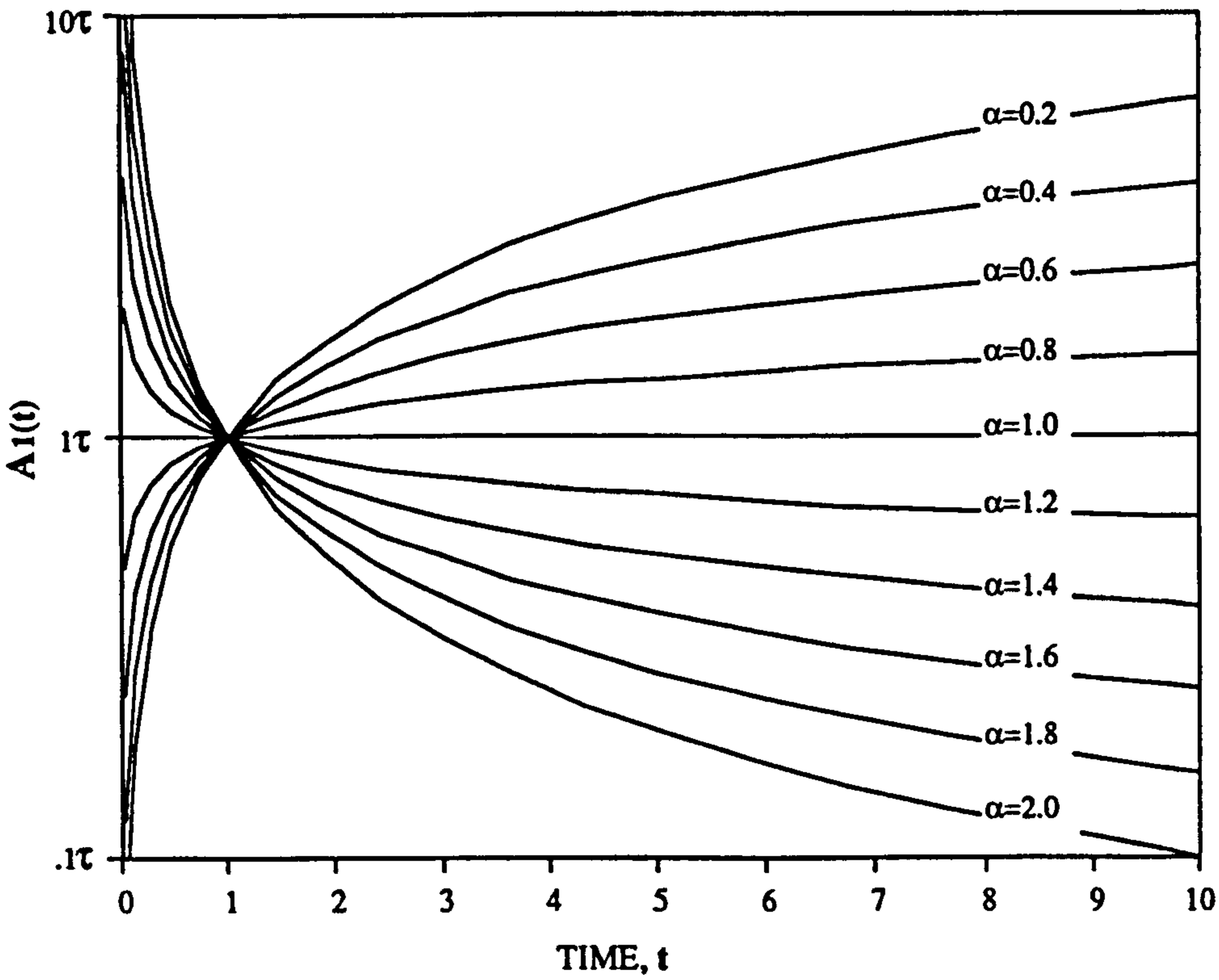

Fig. 5.4 The variation of $A_1(t)$ with time and the parameter α

From the figure it is seen that $A_1(t)$ increases as the time increases when α is less than 1, and decreases when α is greater than 1. While α is equal to 1, $A_1(t) = \tau$ and

Eq.(5.9) becomes Eq.(5.5). Therefore, a static system can be treated as a special case of the dynamic system. Since $A_1(t)$ depicts a dynamic system, it is referred to as the dynamic storage factor. To keep the dimensions at the left-hand and right-hand side of Eq.(5.9) same, it is necessary to change the dimension of τ into $[T]^{\alpha}$ from its previous definition [T] (i.e.the dimension of time).

Inserting Eq.(5.5) and Eq.(5.10) into Eq.(5.9) we obtain:

$$\frac{dQ}{dt} = \frac{1}{\tau} t^{\alpha-1}[\eta R(t) - Q(t)] \tag{5.11}$$

By comparing Eq.(5.11) with Eq.(5.6), the meaning of parameter α becomes clear. It indicates the stability of the system physical structure (i.e. the basin magnitude, the mean length of interior channel links and the velocity of flow translation). Consequently, may be referred to as a stability factor.

Knowing Q(0)=0, for a constant input, R, the solution of Eq.(5.11) is of the form:

$$Q(t) = \eta R[1 - e^{-t^{\alpha}/(\alpha\tau)}] \tag{5.12}$$

This is the discharge from the dynamic linear reservoir under a consistent input. For a unit pulse input which terminates immediately after being applied, Eq.(5.12) becomes:

$$H(t) = \frac{\eta t^{\alpha-1}}{\tau} e^{-t^{\alpha}/(\alpha\tau)} \tag{5.13}$$

Eq.(5.13) is the PR function of the dynamic linear reservoir because convoluting it with a constant R can yield Eq.(5.12). This PR is an analogue to the Weibull PDF, which can more flexibly represent the storage effect of one linear reservoir than Eq.(5.7). However, when the system is large, Eq.(5.13) could be more or less

inadequate as the system outflow at a time step is not determined by one local storage reservoir but by a number of cascaded contributing elements.

If *n* number of isochrones could be drawn to represent the time required for each local element of rainfall bounded by two adjacent isochrones to reach the system outlet, then the system can be treated as *n* number of cascaded dynamic linear reservoirs. The resultant discharge is proportional to t^x and H(t) because the cumulation of contribution area is proportional to t^x. In other words, the discharge is defined by the combined effect of storage and routing (Edson, 1951, Nash, 1957):

$$h(t) = F\,H(t)\,t^x \tag{5.14}$$

Where F and x are coefficients. Since the integration of h(t) over the range from 0 to infinity must be equal to the percentage runoff η, it appears that:

$$F = \frac{\eta}{\int_0^{\infty} H(t)t^x dt} \tag{5.15}$$

To facilitate the integration, let $x = \alpha(n\text{-}1)$ and $t^{\alpha} = \alpha\tau z$, then

$$\int_0^{\infty} H(t)t^x dt = \eta\int_0^{\infty} (\alpha\tau z)^{n-1}e^{-z}dz = \eta(\alpha\tau)^{n-1}\Gamma(n) \tag{5.16}$$

Thus,

$$F = \frac{1}{(\alpha\tau)^{n-1}\Gamma(n)} \tag{5.17}$$

Inserting F and Eq.(5.13) into Eq.(5.14) we get:

$$h(t) = \frac{\eta\alpha t^{n\alpha-1}}{(\alpha\tau)^n \Gamma(n)} e^{-t^\alpha/(\alpha\tau)} \tag{5.18}$$

This PR is an analogue to the GW PDF (see Chapter 4). Similar to PR-B, Eq.(5.18) can be made more flexible by incorporation of the lag time:

$$h(u) = \frac{\eta\alpha(u-\Delta+1)^{n\alpha-1}}{\tau^n \Gamma(n)} e^{-(u-\Delta+1)^\alpha/\tau} \tag{5.19}$$

Where τ is equivalent to $\alpha\tau$ used in Eq.(5.18) and t has been changed back to its original notation, u.

Eq.(5.19) is the desired PR function. For convenience it is referred to as PR-C. Figure 5.5 shows the characteristics of PR-C varies with its parameters. From the figure it is seen that parameter:

η	proportionally changes the amplitude of h(u) at each time point;
n	mainly determines the peak, time to peak and shape of the rising limb;
τ	mainly portrays the peak, time to peak and shape of the recession limb;
Δ-1	defines the lag time or when the PR starts to rise;
α	plays a combined role of the parameter n and τ.

The moments of PR-C around its origin have been given in Appendix-I, and the other properties of PR-C are:

1) Time to peak position, U_p:

$$U_p = [\tau(n-1/\alpha)]^{1/\alpha} + \Delta - 1, \quad \text{where } U_p \geq \Delta - 1 \tag{5.20}$$

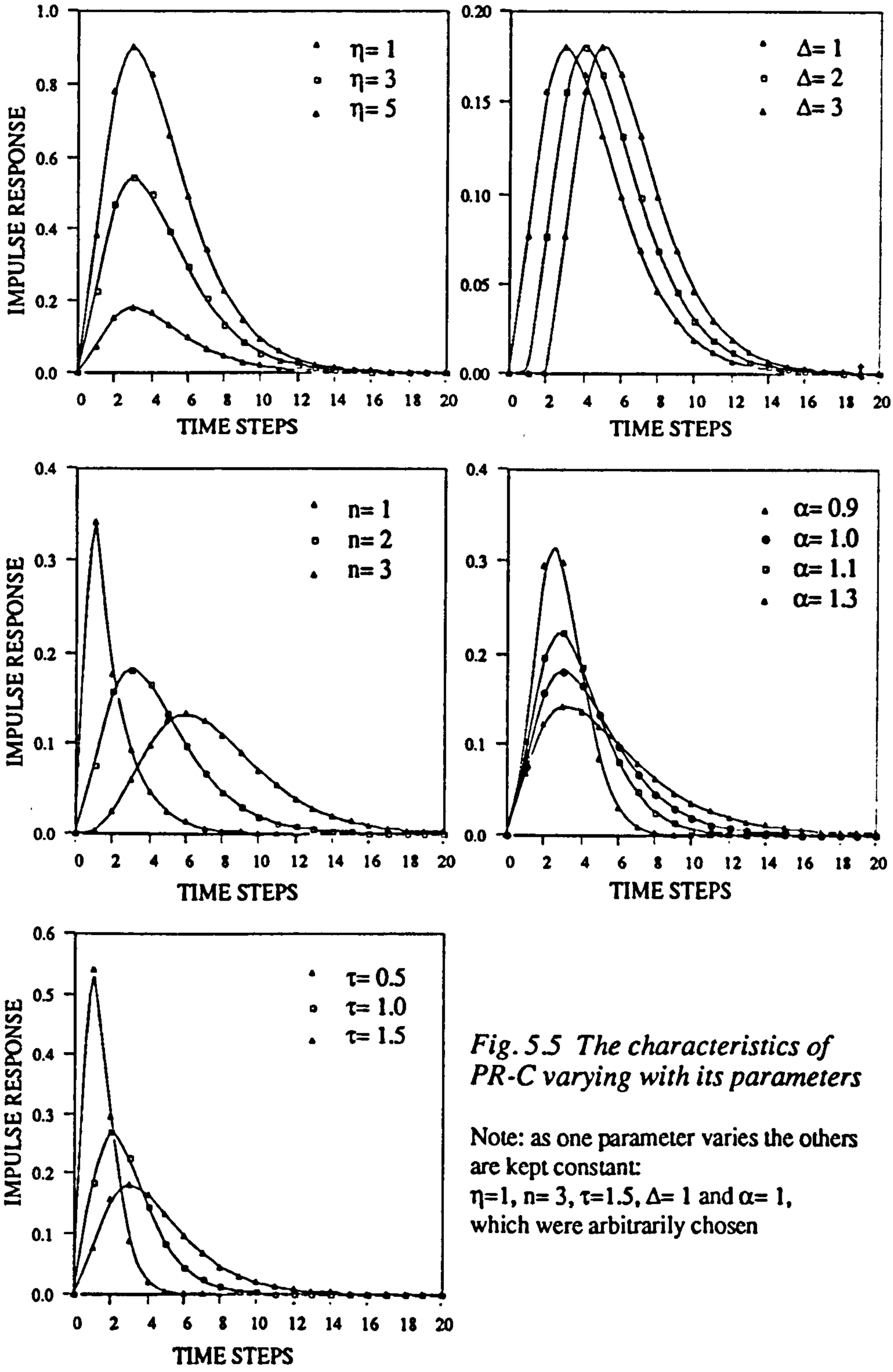

Fig. 5.5 The characteristics of PR-C varying with its parameters

Note: as one parameter varies the others are kept constant:
η=1, n= 3, τ=1.5, Δ= 1 and α= 1, which were arbitrarily chosen

2) The inflection point, U_i:

$$U_i = \left\{\frac{\tau}{2\alpha}\left[2\alpha n + \alpha - 3 + \sqrt{\alpha^2(4n+1) - 6\alpha + 1}\right]\right\}^{\frac{1}{\alpha}} + \Delta - 1, \quad U_i \geq U_p \tag{5.21}$$

As U_p must be greater than or equal to Δ-1, α need not to be less than 1/n. In general, the valid range for each of the PR parameters is:

Percentage runoff:	$\eta \geq 0$
Number of isochrones:	$n \geq 1$ (decimal or integer)
Static storage factor:	$\tau > 0$
Lag time:	$\Delta\text{-}1 \geq 0$
Stability factor:	$\alpha \geq 1/n$

Note, if α is equal to 1/n, then the resultant PR will be a lagged exponential decay.

The validity of PR-C lies in the observation that:

1) Drainage systems can be assumed as behaving like linear storage reservoirs;

2) The same change in the system storage occurring at different times may not necessarily result in the same change in the outflow or vice versa due to the temporal variations in the storage factor. Bras (1990, page 396) states that: 'in fact, the storage factor is rarely a constant throughout the whole recession and may vary with season and soil moisture condition';

3) In addition to the special cases which have been spotted by Edson (1951), Nash (1957), Dooge (1959), Gray (1961, 1973), Diskin (1964), W. O. Maddaus and P. E. Eagleson (1969), another interesting special case of PR-C was found by Karlinger and

Troutman in 1985 through a totally different approach, which strongly support the validity of PR-C. Karlinger-Troutman's asymptotic PR function was parametrised based on the basin magnitude, the mean length of interior stream links and the velocity of translation:

$$h(u)=\frac{u}{2\vartheta(\ell/v)^2}e^{-\frac{u^2}{4\vartheta(\ell/v)^2}} \tag{5.22}$$

Which can be related to the PR-C by $\eta = 1$, $n = 1$, $\tau = 4\vartheta(\ell/v)^2$, $\Delta = 1$ and $\alpha = 2$. Where, ϑ is the basin magnitude, ℓ, the mean length of interior stream links and v, the velocity of flow translation. Note this model also provided a physics-based representation of the static storage factor, τ. In addition, a similar PR function to Eq.(5.22) has been proposed by Lienhard in 1964:

$$p(t)=\frac{2t^{2n-1}}{\tau^n\Gamma(n)}e^{-t^2/\tau}$$

The number of ways in which a raindrop could find its way to the gauging station after time t is proportional to t^{n-1}.

4) A PR function is defined by the combined effects of storage and routing (Edson, 1951 and Nash, 1957).

These facts manifest that PR-C is a valid and general conceptual PR function. The model has significant theoretical advantages that make it more useful. Further improvement is possible by introducing more parameters and another two alternative PR functions of the DLR have been presented in Appendix-II.

By substituting PR-C into Eq.(5.3) with the memory length, M, taking an adequately large integer so that the sum of the remainder of h(u), u = M+1, M + 2,

$\cdots$, is negligible, a deterministic (no random component) model can be formed. The model is a simplest representation of a relationship between the pulse input R_t and output Q_t. Note, where the model input data resolution is 1 unit time step. Otherwise, Eq.(5.3) can be rewritten into:

$$Q_t = \sum_{u=1}^{M}\left[h(u) \sum_{i=(u-1)\chi}^{u\chi-1} R_{t-i} \right] \quad ; \quad t = 1, 2, 3, \cdots \tag{5.23}$$

This model allows one to study the effect of data resolution on the modelling accuracy. Where χ ($\geq$1) is the discretising time interval of the model input in steps, and h(u) is a χ–step PR function. If χ is equal to 1 then the input data resolution is identical to the system discretising resolution. For different input data resolutions, the PR will be different and correspondingly, will yield a different modelling accuracy. The input time series arises by summing or aggregating the original time series over a predetermined time interval, χ, hence is an averaged discrete series. Because the averaged series is smoother than the original system realisation, this means the output is generated by filtering a pre-smoothed data series. For example, if χ=2, then the output will be $Q_1 = h(1)R_1$, $Q_2 = h(1)(R_2+R_1)$, $Q_3 = h(1)(R_3+R_2)+h(2)R_1$, $\cdots$. Physically, this is similar to what is happening in a telemetered gauging system (Powell, 1985). While using a smoothed input data series a direct benefit is that random errors contained in the original data may be eliminated to some extent so that a more accurate outcome can be obtained. Providing χ is not larger than a permitted value the incorporation of χ into the model should not result in an intolerable modelling error. A rule for determination of a suitable input data resolution will be discussed in Chapter 8. For convenience of description, Eq.(5.23) is referred to as the Naive CPTF model. This model is not an empirical model because its parameters are uniquely defined by PR-C. It can be identified through a PR-to-CPTF approach.

The Naive CPTF model has a weak point, the measured flow is not able to be fed back. Consequently, it is unable to use the state-updating technique to enhance its performance in real-time. To overcome this shortcoming, a more flexible and advanced CPTF model is derived by hybridising PR-C with the structure of the NCTF models.

5.2.3 Hybrid Linear System Approach

The Naive CPTF model has the advantages of conceptual explainability of its parameters and is easy to be identified. Unfortunately, it lacks the state-updating capability. As NCTF models are efficiently structured and naturally suitable for state-updating in real-time (Harpin, 1982, Reed, 1984), a better real-time model may be developed by hybridising the advantages of the two models.

Rewriting the NCTF model in Eq.(5.2) in terms of the backward shift operator, $B = 1-\nabla$ as:

$$Q_t = \frac{\zeta_0 B^{\Delta-1} - \sum_{u=1}^{s} \zeta_u B^u B^{\Delta-1}}{1 - \sum_{u=1}^{r} \Theta_u B^u} R_t \qquad (5.24)$$

Where Θ_u and ζ_u will be referred to as the model parameters, which are different from the PR parameters.

Since $Q(t) = \sum_{u=1}^{M} h(u) B^{u-1} R_t$, we have

$$\left[\zeta_0 - \sum_{u=1}^{s} \zeta_u B^u\right] B^{\Delta-1} = \left[\sum_{u=1}^{M} h(u) B^{u-1}\right]\left[1 - \sum_{u=1}^{r} \Theta_u B^u\right] \qquad (5.25)$$

On equating coefficients of B, it is found that

$$\zeta_0 = h(\Delta) \tag{5.26}$$

$$\begin{bmatrix}\zeta_1\\ \zeta_2\\ \vdots\\ \zeta_s\end{bmatrix} = \begin{bmatrix}h_\Delta & h_{\Delta-1} & \cdots & h_{\Delta+1-r}\\ h_{\Delta+1} & h_\Delta & \cdots & h_{\Delta+2-r}\\ \vdots & \vdots & \cdots & \vdots\\ h_{\Omega-1} & h_{\Omega-2} & \cdots & h_{\Omega-r}\end{bmatrix} \times \begin{bmatrix}\Theta_1\\ \Theta_2\\ \vdots\\ \Theta_r\end{bmatrix} - \begin{bmatrix}h_{\Delta+1}\\ h_{\Delta+2}\\ \vdots\\ h_\Omega\end{bmatrix} \tag{5.27}$$

$$\begin{bmatrix}\Theta_1\\ \Theta_2\\ \vdots\\ \Theta_r\end{bmatrix} = \begin{bmatrix}h_\Omega & h_{\Omega-1} & \cdots & h_{\Omega-r+1}\\ h_{\Omega+1} & h_\Omega & \cdots & h_{\Omega-r+2}\\ \vdots & \vdots & \cdots & \vdots\\ h_{\Omega+r-1} & h_{\Omega+r-2} & \cdots & h_\Omega\end{bmatrix}^{-1} \times \begin{bmatrix}h_{\Omega+1}\\ h_{\Omega+2}\\ \vdots\\ h_{\Omega+r}\end{bmatrix} \tag{5.28}$$

where $\Omega = \Delta + s$ and h_u is same as h(u) in the matrix equations. Solving Eq.(5.28) need considerable efforts. Without biasing from the initial purpose, that is, to introduce state updating ability into the Naive CPTF model, the model order, *r*, is defaulted to be a value of 1. Thus the model becomes a first-order Markov process in which the current state only depends on one previous state. To ensure an adequate reproduction of the PR function, a sufficiently large *s* is required. The method for determination of *s*, will be discussed in the next chapter.

Substituting the estimated Θ_u, ζ_u into Eq.(5.24), the discharge at any time t (>0) can be calculated as:

$$Q_t = \Theta_1 Q_{t-1} + \zeta_0 R_{t-(\Delta-1)} - \sum_{u=1}^{s}\left[\zeta_u R_{t-u-(\Delta-1)}\right] \;;\; t = 1, 2, 3, \cdots \tag{5.29}$$

where the model input data resolution is at a unit time step. Otherwise, Eq.(5.29) can be rewritten into:

$$Q_t = \Theta_1 Q_{t-\chi} + \zeta_0 \sum_{i=(\Delta-1)\chi}^{\Delta\chi-1} R_{t-i} - \sum_{u=1}^{s}\left[\zeta_u \sum_{i=(u+\Delta-1)\chi}^{(u+\Delta)\chi-1} R_{t-i}\right] \quad ; \quad t = 1, 2, 3, \cdots \tag{5.30}$$

This equation defines an advanced CPTF model form.

5.3 Summary

A general conceptual pulse response function for a kind of dynamic linear system has been 'identified'. It is uniquely defined by the five PR parameters. Using the PR function, a conceptually parametrised transfer function (CPTF) model was developed, which has two forms. The Naive CPTF model is a linear filter type (i.e. similar to a IUH) whereas the Advanced CPTF model is a Markov Process. They are mutually transferable. The Naive CPTF model is suitable for parameter adaption and the Advanced CPTF model is ready for state updating. For convenience, a CPTF model is denoted as: CPTF (η, n, τ, Δ, α, χ).

The input data resolution of a CPTF model may be different from the system discretising resolution. A lower input data resolution can be obtained by averaging the data points over a larger time step before inputting into the model.

Finally, it is worth mentioning that, although the PR-C is a valid representation of a dynamic linear storage system, the representation may not be unique. For this reason two alternatives have been given in Appendix-II.

CHAPTER 6

IDENTIFICATION OF CPTF MODEL

A Naive CPTF has M, and an Advanced CPTF model has s+1 number of model parameters (see Chapter 5). These parameters all can be derived from the same pulse response function which is uniquely defined by the five PR parameters. The procedure involved in the determination of the PR parameters is referred to as the identification of the CPTF model. The major considerations in development of the procedure were:

- *Fast in computation;*
- *Robust to data noise and*
- *Simple for application.*

While aiming for model identification and updating in real-time the identification procedure has to be fast in computation. This requires the identification method must be simple and robust. The robustness means that a model should be always identifiable and updatable within a noisy environment.

Genetic Algorithms (Lawrence, 1991) were found quite satisfactory in achieving these criteria when compared with the conventional least-square methods. Therefore, it is has been incorporated in the identification procedure. With this procedure, a CPTF model can always be identified and updated in real-time so long as an input and output

relationship is given.

6.1 Identification Procedure

The process of model identification is necessarily iterative, in other words, it should be a process of evolution, adaption, or trial and error. The identification procedure for a CPTF model is illustrated in Figure 6.1.

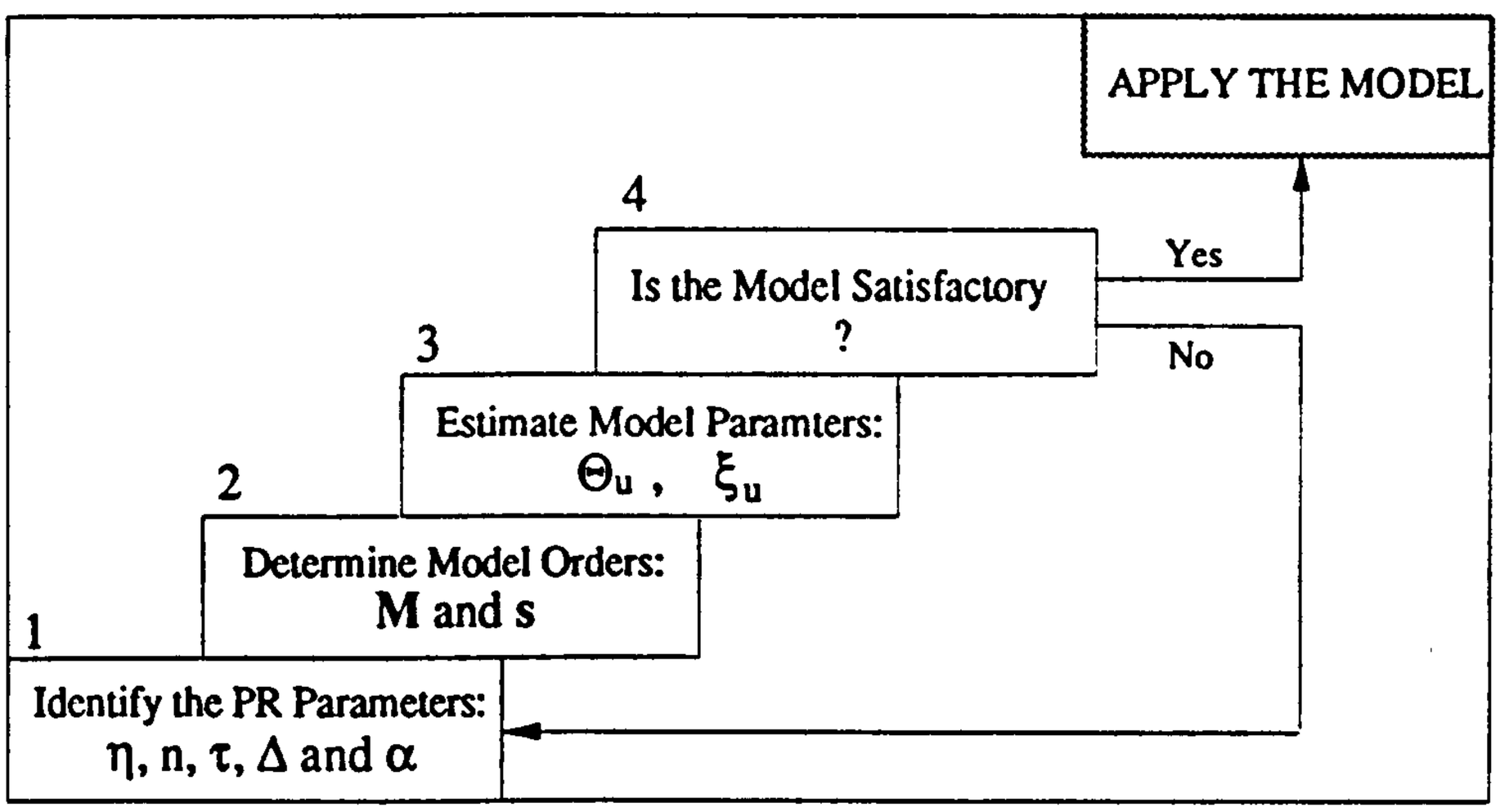

Fig. 6.1 Identification procedure for a CPTF model

Essentially, it is a two-step PR-to-CPTF procedure: 1) Identification of the five PR parameters: η, n, τ, Δ and α, and 2) Estimation of the model parameters: Θ_u and ζ_u. Clearly, for identification of a Naive CPTF model, only the first step is needed.

6.2 Identification of η, n, τ, Δ and α

The Genetic Algorithm plays a vital role in searching a set of satisfactory PR parameters. The PR function that can transform the given input into the required output and minimise the modelling errors is located at a point in five-dimensional

space, $\Xi(\eta, n, \tau, \Delta, \alpha)$. By searching the space, the expected PR parameters, and hence the PR function can be identified.

There are many other available techniques which can be employed to fulfil the searching task, such as the Rosenbrock (1960) 'hill-climbing' technique, dynamic programming, etc. However, the Genetic Algorithm was found to be more flexible, straightforward and satisfactory for implementation than the other methods.

Genetic Algorithms were invented by John Holland (1992) to mimic some of the processes observed in natural evolution. In the view of biological science, natural evolution takes place on chromosomes. A chromosome constitutes a number of genes which are arranged in a linear fashion, responsible for passing on specific properties from parents to offspring. A number of chromosomes make up a population.

Any perturbation of any gene within a chromosome will result in a new chromosome which in turn leads to character divergence of a living being. This is called evolution. Natural evolution is driven by the natural forces such as struggling for existence and natural selection. In order to adapt to the natural world, living beings have developed several techniques for changing their genes and improving their chromosomes, of which, gene copying, random mutation and cross-over of genes are the most important reproduction techniques. Some species only employed a single technique while other species adopt all, the more techniques employed the more chances of evolution. As a result the highly evolved and fittest species will dominant the natural world and those who are not fit to the environment will be eliminated. Based on this principle, a very effective algorithm can be devised for identification of the PR parameters.

Taking any of the five PR parameters, η, n, τ, Δ or α, in the space Ξ as a gene, then any point $[\eta_i, n_i, \tau_i, \Delta_i, \alpha_i]$, $i = 1, 2, 3, \cdots, N$, in Ξ is a chromosome which uniquely defines a PR function. For the sake of clarity, a chromosome will be also referred to

as a parameter vector. The N number of chromosomes make up a population. A chromosome in the population is called a member of the population and the total member number, N, is referred to as population size. Note, a population usually constitutes N members randomly selected from the space Ξ, and the population size is fixed throughout the entire evolution process which terminates at a specified time point. It is expected that by evolving a population, the desired best member can appear in the population. The Genetic Algorithm (GA) is a collective term of the three evolving techniques:

$$\text{GA} \rightarrow \begin{cases} \textit{Gene Copying} + \text{Random Mutation} \\ \textit{Gene Copying} + \text{Cross}-\text{over} \\ \textit{Gene Copying} + \text{Random Mutation} + \text{Cross}-\text{over} \end{cases}$$

To distinguish them from each other, the first is called Random-mutation Genetic Algorithm, the second, Cross-over Genetic Algorithm and the last, Comprehensive Genetic Algorithm. The Gene copying technique can only produce a children generation being identical to their parents generation, whereas both the random mutation and cross-over techniques can result in an evolution effect. Either of the three algorithms can be used to identify a set of desired PR parameters (i.e. chromosome or parameter vector), however, only the Random-mutation Genetic Algorithm and the Comprehensive Genetic Algorithm are recommended here.

6.2.1 Using the Random-mutation Genetic Algorithm

The basic idea is that, a randomly initialised population with a fixed size 1 (i.e. only one member) is evolved within a specified time period, e.g. 10 time units. First the genes of the parent member in the population are reproduced by gene copying. Then, by applying the random mutation technique on the reproduced genes, a child

chromosome with different characteristics from its parent is produced. If the parent is less fit to the given environment than its child then it is replaced by the child otherwise will stay in the population. Such a reproduction-evolution process cycles until the specified time limit is up then the parent member within the population is returned as the identified PR parameter vector. Using this parameter vector a PR-C, hence a Naive CPTF model can be derived. Because there is only one parent member in the population, it is unable to give birth to a children generation by cross-over. Each time only one child chromosome is produced. Evolution is made through the natural selection mechanism which is mimicked by a fitness function:

$$FF = \frac{\sum_{i=t-\delta}^{t}[Q_o(i) - Q_m(i)]^2}{\sum_{i=t-\delta}^{t}[Q_o(i)]^2} \qquad (6.1)$$

Where FF is the dimensionless Fitness Factor

Q_o is the observed time series of flow;

Q_m is the model output time series;

t is an arbitrary time point (e.g. time of forecasting)

δ is an arbitrary time interval.

The fitness factor measures the performance of a candidate CPTF model, hence the identified parameter vector. Eq.(6.1) tries to measure the fitting error as a ratio over the observed flow accumulation during the period from t-δ to t. It is devised to allow different fitness values to be compared regardless of the amplitude of the observed flows. If the fitting is perfect then FF will be zero. By minimising FF, a given time series can be optimally fitted. If *t* and δ are equal to the event duration, then a single PR will be identified, which functions throughout the entire event. Otherwise, multiple PRs are identified, which are attempted to segmentally fit the observed flow series. Q_m can be calculated by convolution of the model input with the PR function

estimated using the identified PR parameter vector.

This algorithm is illustrated in Figure 6.2 and a numerical example illustrating the approach is given in Appendix-III.

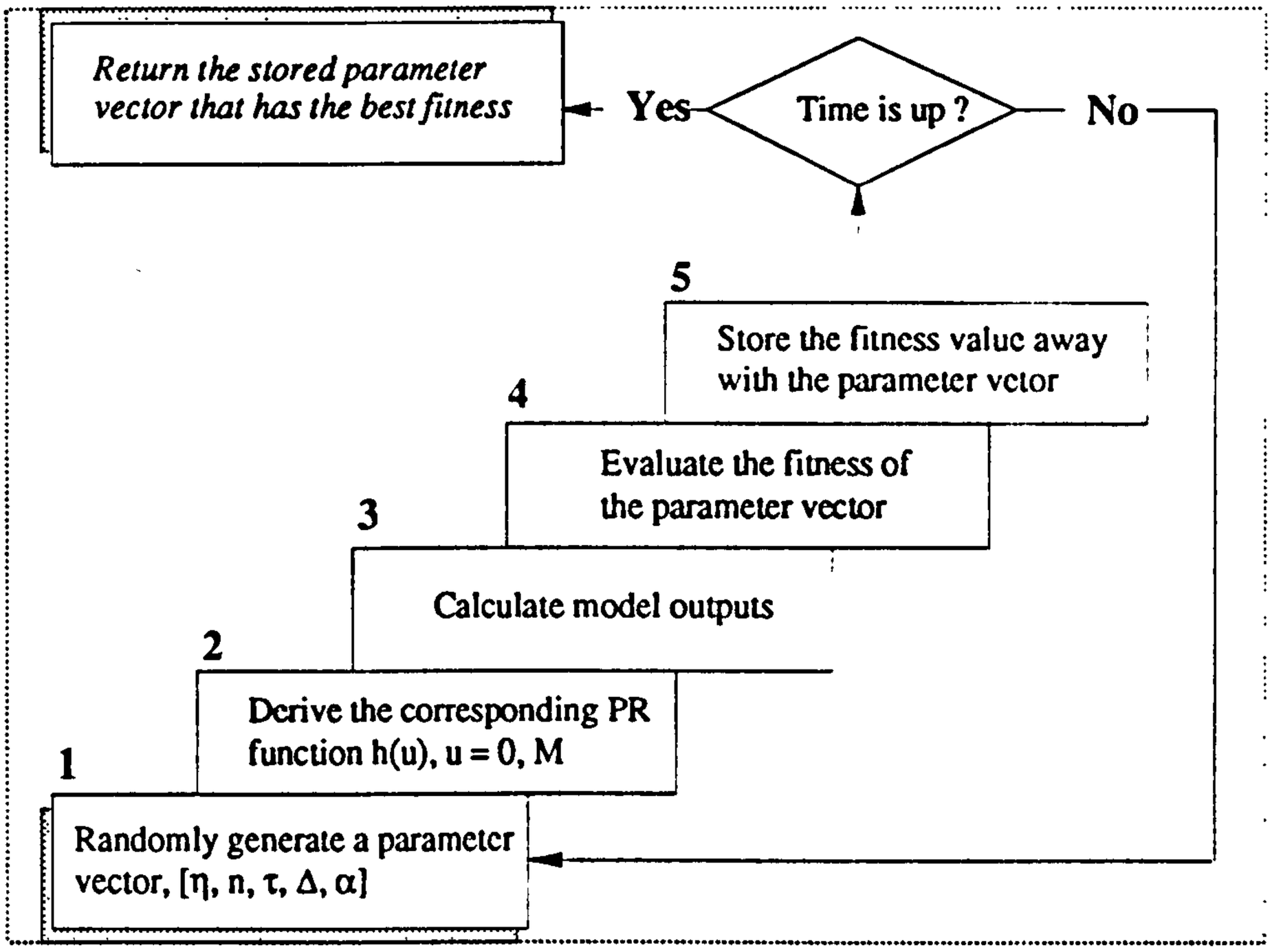

Fig. 6.2 Random Mutation Genetic Algorithm

At each evolving step, random mutation is applied on each of the PR parameters. Let $V = G(V_1, V_2)$ denotes that a random number V is generated by a random number generator G within a range from V_1 to V_2 ($V_1 < V_2$) and the values of V have a uniform probability density $1/(V_1 - V_2)$. The reproduction of a PR parameter vector can be made by running G for each of the five PR parameters in turn with V_1 and V_2 taking different values. For instance: $\eta = G(0.0, 100.0)$, $n = G(1.0, 10.0)$, $\tau = G(0.0, 5.0)$, $\Delta = G(1.0, 10.0)$, $\alpha = G(1.0/n, 5.0)$.

The objective for constricting the value range of V is to avoid overflows to the

computer's capacity and speed up the evolution. Values of V_1 and V_2 can be set according to the drainage system conditions and the valid value range of each PR parameter (see Chapter 5). Usually, the upper limit can be observed or inferred after fitting a number of historical events.

Since the mutation step is not constant, the children chromosomes are produced randomly and the time taken for obtaining an expected solution is not certain. It is dependent on the computer speed and the random number generating algorithm. However, an up-to-now best candidate is guaranteed. If it is not satisfactory, then either a longer evolving time period or the Comprehensive GA should be used. Random-mutation GA is very easy to use and quite reliable. Therefore, it is recommended as a primary method for identifying CPTF models. However, for obtaining a more optimal solution the Comprehensive GA may be used.

6.2.2 Using the Comprehensive Genetic Algorithm

The Comprehensive Genetic Algorithm uses a gene copying technique to reproduce the parents members in a population with a fixed size being larger than 1, and then the genes of the reproduced chromosomes are partially crossed over (i.e. exchanged). Thus a child chromosome carries the genes from both of its parents. It is expected to be different from its parents, hence superior to its parents. However, when the two parents are identical, cross-over can not result in evolution. Thus, cross-over has to be reinforced by the random mutation technique in this case in order to introduce difference into the children generation. After all of the parents members in the population having been crossed over, and randomly perturbed when two parents are identical, by comparing the fitness of the parents generation with the children generation the less-fit parents members are replaced by those children members who are more fit. The fitness factor can be calculated using Eq.(6.1). Population evolution occurs when the less-fit parents members in the population are replaced by the more-fit children. Once having been in the population, the children chromosomes became

parents members of the population. This reproduction-evolution process cycles until the specified time limit is up then return the best members of the population. This algorithm is illustrated in Figure 6.3, and a numerical example illustrating the approach is given in Appendix-III.

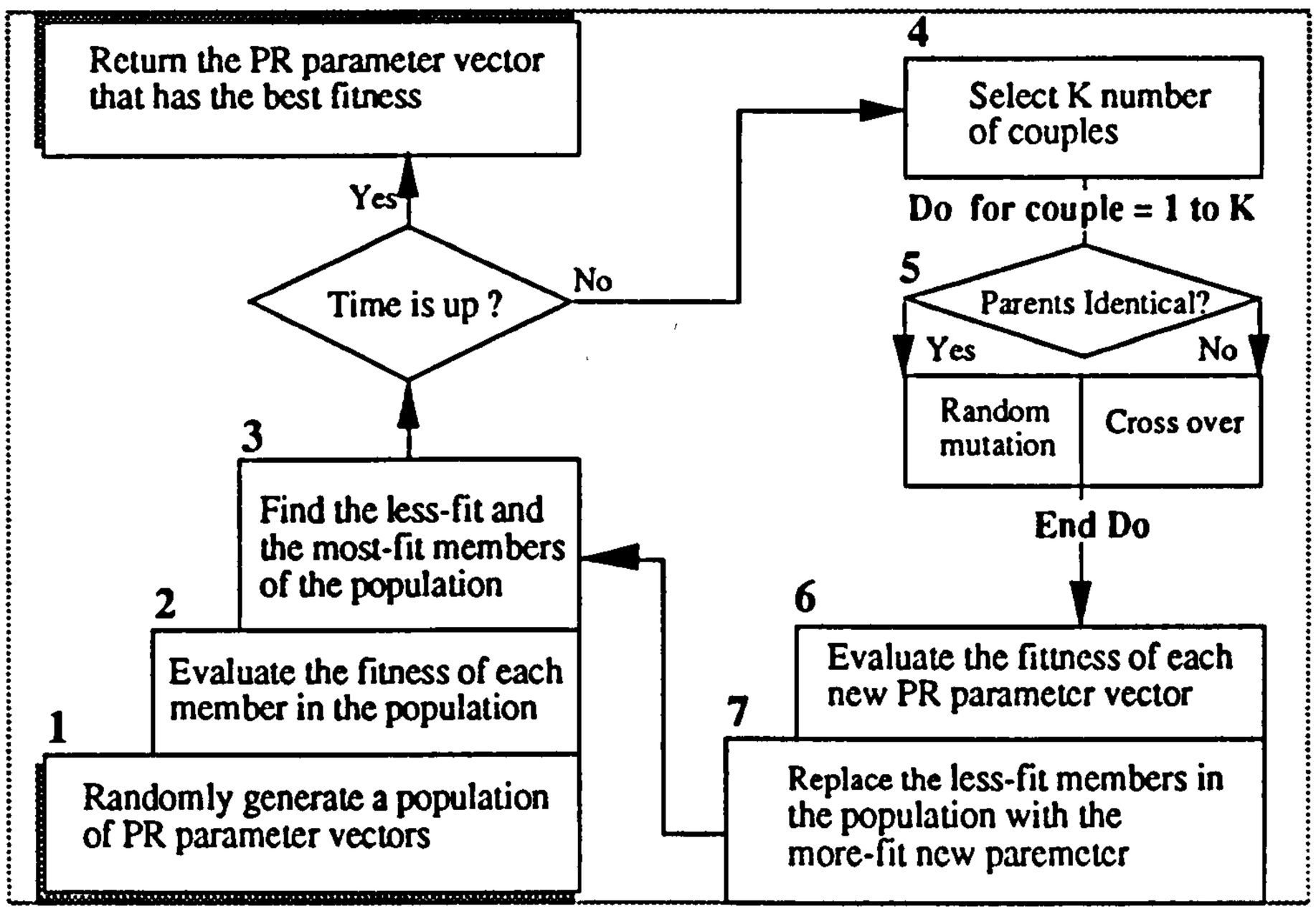

Fig. 6.3 Comprehensive Genetic Algorithm

It is easy to see that the major differences between the Comprehensive and the Random-mutation Genetic Algorithms are that 1) the population size is different and 2) the reproduction techniques are different. The size of the population can be arbitrarily chosen according to the computer capacity. Cross-over is exercised according to the fitness of the parents members. Those who are more fit will be given more chance to reproduce themself. To select a parent member, the *roulette wheel parent selection* technique can be used:

1) Label the members in the population as h_i, i = 1, N and their fitness factors as FF_i,

i = 1, N; where N is the size of the population;

2) Sum the inverse of the fitness factors, $1/FF_i$ of all the members in the population and describe the result as total fitness, Φ;

3) Randomly generate a number υ between 0 and Φ;

4) Accumulate the inverse of the fitness factors, $1/FF_i$, starting from i = 1; if the accumulation is not greater than or equal to υ then continue otherwise return the last member as a qualified parent chromosome;

5) Go to (3) until the required number of couples (e.g. 10) for producing their children generation by mating has been obtained.

Note, assuming a number of J parents members were selected then the total couple number would be equal to:

$$C_J^2 = \frac{J!}{2(J-2)!} = \frac{J(J-1)}{2}$$

The effect of *roulette wheel parent selection* is to return a randomly selected parent. The chance of each parent being selected is proportional to its fitness (i.e. $1/FF_i$).

Another point meriting further explanation is the reproduction techniques. Their function is to create new PR parameter vectors and cause some of the new members to differ from those parents members that stayed in the population. The whole procedure includes 4 steps.

1) During an evolution cycle, the gene copying technique first makes a copy of each selected couple. Then the other two reproduction techniques are applied upon it.

2) cross-over occurs when the couple exchange some of their genes. For identification of a CPTF model, exchanging every genes of the two parents members is meaningless and always exchanging one gene at all times may not be so efficient. Thus a better way is to randomly chose a segment of each parents chromosome then cross-over the chosen segments. This method is named by John Holland as the *one-point cross-over.* The separation point can be randomly determined. For example, assuming the five genes of the parents members are labelled respectively as η_{11}, n_{12}, τ_{13}, Δ_{14}, α_{15} , and η_{21}, n_{22}, τ_{23}, Δ_{24} and α_{25}, a random number generated between 1 to 5 which are uniformly distributed is equal to V, say 2 then the first V number of PR parameters, η and n will be exchanged, this will result in two newborn children chromosomes: η_{21}, n_{22}, τ_{13}, Δ_{14}, α_{15} , and η_{12}, n_{12}, τ_{23}, Δ_{24} and α_{25}. In cases of that the two parents are identical in the selected segment cross-over introduces no diversity in the two newly created children. Under these circumstances the random mutation technique need to be applied.

3) Random mutation guarantees the children PR parameter vectors created differ from there parents. Which genes to mutate ? For the sake of simplicity, random mutation of every gene is recommended. A smaller random perturbation is helpful to give a birth to a best child if the best and near best genes have been contained and spread in its parents members of the population at the later stage of the evolution. However, at the beginning of the evolution a larger creeping step will certainly reduce the time required for finding a solution.

4) Finally the deletion of some of the less-fit parents members of the population makes room for the newly generated but more fit children. The number of parents to be deleted is arbitrary , which may vary from one to the entire population. However, here, it is suggested that the members to be deleted should be less than 50% of the population size because better parents may not always produce better children therefore it is wise to keep the better parents in order to maintain a good quality of the

population. On the other hand, since the number of children to be generated is equal to the number of mating parents selected at each evolution cycle, i.e. =J(J-1), obviously the deleted parents members should be also less than or equal to the newborn children otherwise the population size can not be kept as constant. If all goes well throughout the evolution, a randomly initialised population of unexceptional chromosomes will produce new generations and improve as the parents are replaced by better and better offsprings.

6.3 Determination of the Model Orders: *M* and *s*

The order of Naive CPTF model, M, should satisfy:

$$\sum_{u=M}^{\infty} h(u) \to 0$$

The order of the Advanced CPTF model, *s*, may take a value between 0 and M. It was recognised that if a value is taken to be the time ordinate of the inflection point of h(u), it will suffice in most of the cases. That is, $s = U_i$, where U_i is the time ordinate of the inflection point (Chapter 5). In exceptional cases, it may take a value being equal to M-Δ-1.

6.4 Estimation of the Model Parameters: Θ_u and ζ_u

Knowing the PR function h(u) and the Naive CPTF model's orders, *M*, the parameters Θ_u and ζ_u can be estimated using Eq.(6.2) and Eq.(6.3) (see also Eq. (5.26) and Eq. (5.27) at page 116).

$$\Theta_1 = h_{\Delta+s+1} / h_{\Delta+s}, \tag{6.2}$$

This parameter is always less than 1 and it is the only parameter which governs the speed of flow recession after input has ceased. The reproduction error of the PR function h(u) will only occur when u is greater than $s+\Delta+1$ (i.e. $U_i+\Delta+1$). If the approximation error is unacceptably large then the model order should take a larger value, e.g. $s = M-\Delta-1$. When Θ_1 is equal to zero (i.e. $s = M-\Delta$) the output is a filtered rainfall series and the results will be identical to that which would have been produced by the corresponding Naive CPTF model.

$$\begin{bmatrix} \zeta_0 \\ \zeta_1 \\ \zeta_2 \\ \vdots \\ \zeta_s \end{bmatrix} = \begin{bmatrix} \frac{h_\Delta}{\Theta_1} \\ h_\Delta \\ h_{\Delta+1} \\ \vdots \\ h_{\Delta+s-1} \end{bmatrix} \Theta_1 - \begin{bmatrix} 0 \\ h_{\Delta+1} \\ h_{\Delta+2} \\ \vdots \\ h_{\Delta+s} \end{bmatrix} \tag{6.3}$$

Note there is no need to observe the rule of parsimony because estimation of the parameters $[\zeta_0, \ \zeta_1, \zeta_2, \zeta_3, \cdots, \zeta_S]$ is always feasible and extremely simple. This is different from the identification of NCTF models, which have to obey the principle of parsimony in order to ease the identification procedure and reduce the uncertainty of the parameters to be identified.

6.5 Diagnostic Checks and Updating the CPTF Model

A diagnostic check is an essential stage in the identification of a CPTF model. The objective is to uncover the inadequacy of the identified model and update it if necessary. If there is a lack of fit then the previous stages of the identification procedure need to be repeated until the model's performance is satisfactory. By comparing the new PR parameters with their old values the causes of lack of fit can be diagnosed.

It is assumed that an identified CPTF model using historical events represents the dominant factors that govern the flow convolution procedure within a system. However, such dominant factors are often modified due to the variations which lie within either the rainfall, flow or the catchment conditions. Therefore, the idea is to treat the procedure as a nonlinear and dynamic system. To cope with such a system, the model needs to be upgraded in real-time. Hopefully, in this way the system can be simulated segmentally by a linear model.

Error prediction, state updating and parameter updating are the major real-time model updating techniques. However, only the last two upgrading methods are incorporated in the CPTF model identification procedure, because trying to analyse the time series of simulation or prediction errors and using the obtained information to predict 'future errors' may at best correct a small and stable error quite well, and at worst can make the already poor simulation or forecast awful. A CPTF model can be updated by either state updating, or parameter updating or both in real-time.

6.5.1 State Updating

The outputs from the CPTF model are state variables which can be updated using the telemetered observations as soon as they are available. This technique assumes that if the model performance is well now it will behave satisfactorily in the future. Implementation of state updating is straight forward and takes less time than parameter updating. This makes the technique suitable for real-time application purposes.

6.5.2 Parameter Updating

The CPTF model parameters or PR can be reestimated in real-time. Updating is made after the re-estimation of the PR parameters (i.e. η, n, τ, Δ and α) which may be altered partially or entirely. The PR parameter updating at time *t* requires a search for

an optimal set of η, n, τ, Δ and α within the parameter space so that the measured outputs over the duration from t-δ to t can be optimally fitted by the model outputs.

Table 6.1 shows the main effects which are likely to be resulted from the parameter updating.

Table 6.1 Main effects of parameter updating

PARAMETER	MAIN EFFECTS
η	Proportionally changes the amplitude of PR
n	Mainly determines the peak, time to peak and the shape of the rising limb
τ	Mainly portrays the peak, time to peak and the shape of the recession limb
Δ	Defines the time of lag or first non-zero value of PR
α	Plays a combined part of *n* and τ

Modelling experiences showed that different systems require different upgrading frequencies. However, in general, during an event, the rainfall-to-flow transformation system is dominated by the impulse responses having smaller gains at the earlier stage, and thereafter gradually approaches to a stabilised stage. Therefore, frequent diagnostic checks and updating are necessary during the early period of an event.

6.6 Summary

The identification of CPTF model is a two-step procedure which is different from the conventional least-square method. A CPTF model is identified via a PR-to-CPTF approach. The PR parameters identified at the first step guarantees a physically realisable PR function to be established and from which a Naive CPTF model can be

produced. The model parameters identified at the second step enable a CPTF model of the first-order Markov Process type to be constructed which has more adaptation flexibility than the Naive CPTF model. Naive CPTF model can be updated in real-time using the parameter updating technique whereas the Advanced CPTF model can be updated by state updating or/and parameter updating.

The Genetic Algorithm plays a key role in identification of the PR parameters, which is treated as a collective term of the three evolution (or optimisation) techniques. The universal applicability of the algorithm has not been explored and only those elements capable of achieving the primary aims of this study were concentrated on.

Before carrying out the identification procedure, base flow separation and net rainfall derivation are not required because it is quite difficult to do in real-time. Since the model is intended to be applied by giving the 'raw' input, it should also be identified using the raw input. The changes in the interactions between input and output may be dealt with by the model updating techniques.

CHAPTER 7

CONVERSION OF NON-CONCEPTUAL TRANSFER FUNCTION AND UNIT HYDROGRAPH MODELS

This chapter explains how to convert a static Non-Conceptual Transfer Function (NCTF) and Unit Hydrograph (UH) Model into a CPTF model. The objective is to reduce the workload required for identification of the CPTF models while there already have been some NCTF or UH models available at a modelling site. The significance is that the non-conceptual parameters can be transformed into conceptual parameters therefore may be physically verified or more easily upgraded in real-time.

7.1 Conversion of NCTF Model into CPTF Model

The conversion of a static NCTF model into a CPTF model is quite straightforward. The procedure involves:

- Derivation of PR from the given NCTF model by inputting a unit pulse input;

- Calculation of the percentage runoff factor η which is equal to the accumulation of the derived PR over the range from 0 to infinity;

• Determination of parameter Δ which is the time ordinate of the first non-zero value of the derived PR;

• Evolution of the PR parameters, n, τ and α using the Random-mutation Genetic Algorithm (See Chapter 6 and Appendix-III) to obtain the best fit of the PR of the NCTF model;

• Finding the model orders, M, and s, and parameters, ζ_u and Θ_u using Eq.(6.2) and Eq.(6.3).

Three example CPTF PRs converted from the NCTF models for the River Asker and River Stour in the Wessex region, UK are shown in Figure 7.1, Figure 7.2 and Figure 7.3. The NCTF and the corresponding CPTF models were summarised in Table 7.1.

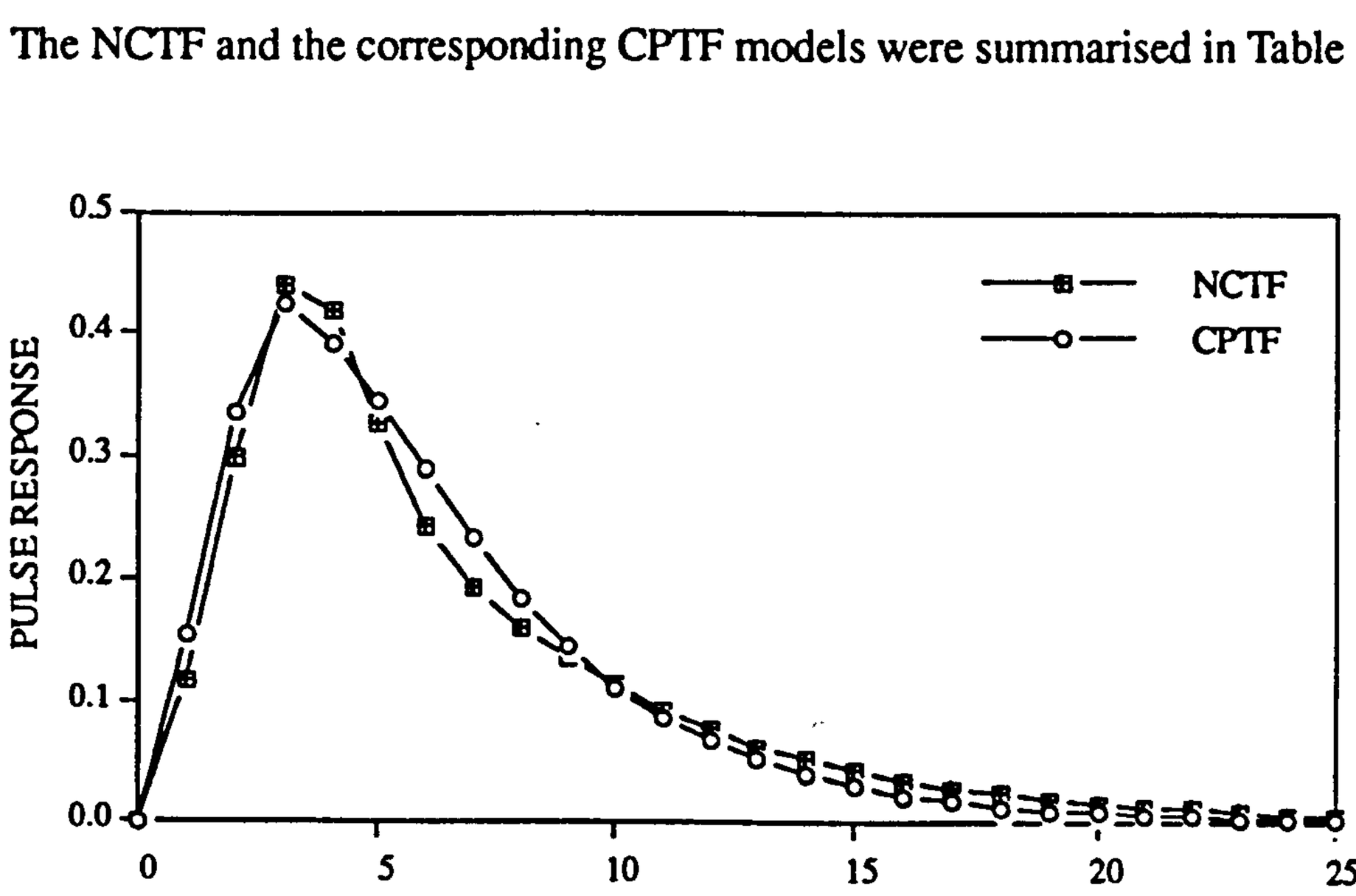

Fig. 7.1 CPTF PR converted from the NCTF model-1 of the River Asker at Bridport

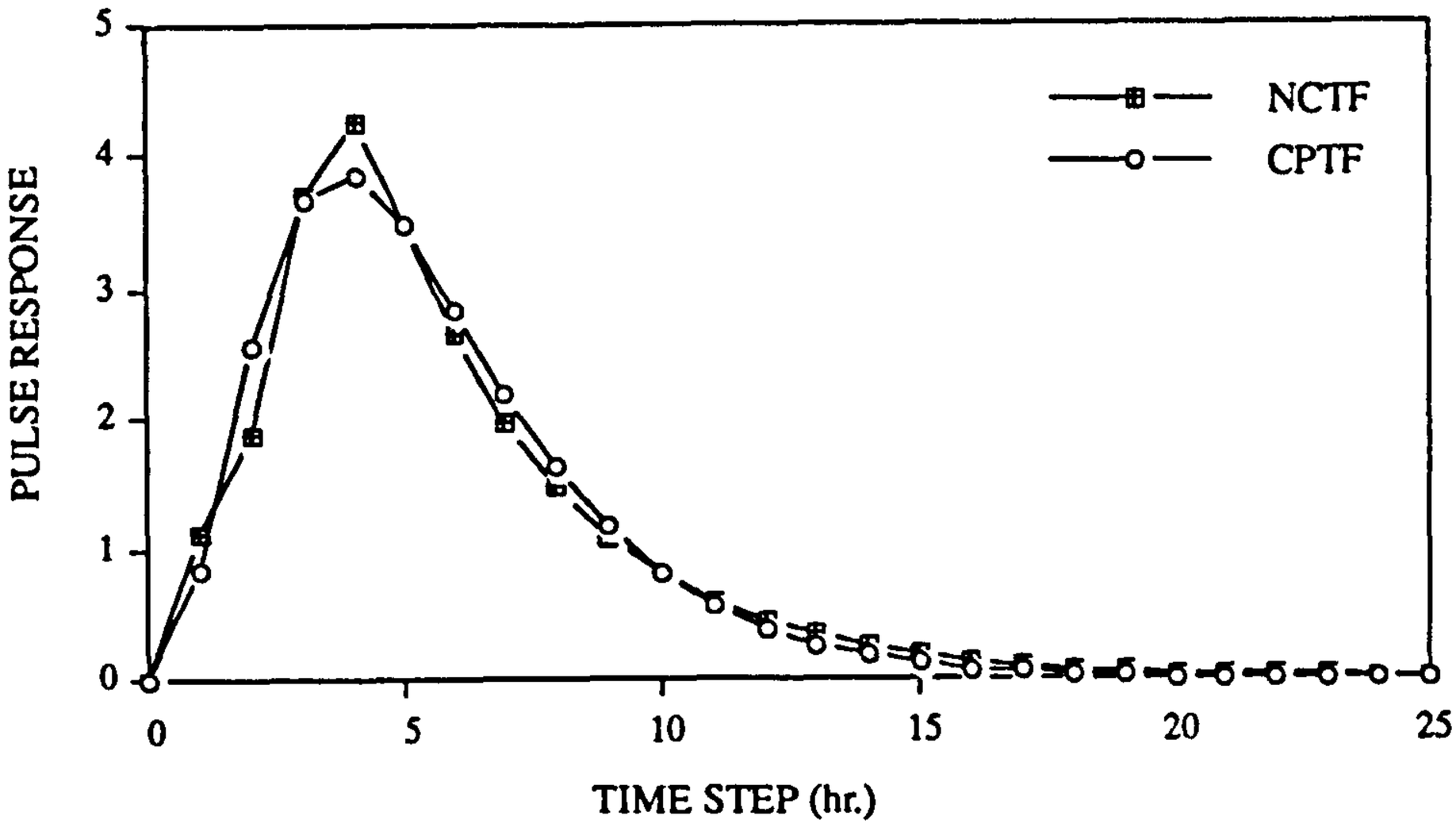

Fig. 7.2 CPTF PR converted from the NCTF model-2 of the River Asker at Bridport

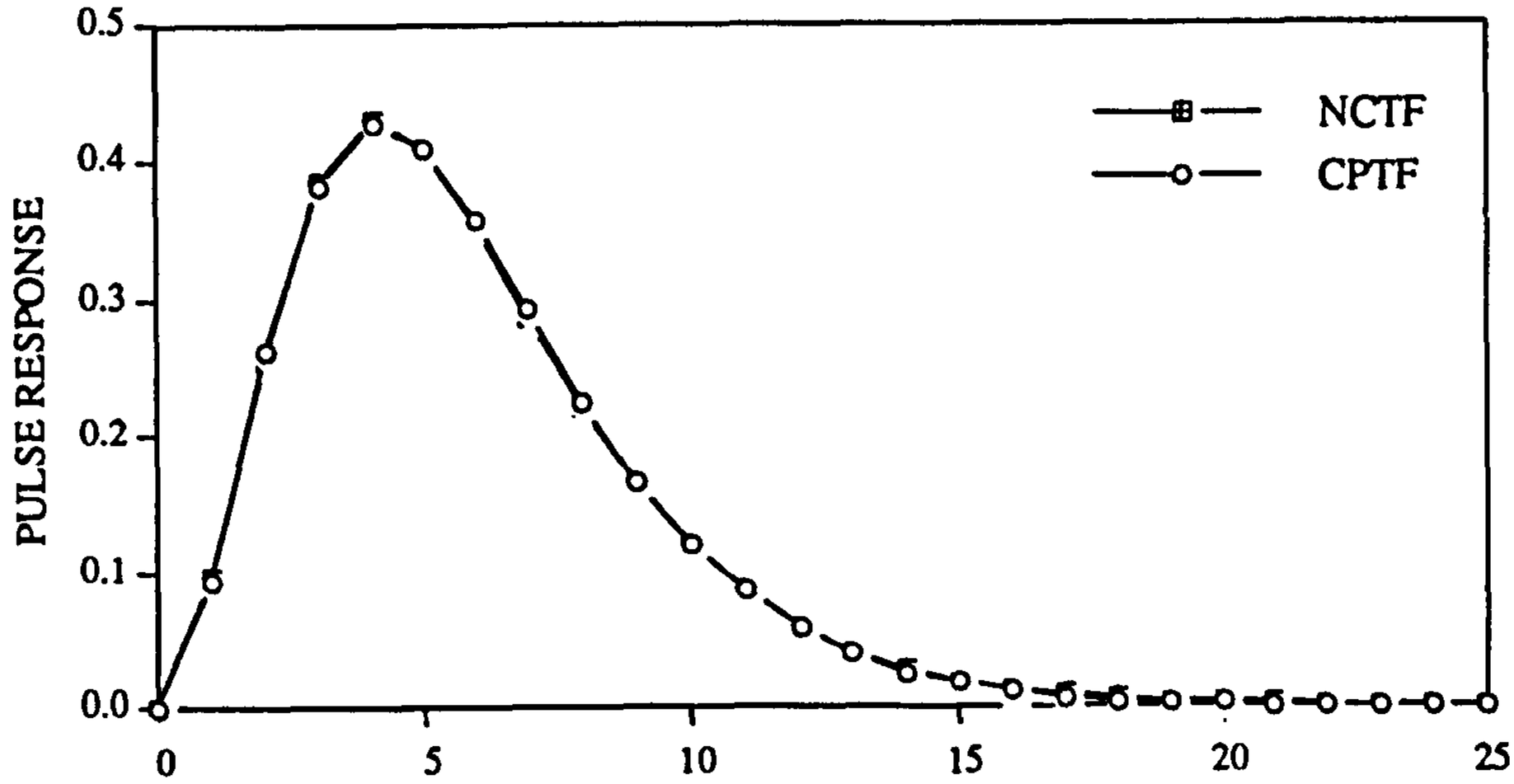

Fig. 7.3 CPTF PR converted from the NCTF model of the River Stour *at Throop*

Table 7.1 NCTF models and the equivalent CPTF models

RIVER	NCTF MODELS $Q_t = \frac{\zeta_0 B^{\Delta-1} - \sum_{u=1}^{s} \zeta_u B^{u+\Delta-1}}{1 - \sum_{u=1}^{r} \Theta_u B^u} R_t$	CPTF MODELS CPTF(η, n, τ, Δ, α, χ)
River Asker (at Bridport)	$\Theta_1 = 1.3756$ $\Theta_2 = -0.7086$ $\Theta_3 = 0.2094$ $\zeta_1 = 0.1183$ $\zeta_2 = -0.1358$ $\zeta_3 = -0.1139$	$\eta = 2.977$ $n = 6$ $\tau = 0.481$ $\Delta = 1$ $\alpha = 0.625$ $\chi = 1$
	$\Theta_1 = 0.9709$ $\Theta_2 = -0.1716$ $\zeta_1 = 1.1116$ $\zeta_2 = -0.8092$ $\zeta_3 = -2.0554$ $\zeta_4 = -0.9915$	$\eta = 24.752$ $n = 5$ $\tau = 0.773$ $\Delta = 1$ $\alpha = 0.807$ $\chi = 1$
River Stour (at Throop)	$\Theta_1 = 1.7300$ $\Theta_2 = -0.9970$ $\Theta_3 = 0.9120$ $\zeta_1 = 0.0951$ $\zeta_2 = -0.0903$ $\zeta_3 = -0.0397$	$\eta = 3.001$ $n = 3$ $\tau = 2.244$ $\Delta = 1$ $\alpha = 1.071$ $\chi = 1$

7.2 Conversion of UH Model into CPTF Model

Converting a UH model into a CPTF model is also very simple. The PR parameters can be derived by directly fitting the UH. For example, the UK National River Authority (NRA), Wessex regional office utilises the Flood Study Report (FSR, 1975) procedure and employs four parameters: Peak flow (h_p), Time-to-peak (U_p), Duration of steep recession (D_w) and Duration of shallow recession (D_b) to synthetically define a UH. See Figure 7.4.

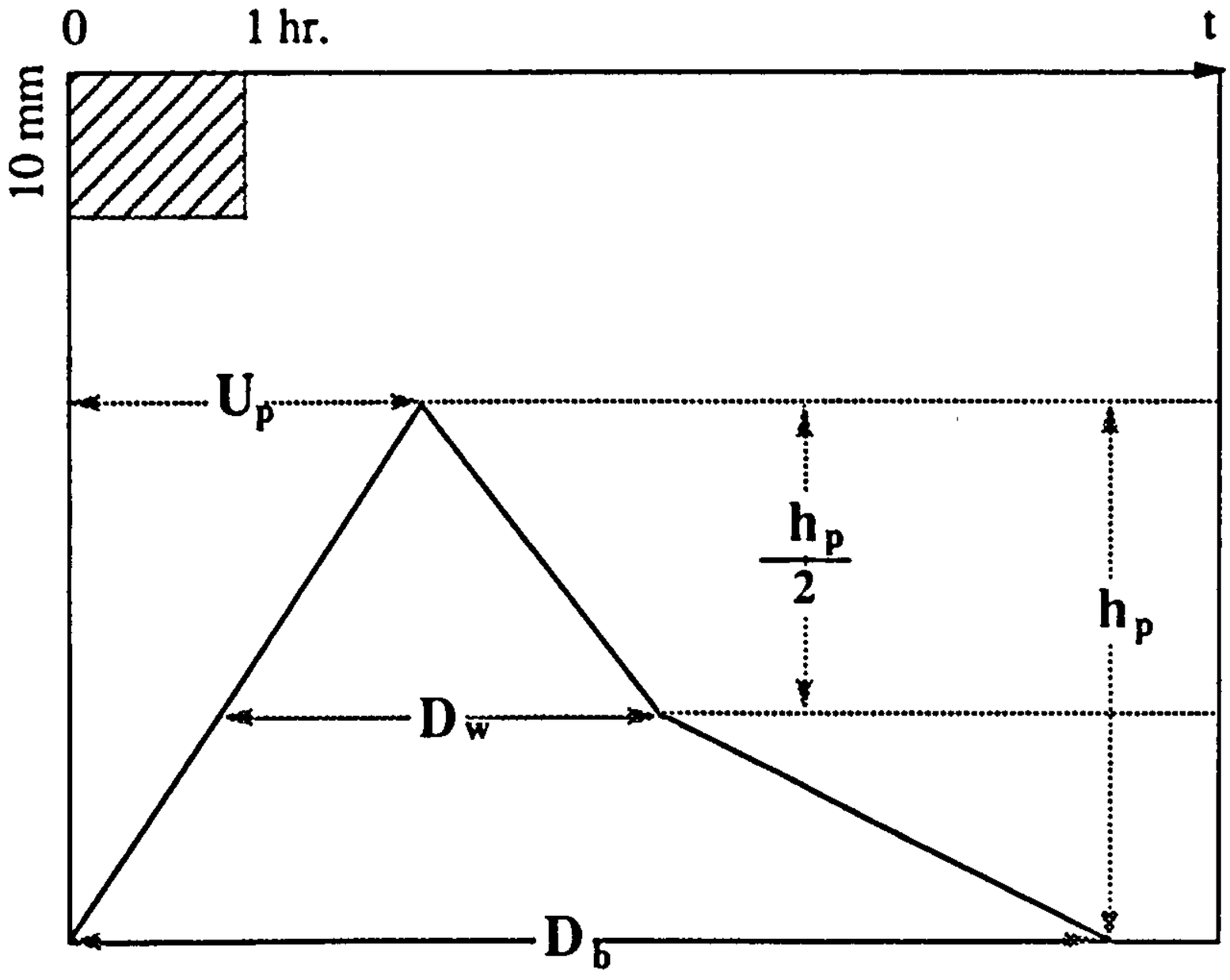

Fig. 7.4 Definition of a UH by the 4 parameters

Table 7.2 shows the UH models used in the region.

Table 7.2 The UH models used by the NRA Wessex office (Source: Han, 1991)

CATCHMENTS	h_p(m^3/s)	U_p(hr.)	D_w(hr.)	D_b(hr
Lovington	40	10	10	26
Halsewater	22	7	10	30
Chrisleborough	20	10	12	25
Bishops Hull	50	10	12	33
Greenham	20	5	8	24
Pen Mill	53	11	11	38

Following procedure details how to convert the above UH models into the equivalent CPTF forms:

- **Estimation of the percentage runoff factor η:**

$$\eta = \frac{h_p}{4}(2D_w + D_b) \text{ (cumecs} \cdot \text{hr/mm)};$$

Note the input rainfall is 10 mm/h and if gross rainfall is used as input, this parameter needs to be re-estimated at application time of the model.

- **Estimation of the time of lag:**

$\Delta = 1$

- **Estimation of n, τ and α:**

Parameters, n, τ and α can be estimated by minimising the fitness factor using the Random-mutation Genetic Algorithm. The numerical example which illustrates how a CPTF model can be fit onto a given time series data using the GA has been given in Appendix-III.

Following this procedure, the given UHs were converted into the PR functions of CPTF model. The results are shown in Table 7.3

Table 7.3 Representing PR parameters of each UH

CATCHMENTS	η*	n	τ	Δ	α
Lovington	460.0	5	1.985	1	0.924
Halsewater	275.1	6	0.825	1	0.664
Chrisleborough	245.0	5	2.230	1	0.957
Bishops Hull	712.5	4	2.835	1	0.923
Greenham	200.1	6	0.654	1	0.631
Pen Mill	795.4	4	2.799	1	0.890

* $m^3 \cdot hr./(s \cdot mm)$

Comparisons between the UHs and the corresponding CPTF PRs are shown in Figure 7.5(A) and Figure 7.5(B).

7.3 Summary

Approximation of an existing NCTF model or UH model by a CPTF model is feasible and simple. The basic idea is to convert the PR function implicitly defined by the non-conceptual parameters into an explicit and conceptually parametrised PR function.

The NCTF, UH and the converted CPTF models will be used to assess the performance of CPTF models in next chapter.

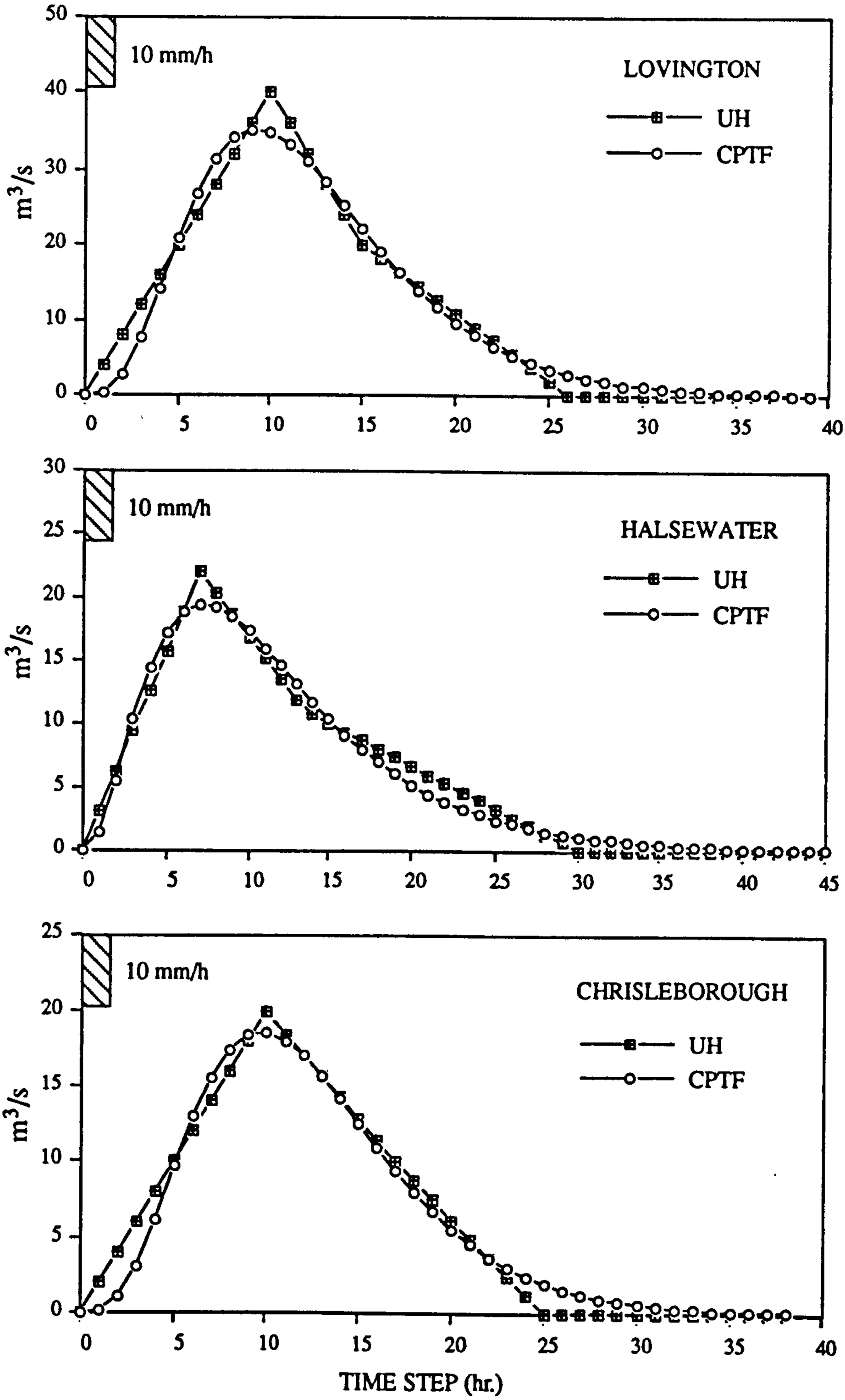

Fig. 7.5 (A) Representation of UH by CPTF PR

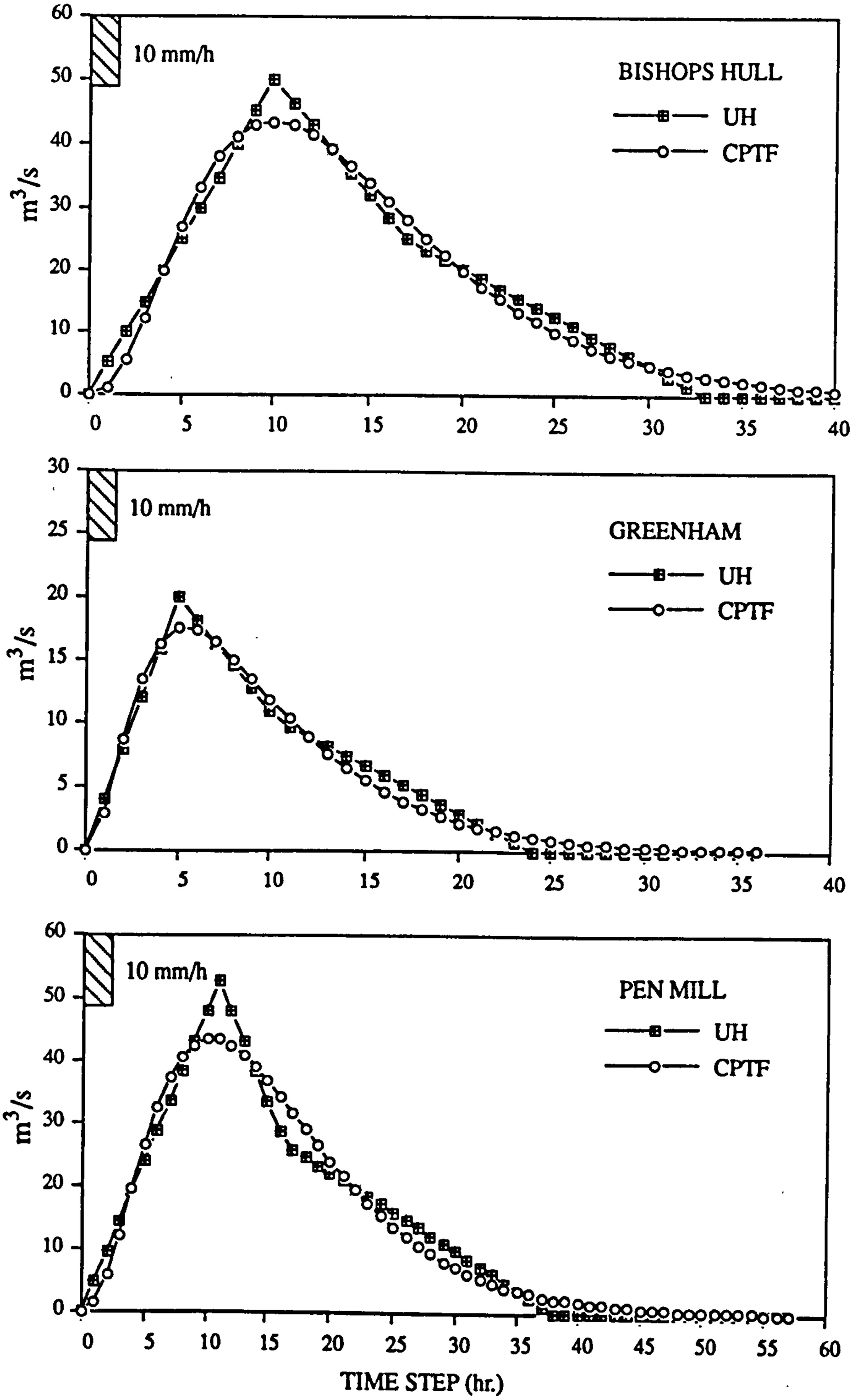

Fig. 7.5 (B) Continuation of Fig. 7.5 (A)

CHAPTER 8

APPRAISAL OF CPTF MODEL

A general assessment on the performance of the CPTF model is not practicable. However, a primary assessment can be made by 1) comparing the CPTF model with the Non-conceptual Transfer Function (NCTF) model and Unit Hydrograph (UH) model, 2) examining the performance of CPTF model in simulation of the actual flow observations and 3) demonstrating the performance of the CPTF model in drainage flow predictions. Two drainage systems having different response characteristics were used for this assessment.

8.1 Comparison Between CPTF and NCTF Models

The CPTF model can be compared with the NCTF model in terms of model philosophy, structure, identification procedure and performance. See Table 8.1.

Philosophically, both CPTF and NCTF models represent transfer from one discrete data series to another. However, CPTF is conceptual model whereas NCTF model is a solution of the linear differential equation and belongs to the physics-based category.

Structurally, both of the models are linear filters of infinite order. However, when expressed in the form of Eq.(5.24), a NCTF model may have a longer memory of the flow part than a CPTF model whereas the CPTF model is a first-order Markov Process

whose current state only depends on one previous state.

Table 8.1 Comparison between CPTF and NCTF models

	CPTF	**NCTF**
PHILOSOPHY	Conceptual	Physics-based
IDENTIFICATION PROCEDURE AND TYPICAL METHOD	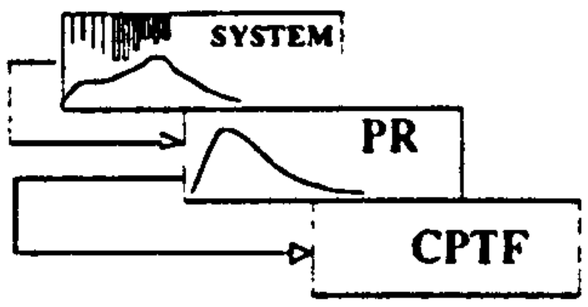	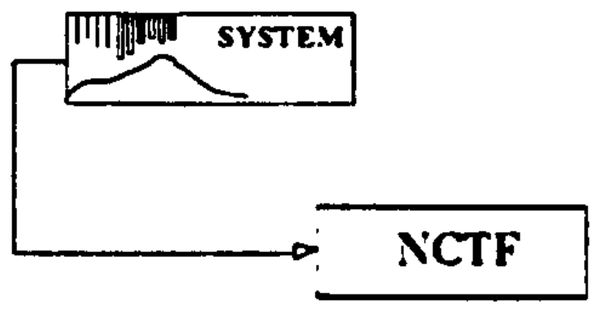
	Genetic Algorithm	Least Square
DEFINTION AND PROPERTIES OF **PR**	$h(u)=\begin{cases}\dfrac{\eta\alpha(u-\Delta+1)^{\alpha n-1}}{\tau^{n}\Gamma(n)}e^{-(u-\Delta+1)^{\alpha}/\tau} & ;u\geq\Delta\\ 0 & ;u<\Delta\end{cases}$	$[\zeta(0)-\sum_{u=1}^{s}\zeta(u)B^{u}]B^{\Delta}=\sum_{u=0}^{t}h(u)B^{u}\,[1-\sum_{u=1}^{r}\Theta(u)B^{u}]$
	ALWAYS: (1) Positive (2) Smooth (3) Stable (4) Identifiable	CAN BE: (1) Negative (2) Fluctuating (3) Not convergent (4) Unidentifiable

NCTF models are usually identified using Least Square, Recursive Least Square methods or following Box-Jenkins' Approach, which is essentially a Data-to-Model procedure whereas the identification of a CPTF model is a data-to-PR procedure. The CPTF model parameters are not directly estimated from the observed input-output data but from the PR function. The identification of PR using the Genetic Algorithm in advance is advantageous, because it enables the PR function that can produce a best fit to the actual observations to be always identifiable for a given input-output relation.

Parameter updating for NCTF models in real-time may not be robust to data errors

whereas the updating of the CPTF model parameters is always feasible. Errors at a small percentage of randomly scattered points will not affect the identifiability and the quality of CPTF model. Using an adaptive CPTF model, various storm conditions and catchment characteristics could be dealt with effectively.

To compare the relative performance of the CPTF model to NCTF model. The three NCTF models used in the NRA Wessex region (Chapter 7) and the corresponding CPTF models which were converted from the NCTF models were compared by providing the same inputs. The differences between the PRs and between the model outputs were quantified using the Fitness Factor, i.e. Eq.(6.1). Comparisons of the hydrographs are shown in Figure 8.1 to Figure 8.3. Note, the model outputs for different river systems were produced by inputting the same radar rainfall series so that the fitness factors may be inter-compared for different models.

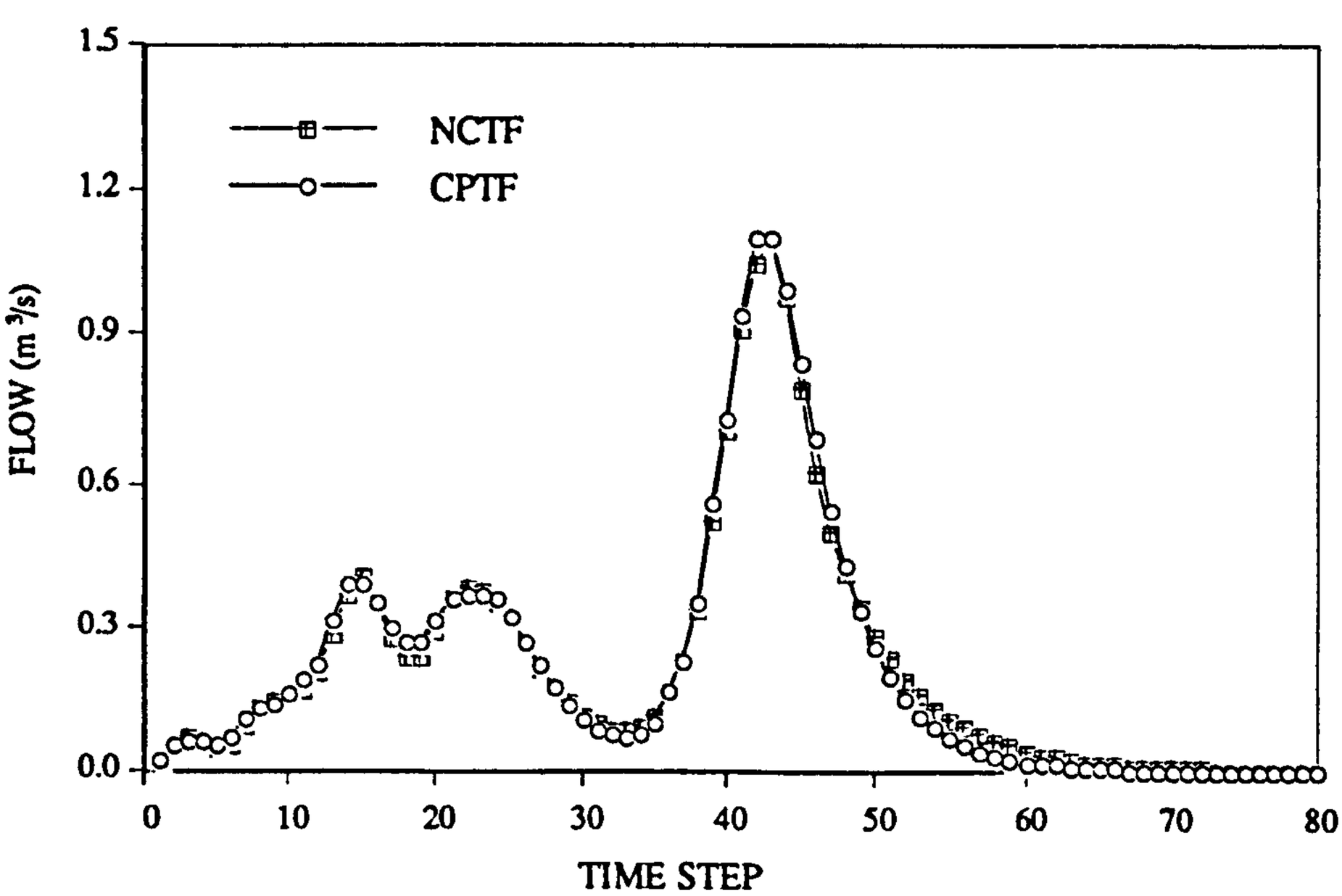

Fig. 8.1 Comparison 1: simulations for River Asker at Bridport

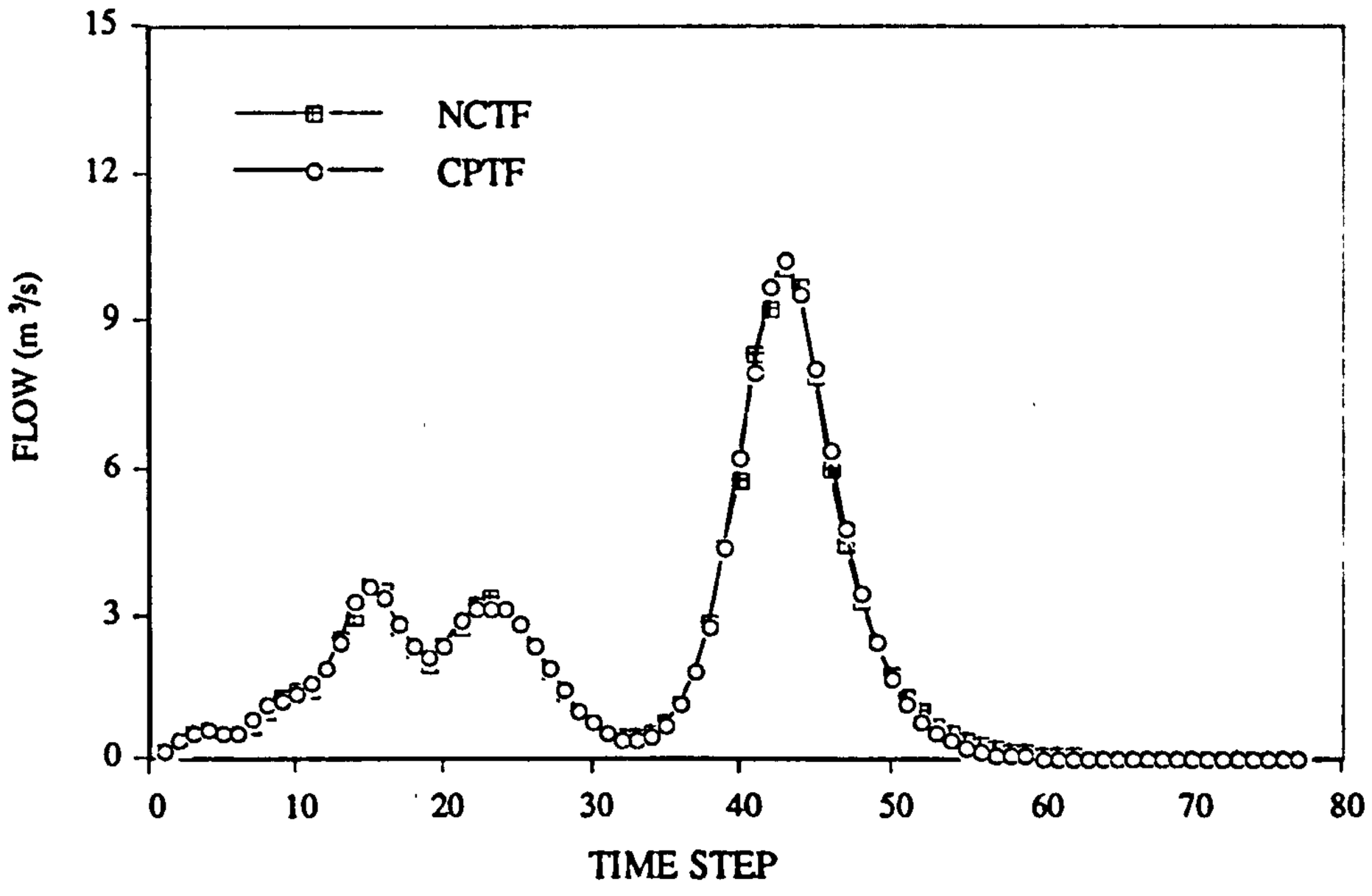

Fig. 8.2 Comparison 2: simulations for River Asker at Bridport

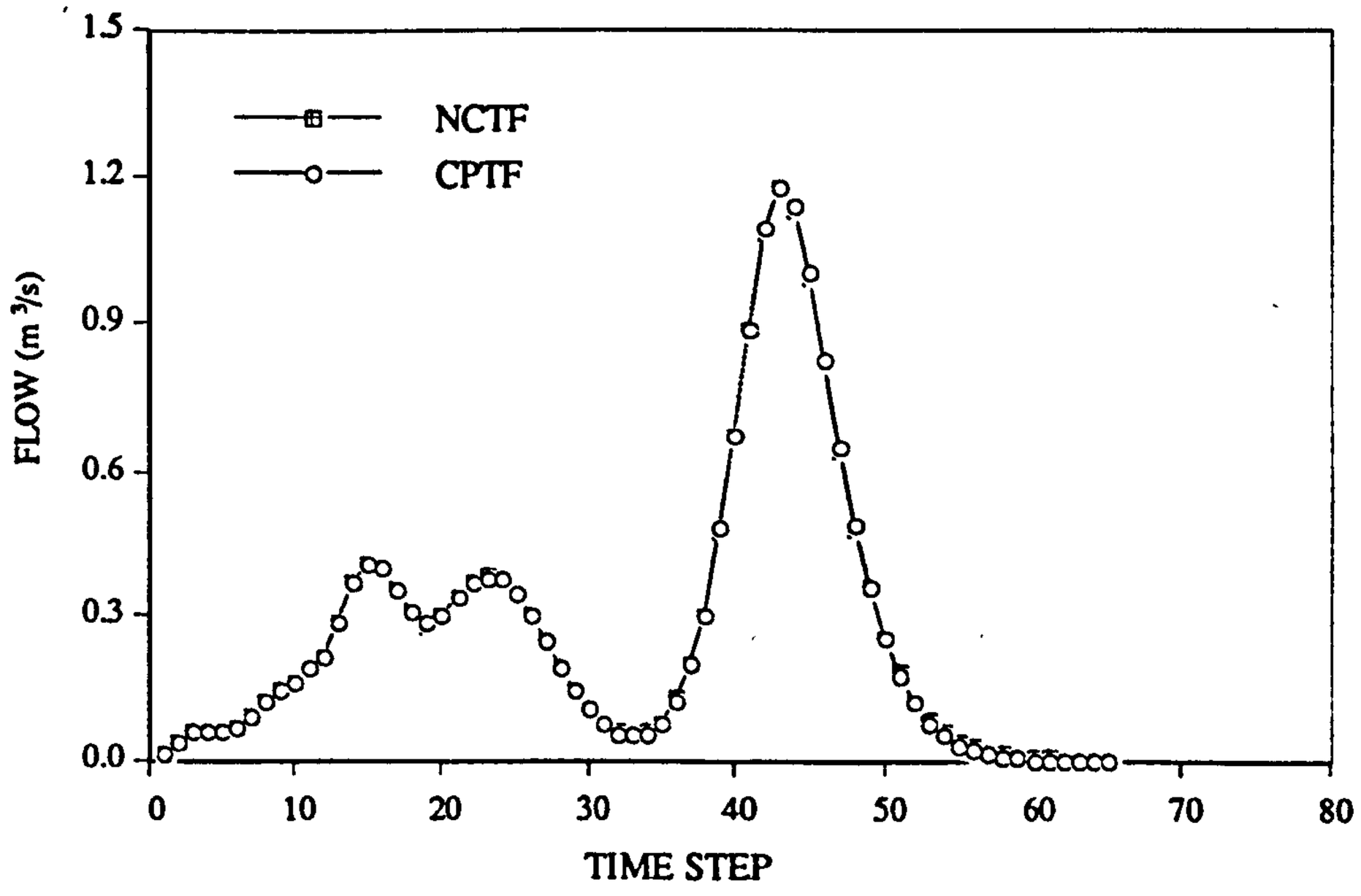

Fig. 8.3 Comparison 3: simulations for River Stour at Throop

It can be seen from the figures that the differences between the flow simulations are quite minor and the performance of the CPTF models will be at least as good as the NCTF models. The fitness factors are shown in Table 8.2, which can be used to compare the performance of CPTF model in fitting the different NCTF models.

Table 8.2 Fitness factors of CPTF model in fitting the NCTF models

MODELS	PR	Flow Simulations
River Asker (at Bridport)	0.0150	0.0043
	0.0130	0.0022
River Stour (at Throop)	0.0002	0.0001

8.2 Comparison Between CPTF and UH Models

Unit Hydrograph models are developed based on a number of clearly defined assumptions (see Bras, 1990). PR-C can be treated as a conceptual Instantaneous Unit Hydrograph (IUH) if it is used by giving the net rainfall input. However, a number of differences may be recognised between UH and CPTF models: 1) the CPTF model is a hybridisation of the IUH model and the NCTF model; 2) the CPTF model is not only a rainfall-runoff model. It can also be devised for flow routing purposes; 3) the CPTF model accepts gross rainfall as input and does not need base flow separation; 4) the CPTF has two forms. With its advanced form previous state observation is able to be fed back for state updating purpose.

The relative performance of the CPTF model to the UH model can be assessed by comparing the existing UH models in the NRA Wessex region (Chapter 7) with the converted CPTF models and by providing the same input rainfall time-series. The results are shown in Figure 8.4 to Figure 8.9.

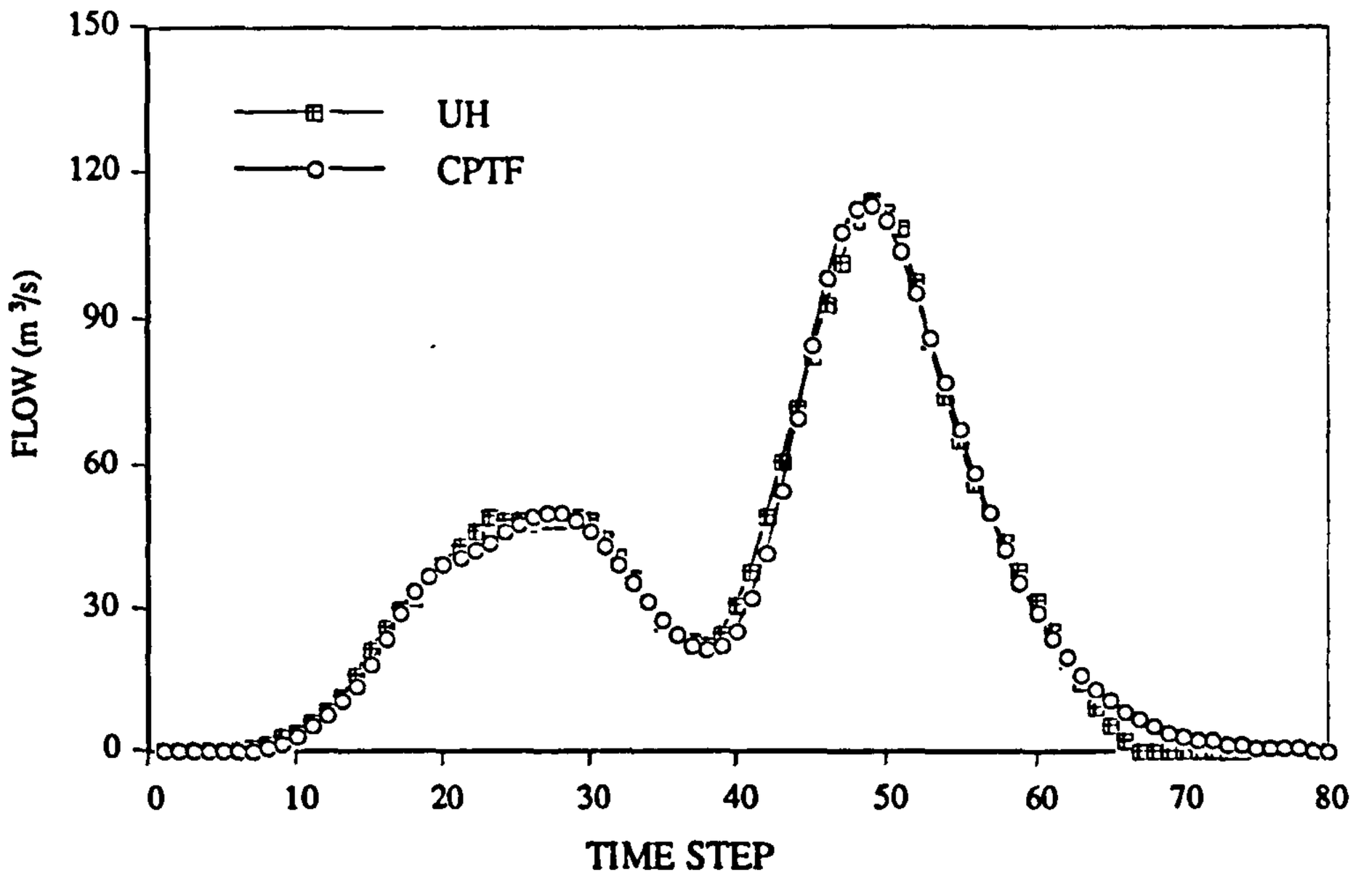

Fig. 8.4 Comparison 1: simulations using the Lovington Models

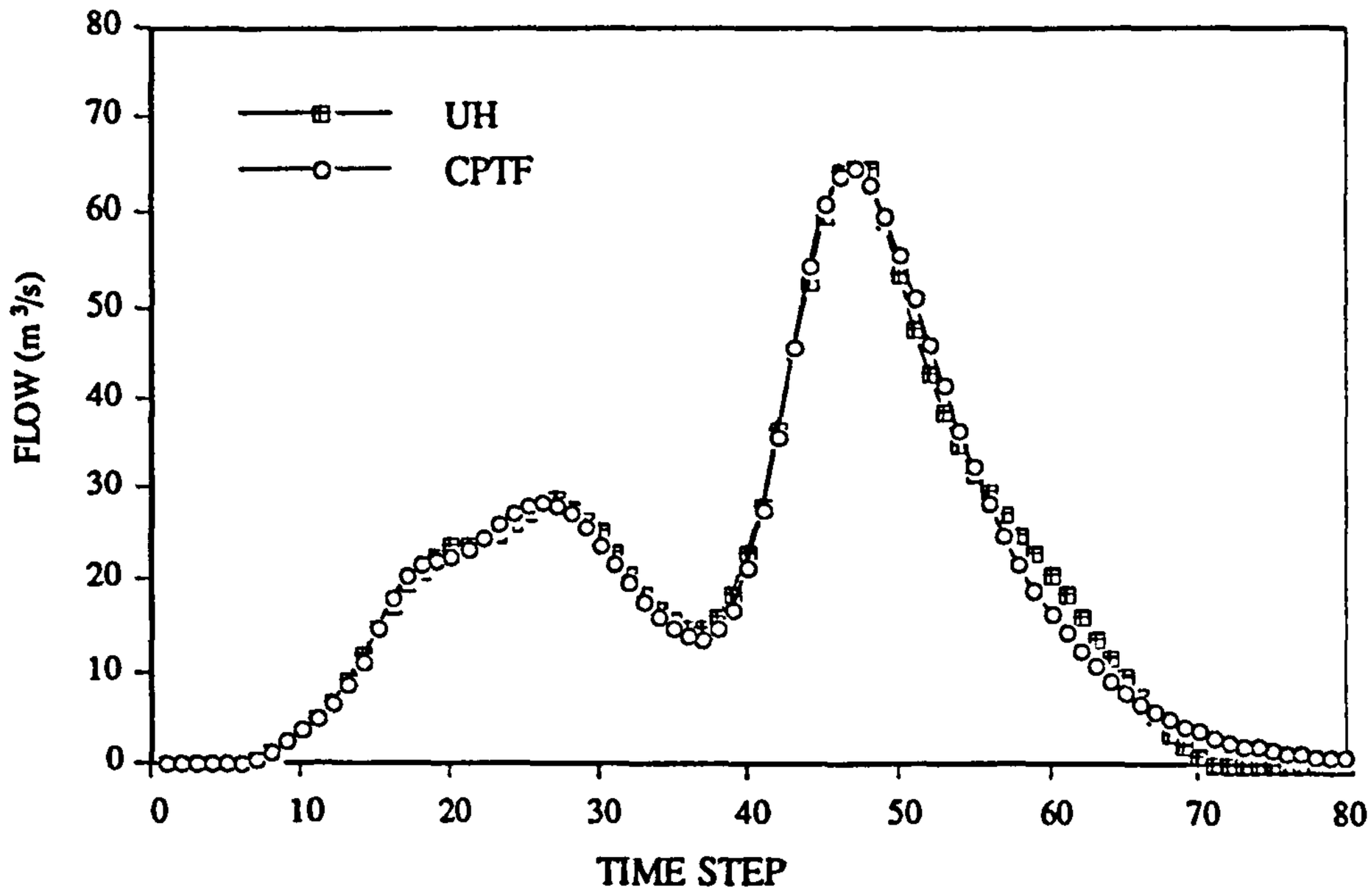

Fig. 8.5 Comparison 2: simulations using the Halsewater Models

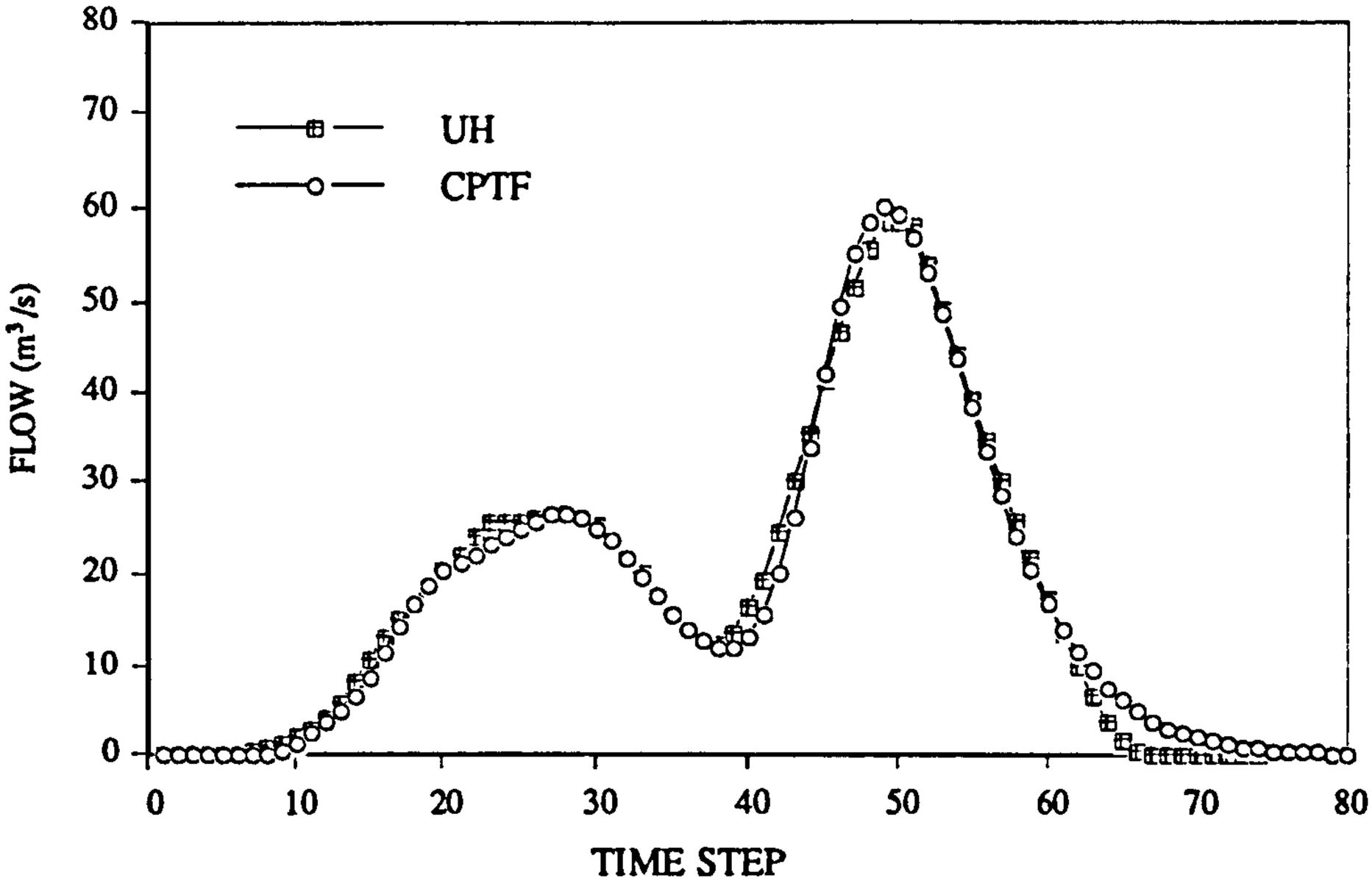

Fig. 8.6 Comparison 3: simulations using the Chrisleborough Models

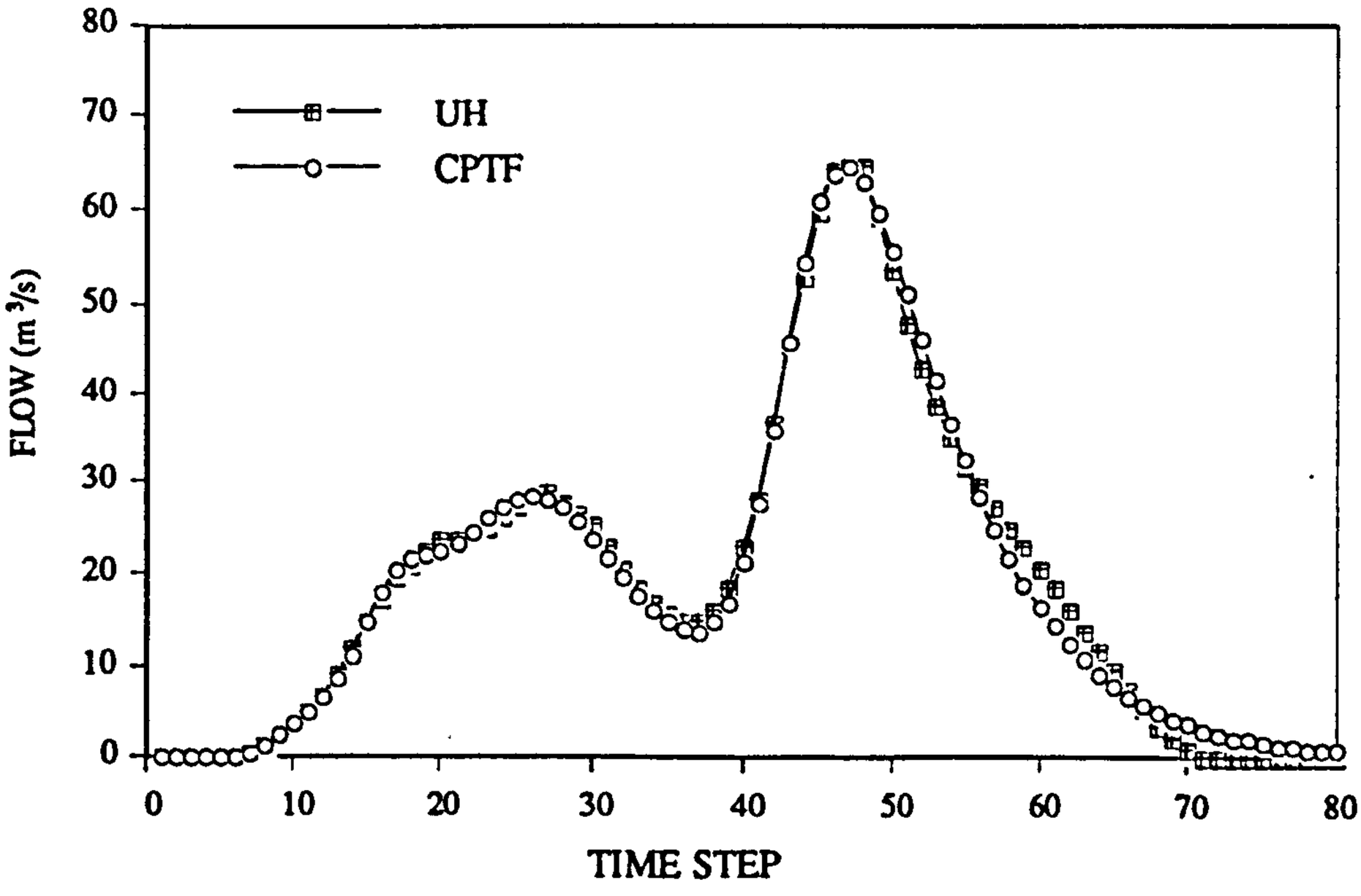

Fig. 8.7 Comparison 4: simulations using the Bishops Hull Models

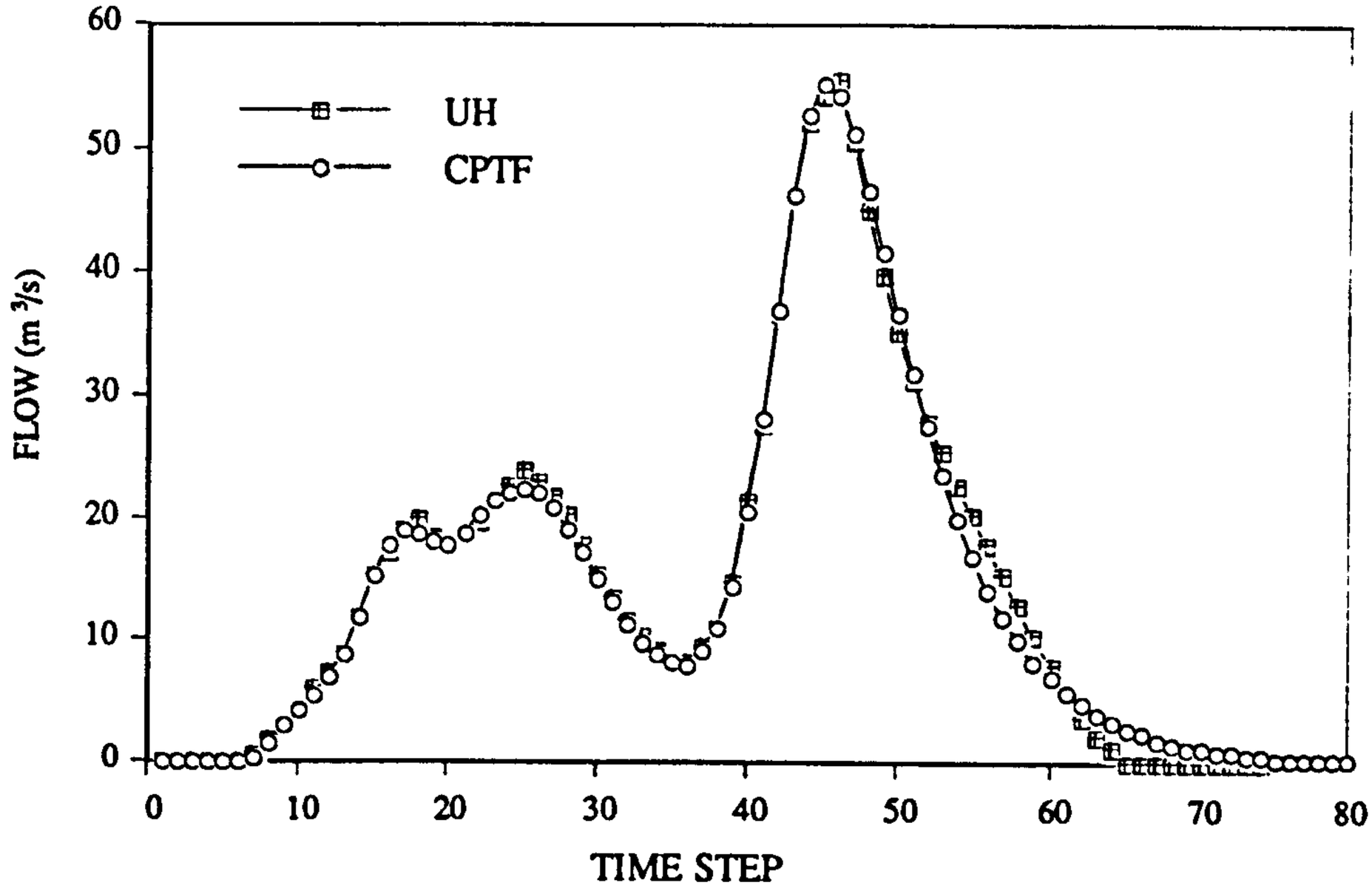

Fig. 8.8 Comparison 5: simulations using the Greenham Models

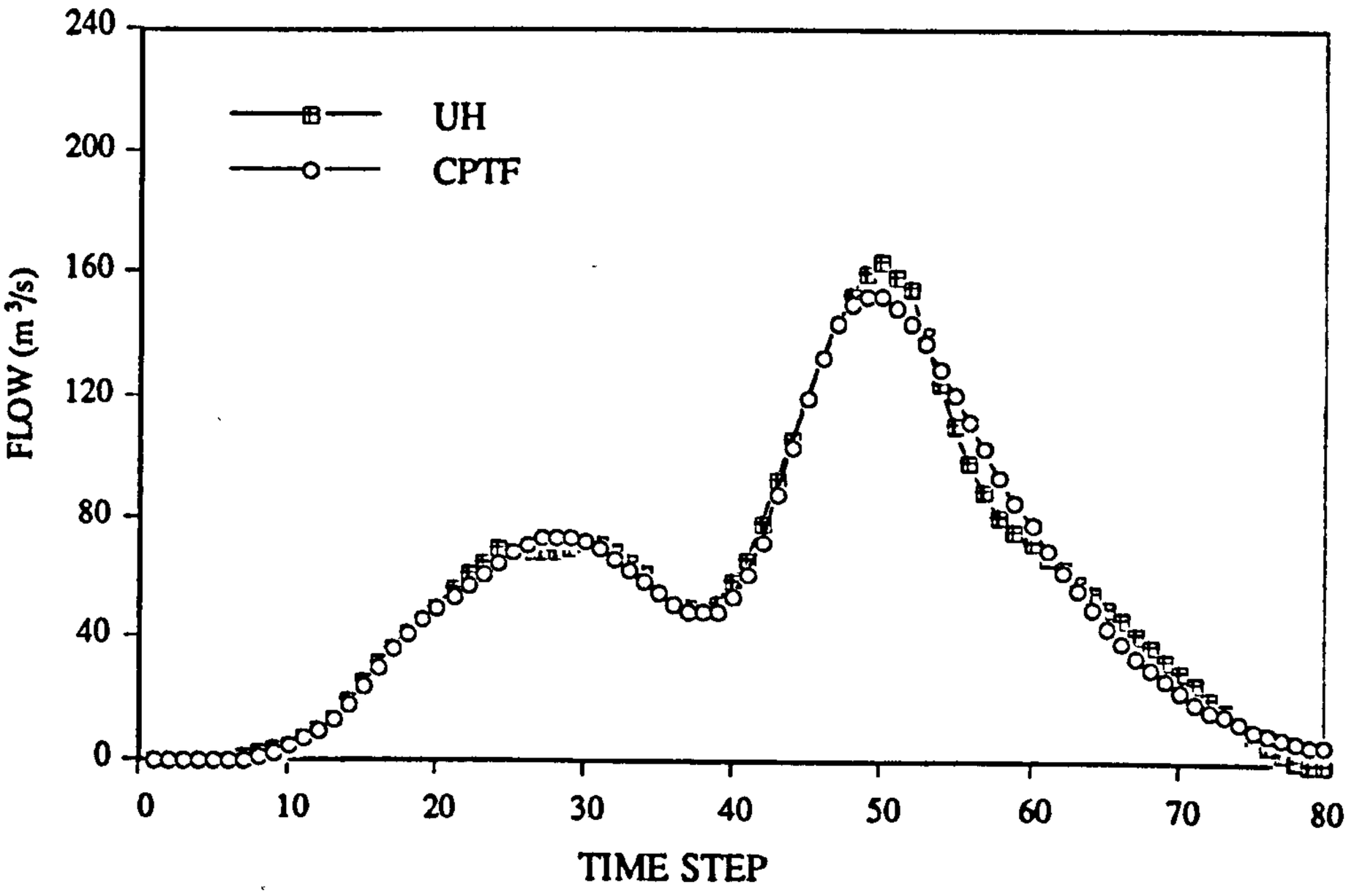

Fig. 8.9 Comparison 6: simulations using the Pen Mill Models

The fitness factors are shown in Table 8.3.

Table 8.3 Fitness factors of CPTF model in fitting the UH models

MODELS	PR	FLOW SIMULATION
Lovington	0.014	0.0039
Halsewater	0.011	0.0035
Chrisleboroug	0.015	0.0051
Bishops Hull	0.010	0.0030
Greenham	0.011	0.0036
Pen Mill	0.016	0.0052

From the results it was recognised that using CPTF model produced more reasonable flow simulations than the UH models.

8.3 Performance in Drainage Flow Simulation

Simulation is defined as the reproduction of the realisations of a real-world system using a mathematical model. Because the CPTF model can be static or adaptive, the assessments may be carried out on two aspects: static simulation and adaptive simulation using the following events.

8.3.1 Events

To assess the performance of CPTF model in flow simulation, two types of data were used in carrying out the assessments. The first type is rainfall-runoff data and the second is sewer inflow-outflow data. The rainfall-runoff events were shown in Table 8.4 which were collected at a 1-hour temporal resolution from the Blackford Bridge

catchment in the Northwestern England region, and the telemetered urban drainage flow events were shown in Table 8.5, which were observed in the Wythenshawe catchment in Greater Manchester (UK) at a 10-minute temporal resolution.

Table 8.4 The rainfall-runoff events

RAINFALL	DURATION (hr.)	PEAK (mm/h)	AVERAGE (mm/h)	DEPTH (mm)
BL820102	42	1.100	0.167	7.02
BL820203	10	1.350	0.554	5.54
BL820625	31	1.580	0.290	9.00
BL820817	17	1.650	0.538	9.14
BL840205	25	2.080	0.480	12.01
BL851029	15	1.250	0.341	5.12
BL861229	38	2.050	0.603	22.92

RUNOFF	DURATION (hr.)	PEAK (m^3/s)	AVERAGE (m^3/s)	VOLUME (m^3)
BL820102	66	30.110	7.850	1865160
BL820203	32	3.540	0.692	79776
BL820625	58	11.520	1.833	382788
BL820817	38	14.610	3.184	435564
BL840205	50	37.800	9.166	1649880
BL851029	42	15.880	5.000	755928
BL861229	60	71.270	21.526	4649580

Table 8.5 The inflow-outflow events

INFLOW	DURATION (hr.)	PEAK (m^3 /s)	AVERAGE (m^3 /s)	VOLUME (m^3)
RN930903	144	4.220	0.886	76524
RN930904	48	16.930	3.064	88248
RN930905	48	6.690	1.629	46926
RN930906	36	12.130	1.596	34470
RN930907	73	0.510	0.319	13974
OUTFLOW	**DURATION (hr.)**	**PEAK (m^3 /s)**	**AVERAGE (m^3 /s)**	**VOLUME (m^3)**
RN930903	144	11.000	3.948	341130
RN930904	48	35.980	9.395	270582
RN930905	48	18.490	5.280	152064
RN930906	36	34.780	6.772	146274
RN930907	73	2.390	1.673	73284

8.3.2 Comparisons

For each input-output event shown in Table 8.4 and Table 8.5, simulated hydrographies were respectively produced statistically and adaptively using the Naive CPTF model and Advanced CPTF model.

In static simulation mode, an optimum Naive CPTF model was identified using the Random-mutation Genetic Algorithm (Chapter 6) for each event, then the corresponding Advanced CPTF model was derived from it. The identified PR parameters for different resolutions (i.e. χ) of the model input were shown in Table

8.6(a), Table 8.6(b) and Table 8.6(c).

Table 8.6 (a) Identified PR parameters for χ=1

EVENTS	PR PARAMETERS IDENTIFIED for $\chi = 1$				
	η	n	τ	Δ	α
BL820102	79.697	4	1.296	1	0.813
BL820203	4.250	2	2.057	3	1.050
BL820625	13.204	5	3.117	1	1.316
BL820817	13.711	4	1.651	4	1.344
BL840205	36.988	5	1.537	5	1.019
BL851029	41.113	3	1.257	3	0.733
BL861229	58.173	5	2.991	2	1.156
RN930903	4.456	2	1.584	1	2.002
RN930904	3.030	1	3.324	1	1.773
RN930905	3.165	5	0.264	1	0.901
RN930906	3.346	4	0.387	1	0.997
RN930907	4.469	6	0.281	1	2.287

Table 8.6 (b) Identified PR parameters for χ=3

EVENTS	PR PARAMETERS IDENTIFIED for $\chi = 3$				
	η	n	τ	Δ	α
BL820102	27.062	3	1.324	1	1.126
BL820203	1.281	2	1.101	2	2.369
BL820625	4.335	1	3.201	2	1.804
BL820817	5.891	4	0.737	2	2.410
BL840205	11.290	3	2.769	2	1.903
BL851029	12.514	2	3.204	1	1.590
BL861229	19.335	5	1.489	1	1.399
RN930903	1.345	4	0.593	1	0.767
RN930904	1.312	1	2.132	1	2.286
RN930905	1.017	2	1.561	1	2.336
RN930906	1.124	5	0.274	1	1.144
RN930907	1.761	3	1.351	1	2.345

Table 8.6 (c) Identified PR parameters for χ=6

EVENTS	PR PARAMETERS IDENTIFIED for $\chi = 6$				
	η	n	τ	Δ	α
BL820102	13.329	5	0.337	1	0.887
BL820203	0.937	4	0.524	1	1.989
BL820625	2.590	4	0.664	1	2.109
BL820817	2.781	3	1.204	1	2.474
BL840205	6.187	1	2.031	2	2.491
BL851029	6.308	2	1.309	1	1.676
BL861229	9.255	2	1.102	2	2.072
RN930903	0.690	2	2.174	1	2.228
RN930904	0.450	5	0.311	1	1.322
RN930905	0.563	4	0.605	1	1.560
RN930906	0.871	3	0.601	1	2.230
RN930907	1.053	5	0.459	1	2.154

In adaptive simulation mode, the model parameters were updated for each simulation step using the Random-mutation Genetic Algorithm.

In addition, in order to know the simulation accuracy when the model input data resolution χ is different from the system's discretising resolution, the simulations were carried out respectively for χ taking 1, 3 and 6 time steps.

In brief, the comparison scheme constitutes two simulation modes, two model forms, three model input data resolutions, two catchments and 12 events, see Table 8.7.

Table 8.7 Scheme for comparing different simulations

Mode \ Model Form	Naive CPTF	Advanced CPTF
STATIC	$\chi = 1$	$\chi = 1$
	$\chi = 3$	$\chi = 3$
(PARAMETER) ADAPTIVE	$\chi = 6$	$\chi = 6$

The results are shown in Figure 8.10, Figure 8.11 and Figure 8.12, which indicate the performance of CPTF model.

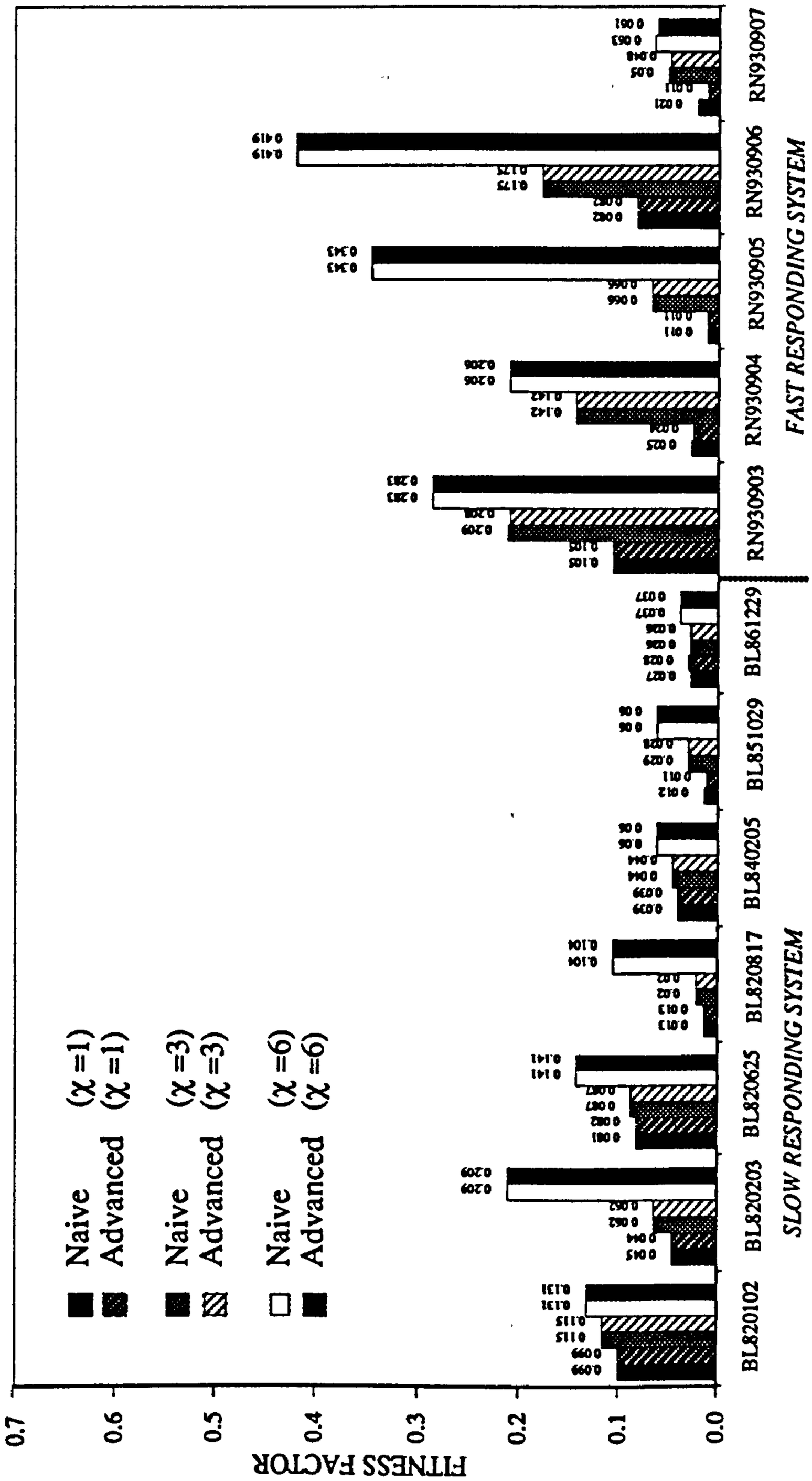

Fig. 8.10 Comparisons of the static simulation errors
(1) fordifferent systems and events
(2) between Naive CPTF model and Advanced CPTF model
(3) as the model discretising interval, χ, takes different time steps

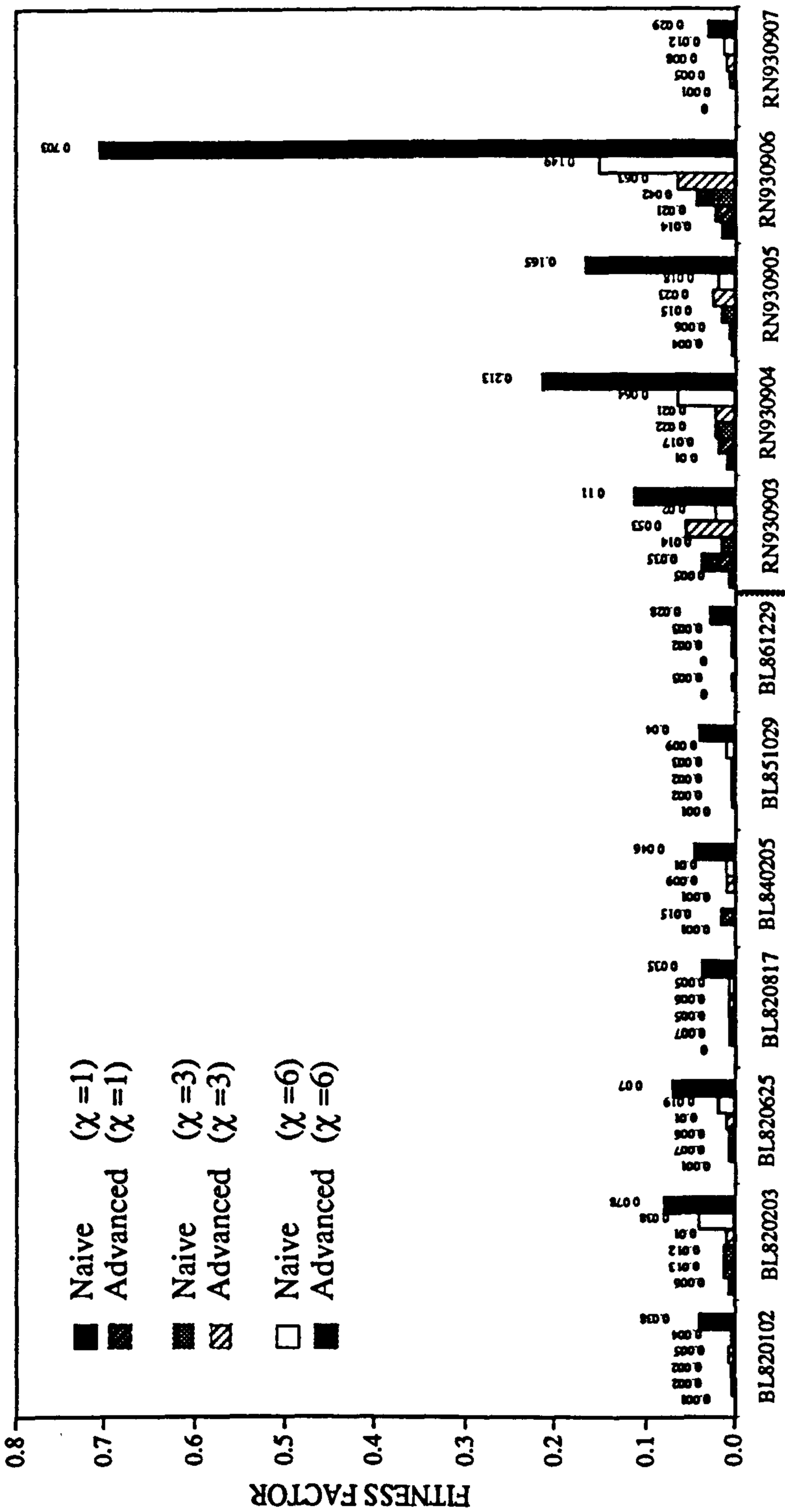

Fig. 8.11 Comparisons of the adaptive simulation errors
(1) fordifferent systems and events
(2) between Naive CPTF model and Advanced CPTF model
(3) as the model discretising interval, χ, takes different time steps

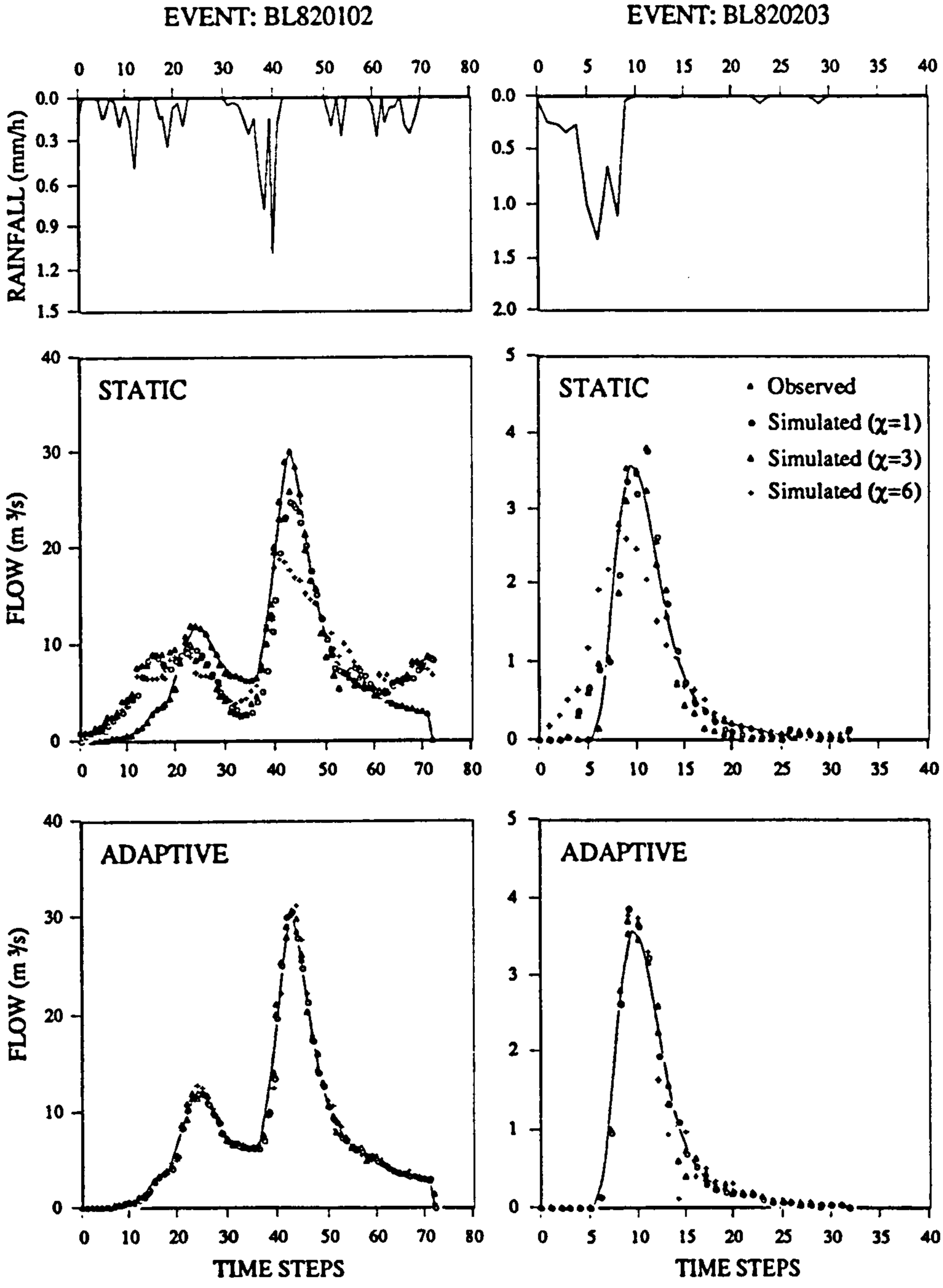

Fig. 8.12 (Event 1-2) Comparison of the simulated and observed hydrographs

Note: The vertically flipped graphs show the model inputs. The static and adaptive simulations were respectively made for different model discretising intervals (χ=1, 3, 6 steps)

(To be continued)...

Figure 8.12 continued....

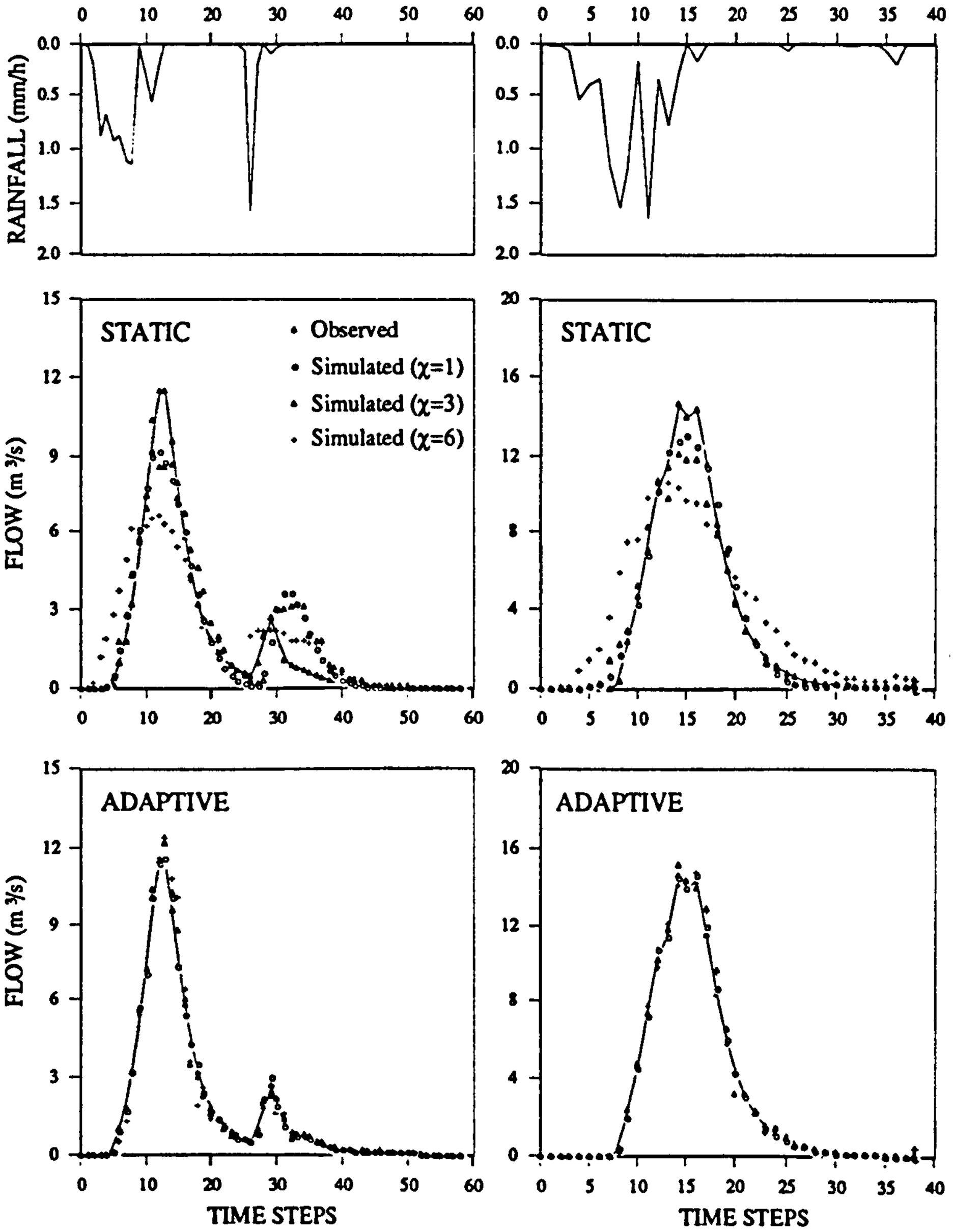

Fig. 8.12 (Event 3-4)

Figure 8.12 continued....

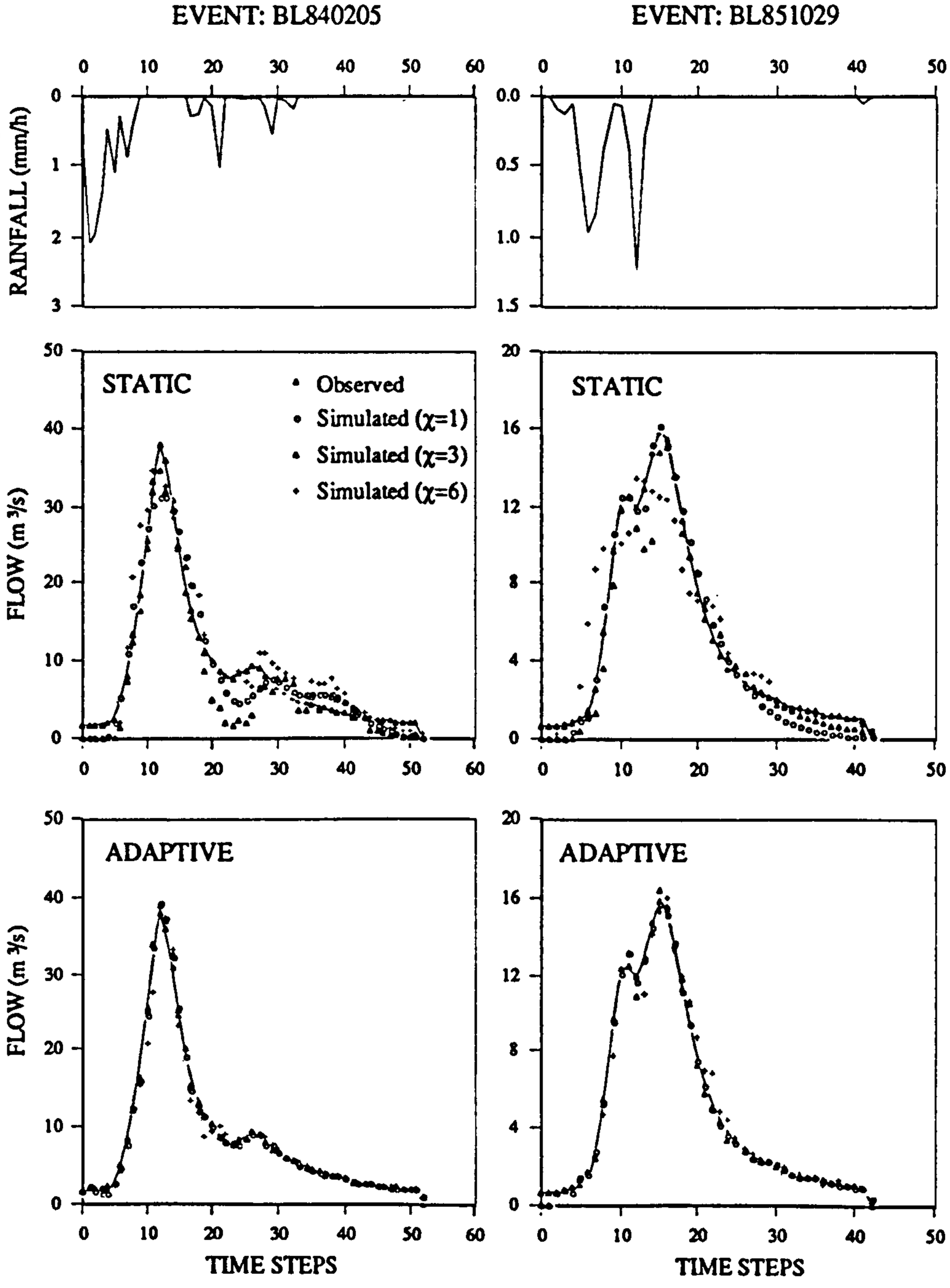

Fig. 8.12 (Event 5-6)

Figure 8.12 continued....

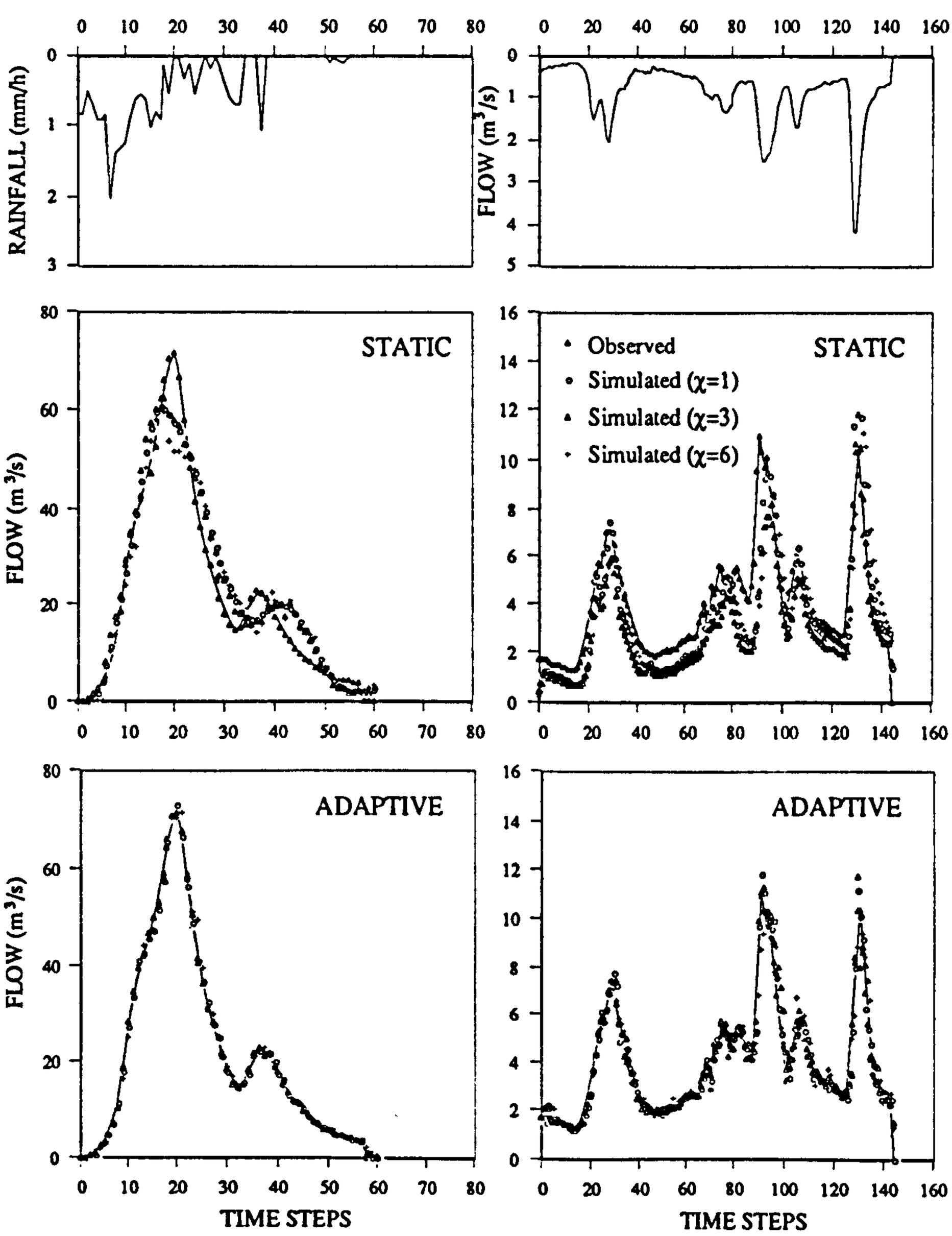

Fig. 8.12 (Event 7-8)

Figure 8.12 continued....

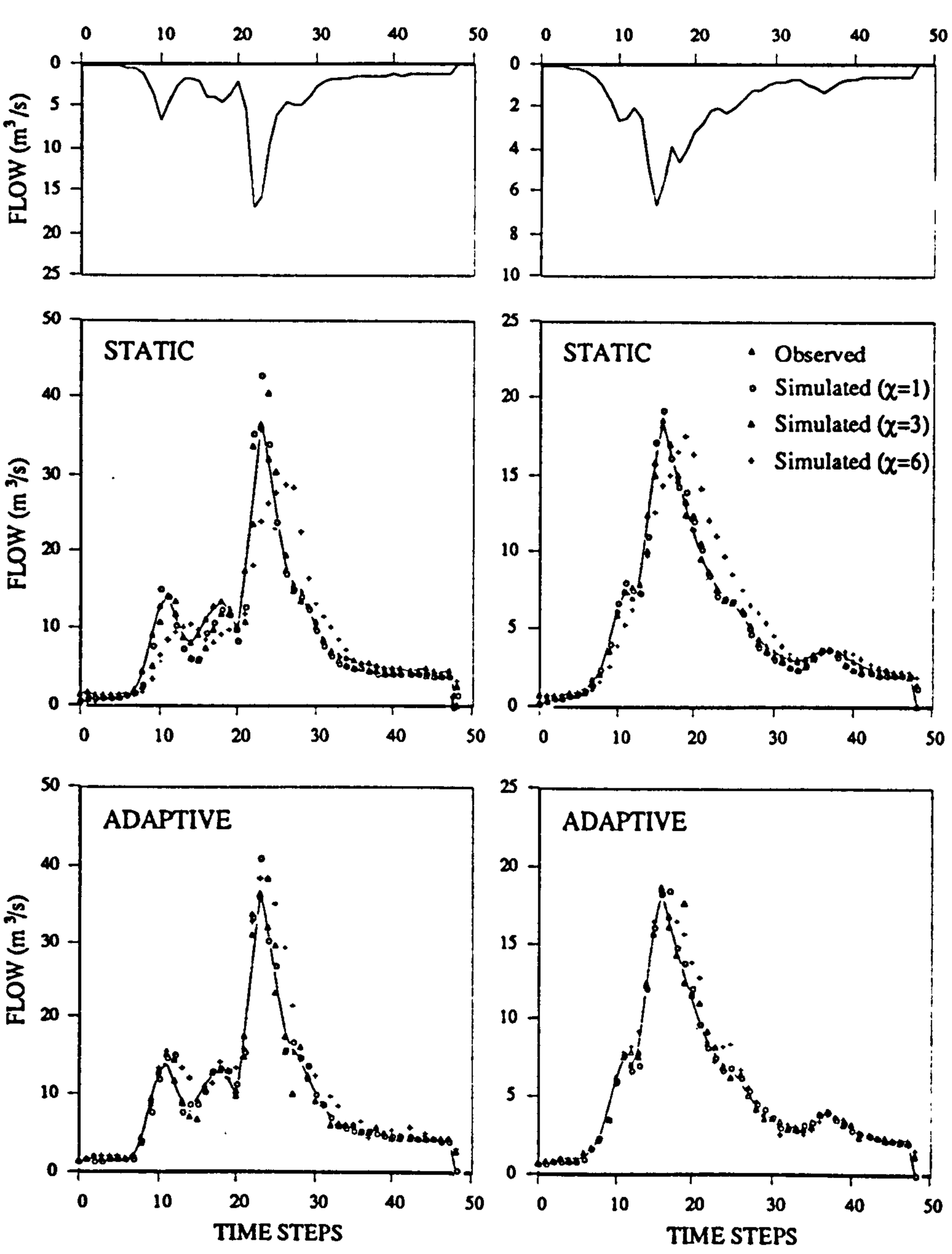

Fig. 8.12 (Event 9-10)

Figure 8.12 continued....

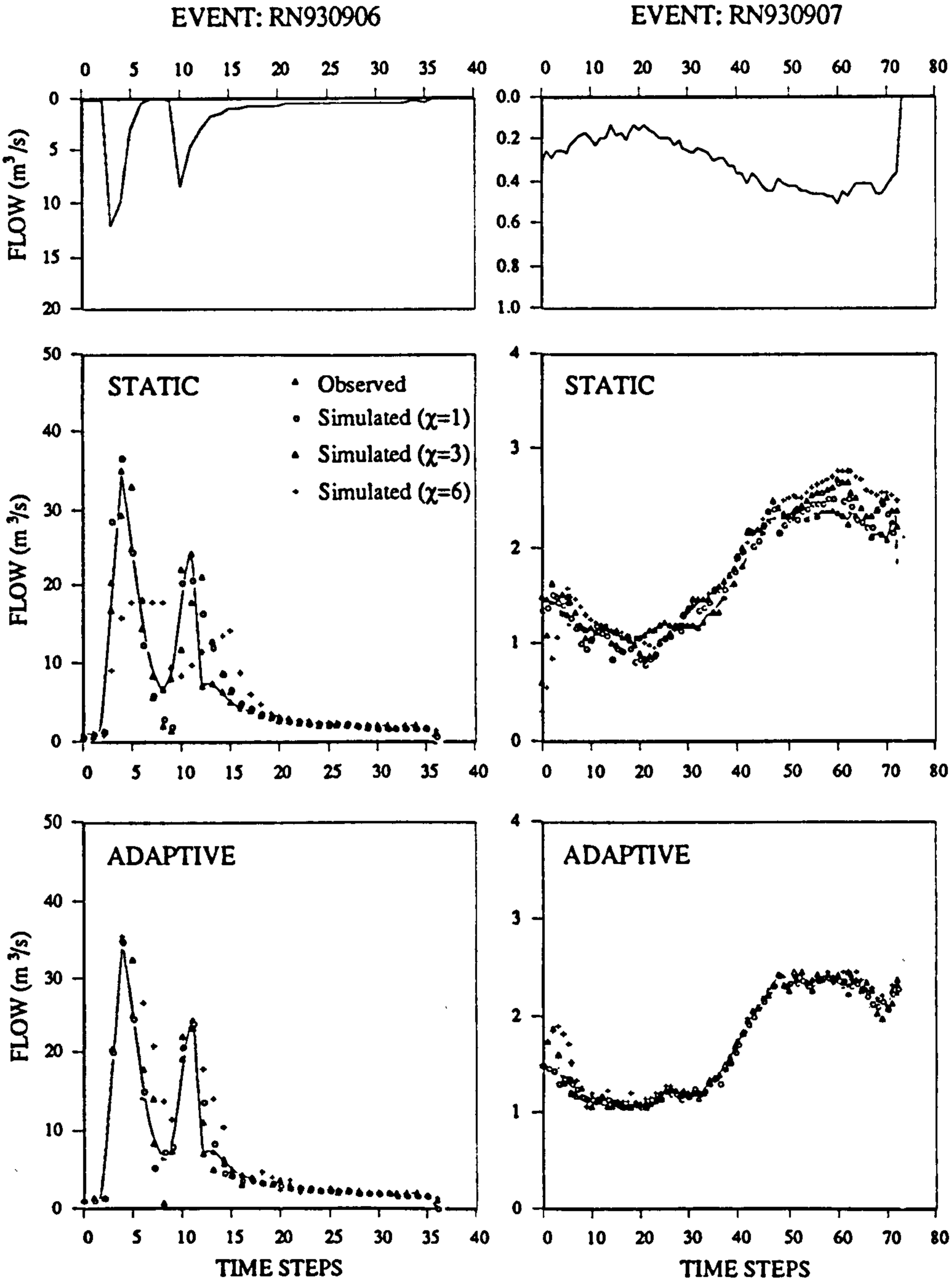

Fig. 8.12 (Event 11-12)

Figure 8.10 shows the comparisons of the static simulation errors, Figure 8.11 shows the comparisons of the adaptive simulation errors and Figure 8.12 compares the twelve simulated hydrographs with the observed hydrographs. The vertically flipped graph at the top of each figure is the model input when χ=1. For the sake of simplicity, only the hydrographs produced using the Naive CPTF model were shown in the figure. The comparisons revealed that :

(1) in static simulation mode, the performance of a Naive CPTF model and Advanced CPTF model was almost identical, especially when the model input data resolution is high (i.e. χ is small). This is just what has been anticipated since the Advanced CPTF model has an almost identical PR to the Naive CPTF. The relation between the model input data resolution and the modelling errors will be further discussed in next section

(2) in (parameter) adaptive simulation mode, the Naive CPTF model produced better results than the Advanced CPTF model. Due to the incompatibility of the updated PR with the old state estimation or the independency of the previous model estimation to the present estimation the Advanced CPTF model produced considerably larger simulation errors when the model input data resolution is low (i.e large χ). This result suggests that, if the model input data resolution is too coarse it is not feasible to use an Advanced CPTF model for the purpose of a parameter adaptive application. Going further, parameter updating must be exercised with caution for any TF model that constitutes flow terms, which confirms the earlier results of Harpin (1982).

(3) in general the adaptive simulations using Naive CPTF model were more accurate than the static simulations. With the adaptive CPTF model utilised for the inter-comparisons, it was able to simulate the urban drainage systems, and the accuracy was dependent on the input data resolutions (see also Chapter 3).

8.4 Discretising Rule for Model Input

A rainfall-to-runoff or flow-to-flow event is a continuous system in time, however, usually approximated by a discrete system in operational hydrology. There are two types of discrete time series as described in Chapter 3. While the input to a CPTF is an averaged time series then the smoothing effect occurs, which helps to eliminate the random errors (i.e white noise) from the original system realisation. However, will this also distort the original time series and result in modelling errors?

A natural catchment is a low pass filter (Cluckie, 1989), which is mimicked by the PR function (eg. PR-C). Theoretically, any variance embodied in the input data with higher frequency than that allowed to pass the filter will be eliminated from the model output. Therefore, so long as the smoothing due to a decrease in the input data resolution does not cause a loss of the low frequencies that are able to pass the filter then the removal of the higher frequencies is harmless. This is because the higher frequencies in the input data will be eliminated by the model anyway. Which frequencies will be eliminated is dependent on the filter characteristics, such as the length of the filter (i.e. number of ordinates).

Isermann (1980) found that, a suitable χ should satisfy: $T_{95}/15 < \chi < T_{95}/6$, where T_{95} is the time when the accumulation of the PR over the range from Δ to T_{95} has reached 95% of the total accumulations over the range from Δ to ∞. However he revised this rule into $T_{95}/15 < \chi < T_{95}/4$ in 1981. The upper boundary was increased 1.5 times. Differing from Isermann, Bittanti and Scattonlini (1982) used T_{90} as the reference point and suggested a rule as $T_{90}/15 < \chi < T_{90}/5$. Similar to this rule, Powell and Cluckie (1985) stated that χ should satisfy $T_{90}/20 < \chi < T_{90}/10$. All these rules have confirmed that an appropriate model input discretising interval is dependent on the filter length and the major filtering effect is achieved by the first few values of the filter. Nevertheless, of these rules which should be observed?

As it is felt that the choice of the reference point in developing the above rules was too arbitrary and subjective, an alteration was investigated by looking at the relation between the simulation errors and the inflection point U_i, which is concededly an objective indicator of the turning point of the system's intrinsic property. A careful study of the relationship between the input data resolution and the performance of the static Naive CPTF model revealed that, the simulation errors have a strong correlation with $[U_i-\Delta+1]/2$, which is Half Of the Lag-To-Inflection Duration (HOLTID). See Figure 8.13.

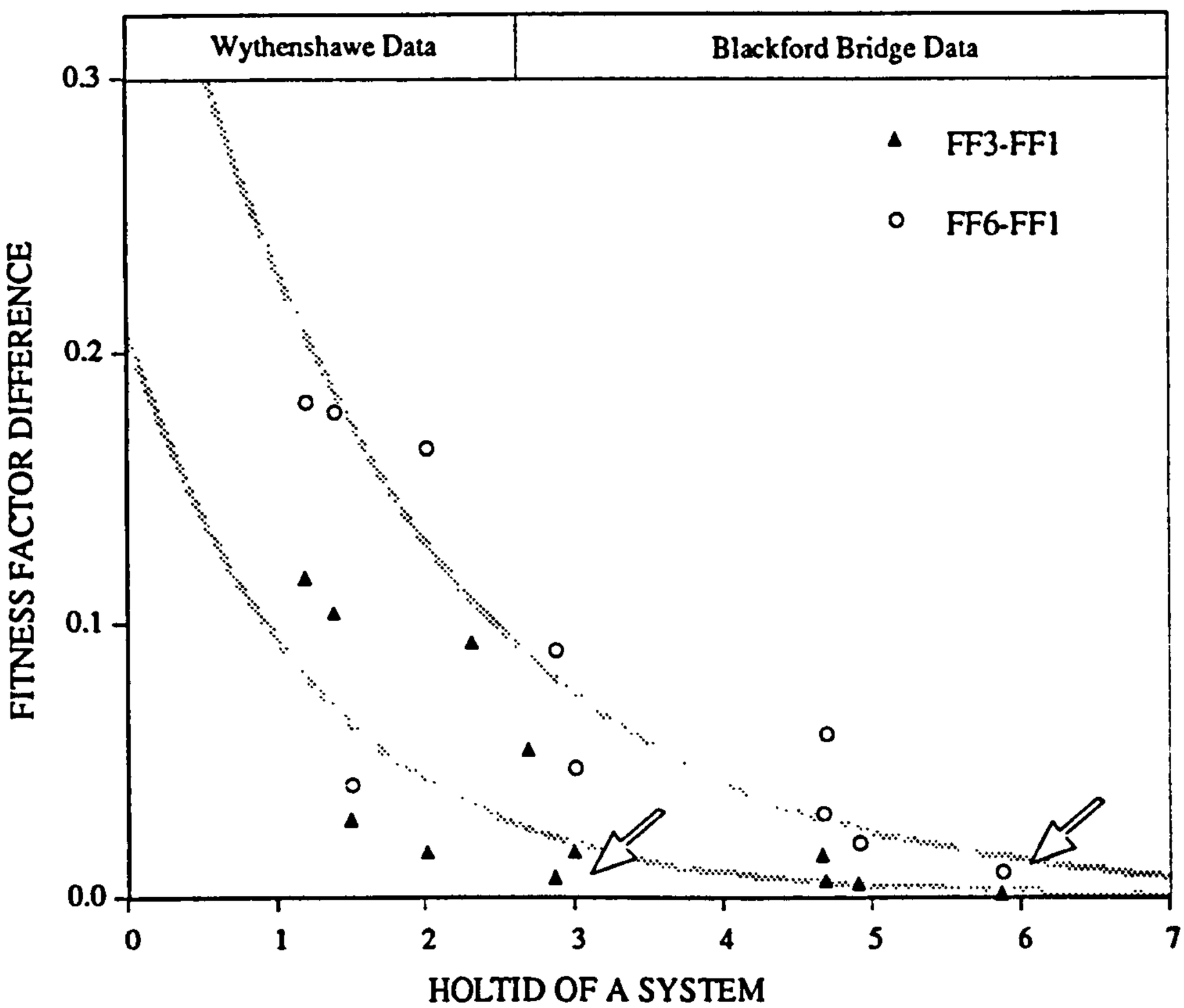

Fig. 8.13 Relationship between the simulation errors and HOLTID

Note: The differences between the fitness factors (i.e. simulation errors) were calculated as FF3-FF1 and FF6-FF1, where FF1 FF3 and FF6 respectively is the simulation error produced when the data resolution of model input is χ=1, χ=3, χ=6 steps. The arrows are pointing to the systems that has a 3-step and 6-step HOLTID respectively. Simulation errors were significant if the input data resolution was greater than the system's HOLTID.

The figure shows the error increments resulting from the reductions in input data resolutions respectively from 1 step to 3 steps and from 1 step to 6 steps. The arrows in the figure are pointing to the systems having a 3-step and 6-step HOLTID respectively. For the system with a 3-step HOLTID, using χ=6 produced more significant simulation errors than using χ=3, whereas for the system with a 6-step HOLTID the errors produced when χ=3 and χ=6 were quite close to each other. This indicates: if the input data resolution χ is larger than the system's HOLTID (i.e χ > HOLTID), then significant simulation error will occur.

Based on this discovery, a rule for judging the adequacy of an input data resolution to a hydrological model is suggested as:

$$\chi \leq \frac{U_i - \Delta + 1}{2} \quad ; \quad \chi = 1, 2, 3\cdots \tag{8.1}$$

Where, the HOLTID is in steps and can be derived using the model's PR function which need to be identified from the system's realisations. The rule says 1) the model input data resolution may take any value being shorter than or equal to the HOLITD; 2) If the derived HOLTID is greater than 1, it means that the system's discretising resolution is fine enough and a larger χ, say 2, is likely to be feasible; otherwise 3) it means that the system's discretising resolution is possibly not adequate. Therefore, a smaller discretising interval should be examined in making the observations of the system.

The effect of resolution reduction in the model input data on the PR functions is illustrated in Figure 8.14, which shows the PR functions identified for each event and input data resolutions (i.e. χ =1, 3 and 6) for the two catchments.

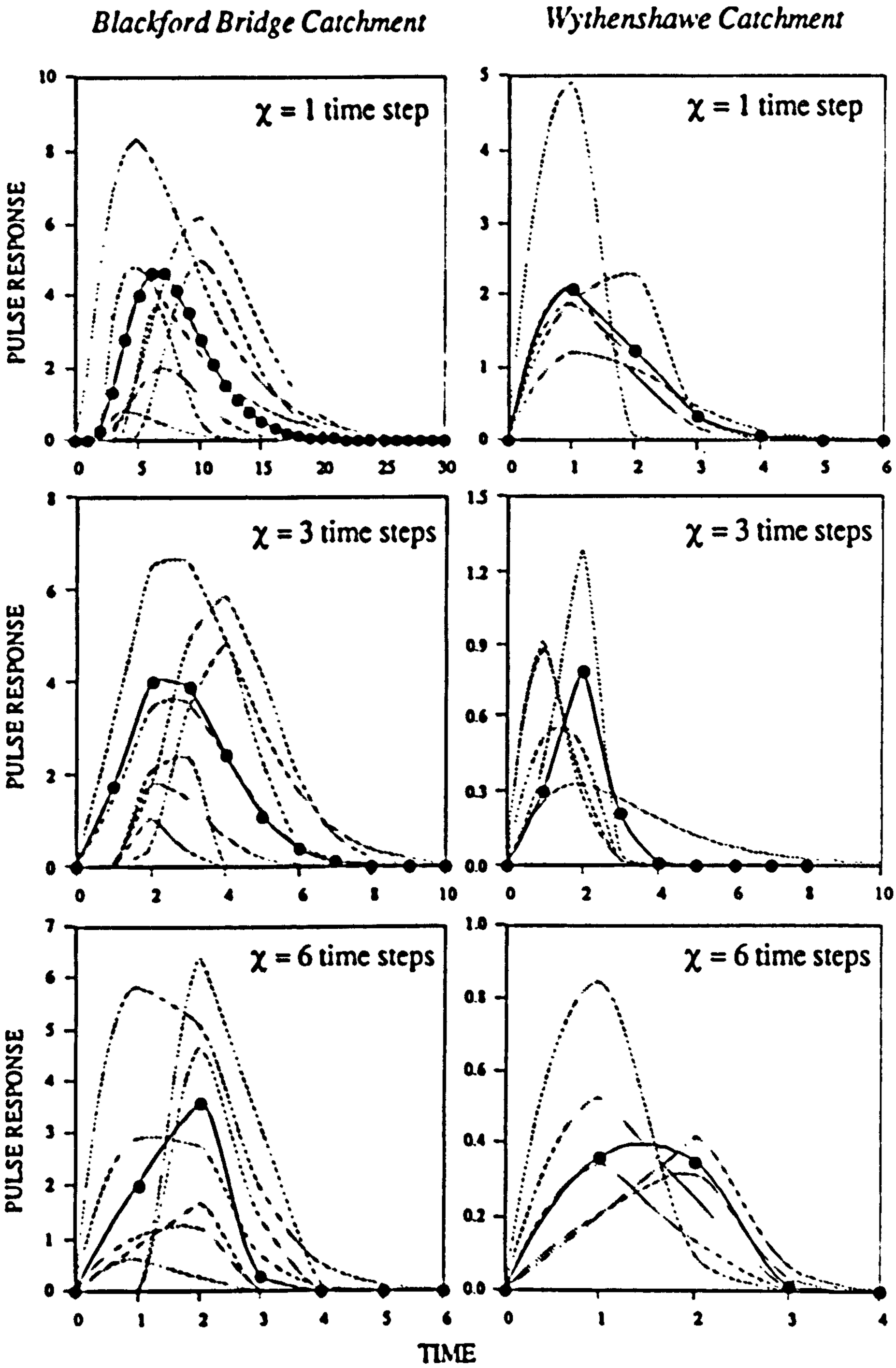

Fig. 8.14 Pulse Responses identified for different input data resolutions

(Note: the time interval is χ steps and the solid lines are the average PRs)

Resolution reduction produced a shrink of the PR ordinate numbers. Clearly, an increase in the data resolution will yield a reverse effect. The solid line shown in the figure is the average PR calculated using the mean value of each PR parameters. It is assumed that an average PR represents the mean condition of a catchment which is defined by the mean PR parameters.

At this point, it can be stated that the reduction of temporal data resolution due to averaging does not necessarily mean the reduction of modelling accuracy providing that the reduced resolution is still less than the system's HOLTID. HOLTID is the lowest resolution of the input data applicable to a model. With this conclusion the analysis that had been conducted previously in Chapter 3 on the temporal data resolution issue is made complete here.

8.5 Performance in Drainage Flow Prediction

From the simulation results, the performance of the CPTF model in simulation of an UDS has been seen as satisfactory, especially when an adaptive CPTF model is used. However, this does not automatically mean that the model can yield high-quality predictions. Various aspects being relevant to the system characteristics and the model will affect the prediction quality, of which, the system linearity and stability are the two dominant factors. Stability is the degree of temporal dependency of the successive observations and linearity is the way that the system's output level reacts on the input. If a model is able to well represent the system's linearity then it is regarded as qualified for being a forecasting model. CPTF model is such a model because the PR parameters of CPTF model has excellent adaptability in coping with the system's linearity, i.e. same input is allowed to produce different percentage outputs over different durations. However, its forecasting performance will be dependent on the system's stability. Prediction lead time, determined on the assumption that the model fitted to past data will also be true in the future, is generally too absolute because the system may not be stable; no stability no forecasting.

Having made the responsibility of a CPTF model in prediction clear, its performance was demonstrated with reference to the two simulated hydrological systems again and with the following assumptions and description conveniences:

- Forecasting time is the time when flow prediction is to be made;
- Forecasted time is equal to the forecasting time + lead time;
- Model parameter updating is made at every forecasting step;
- Input data are available up to the forecasted time;
- Flow prediction for a lead time of 1-step, 3-step or 6-step are required.

The flow prediction procedure is shown in Figure 8.15.

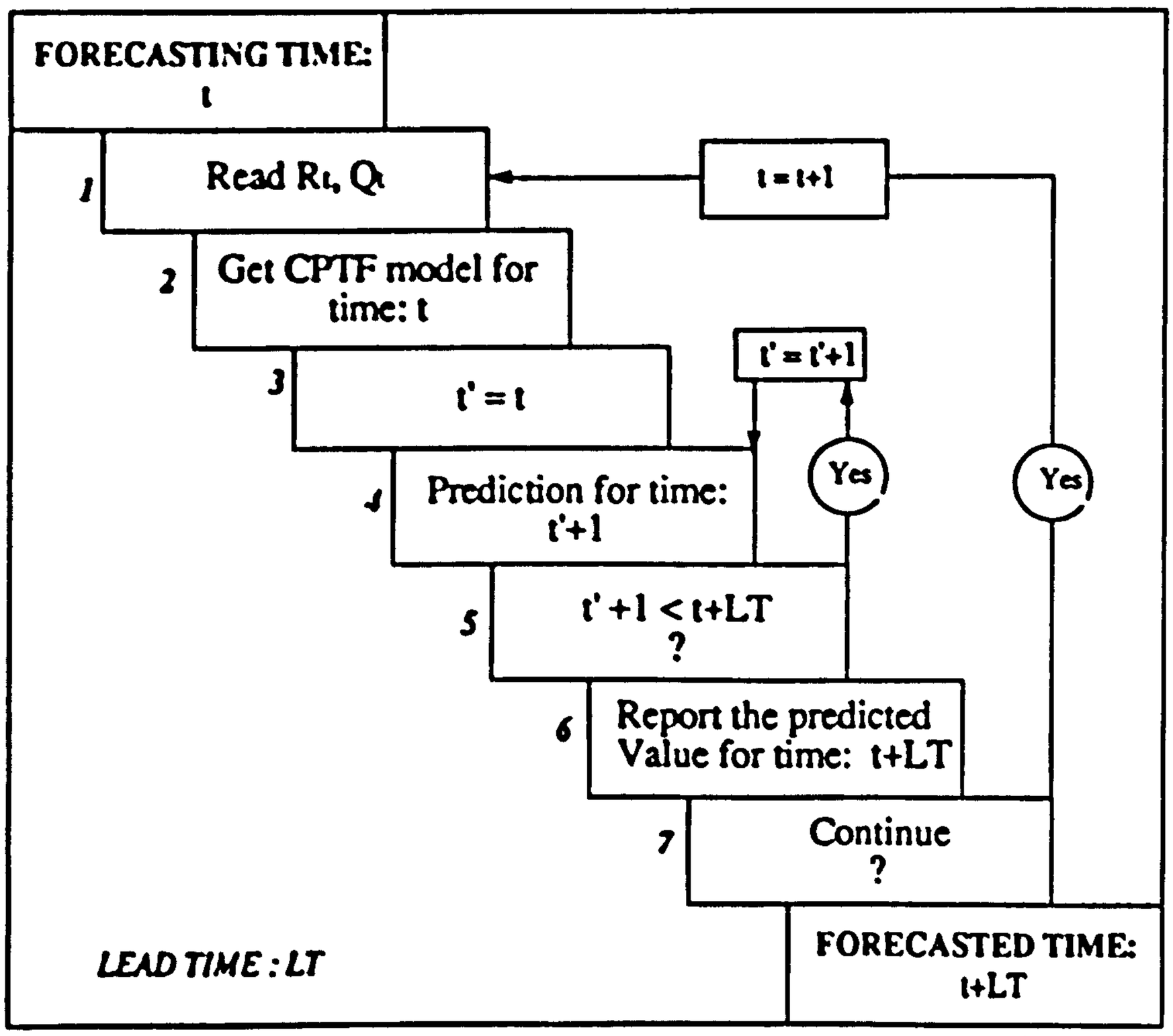

Fig. 8.15 Prediction procedure

It is progressive forecasting made step by step. A prediction for a lead time, LT, will be made for a number of LT successive time steps: t+1, t+2, ···, t+LT starting from the forecasting time, t. However, when a Naive CPTF model is used, prediction can be made directly for the time LT steps ahead, because there is no need to derive the intermediate predictions. The most important stage is the second stage when if the forecasting is made in static mode then an average model will be always used otherwise the model's parameter or state will be updated.

For each input-output event listed in Table 8.4 and Table 8.5, the predicted hydrographs were produced respectively using the Naive CPTF model and Advanced CPTF model. The scheme for comparing different predictions is shown in Table 8.8.

Table 8.8 Scheme for comparing different predictions

<table>
<tr><th>Prediction Mode</th><th colspan="2">Model Form</th><th>Leading Time (steps)</th></tr>
<tr><td>STATIC</td><td colspan="2">Average Naive CPTF</td><td rowspan="3">LT = 1

LT = 3

LT = 6</td></tr>
<tr><td rowspan="2">ADAPTIVE</td><td>PARAMETER UPDATING</td><td>Naive CPTF</td></tr>
<tr><td>STATE UPDATING</td><td>Average Advanced CPTF</td></tr>
</table>

In static prediction mode, the average Naive CPTF model was used with its PR being the average PR derived as χ =1 step (see Figure 8.14).

In adaptive prediction mode, the predictions were made respectively by the parameter adaptive Naive CPTF model and the state adaptive Advanced CPTF model. The later was derived using the average PR derived as χ =1 step.

In order to know the prediction accuracy when the lead time, LT, takes different time

steps the static and adaptive predictions were carried out respectively for LT taking 1, 3 and 6 time steps.

Figure 8.16 shows the comparisons of the prediction errors.

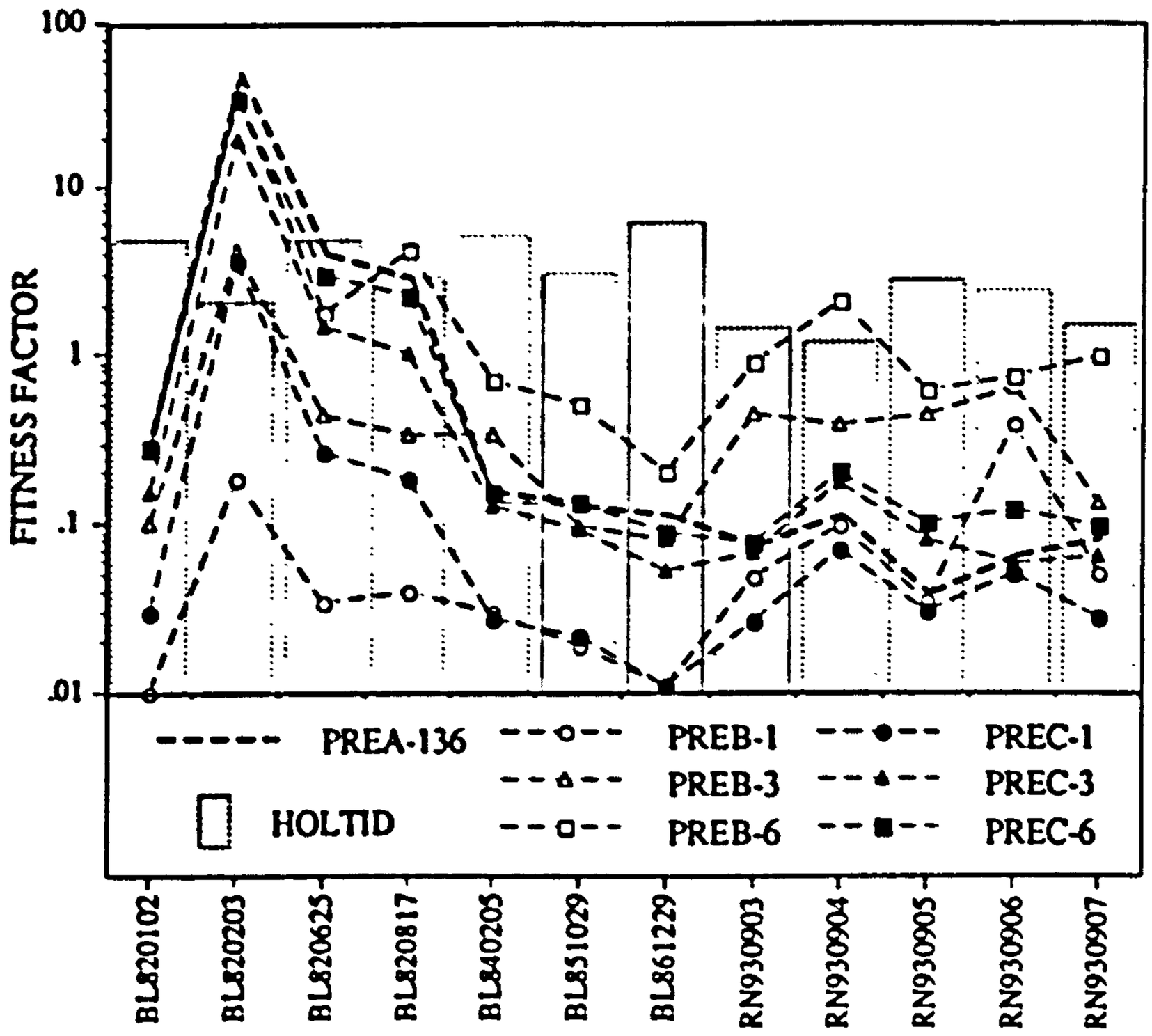

Fig. 8.16. Comparison of the prediction errors

(Note: PREA: Static prediction using the average Naive CPTF models. PREB-LT, LT-step ahead adaptive prediction using the parameter adaptive average Naive CPTF models. PREC-LT, adaptive prediction using the average Advanced CPTF models with state updating.)

In the figure, PREA keys the static predictions. As the predicted flows were made by convoluting the inputs with the average Naive CPTF models, therefore, the predicted hydrographs and prediction errors are identical for any lead time. Such predictions are sometimes called simulative predictions; PREB denotes the adaptive predictions which were produced using the parameter adaptive Naive CPTF model and PREC, the adaptive prediction made using the average Advanced CPTF model with state updating. The system HOLTID values were also shown in the figure (vertical bars).

It can be seen from the figure that prediction errors varied with the system characteristics, lead time and the prediction mode:

(1) The performance of a static average CPTF model (i.e. PREA) is determined mainly by the characteristics of the individual PRs of each event from which the average PR was derived. It is evident that for the system labelled as RN the performance of the model was quite promising because the average PR was representative. However, an average static CPTF model was not adequate for predicting flow for the catchment labelled as BL, whose PR was highly variable among the events.

(2) The performance of an adaptive CPTF model with parameter updating (i.e. PREB) was mainly dependent on one factor: the HOLTID. Given, a HOLTID, the prediction errors increased as the lead time increased, however, with a same lead time, the longer HOLTID, the smaller errors in general. Since the model can adjust itself, the poor representability of the static average model could be mitigated to some extent. e.g. the improvements achieved for the catchment labelled as BL. However, in cases when the average models were representative the performances of the parameter adaptive CPTF model were not able to compete with the state adaptive CPTF model (PREC) or even with the static average CPTF model (PREA). This means if a model is well representative at the time 't' may not be well representative at 't+1'.

(3) The performance of an average CPTF model with only state updating (i.e. PREC)

was dependent on two factors, the variability in the system PR and the HOLTID of the system. Roughly, three situations were recognised:

i) *The* average *model was not representative;* e.g. the model of the Blackford Bridge system. The static predictions were improved by state updating, especially, when the lead time is relatively short compared to the HOLTID of the system.

ii) *The* average *model was representative and the lead time was short compared to the HOLTID of the catchment;* In this situation, the model's performance was apparently superior to the static average model. e.g. PREC-1 for the events of Wythenshawe system labelled as RN.

iii) *The* average *model was representative and the lead time was relatively long*; The state updating caused larger prediction errors than the static predictions due to the feedback of independent observations . e.g. PREC-3 and PREC-6 for the events of the Wythenshawe system. This was the only situation when the state adaptive average CPTF model could not beat the static average model.

In summary, the prediction errors were strongly correlated to the system's HOLTID, which determines the dependency of the observations to each other and therefore sets the possible prediction accuracy that may be achieved using a CPTF model. For those systems having wider variation range of the PR, using a parameter adaptive CPTF model can achieve better prediction results; whereas for those having less PR variability using an average state adaptive CPTF model is a wise choice.

Comparisons of the statically and adaptively predicted hydrographs with the observed hydrographs (12 events) were shown in Figure 8.17. The vertically flipped graph at the top of each figure is the model input at $\chi=1$.

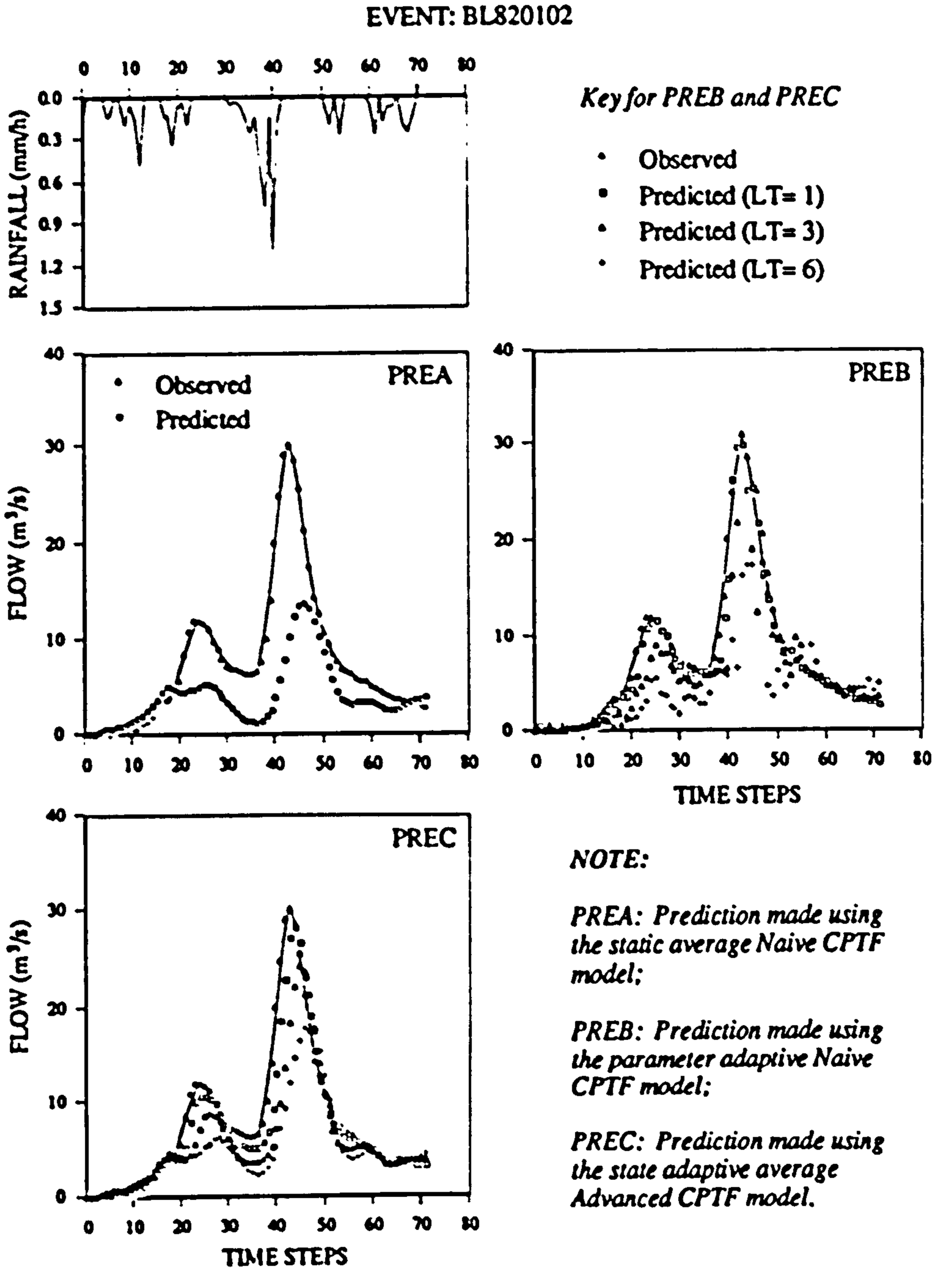

Fig. 8.17 (Event 1) Comparison of the predicted and observed hydrographs

Note: The vertically flipped graphs show the model inputs. The static and adaptive predictions were respectively made for different lead time steps (LT=1, 3 and 6 steps)

(To be continued)...

Figure 8.17 continued...

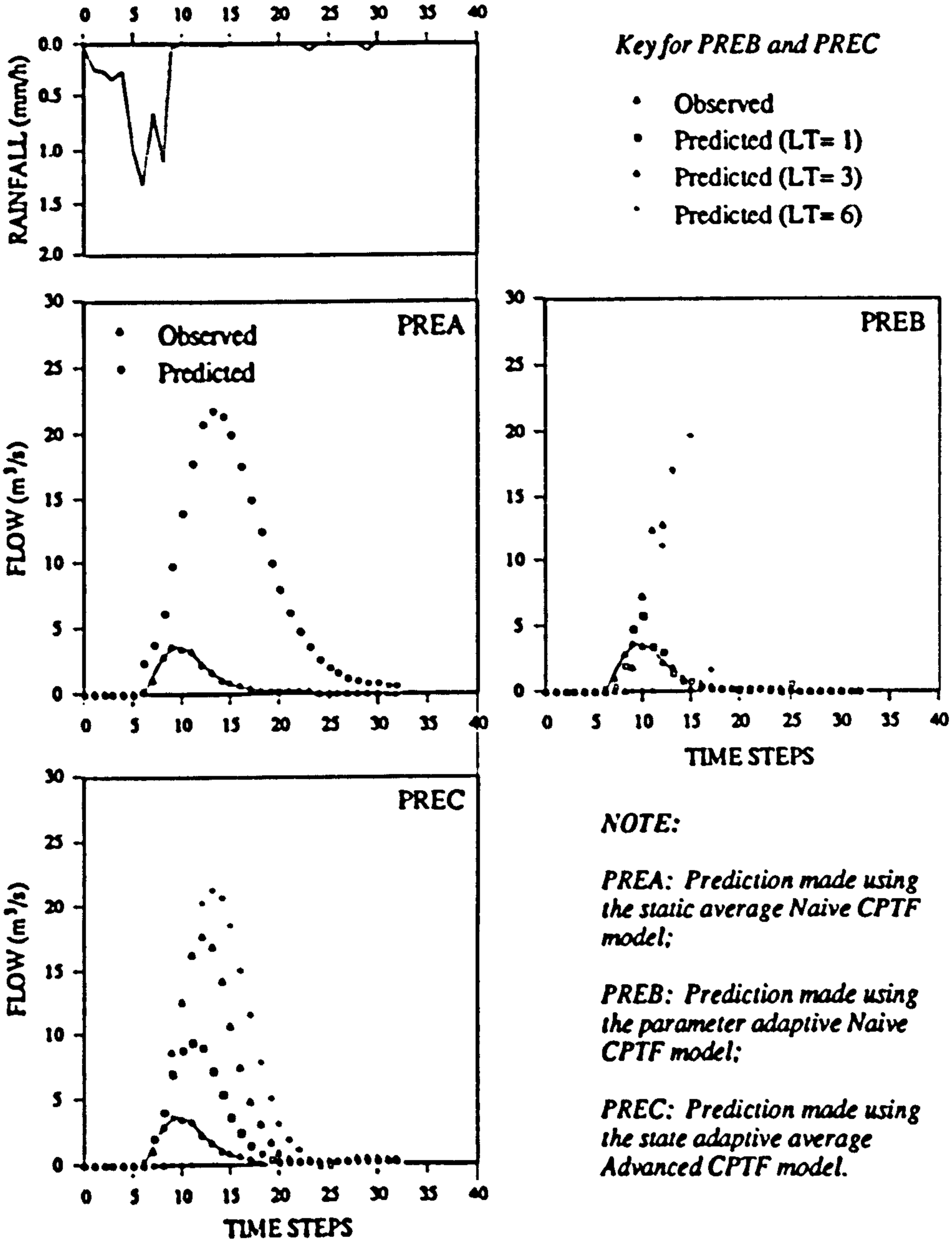

Fig. 8.17 (Event 2)

Figure 8.17 continued...

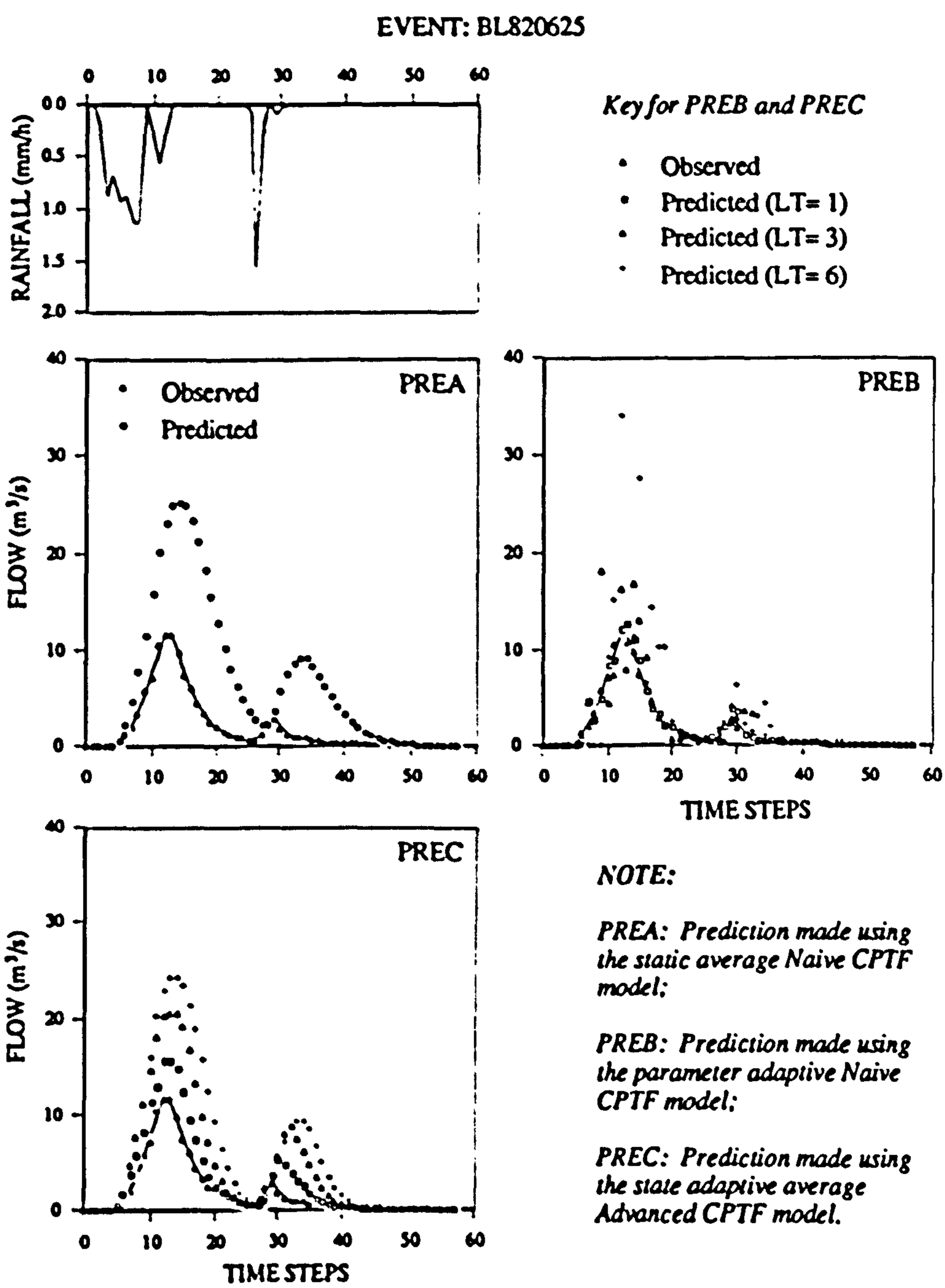

Fig. 8.17 (Event 3)

Figure 8.17 continued...

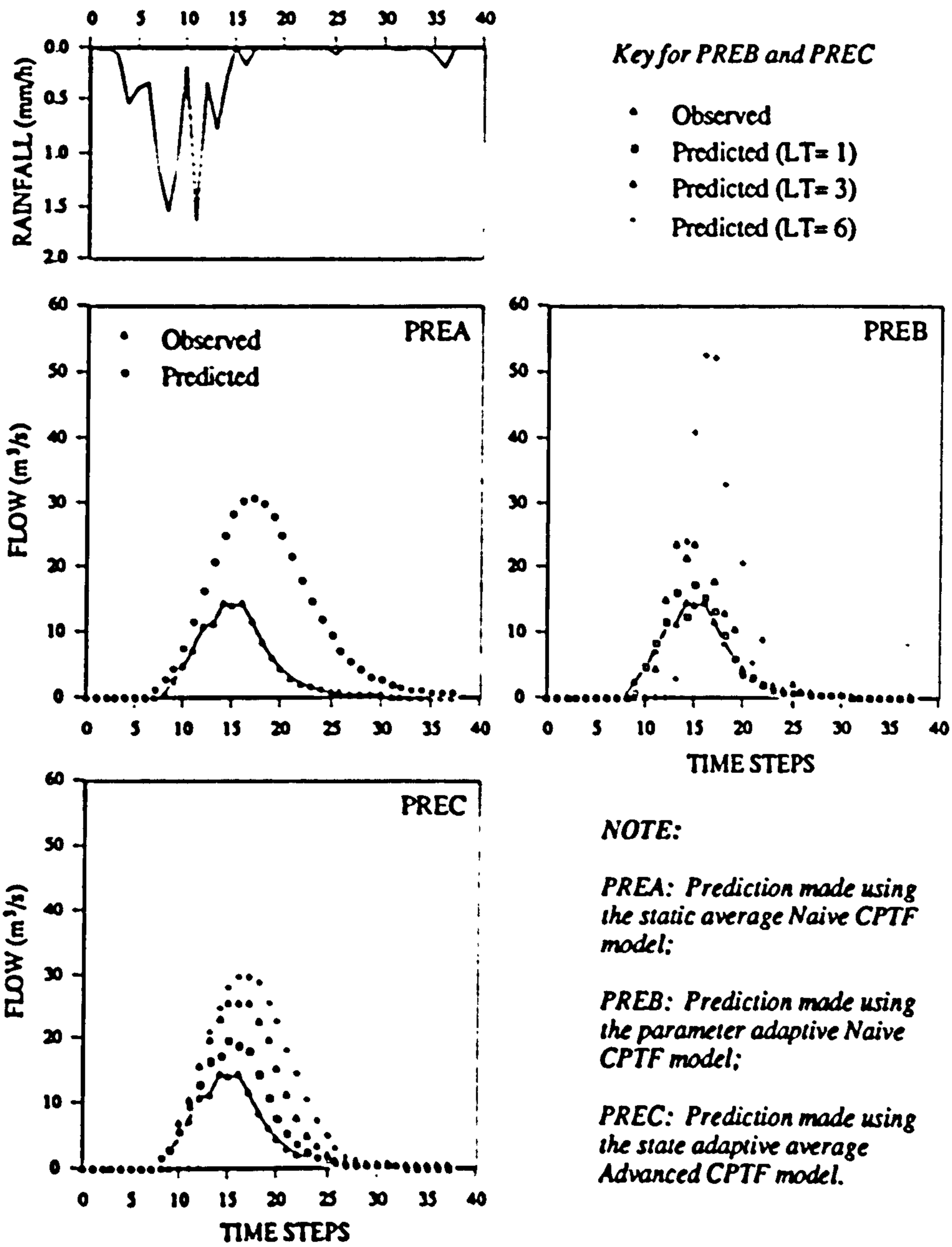

Fig. 8.17 (Event 4)

Figure 8.17 continued...

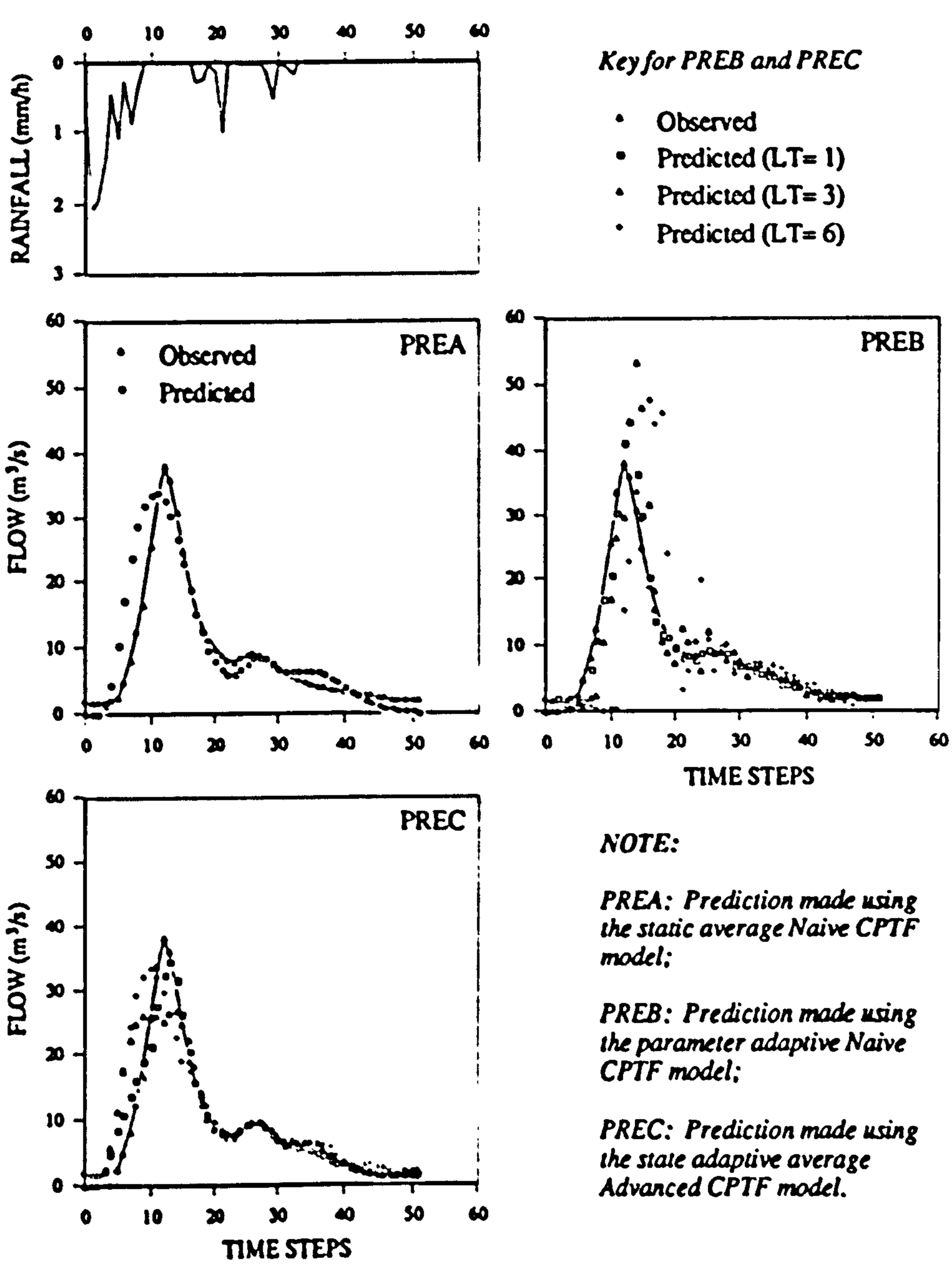

Fig. 8.17 (Event 5)

Figure 8.17 continued...

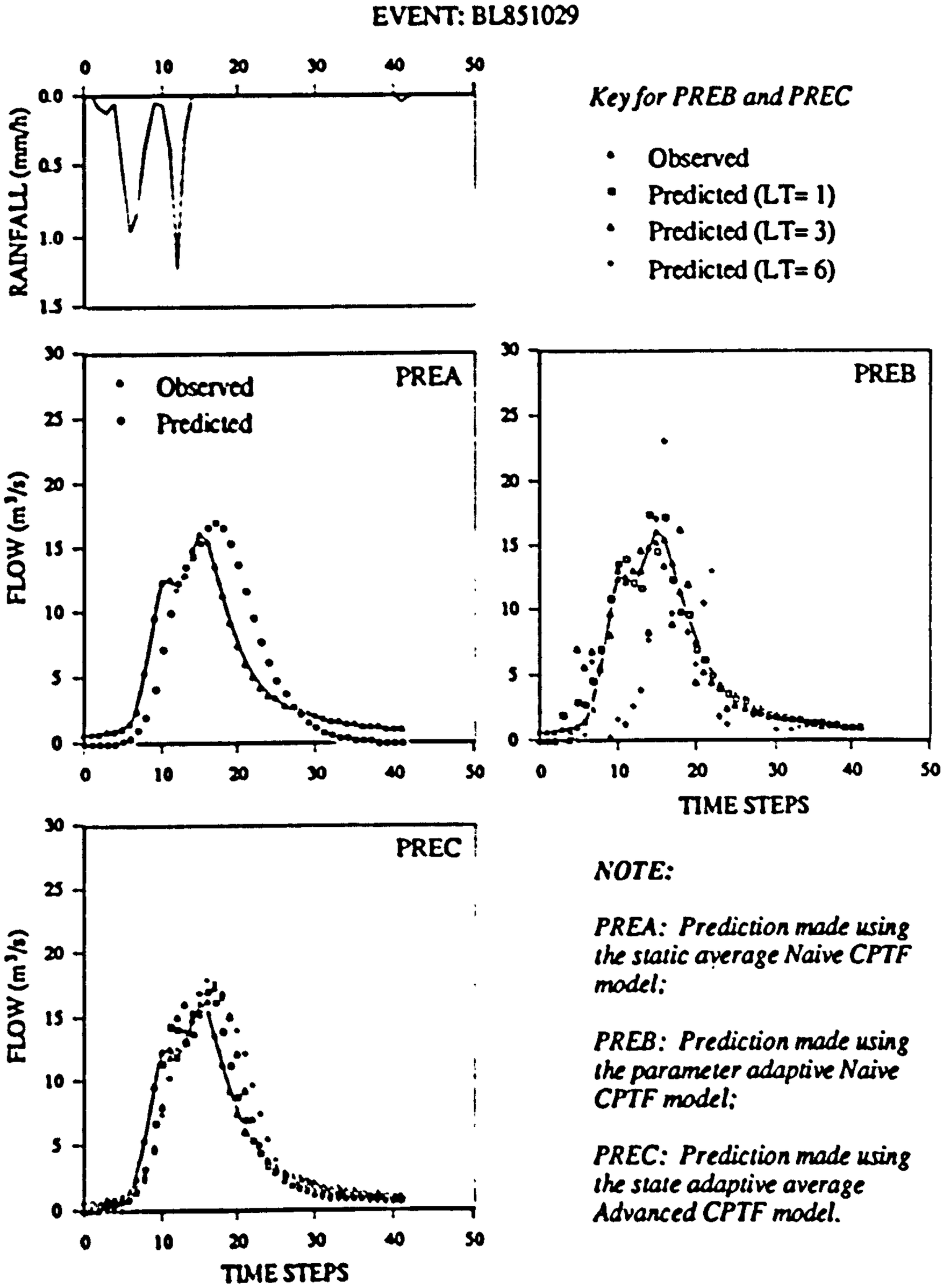

Fig. 8.17 (Event 6)

Figure 8.17 continued...

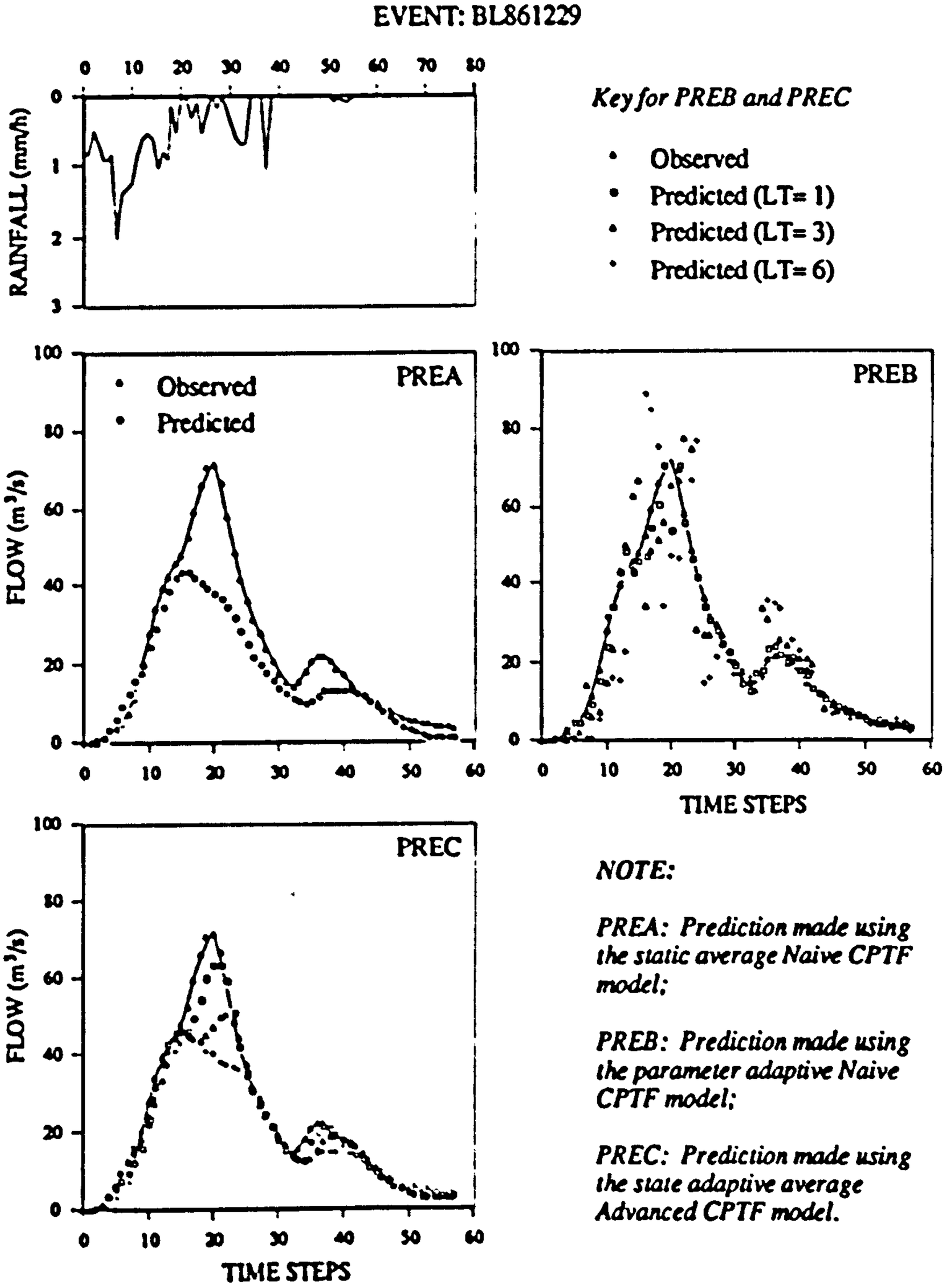

Fig. 8.17 (Event 7)

Figure 8.17 continued...

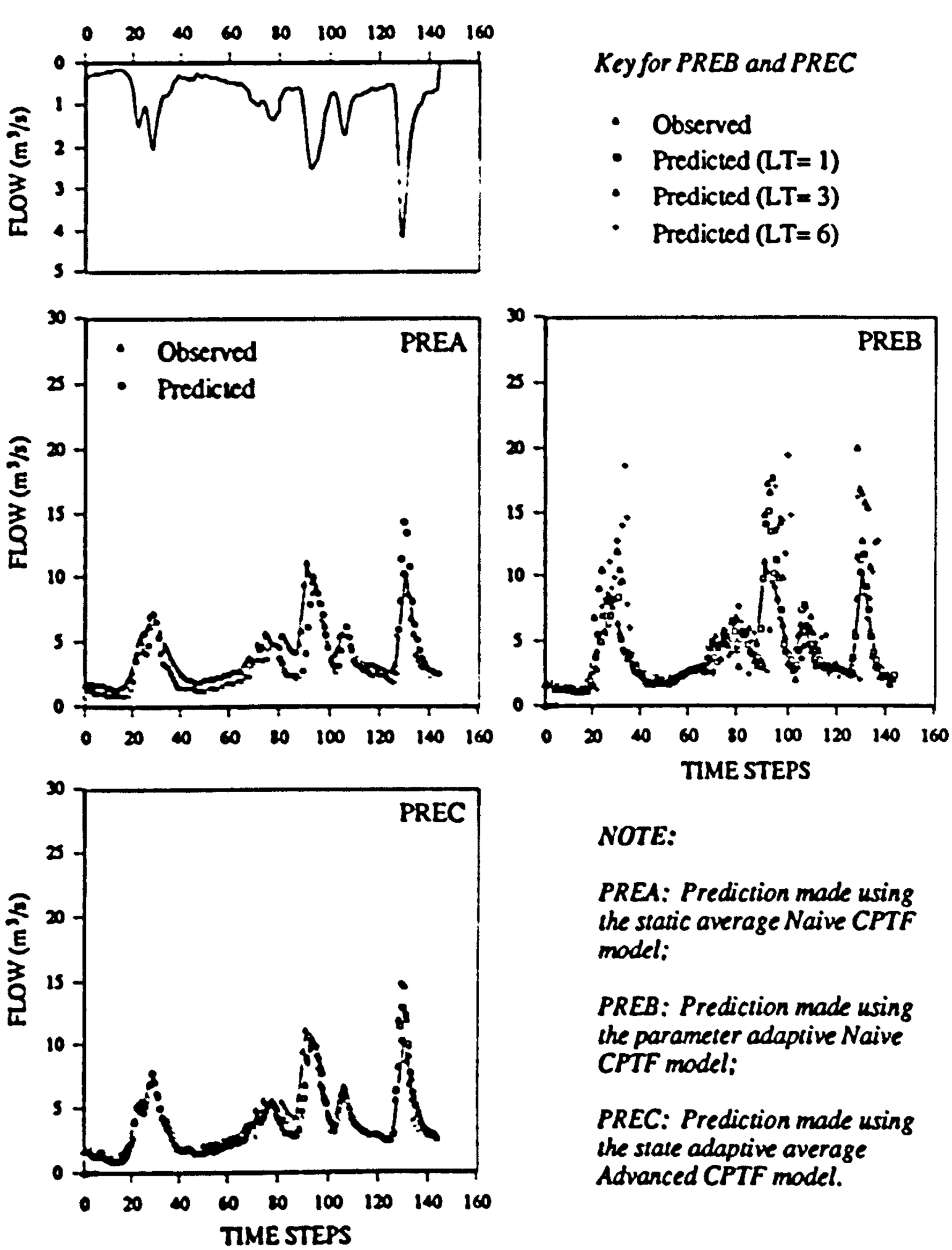

Fig. 8.17 (Event 8)

Figure 8.17 continued...

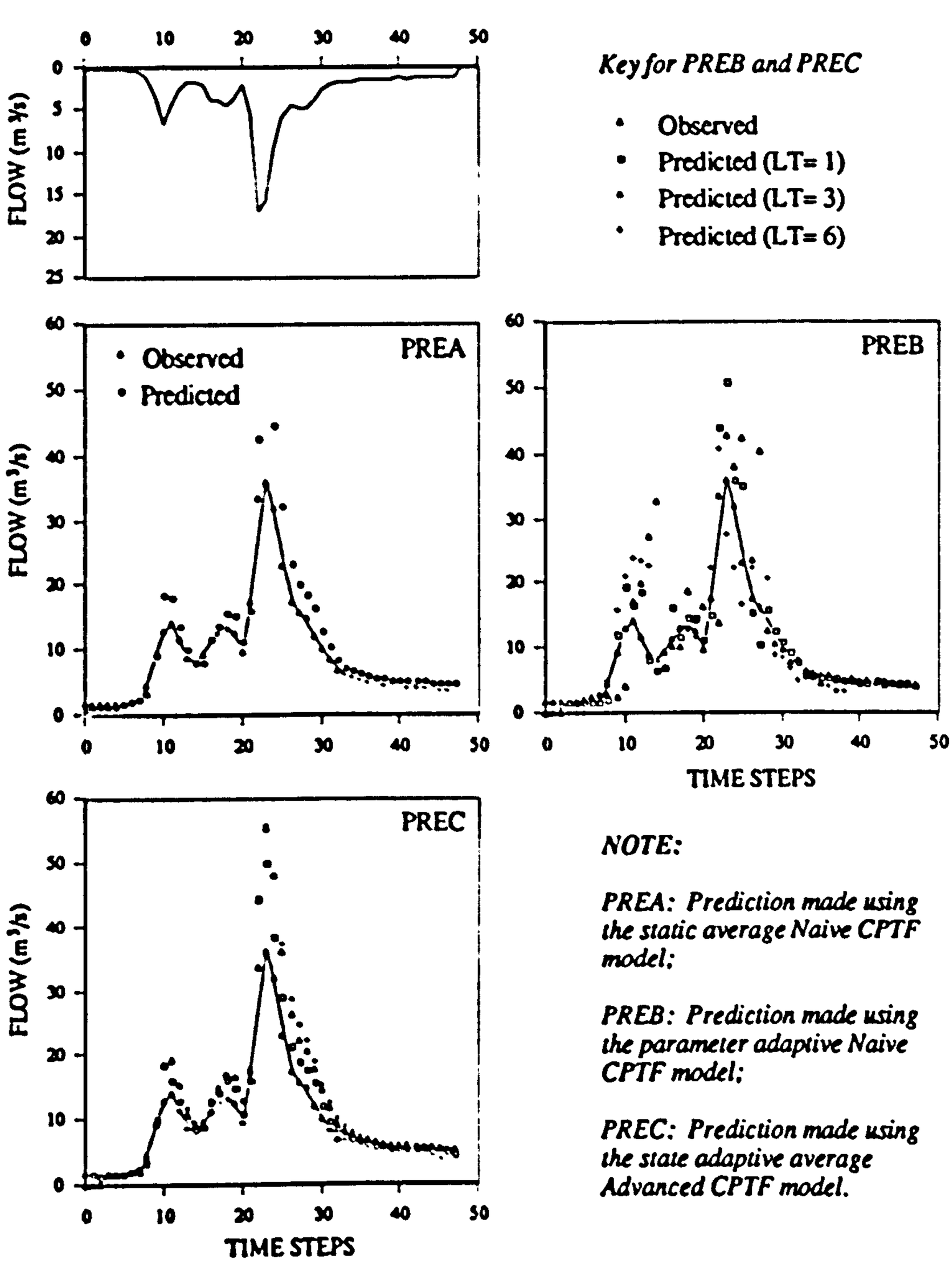

Fig. 8.17 (Event 9)

Figure 8.17 continued...

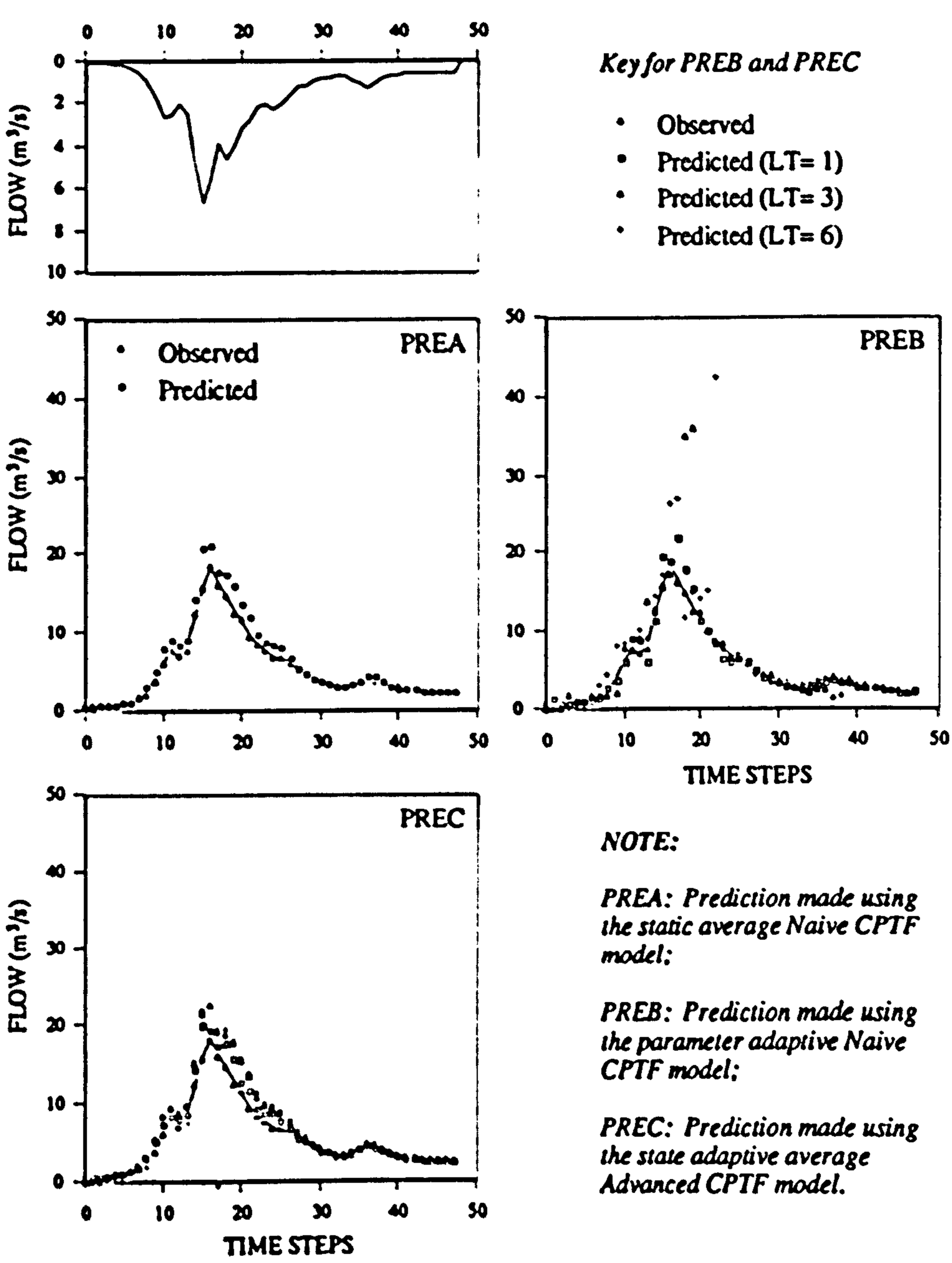

Fig. 8.17 (Event 10)

Figure 8.17 continued...

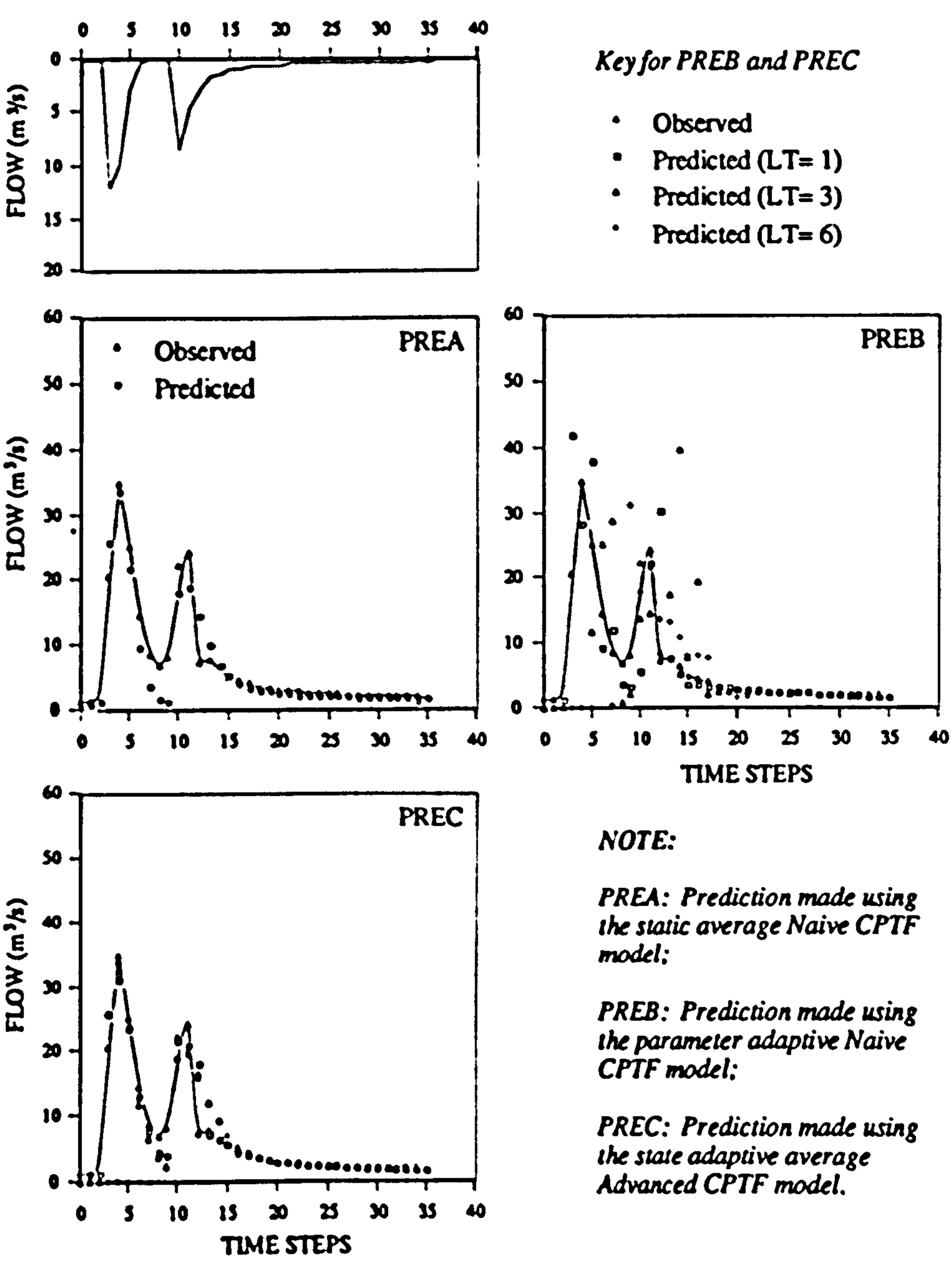

Fig. 8.17 (Event 11)

Figure 8.17 continued...

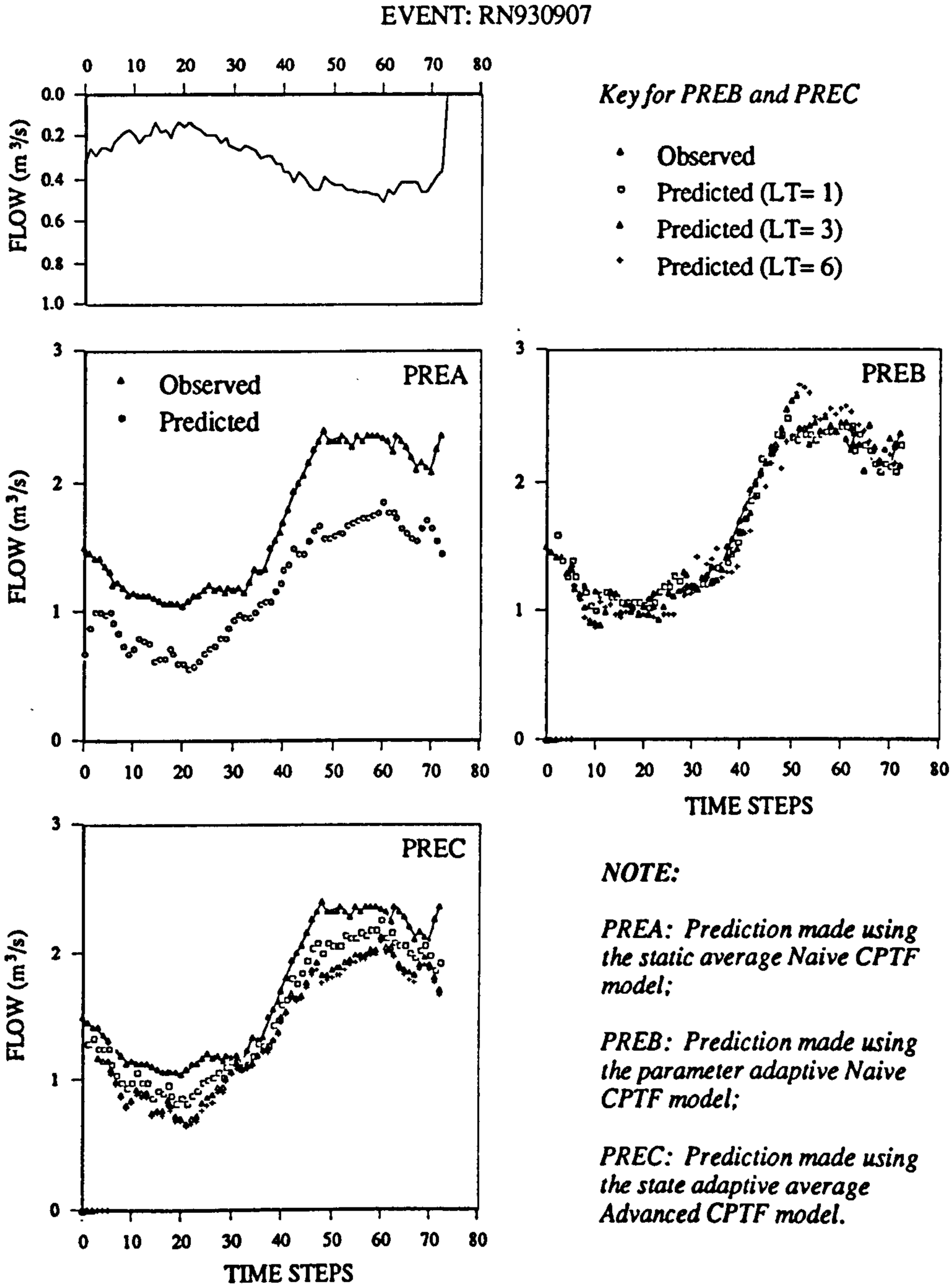

Fig. 8.17 (Event 12)

8.6 Summary

(1) CPTF model is simple, adaptable, robust and maintainable, therefore is suitable for real-time urban drainage flow simulations and predictions.

(2) The performance of a CPTF model is at least as good as a NCTF model in flow simulations. However, for adaptive forecasting applications, CPTF model is more robust and flexible than the NCTF model.

(3) Naive CPTF model can be used to adequately mimic a UH model. However, unlike the UH, no constraints were explicitly imposed during the development of the model. Net rainfall derivation and base flow removal is not obligatory because the same input is allowed to yield different output levels and over different durations.

(4) The Half Of the Lag-To-Inflection Duration (HOLTID) is a dominant factor which governs the validity of a model input data resolution and determines the model's performance in simulation and prediction.

(5) The performance of a CPTF model in simulation of a drainage system is generally satisfactory. However, the simulation errors increases as the input data resolution decreases. When the discretising time interval of the model input is greater than the HOLTID, the increase will be significant.

(6) For operational flow prediction purposes, a CPTF model may be adopted based on the PR variability of a system: i) if the PR function is less variable then an average CPTF model with state updating will suffice, otherwise, ii) a parameter adaptive CPTF model should be used. Since the PRs of urban drainage systems are less variable than that of the rural systems, the state adaptive average CPTF model has considerable potential for use in the RTC of UDSs.

CHAPTER 9

THE ACCURACY OF RADAR RAINFALL DATA FOR MODELLING

Incorporation of radar rainfall into active control for urban drainage systems has been a perceived possibility (Shepherd, 1987). However, as precipitation is one of the most variable hydrological process this raises a problem when using weather radar to study the process, that is, the accuracy of radar rainfall estimates of precipitation. With the development and application of weather radar systems, this problem has been extensively studied over the past years (see Battan, 1973, Collier, 1989) and a number of major error sources have been recognised (Collier, Larke and May, 1983). As it is unable to obtain the true precipitation measurements subject to the inability of the current rainfall measuring devices, the existing conclusions on the accuracy of radar rainfall data were made on a relative basis, for instance, by comparing the radar observations with the 'ground truth' obtained by ground raingauge. For meteorological application purposes, this is the only and feasible approach that can be opted to quantify the accuracy of radar rainfall measurements. However, for hydrological application purposes, the quantification is inadequate and needs to be extended since the accuracy of radar rainfall data required for weather forecasting may be different from that for input into a hydrological model.

During this analysis, it is assumed that radar rainfall data is used in the urban hydrology context. The problem is addressed following a two-step procedure: 1) by comparing the single-site rainfall data with the observations of a co-located telemetry

raingauge network. Raingauge rainfall is taken as the 'ground truth'; and 2) by comparing the simulated hydrographs with the observed drainage flows. The observed hydrographs serve as an ultimate criteria in justification of the accuracy of radar rainfall data.

9.1 Data Acquisition

Two types of data are used in the following analyses, the rainfall data were observed by the Hameldon Hill radar system and the raingauge network in the Bolton catchment, and the urban drainage flow data were obtained through a telemetry system installed in the Bolton drainage system. The locations of the radar and raingauge network has been previously shown in Figure 3.1.

9.1.1 Radar Rainfall Data

A time-space series rainfall with a 2-km spatial resolution is used in this study, which was continuously observed over a duration from 00:00 GMT on 26 October to 00:00 GMT on 13 November 1989 (18 days) and at least seven independent storms are recognisable from the data. The basic rainfall intensities were measured instantaneously at every 5 minutes, accurately synchronised, and given an automatic real-time on-site calibration (see Chapter 2). However, to reduce the computation load, hourly rainfall was used in this analysis, which was produced by accumulation of the 5-minute data. The accuracy of calibrated rainfall data is the primary focus of this study.

9.1.2 Raingauge Network Data

Bolton catchment has long been known as having widespread spatial variability during storm times. For a short term flow surveys, 10 telemetry raingauges were established in the catchment to measure the full extent of the spatial effect, and more particularly

rainfall movement. Unfortunately one raingauge failed to give readings due to the dead flies deposited in it! So only 9 raingauges were in operation. The raingauges are tipping bucket type at an accuracy of 0.2 mm/tip. The data was measured over the same duration and area as the radar rainfall data. A temporal resolution of 2 minutes was used for recoding the rainfall data (i.e. number of tips per two minutes). The hourly data used in this analysis was produced by accumulation of the 2-minute data.

9.1.3 Grid Rainfall Estimation Using Raingauge Data

The relative accuracy of radar rainfall data to the raingauge measurements can be assessed using the grid rainfall (i.e. distributed) or the areal rainfall (i.e. lumped). In this analysis, both of the prospects are intended to be compared with the raingauge data. Therefore, the raingauge grid rainfall for each 2km by 2km grid has to be derived from the point raingauge measurements.

A reliable and computer-based objective method with appreciable simplicity in estimating the grid rainfall from raingauge observations is desired. Over the last 50 years or so several methods for estimating grid and areal rainfall from data supplied by a raingauge network have been proposed. These techniques may be grouped into the following broad categories: (1) using the near neighbour gauges either individually or by arithmetic averaging; (2) using the objective or subjective isohyetal analysis; (3) using the Theissen polygon procedure; or (4) using the reciprocal distance square (RDS) methods (Collier 1986). Generally each of the techniques has its advantages on certain aspects but not the whole. Low accuracy of the estimated data or tediousness in use are their main drawbacks. In this study, a RDS method developed based on the Modified Shepherd Method (Franke and Neilson 1980) is used due to its simplicity and effectiveness.

(1) The Basic and Modified Shepherd Method

Raingauge rainfall is a point measurement. The mean depth (mm) over a square area is called grid rainfall and the mean depth over a number of grids is called areal rainfall. Such a definition is just for description convenience. Grid rainfall can be derived using a number of point rainfalls by interpolation.

The Basic Shepherd Method is a two-dimensional surface interpolation procedure, described in Shepherd (1968). It constructs an interpolating surface z=F(x,y) through a set of M scattered data points (x_i, y_i, R_i) using

$$F(x,y) = \frac{\sum_{i=1}^{M} W_i R_i}{\sum_{i=1}^{M} W_i} \qquad (9.1)$$

Where $W_i = 1/d^2$ is the weight of a raingauge and $d^2 = (x - x_i)^2 + (y - x_i)^2$ is the distance of a raingauge from a point.

This method is global in that the interpolated value at any point depends on all the data within the raingauge network. This will result in erroneous interpolation if the rainfall surface varies significantly. Therefore, a modification was made to Eq.(9.1) by Franke and Neilson (1980), whereby the method becomes regional by adjusting each W_i to be zero outside a circle with centre (x_i, y_i) and some radius, r_c. In this way each raingauge is assumed only contributes adequate information up to a distance of r_c. Hereafter, r_c is referred to as Confident Interpolation Radius of a raingauge or CIR.

To further improve the performance of the basic Shepherd Method, a quadratic surface is fitted by weighted least-squares to data local to (x_i, y_i, R_i) and forced to interpolate (x_i, y_i, R_i). In this context, a point (x,y) is defined to be local to another point if it lies within some distance r_L from it. Each point within r_L is supposed to take the value defined by the quadratic surface. Hereafter r_L is referred to as the Local Interpolation Radius of a raingauge or LIR. Obviously, $r_L \leq r_c$.

(2) The Technique Used in This Study

The technique used in this study is developed based on the Modified Shepherd Method, in which rainfall field is considered as spatially varying and a raingauge can only provide acceptable rainfall information to a limited range, r_c. However, a clear approach has been proposed for determination of the CIR and the LIR.

It is posiible to subjectively determine a CIR so long as the 'point' measurements are used to provide areal rainfall information. Nevertheless, the determination should be a matter relative to the density of raingauges (i.e. the number of raingauges per km^2). In this analysis CIR is defined as the radius of a circle which has an area being equal to the inverse of the mean raingauge density. This definition states that a raingauge is only required to provide precipitation information for the mean area controlled by it. In extreme case, if only one raingauge is available over an interested area then the precipitation information has to be inferred from it anyhow for the whole area. The CIR determines the average accuracy of the interpolated rainfalls. All raingauges within a circle of CIR can be used confidently to interpolate the rainfall value for the centre of the circle. Beyond CIR, some times raingauges have to be used, nevertheless, the interpolated rainfall is no longer considered as having the average data accuracy.

Assuming that rainfalls are to be interpolated for each grid centre of a grid network, any grid may be categorised into one of the three groups according to the distance from the grid centre to its nearby raingauges: (1) there are no adjacent raingauges located within the CIR. At such a grid point, rainfall value can only be estimated by making the best use of the raingauge network and three nearest raingauges located in different directions are forced to interpolate the rainfall for the grid. of course, the interpolated value has a lower-than-average accuracy; (2) there are adjacent raingauges within the interpolation radius but none of them is local to the point. At such a point the rainfall value is interpolated by Eq.(9.1) using all of the raingauge measurements, and (3)

there are raingauges local to the point (i.e within the LIR). At such a point, the rainfall value takes the measurement of the nearest raingauge.

Shearman et. al. (1975) adopt a factor being 10% of the 5-km grid interval (i.e 500m) as the LIR. In this study, LIR is defined as being equal to 5% of the CIR. For example, if the mean area controlled by a raingauge is 25 km^2, then the CIR would be 2.82 km and LIR, approximately 140m.

Figure 9.1 illustrates the contribution weight of a raingauge varying with the distance from the rainaguge.

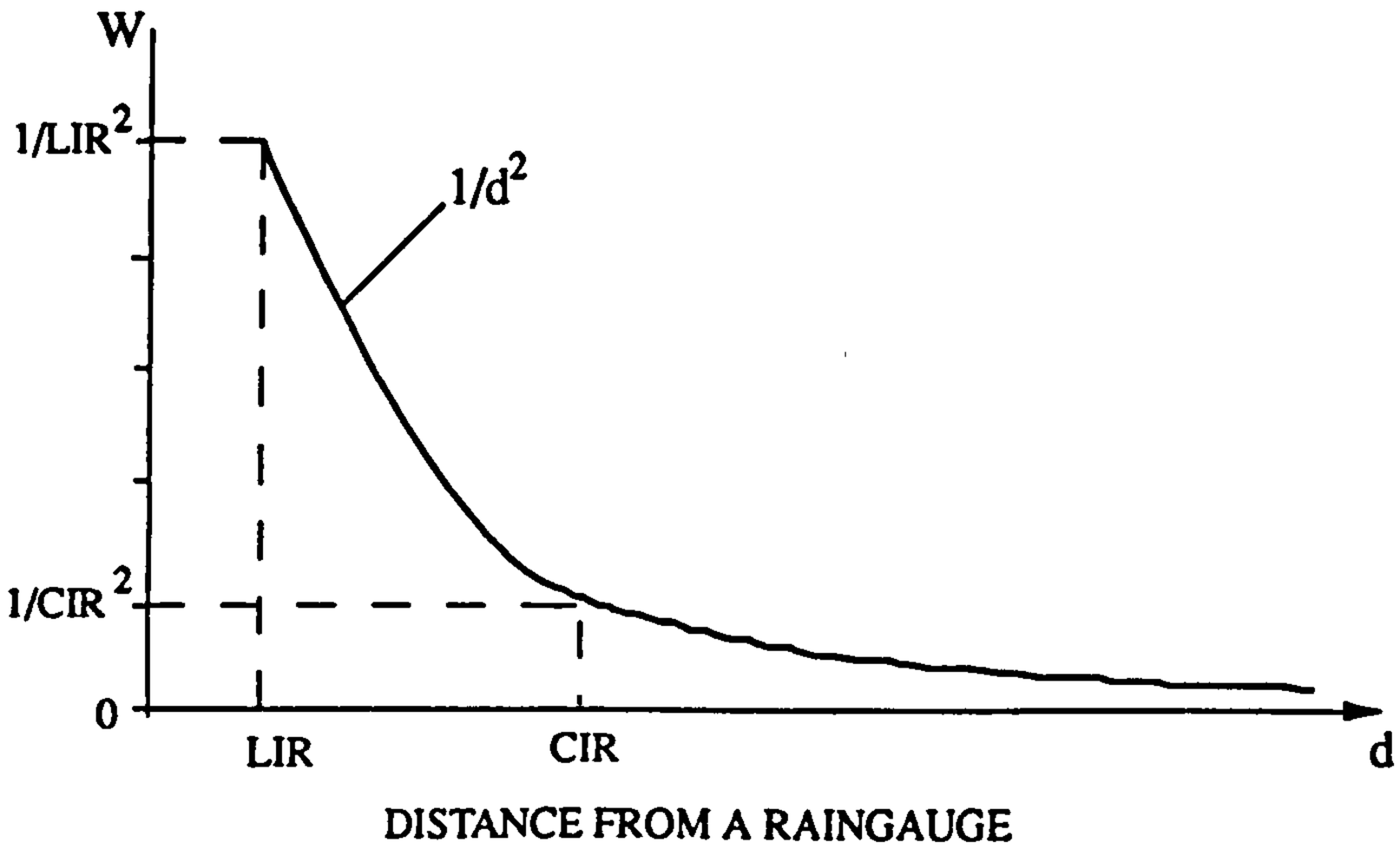

Fig. 9.1 The contribution weight of a raingauge attenuates with the increase in distance

A number of interpolation examples were shown in Figure 9.2. Nine raingauges were sited within the catchment with a density being 1 gauge per 13 km^2. The CIR and LIR is, therefore, respectively about 2km and100m. Rainfall values are required for each grid centre of the 2km by 2km grid network.

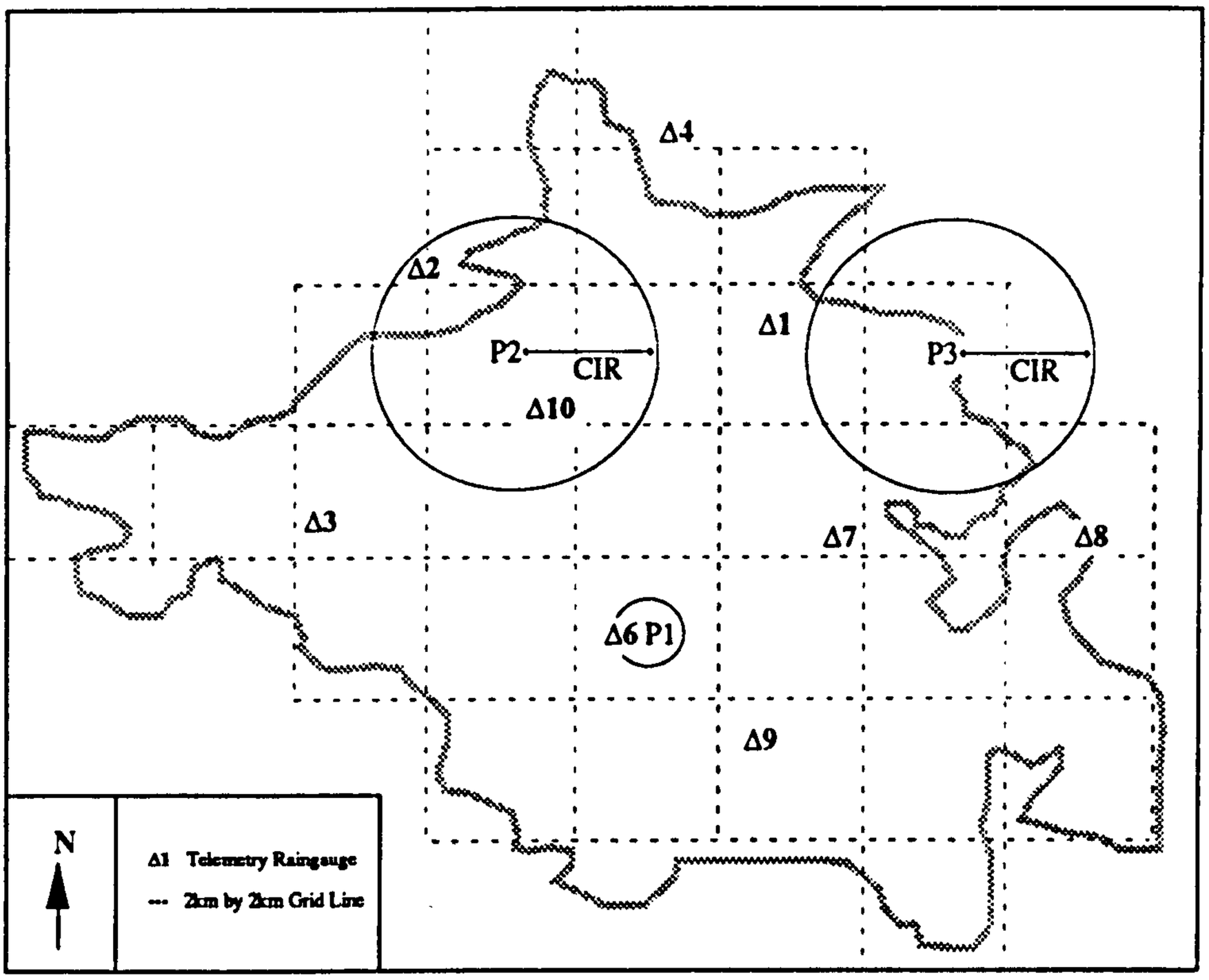

Fig. 9.2 Estimation of rainfall for a grid point

Case 1: At the grid centre labelled as p_1, raingauge Δ6 is located within the LIR, Consequently the rainfall value of point p_1 is taken to be the observation of Δ6.

Case 2: At grid point P_2, two raingauges, Δ2 and Δ10 were sited within the CIR from the point, so the rainfall at this point is interpolated by Eq.(9.1) using the two raingauge observations.

Case 3: At the grid centre P_3, none of the raingauges were sited within the distance of CIR, so the rainfall at this point was interpolated by Eq.(9.1) using the three nearest raingauges , Δ1, Δ7 and Δ8 which are located in three different directions.

The areal rainfall is taken to be the mean value of the grid rainfall estimates.

9.2 Comparison of Radar and Raingauge Rainfall

Radar rainfalls are discrete time-space series. Therefore, assessment of the relative radar rainfall accuracy to the raingauge rainfall can be made by 1) comparing the areal rainfall hyetographs, 2) comparing the accumulative rainfall hyetograph; 3) comparing the grid rainfall depths and 4) comparing the resulted runoff hydrographs. The assessment factor (Collier, 1986) may be used as an objective indicator of the radar rainfall accuracy, which is defined as the ratio of radar measurements divided by the co-located raingauge measurements: AF=R/G.

9.2.1 Accuracy of Radar Rainfall Intensities

Figure 9.3 shows a comparison between the radar and raingauge hyetographs over the entire duration from 00:00 GMT on 26 October to 00:00 13 November 1989. The accuracy of radar rainfall is indicated by the AF values plotted at the top of the figure.

It can be seen from the figure that the timings of the radar and raingauge measurements matched fairly well, and the AF varied within a range from 0 to 10. However, at most of the time it was between 0 and 2.

9.2.2 Accuracy of Radar Rainfall Accumulations

The areal accumulative rainfalls were derived using the radar and raingauge grid rainfalls for the whole catchment. The result was shown in Figure 9.4, which indicates that radar measured less rainfall than the raingauge network in general. This could be caused by insufficient radar rainfall data calibration or inaccuracy of the raingauge data.

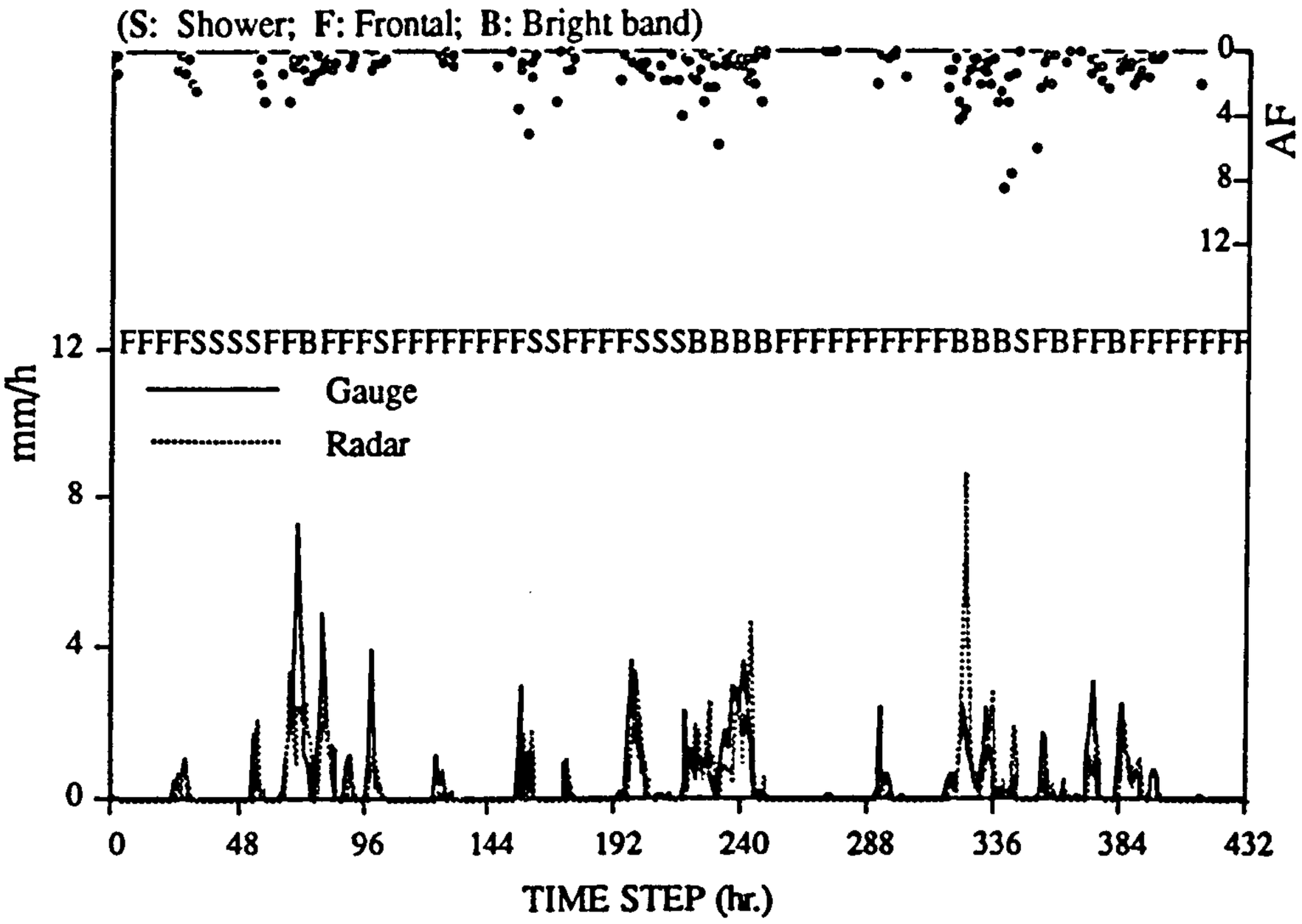

Fig. 9.3 Comparison of hyetographs

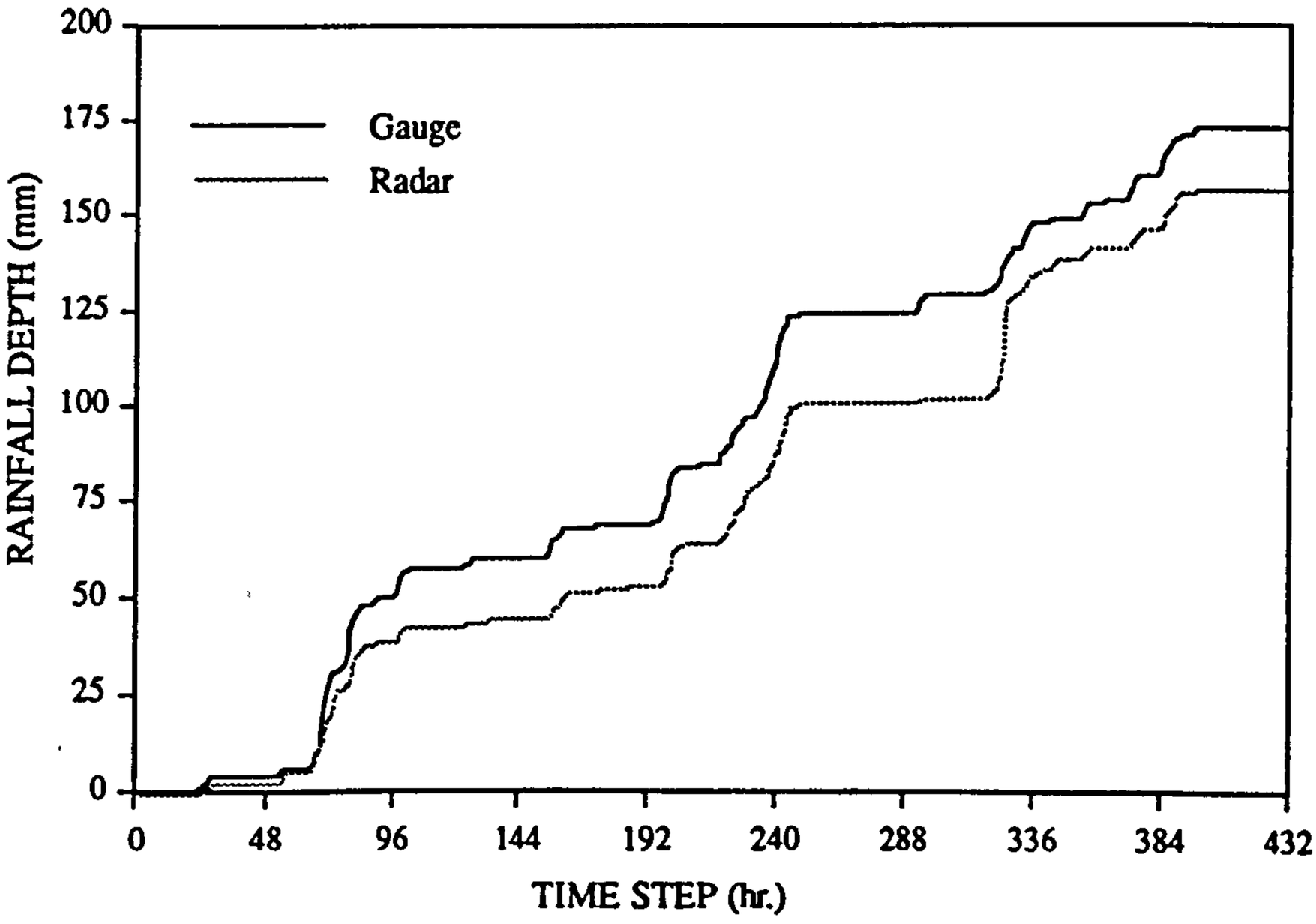

Fig. 9.4 Comparison of rainfall accumulations

Noticing that the AF varied abruptly with time, it is suspected that bright band effect might have played a major part in causing the variations. Consequently, the dominant rainfall types over the time period from 00:00 GMT on 26 October to 00:00 GMT on 13 November 1989 were checked and the results were shown in Table 9.1 and Figure 9.3. The rainfall types were identified at the Hameldon Hill radar site by the automatic algorithm (Chapter 2).

Table 9.1 Dominant rainfall types

Time Period (hr.)	Rainfall Type	Time Period (hr.)	Rainfall Type
1-24	F	204-217	S
25-53	S	218-248	B
54-65	F	249-320	F
66-74	B	321-330	B
75-97	F	331-340	S
98-105	S	341-353	F
106-154	F	354-357	B
155-170	S	358-371	F
171-194	F	372-377	B
195-203	S	378-432	F

(S: Shower; F: Frontal; B: Bright band)

It was found that the periods when radar rainfall was overestimated are coincided with the bright band situations. However, it is also noticed that bright band did not result in rainfall overestimation in all of the cases. For example over the duration from 66 to 74 hours, the radar rainfall was actually underestimated. In such cases, it is likely that either the rainfall types were wrongly assessed or the data was ineffectively calibrated or the raingauge measurements were inaccurate or unrepresentative.

In brief, radar hourly areal rainfall intensity (mm/h) was underestimated most of the time and the areal rainfall depth (mm) was also underestimated compared to the raingauge network observations.

9.2.3 Spatial Variation of the Assessment Factor

The lumped hourly radar rainfall measurements (intensity and depth) were below that recorded by the co-located raingauge network, however it is likely that, the relative underestimation of rainfall by radar should not be the same for every grid point. The accuracy of radar rainfall may have a range dependent feature. To prove this, the variation of the AF as a function of radar range was investigated.

Since the deviation between radar and raingauge rainfall is also dependent on the rainfall types in addition to the radar range, each event was selected as only having one dominant rainfall type in order to eliminate the impacts of rainfall types. A total number of 9 storms were extracted from the 18-day time-space series rainfall, which were shown in Table 9.2 and Table 9.3.

To carry out the investigation respectively for each of the three rainfall types, firstly rainfall depths of the radar and raingauge rainfalls for each grid cell were derived and then the AF values were calculated. The results were shown in Figure 9.5, Figure 9.6 and Figure 9.7, which indicate the AF varying with the distance from a cell to radar. Within a range from 15 km to 35 km the assessment factor varied from 0.5 to 2.0 for both of the shower and frontal-type storms, however, reached as much as 4.5 in the bright-band case on 8/11/89. It decreases with a increase in the radar range. This means that radar detected more rainfalls at close ranges and less at the further ranges than the raingauge network. At a range of about 20 km the assessment factor reached a value of 1, which indicates that the radar rainfall measurements were the same as that from the raingauge network.

Table 9.2 Data from radar

Day/Month	Type	Time	Duration (hr.s)	Beam Elevation	Average Rain Totals (mm)
27/10	Shower	00:00-09:00	10	1/2 Degree	2.7
01/11	Shower	11:00-21:00	10		6.6
08/11-09/11	Shower	19:00-05:00	10		6.1
29/10	Frontal	03:00-13:00	10		11.4
31/10	Frontal	03:00-13:00	10		1.1
10/11-11/11	Frontal	18:00-17:00	23		10.3
04/11-05/11	Bright Band	02:00-08:00	30		36.3
28/10-29/10	Bright Band	17:00-02:00	9		20.1
8/11	Bright Band	08:00-20:00	12		28.6

Table 9.3 Data from raingauge network

Day/Month	Time	Duration (hr.s)	Average Rain Depth (mm)
27/10	00:00-09:00	10	3.3
01/11	11:00-21:00	10	7.2
08/11-09/11	19:00-05:00	10	6.9
29/10	03:00-13:00	10	17.0
31/10	03:00-13:00	10	3.0
10/11-11/11	18:00-17:00	23	12.2
04/11-05/11	02:00-08:00	30	40.2
28/10-29/10	17:00-02:00	9	12.2
8/11	08:00-20:00	12	25.3

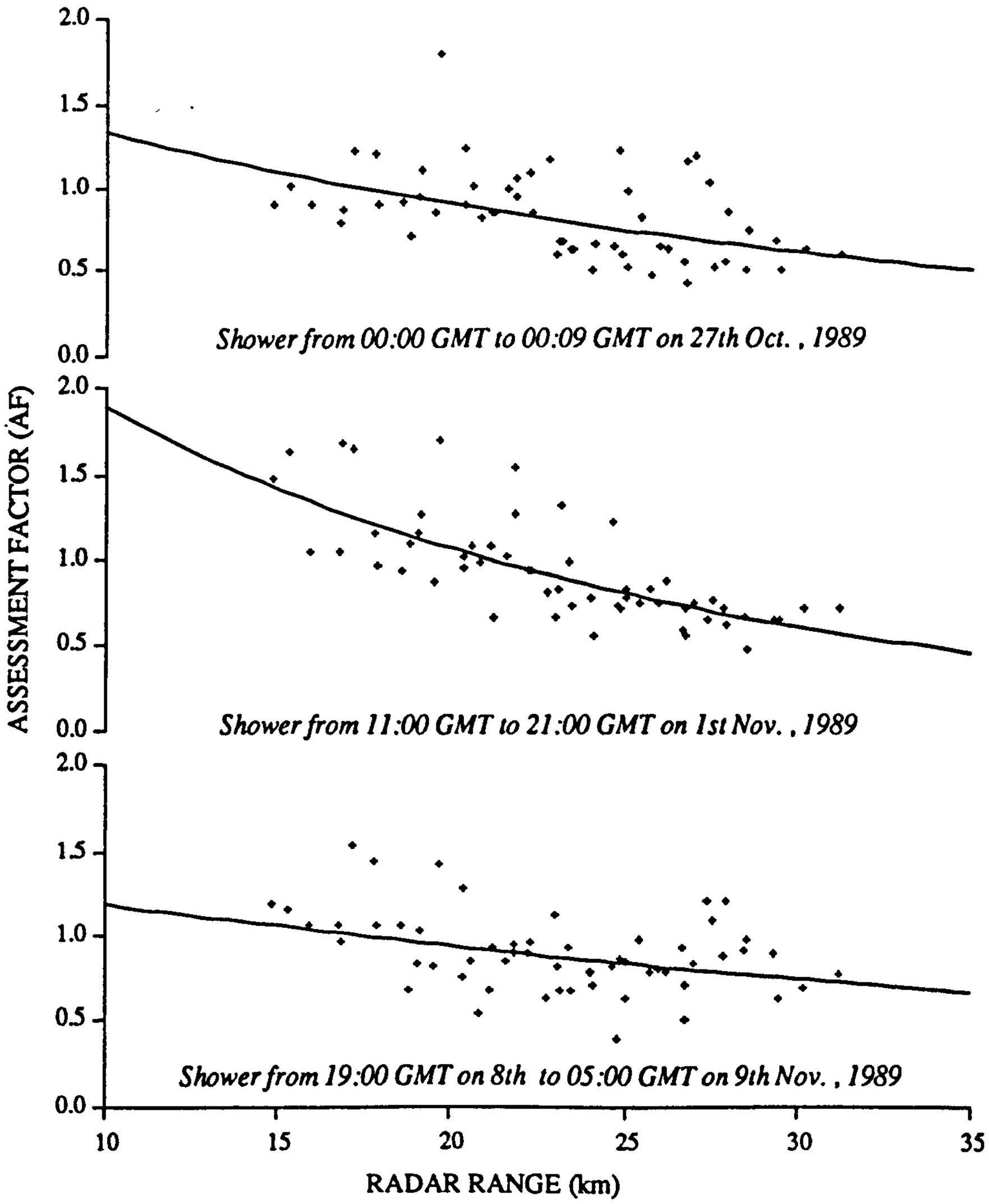

Fig. 9.5 The accuracy of the shower-type radar rainfall depth varies with the radar range

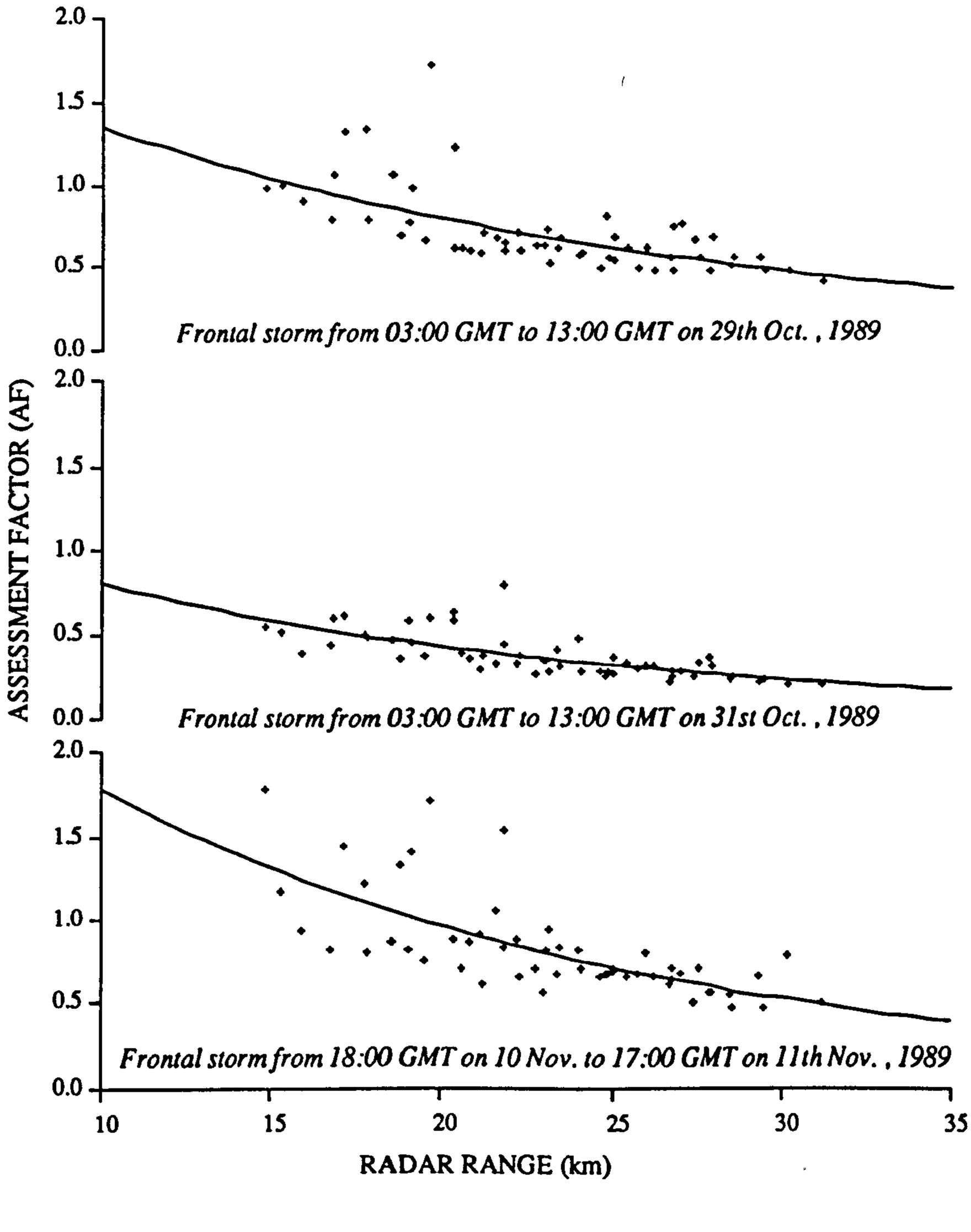

Fig. 9.6 The accuracy of the frontal-type radar rainfall depth varies with the radar range

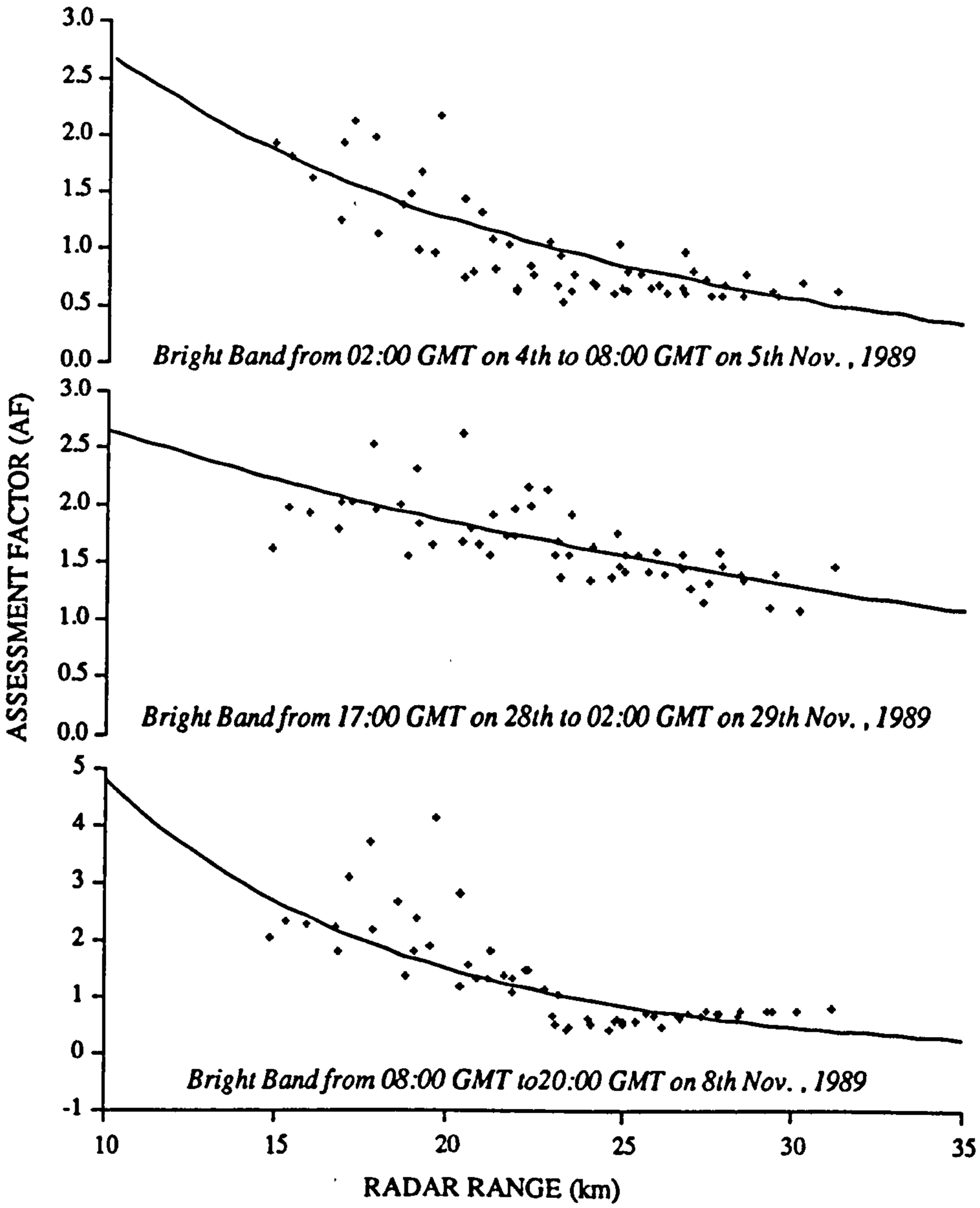

Fig. 9.7 The accuracy of the Bright-band-type radar rainfall depth varies with the radar range

Although there may exist exceptions, the above variation features certainly reflected the factors of the catchment topography, radar technology and the storm developing regime. For instance, ground clutter tends to have more effect on the rainfall observations at the shorter range than the further ranges. Besides, the detectability of

radar is reduced at longer ranges due to power attenuation. These factors certainly affected the accuracy of radar rainfall in space. To probe the absolute extent to which the radar rainfall accuracy was reduced, a further comparison needs to be carried out within the hydrological context though the present study provides some clear indications of the way forward in this area of 'ground-truth' interpretation.

9.3 Flow-simulation Accuracy Using Radar Rainfall

An implicit assumption in which the raingauge observations are taken as the 'ground truth' has been used in carrying out the previous assessments. It is not reliable to draw a conclusion if only based on the assessments because raingauge measurements have long been known as point measurements which are unable to represent the spatial variations of precipitation, and a more objective criteria is required. Consequently, it is necessary to conduct an analysis on the accuracy of urban drainage flow simulation using radar rainfall data. It is envisaged that with the same simulation model if using radar rainfall can produce smaller simulation errors than using the raingauge rainfall then it means radar rainfall data are more accurate than the raingauge data, the vice the versa.

Aiming for the RTC of the drainage system, a set of telemetry flow sensors were installed in the Bolton catchment during a short term flow surveys. Figure 9.8 shows the location of the sensors which measure flows coming out of the two river valleys at the upper stream part of the catchment. Sensors (transducers) were positioned to measure depth and velocity of the flow. Depth sensors are of the 'Milltronics' ultrasonic pulse-echo type situated above the flow and have an operating range of 0.6-4.2 m. Generally, the telemetry system worked well, however, experience has shown that the depth sensors are more reliable than the velocity sensors. Therefore only the depth measurements were used in this analysis. The flow depth data were collected continuously over the duration from 00:00 GMT on 26 October to 00:00 GMT on 13 November 1989 (18 days). The equation used to convert the depth to flow is:

$$Q = \frac{1.49}{n_0}\sqrt{s_0}(w \cdot d)^{5/3}(w + 2d)^{3/2} \qquad (9.2)$$

Where Q is flow (Cumecs)

n_o is the Manning roughness coefficient (=0.02)

s_o is the bed slope (=0.0012)

w is the width of the box pipe cross section(= 2.133 m)

d is the flow depth (m)

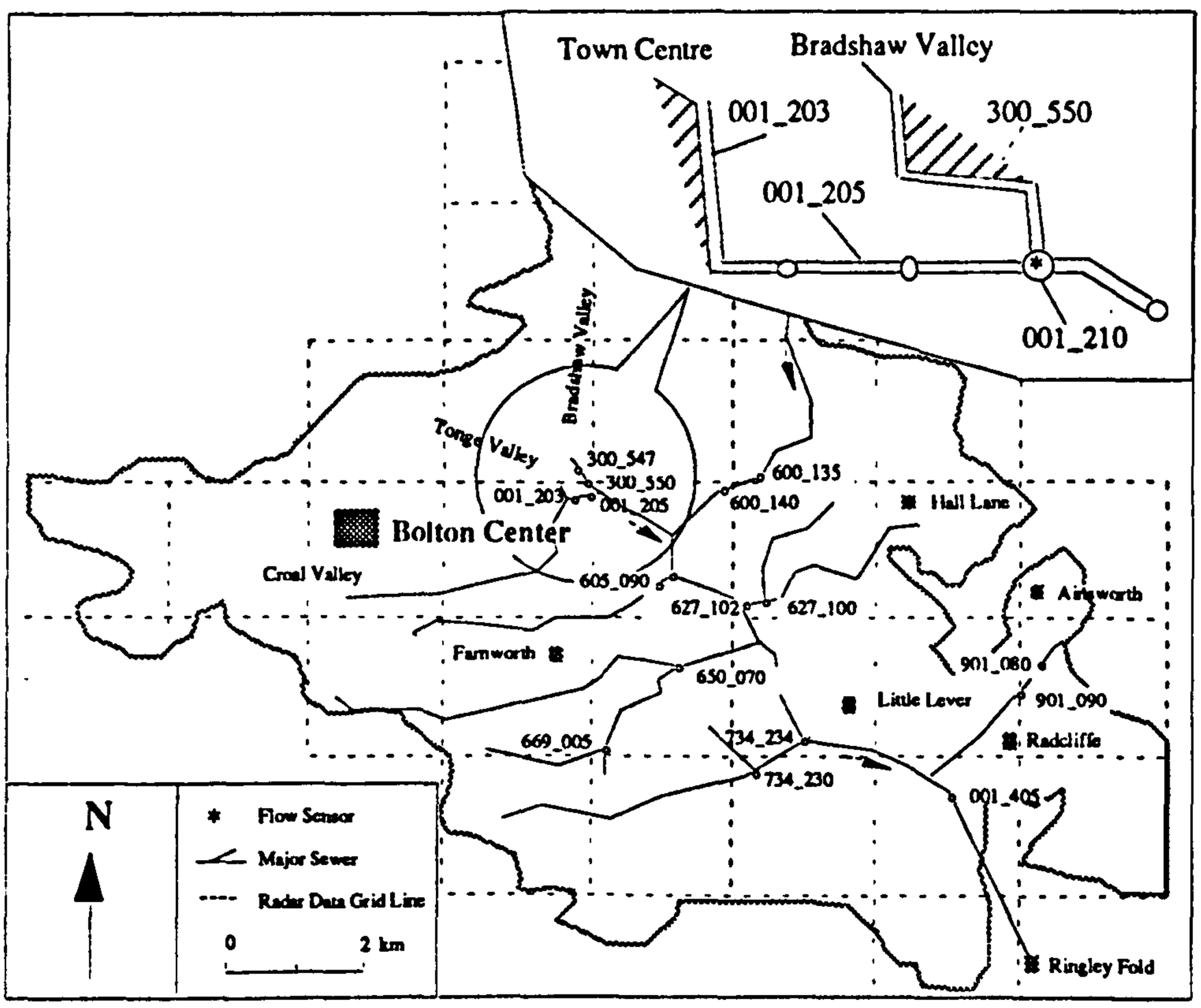

Fig. 9.8 Location of the flow sensor

Since it was not possible to obtain the actual physical parameters of the drainage system, the CPTF model was adopted as a tool for the transformation of the hyetographs into the hydrographs. The procedure involves two steps: 1) identification of a fittest CPTF model using the *raingauge rainfall hyetograph* and the observed hydrograph; 2) transformation of the radar and raingauge hyetographs into hydrographs. Because the model is identified using the raingauge rainfall, if the flow transformed from the raingauge rainfall is not closer to the observed flow than that from the radar rainfall, then the radar rainfall data should be regarded as more accurate than the raingauge data.

The input radar and raingauge hyetographs are shown in Figure 9.9 and the observed hydrograph is plotted in Figure 9.10. The lumped rainfall hyetographs were derived by averaging the grid rainfalls over the flow contribution area (40 km^2). Using the raingauge rainfall hyetograph and the observed hydrograph a Naive CPTF model was identified as: CPTF(η=1.144, n=2, τ=2.112, Δ=1, α=0.664, χ=1) and the corresponding advanced CPTF model is:

$$Q_t = 0.8937Q_{t-1} + 0.0927R_t + 0.0054R_{t-1} + 0.0011R_{t-2} \qquad (9.3)$$

where the model input rainfall (R) data resolution is equal to the output flow (Q) data resolution which was 1 hour. With this model the radar rainfall and raingauge rainfall were transformed into hydrographs, which are shown in the Figure 9.10 together with the observed hydrograph. The comparison indicates that, in general, radar rainfall yielded a similar output from the model to that produced using the raingauge rainfall except for several short periods when bright band effects were present in the data.

To quantitatively compare the simulation errors, a simple percentage error index was used, which is defined as:

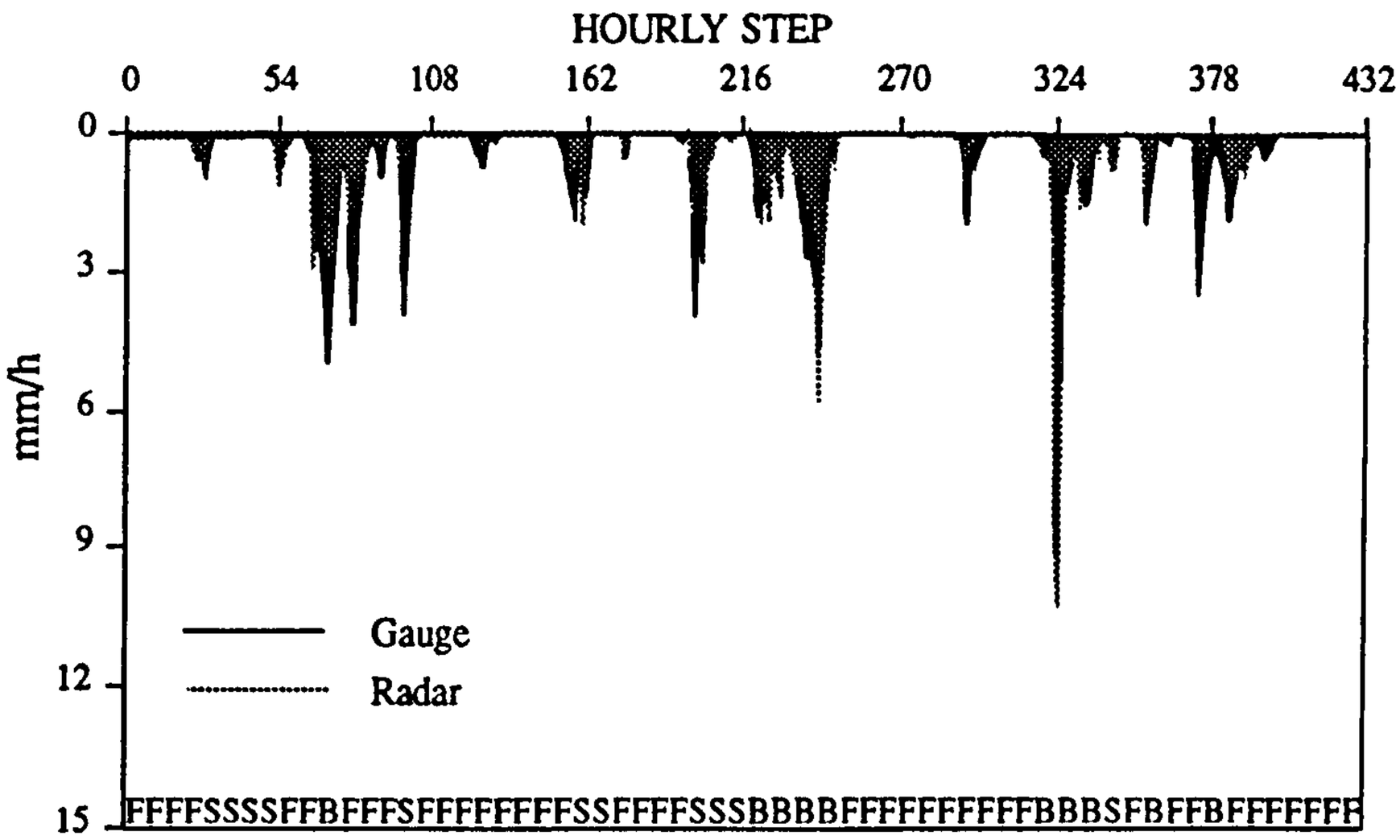

Fig. 9.9 Input radar and raingauge hyetographs to the contribution area

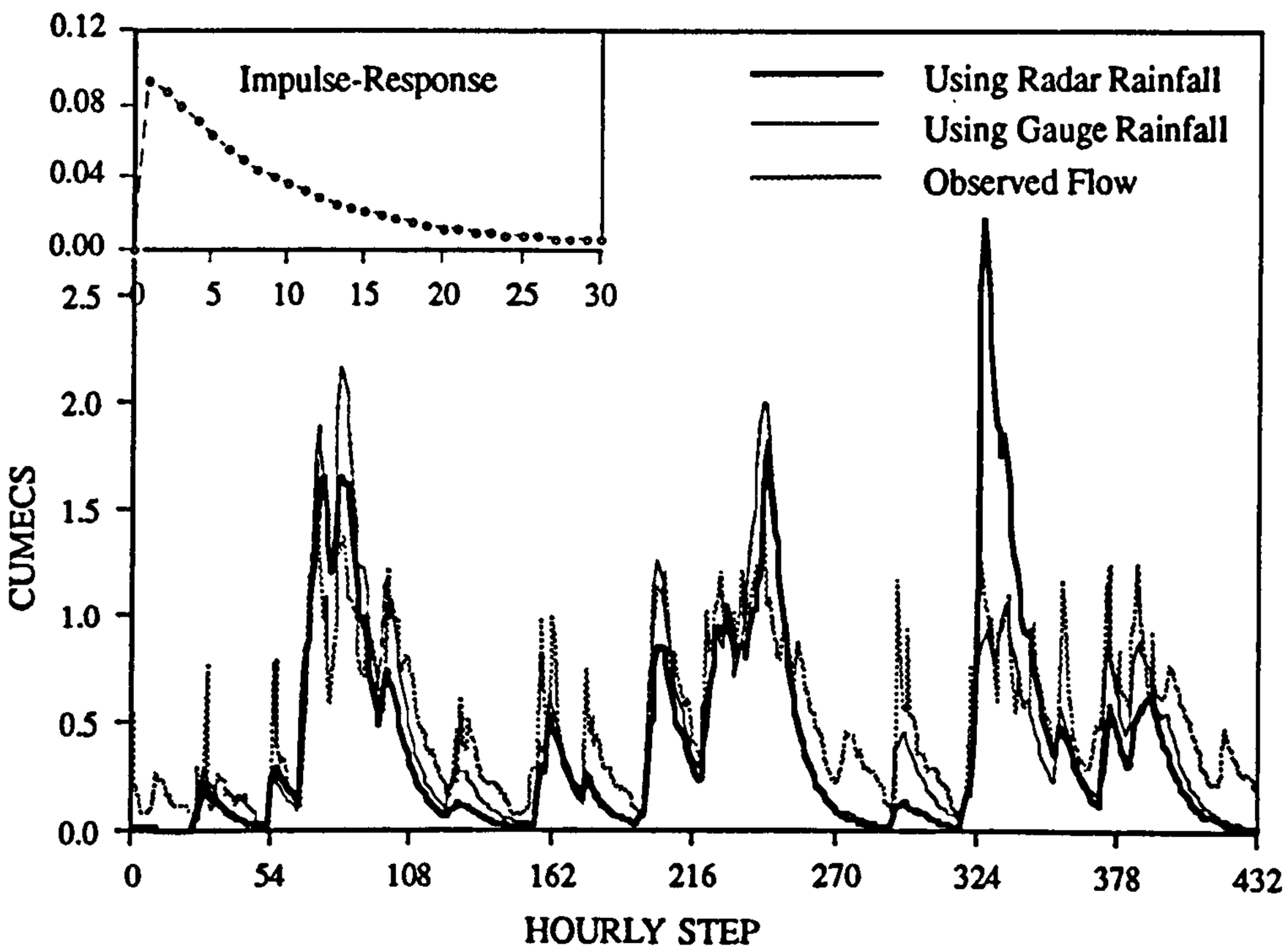

Fig. 9.10 Comparison between the simulated and observed hydrographs

$$PE = \frac{Q_s - Q_o}{Q_o} \times 100\% \qquad (9.4)$$

Where PE is the percentage error;

Q_s is the simulated flow and

Q_o is the observed flow of a time step.

Figure 9.11 shows the comparison of the simulation errors produced using the radar and the raingauge data respectively at each hourly time step over the entire duration of 432 hours.

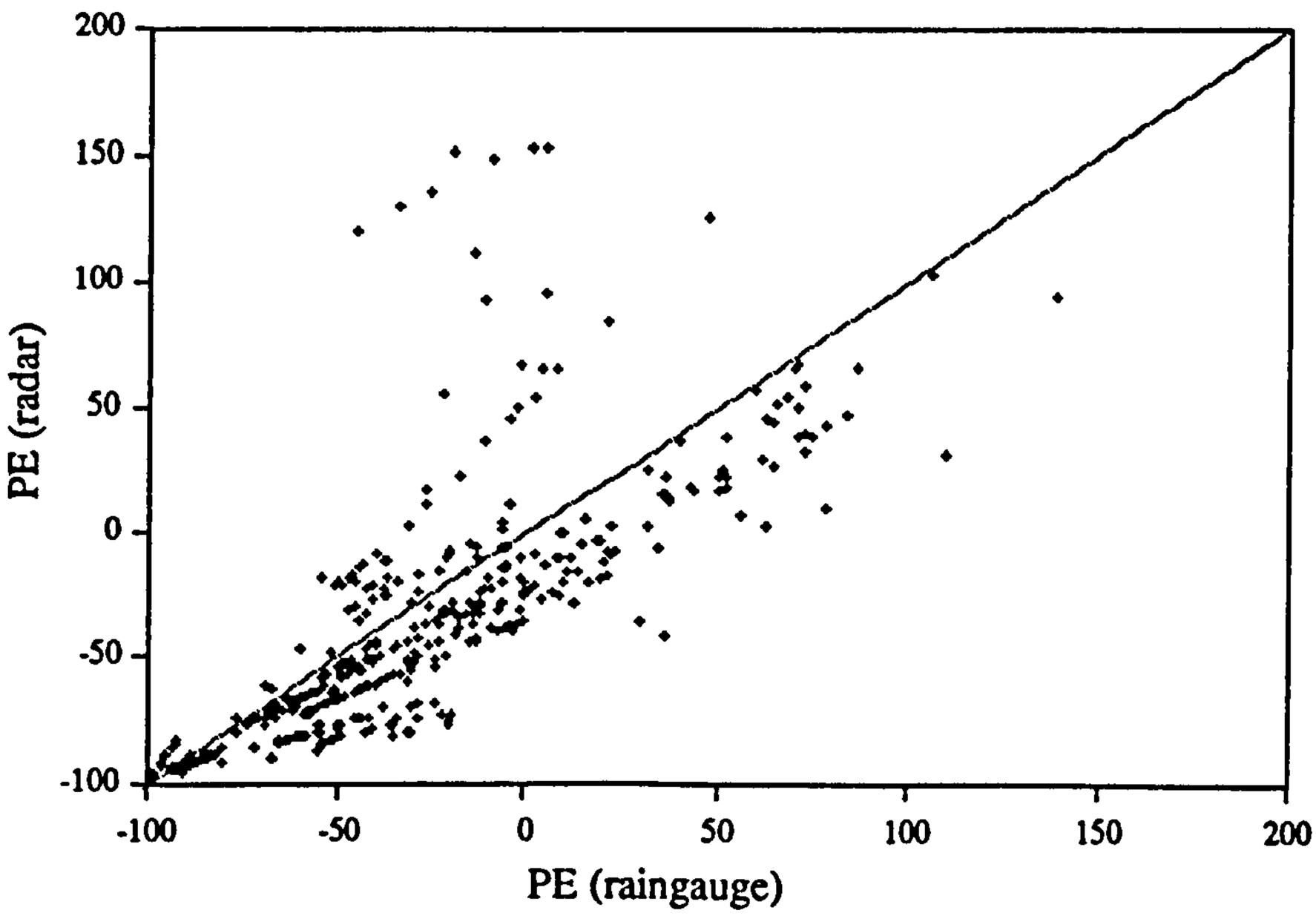

Fig. 9.11 Comparison of the flow simulation errors

The vertical axis is the PE produced using the radar rainfall data and the horizontal axis shows the PE resulted from using raingauge rainfall. The diagonal dotted line in the figure indicates the position where both of the simulations have equal distance to the

observed hydrograph. If a point is below the line then it means that the raingauge rainfall produced larger flow simulation error than the radar rainfall, the vice the versa. As most of the points were apparently below the line, this indicates that the radar rainfall data used in the analysis was more accurate than the raingauge measurements. Going further, if a model is identified using the radar rainfall, the flow simulation using radar rainfall would be more accurate than that using the raingauge rainfall. A model inherently infected by errors at its identification time may be more resilient and performs better than a genuine model in a noisy environment during the post-identification period. This implies that a model can mitigate the imperfectness of input data! Without loosing generality, it may be stated that the accuracy of the areal rainfall estimates of Hameldon Hill radar is at least as accurate as the raingauge measurements within a range of less than 35 km.

9.4 Summary

Radar rainfall accuracy is a time, space, storm type and radar device dependent issue. Hameldon Hill radar overestimated the rainfall depths within a range shorter than about 20km and underestimated the depths beyond that range when compared with the raingauge data. The areal radar rainfall depth was smaller than that estimated using the raingauge data except for some of the bright band situations. However, using the hourly areal radar rainfall produced a more accurate reproduction of the observed flow hydrograph than using the raingauge rainfall. This means 1) despite the radar rainfall estimates being not perfect they do represent the major spatial distribution characteristics of a rainfall field; 2) even with the densely scattered raingauge network (i.e. 1 gauge per 13 km^2), it was not possible to derive an adequate and representative areal rainfall; 3) improvement of the weather radar performance under Bright-band conditions is much-needed and current developments utilising vertical pointing X-band radars to investigate vertical reflectivity profiles will prove important in understanding this aspect of radar meteorology and hence offer the potential to improve the radar hydrology.

CHAPTER 10

THE POTENTIAL BENEFITS OF REAL-TIME CONTROL USING RADAR RAINFALL DATA ON THE FYLDE

The name Fylde, meaning creation of 'fields', first appeared in the 17th century when successive waves of settlers to the area had created one of the richest farming regions in the Northwest of England. The Fylde is now better known for its bathing waters and the pleasure beaches. The length of the Fylde Coast included in current studies on stormwater management is about 22 km, the width is 6 km and total area is approximately 132 km^2. The area is relatively flat. Its central part is higher than the Northern and Southern subareas, and the average ground level is about 15 meters (AOD). The river Wyre runs along the North-Eastern boundary and flows into the Irish sea at the port of Fleetwood. Figure 10.1 shows the primary topographical features of the Fylde Coast.

In 1750, Blackpool first appeared on the map of the Fylde coast and soon the area received an increasing number of residents and travellers. The original land draining system was then combined with the trade effluent and domestic foul system which essentially forms the present day policy in relation to the design of urban drainage systems in the region. Presently, there are eight significant bathing areas along the Fylde Coast, which have been identified as locations where the requirements of the European Community Bathing Water Directive (Council of the European Communities, 1976) should apply.

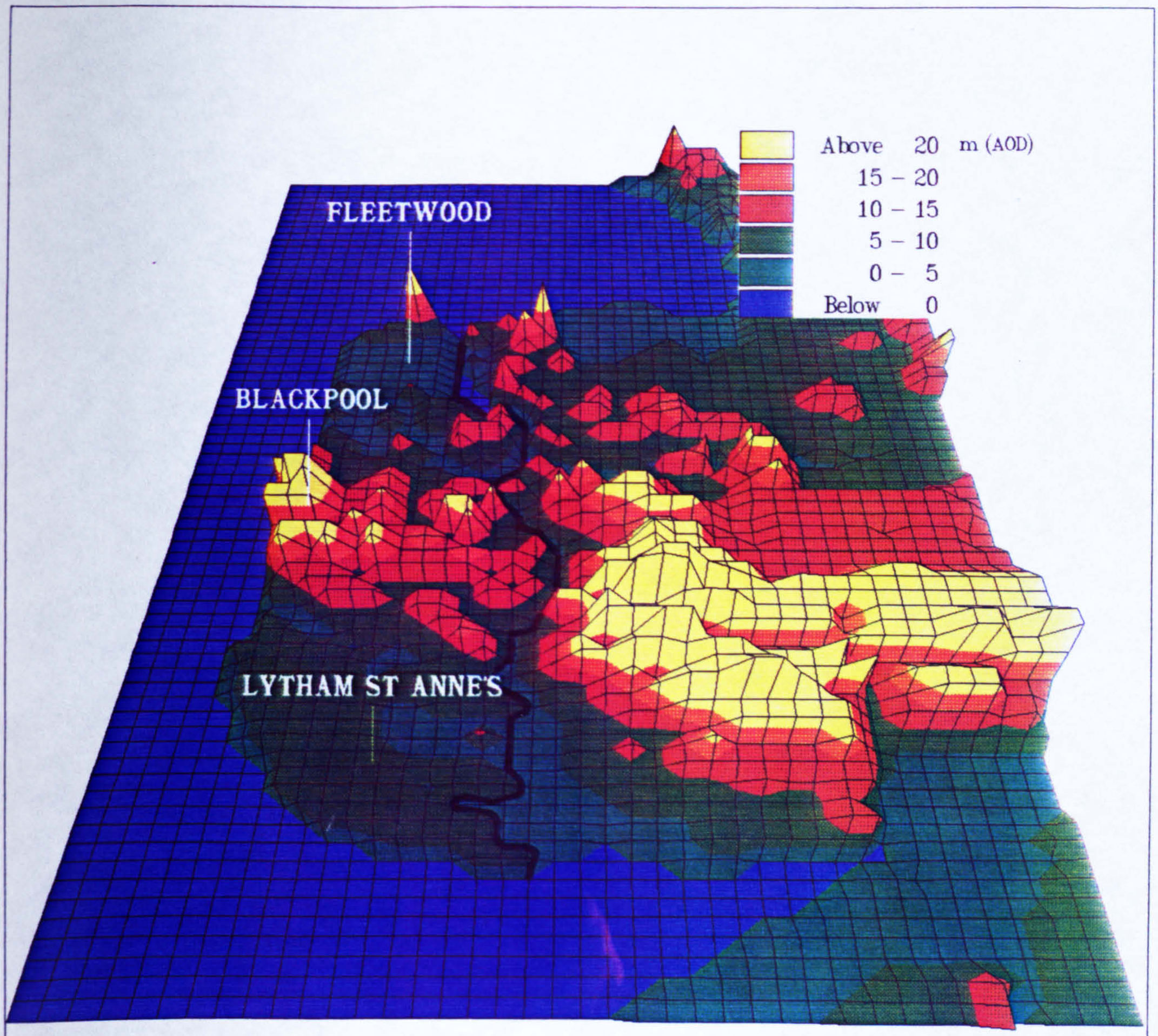

FIG. 10.1 FYLDE COAST TOPOGRAPHY

Blackpool however has been described as Britain's dirtiest bathing beach according to data for 1992 collected by the National Rivers Authority. In a study of more than 400 bathing beaches in England and Wales, designed under the European directive on bathing waters, Blackpool south registered the highest average coliform count at 8000 in 100 millilitres of water (New Scientist, 1993). The major objectives of the current rehabilitation projects focusing on the Fylde system are to protect the bathing water for coastal communities and ensure the discharges of storm water do not prejudice compliance with the requirements of the EC Bathing Water Directive. To achieve this objective, North West Water Ltd. (NWW) has budgeted approximately £150M to clear up the beaches by capital investment in the region's urban drainage infrastructure: ***Phase 1:*** *To construct a biological secondary treatment works at Fleetwood.* ***Phase 2:*** *To construct 3 interconnecting interception tunnels along the Fylde Coast.* The tunnel is designed to have sufficient capacity for storm storage purposes, to collect the flows currently discharging from the five local outfalls and convey them to the treatment works in Fleetwood. At present time, sewer flows from the local outfalls are discharged to sea after coarse screening. In the future, the final treated flow disposal will be made via a new longer sea outfall to be constructed in Fleetwood. The existing outfalls will be retained as emergency outlets to release the excessive water during extreme events. ***Phase 3:*** *To construct a new longer sea outfall in Fleetwood.* ***Phase 4:*** *To install a RTC system in the future Fylde system after completion of the first three phases of works.*

The preparatory works related to Phase 4 is initiated by the present study. This study is carried out to identify the potential for real-time control in the Fylde system and demonstrate a prototype application of radar rainfall data in studying the real-time UDS control problems. The major topics to be addressed include: 1) subcatchments along the Fylde Coast; 2) the existing sewer network models; 3) RTC control strategy and operation strategy; and 4) the potential benefits of RTC.

10.1 Subcatchments Along the Fylde Coast

The Fylde Coast comprises 7 subareas from North to South: Fleetwood, Cleveleys, Thorton, Poulton-le-Fylde, Blackpool North, Blackpool Central-South and Lytham St. Anne's. The subareas are drained by four physically independent combined sewer systems. The systems convey both domestic foul water and storm water mainly by gravity. Discharges of the coarsely screened sewage water are presently mainly made from five local sea outfalls via pumping stations at: Chatsworth Avenue serving the Fleetwood area, Anchorsholme serving Blackpool North, Thorton and Cleveleys areas (in the future this outfall may serve Poulton-le-Fylde as well), Manchester Square and Harrowside outfall serving the Blackpool Central-South area and Fairhaven serving Lytham St. Anne's in the South. Currently the sewer flow from Poulton-le-Fylde discharges to a small treatment works at Skipool Creek on the West bank of the Wyre estuary. NWW has planed to divert the flows from this area into the Anchorsholme system. Poulton-le-Fylde, Thorton and Cleveleys are drained essentially by separated systems however there are cross connections between the storm water drainage system and foul water sewer system. Consequently the separated systems are effectively combined systems. The maintenance of the four sewer systems is the responsibility of the three local district offices appointed by NWW: The NWW office in Preston is responsible for its part over Fleetwood, Thornton Cleveleys and Poulton-le-Fylde areas, Blackpool Borough Council for Blackpool North and Blackpool Central-South and Fylde Borough Council deals with Lytham St Anne's.

Based on the layout and configuration of the drainage systems, the Fylde Coast can be subdivided into four subcatchments which will be referred to by the names of the final outfalls hereafter: Chatsworth Avenue, Anchorsholme, Manchester Square and Fairhaven. Poulton-le-Fylde is treated as a part of the Anchorsholme subcatchment, and Staining which is a small town to the East of Blackpool is included in the Manchester Square subcatchment. The boundaries between these subcatchments are mainly located on the water divide.

A different stormwater management strategy has been proposed by NWW for the Fairhaven subcatchment and this study was therefore concentrated on the three Northern subcatchments as shown in Figure 10.2 though some information relating to the Fairhaven subcatchment is also presented.

There are a number of ancillaries in the Chatsworth Avenue subsystem. In addition to the Chatsworth Avenue pumping station, there are four interior pumps and three Combined Sewer Overflows (CSOs) which discharge into the Wyre estuary. The system has very limited storage capacity.

In the Anchorsholme subcatchment, the Warren Drive tank sewer and Moor Park tank are the two major storage facilities. The off-line Moor Park tank has a storage capacity of 11300.00 m^3 and the Warren Drive tank sewer has a capacity 5420 m^3. These figures indicate that considerable storage volumes are available. Except for the Anchorsholme pumping station, there is no interior pumping station or additional CSOs in this particular subcatchment. Regulators are installed at Moor Park Tank and the Anchorsholme pumping station for controlling the inflows.

The Manchester Square subcatchment is drained by two subsystems: the High-level subsystem and the low-level subsystem respectively. Two pumping stations are used at Manchester Square to pump flows from the higher level and low level systems into the sea. Regulators are installed for controlling the inflows. Besides, an emergency outfall: the Harrowside outfall also operates within the subcatchment. The High-level system collects sewer water from the central and part of the southern areas. A number of small submersible pumping stations, maximally consisting of two pumps, are used for lifting the sewerage flows from the low lands of the South-eastern area (Marton) into the low-level subsystem and in turn further lifted by the Lennox Gate pumping station which is an interior relay pumping station in the low-level system.

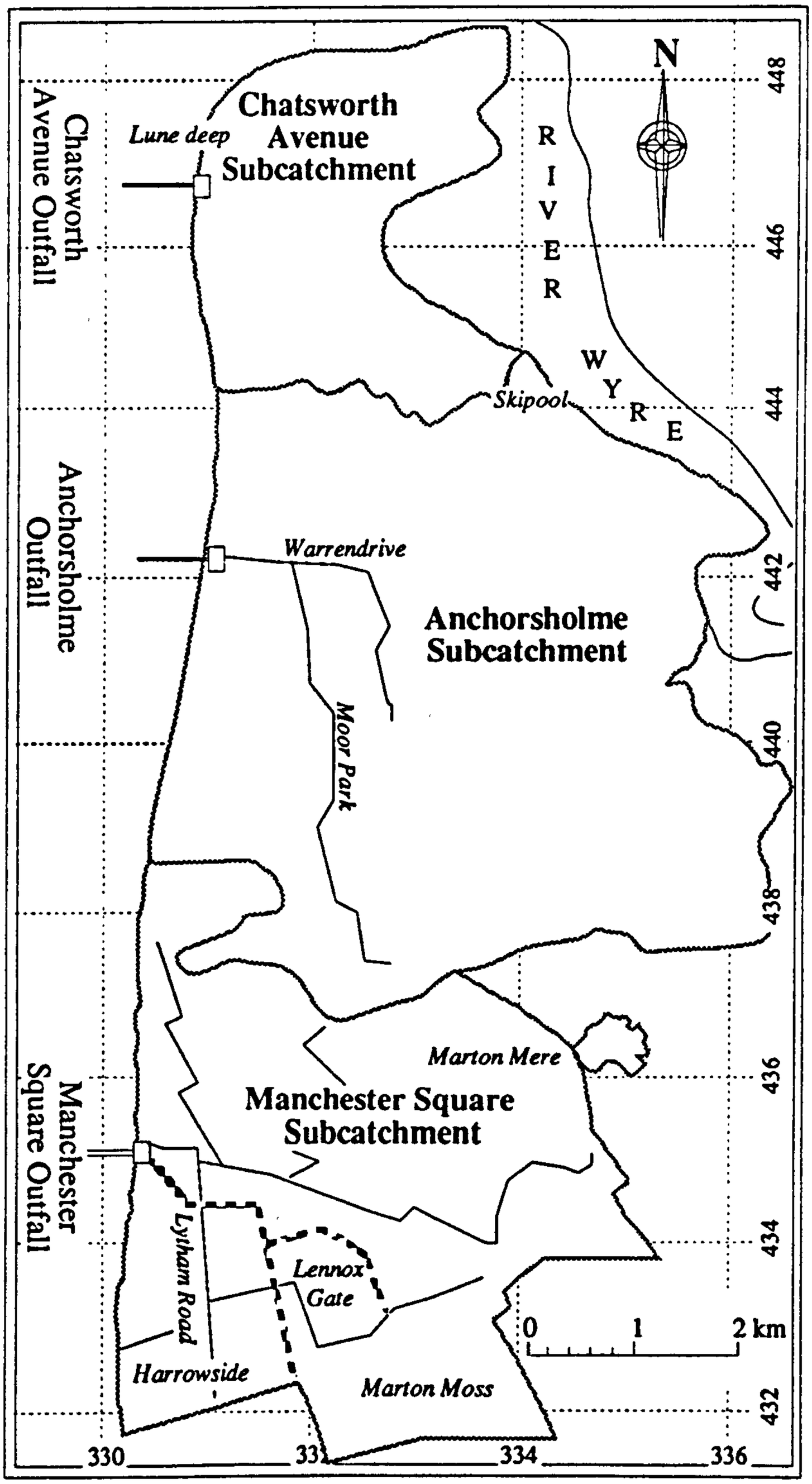

Fig. 10.2 The three Northern subcatchments

(Note:the thick dashed lines are the major low-level sewers)

CSOs from Lennox Gate are diverted to the Harrowside outfall. A new pumping station has just been installed at Harrowside for lifting flow into the Lytham road sewer which is the principal sewer for the Southern area of Blackpool. A total number of 19 pumping sites and 16 CSOs have been identified in the Manchester Square subcatchment. Some of the CSOs discharge into Marton Mere through a system of Dykes and the others discharge directly into the Irish sea via the main outfalls.

10.2 EXISTING SEWER NETWORK MODELS

In the past years, NWW have executed a number of projects to carry out review and rehabilitation schemes in the Fylde Coast area. The earlier modelling works can be dated back to 1985 when the initial WASSP models were created by WRc under contract, though in conjunction with local council staff. Most of the existing WASSP models were produced in 1987 by WRc using upgraded information from a series of sewer surveys carried out during this period. Later in 1988, NWW used a newly developed method of integrating sewer network modelling with marine water quality impact modelling. This was to determine how various storm water management strategies would affect the effects of different degrees of treatment and outfall location for the base flow during relatively dry weather and during periods of light rain.

Storm water volumes have usually been generated by utilising complex sewer hydraulic models such as WASSP or its more recent refinement WALLRUS. Since it was not possible to specify complex control rules for the operation of pumps at the head works of storm overflows and the cost of simulating long sequences of storms was prohibitive. A simplified model, SMARTS (Hutchings and Dempsey, 1991), which links the WASSP/ WALLRUS percentage runoff equation with a simple time/area approach was used to model catchment shape with a simple representation of attenuation involving a non-linear reservoir. The model was developed by WRc under contract to NWW and could be executed on a computer much more quickly than traditional WASSP/WALLRUS studies and also allowed for the incorporation of

relatively complex control rules for stormwater pumping (Crawshaw and Head, 1988). Following the results of the Fylde stormwater management study review of sewer modelling in 1990 and 1991, the WASSP and SMARTS models were further upgraded for all of the subcatchments except for the Manchester Square subcatchment where WASSP models were converted into WALLRUS models (Orman, 1991). Mott MacDonald UK Ltd. produced an independently calibrated WALLRUS model for the Chatsworth Avenue subcatchment and a layout map for the modelled pipes in 1992. The model was more detailed than previous studies had produced. In the Anchorsholme and Manchester Square subcatchments, several elements of small detailed models have been produced by the Blackpool Borough Council staff directly, these have been applied to a number of localised rehabilitation projects for North Park Drive and the Harrowside area, et. al. A list of the available WASSP/WALLRUS models as identified for this report is given in Table 10.1. Figure 10.3 shows the extent of the areas having been modelled at this time. The gradient of shading indicates the relative extent of the modelling.

The currently available models to this study for the Chatsworth Avenue subcatchment are fairly coarse. Only a small number of the major sewers are modelled. The total modelled sewer length is about 17 km and the total contributing area is approximately 459 hectares, of which 37.6% is impervious (Paved area+ Roof area).

Anchorsholme subsystem has a total modelled sewer length of approximately 158 km and the total contributing area is about 1225 hectares, of which 43.7% is impervious. Some parts of the catchment have been extensively modelled such as the Thorton, Cleveleys and Poulton-le-Fylde areas.

The total modelled sewer length in the Manchester Square subcatchment is about 84 km and the total contributing area is approximately 1614 hectares, of which 46.8% is estimated as being impervious. A considerable in-sewer storage capacity is available. However, no current models are suitable for provision of a confident volume

assessment on the capacity.

Table 10.1 The available WASSP/WALLRUS models

SUBCATCHMENTS AND MODELS		NOTE
CHATSWORTH AVENUE	CHATSWORTH_EX1987.SSD CHATSWORTH_UG1988.SSD	CHATSWORTH_EX1987.SSD is the existing model. CHATSWORTH_EX1988.SSD is the upgraded model .
ANCHORSHOLME	NASALT.SSD ANCHORHOLME_EX1988.SSD ANCHORHOLME_UG1990.SSD	ANCHORHOLME_EX1988.SSD is the existing model which was expended and upgraded from NASALT.SSD created in 1986 with the Cleveleys and Thorton submodels amended. ANCHORHOLME_UG1990.SSD is the upgraded model with Poulton-le-Fylde model attached. Most upgrading options are in the secondary subcatchments
MANCHESTER SQUARE	MANCHSQUARE _EX1991.SSD MANCHSQUARE _UG1991.SSD MANCHSQUARE _UG1992.SSD NPD-13.SSD	MANCHSQUARE_EX1991.SSD is the existing model. MANCHSQUARE_UG1991.SSD is the upgraded model produced on version 1.3 of WALLRUS. MANCHSQUARE_UG1992.SSD is the upgraded model. This model is just used for looking at Lennox Gate pumping station. NPD-13.SSD was created by Blackpool Council in 1988 to find a solution for the area from North Park Drive to White Gate Drive.

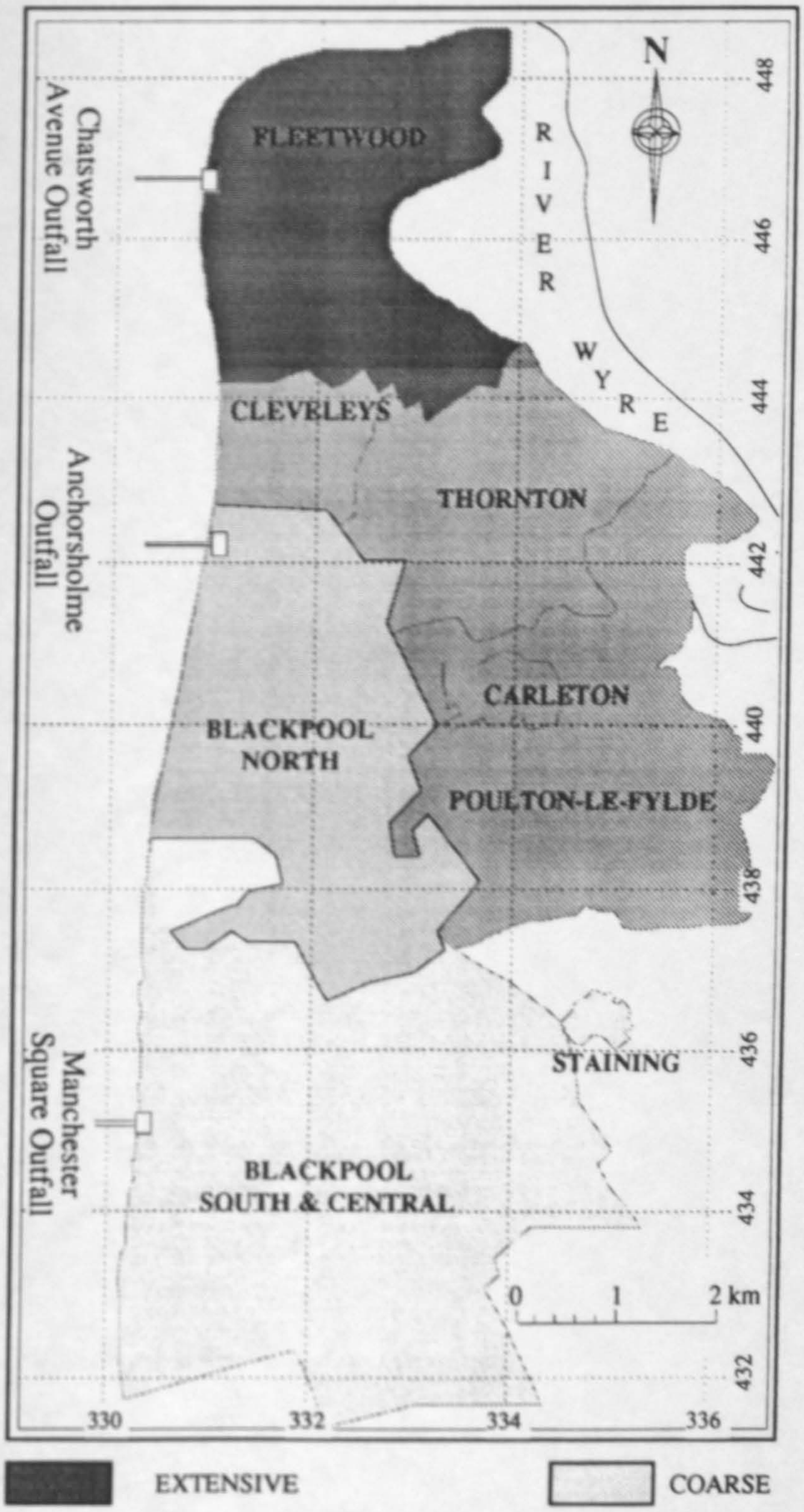

Fig. 10.3 The modelled areas and the relative extent of modelling

10.3 RTC Strategy and Operation Strategy

RTC for a UDS is aimed to realise its function and optimise its performance. Conventionally, storage facilities, flow bifurcations and CSO diversions are constructed wherever necessary to prevent the system from being destructively surcharged or causing flooding. To regulate flows within the system, control devices such as penstocks, flow gates, valves and weirs are usually used. A common feature of such conventional controls is that their settings will not vary with time once having been set. Conventional controls are passive controls. The fixed settings sometimes cause the control system to appear powerless in limitation of the CSO volume even if storage capacity is still available. This problem can be mitigated to some extent by application of RTC.

RTC is a generic description of reactive and predictive control procedures. In reactive control mode, control decision and operation is made in correspondence to the current system status defined by the state variables: the inflow depth/rate, in-sewer flow depth/rate, outflow depth/rate and utilisable storage capacity. Under predictive control mode, control operation is triggered by the predicted system state variables. The natural process of sewer flow integration can be artificially attenuated and smoothed by the regulating operations of RTC procedures.

A RTC strategy is defined by four components, control scope, controller, control objective and control mode, which determine the level of the control strategy. Based on these four components, the RTC strategies for UDS can be generally classified into 54 categories of two levels. See Table 10.2. For example, the *Global-Automatic-**Reactive*** control of CSO *Quality and* pass-forward flow *Quantity* for treatment is a low-level RTC strategy, whereas *Global-Automatic-**Predictive*** control of CSO *Quality and* pass-forward flow *Quantity* for treatment is a high-level RTC strategy. A conventional control (passive) strategy is a basic level control and can be employed to

control the sewer flow quantity within a local scope.

Table 10.2 Classification of RTC strategies

CONTROL SCOPE	CONTROLLER	CONTROL OBJECTIVE	CONTROL MODE
Local	Manual	Quantity	Reactive
Regional	Semiautomatic	Quality	Predictive
Global	Automatic	Quantity & Quality	

Control scope is the portion to be controlled in a UDS. It can be a point, a number of interactive branches or all of the branches. To control the flow at a point, a local control strategy will be enough though perhaps not 'optimal', and coordination among the control devices located at different locations may not be required. However, to achieve regional control objectives, the control of multiple branches requires the coordination of the control operations carried out for the interrelated branches. Without coordination the regional control objectives can not be achieved with maximum efficiency and minimum efforts. It is the coordination and efficiency that sets the regional control apart from the regionally local control (i.e. without coordination among the control devices) which also can achieve the regional control objectives. Global control strategy is formed by coordination among all of the control devices or cab be practicably realised by coordination of the the regional control subsystems using hierarchical procedures.

In principle, problems , e.g. CSO and flooding, can be broadly categorised into three types based on the affected spatial domain: local, regional and global. Though local problems can be tackled by local control strategies solely, the solution may be just a tradeoff with new problems occurring elsewhere in a sewer system as a result of the

original solution. For example, the CSO problem at a point downstream if reduced by shutting a penstock may result in the increase of CSO volume at another site upstream. Accordingly, local controls are only suitable for implementation at the locations where the problem can be trapped and completely removed rather than just partially cured or passed over to their neighbours. To avert future unforeseen peril, the number of uncoordinated local controls should be kept to minimum. If a problem can not be solved satisfactorily by a local control strategy then it becomes regional problem. The removal of regional problems requires a regional control strategy, i.e. coordination of the control operations for the involved local control devices. During most of the time, control tasks can be fulfilled by the local control strategies reinforced by regional control strategies. However, once the problems become global, they can not be solved effectively by the local and regional strategies and a global control is required. For example, to properly and efficiently utilise the future Fylde intercepting tunnel, a global control strategy has to be applied, which requires the coordination among the district management offices if the current sewer management contracts continue to take effect.

A controller can be a human operator (Manual), a piece of simple circuit board, or a complex system, e.g. a computer system (Automatic). In most cases it is the automatic system aided by a human operator (Semiautomatic). A controller is different from a regulator or a control device. The movement of a regulator can be driven by any type of power while being controlled by a controller who determines how the regulator should move.

Control objectives indicate the target to be achieved by implementation of a control strategy. Though the ultimate objective is to control the quality of the receiving surface water body which is often achieved by control of the flow quantity at the first place.

Control mode is the way that the regulators or control devices react to the system status. There are three possible modes: passive, reactive and predictive. Settings of regulators are time-invariant if under passive control. The settings are modified on the

basis of currently measured/predicted values of the state variables in reactive/predictive modes. Since each control mode requires different levels of control expertise, the control strategies can be broadly categorised into three different levels based on the control modes: basic level (passive), low level (reactive) and high level (predictive). The control operations in a RTC system can be incremented from one level to another at a regular step. In cases of control system malfunction, the switching from RTC levels to the basic level must be guaranteed as a fail save aspect of system design.

Discrete settings for all of the regulating devices can be preset based on the potential system status, e.g. flow levels. The time sequence of the set points of all control devices is called the operation strategy. The effect after application of the operation strategy is the increase in utilisation of storage volume and reduction of CSO volume, the more significant the effect then the better the operation strategy. An optimal operation strategy may be yielded from the optimal control operation at each regulating time step.

The above concepts concerning control strategy and operation strategy provide guidelines for the design and operation of the future Fylde RTC system. The selection of a control strategy can be made by determining the control scope, controller, control objective and control level in sequence. Often, the choice of a control strategy is subjected to economic feasibility. From the experiences of Trodda, Labadie and Grigg (1977), Papageorgiou (1983), Shilling (1985), Shilling and Semeke (1985), Shilling (1987), Larson (1990) and Weyand and M. Dolimann (1990), the unmanned large scope control is impracticable because a number of staff have to be available at all times during the control operation for supervision and maintenance purposes. As manual control strategies have been outdated, consequently, the use of a semiautomatic strategy in the first instance is strongly recommended, that is, an automatic system aided by human operator. The human operator will be needed in critical situations such as a severe storm event or system malfunctioning. However, it is unlikely that the use of a single strategy will be the best. For the purpose of reducing operational costs, the

system may be controlled in passive mode during a considerable proportion of the control time when the passive controls are able to cope with the situations. In addition, the use of local control strategies may be helpful for reducing the number of decision variables, and consequently for reducing the operational complexities.

10.4 RTC System

The physical realisation of control strategies is a control system. A RTC system comprises four components:

1) an information logging subsystem;
2) a data transferring subsystem;
3) a data analysing and decision making subsystem and
4) a regulating subsystem.

As there may be different configurations of a control system, hence, there exist more than one approaches to realise it for a given control strategy. Finding a most economic and efficient configuration is another challenging engineering aim which needs to be considered in the development of an 'optimal' RTC system.

Weather radars, raingauges, flow level sensors, flow velocity sensors are the crucial components of the information logging subsystem. Data transferring subsystem refers to the telemetry or devices used to transmit the logged data into the third subsystem: data analysing and decision making subsystem. The regulating subsystem comprises regulating devices such as penstocks, flow gates, valves and weirs. The data analysing and decision making subsystem is the core of the control system, where control operation strategies are generated and operational instructions are issued based on the system state which is analysed or predicated by a set of mathematical models.

10.5 Potential Benefits of RTC

RTC for UDSs has increasingly become an international interest. In many places over the world, a number of large experimental RTC systems have been developed and practically operating (Norreys, 1991) such as in Seattle and Detroit, USA. The former is a semiautomatic reactive control system and constitutes 21 pumping stations and 16 regulators. No rainfall runoff information is used. The later is a semiautomatic predictive control system. Radar rainfall data are used. There are 247 flow level sensors installed in the system.

Within the Fylde system, RTC techniques have been applied to some extent. For example, at the major pumping stations, pumps and penstocks are already reactively under the control of Programmable Logic Controller (PLC). Most of the RTC control strategies applied are based on local reactive control strategies. The regulating operation is triggered by the local flow information sensed by ultrasonic sensors. The experiences gained throughout the construction and operation of the current generation of RTC devices in the pumping stations and storage tanks will provide invaluable foundation upon which the RTC system can be further developed.

Given a storm event, the potential benefits of using RTC are: 1) the frequency and total number of CSOs can be reduced for those systems having insufficient storage capacity; 2) CSO can be prevented from occurring if the systems having just enough storage capacity and 3) a better performance can be guaranteed through well-planed maintenance and operation of the systems which have extra storage capacity.

10.5.1 Assessment Methodology

A general quantification of the benefits to be potentially gained through the application of RTC using radar rainfall is impossible at this time. The most practicable way to provide a good indication of the potential benefits is to carry out the assessment by

assuming a realistic and practicable control system and control operation strategy. The objective of this assessment is to indicate what proportion of the CSO volume which may spill during an event under conventional (i.e. passive) control can be reduced by using a simple predictive RTC strategy for a given system storage capacity.

System performance under the passive controls can be simulated using the WASSP model. By analysis of the inflow, continuation flow and overflow hydrographs, the inflow-storage-outflow relationship and the utilisation extent of the storage capacities can be identified. Thus the flow conditions at the control locations can be predicted. Knowing where the control settings are inappropriate, alternative settings can be applied. After reset the settings the system can be simulated again. By comparing the CSO volumes which spilled during each of the two simulation runs, the reduction of CSO volumes due to the alternation of the original inappropriate settings can be estimated. This procedure represents a one-step predictive RTC operation strategy and will yield the minimum control efficiency.

As it was not possible to carry out the assessment over the full scope of the Fylde system due to the lack of appropriate models, the Anchorsholme subsystem was chosen for the assessment because: 1) its model has been recently upgraded and verified by WRc and Blackpool Council staffs and 2) the corresponding sewer layout map is available which enables the model to be upgraded into a fully spatial version and to accept distributed rainfall input. Using the model, nine synthetically distributed radar rainfall events were examined. In addition, because different data resolutions may produce different results, for comparison purposes, the corresponding lumped rainfall events were also examined.

10.5.2 Selection of Rainfall Events

A distributed storm comprises a number of grid based time-series rainfalls. If lumped spatially, not only the grid rainfall intensities but also the grid rainfall totals (i.e.

accumulations over the entire storm duration) will be smoothed. Since grid rainfall total and duration are also two dominant impacting factors on the CSO volume in addition to the grid rainfall intensity, to ensure that the CSO volumes spilled during different storms (i.e. distributed and lumped) are mutually comparable, *the grid rainfall durations and totals have to be chosen as being same for a given storm.* For this reason, a series of synthetic storms were developed from actual radar storms and used to examine the behaviour of the subsystem over a series of storm depth durations.

There are two approaches to define a synthetically distributed storm. One is to get an actual distributed storm and modify it so that the above criteria can be met. This will result in a storm with some of its grid rainfall time-series are artificially generated using mathematical techniques. Such a storm is advantageous if it were used for investigating the effects of storm movement in relation to the peak runoff of a particular storm (Shepherd, 1987). Another alternative approach is to get a number of actually observed grid rainfall time-series of the approximate same scale defined by the storm duration and return period, and then randomly transpose the grid time-series rainfalls into the interest catchment to form a synthetically distributed storm. This means, given its scale the spatial distribution of a storm can be assumed as being random. For a given catchment, it is unlikely that two storms having the same scale (i.e. same duration and return period) can be found with the same spatial distribution pattern. Therefore, in this study the second approach was adopted, which generates a storm by:

1) Selection of grid time-series rainfalls of the required scale from the radar archive;
2) Transposition of the selected grid time-series rainfalls into the catchment.

Since the Anchorsholme catchment is covered by six radar rainfall grids (2km by 2km), each event constitutes 6 grid rainfall series of the same scale (i.e. equal duration and return period). In order to obtain a sufficient number of events from the limited data archive, following criteria were used:

1) Rainfall duration (D) has to be 60 minutes or 105 minutes or 165 minutes;

2) The return period (T) has to be 1 year or 2 years or 5 years.

Based on these criteria, a total number of 54 time-series grid rainfalls were selected from the Hameldon Hill radar rainfall measurements, which made up 9 synthetically distributed storms as shown in Table 10.3. The six time-series rainfalls (from G1 to G6) of each storm were randomly transposed to the 6 grids over the catchment. In the table, rainfall depths were calculated as the grid rainfall accumulations over the entire storm duration and the average of the six grid rainfall totals of a storm (i.e. areal rainfall) is shown in the last column.

Table 10.3 Nine synthetically distributed storms

TIME-SERIES RAINFALLS	RAINFALL DEPTH (MM)						AVERAGE (mm)
	G1	G2	G3	G4	G5	G6	
D060 Min.T1Year	11.9	12.3	12.7	11.0	12.7	12.9	12.3
D105 Min.T1Year	17.6	16.3	14.9	17.2	16.3	13.8	16.0
D165 Min.T1Year	19.7	19.0	20.2	17.1	18.6	27.3	20.3
D060 Min.T2Year	13.7	15.0	14.4	12.9	12.9	15.0	14.0
D105 Min.T2Year	19.7	16.3	18.2	14.5	14.7	17.3	16.8
D165 Min.T2Year	20.3	18.9	20.6	19.4	18.1	19.9	19.5
D060 Min.T5Year	18.4	16.9	17.1	17.3	19.1	15.3	17.4
D105 Min.T5Year	21.3	21.0	22.0	22.3	20.4	19.4	21.1
D165 Min.T5Year	24.4	24.3	24.6	25.2	25.0	25.1	24.8

Figure 10.4 to Figure 10.12 shows the spatial distribution patterns of the 9 synthetically distributed storms.

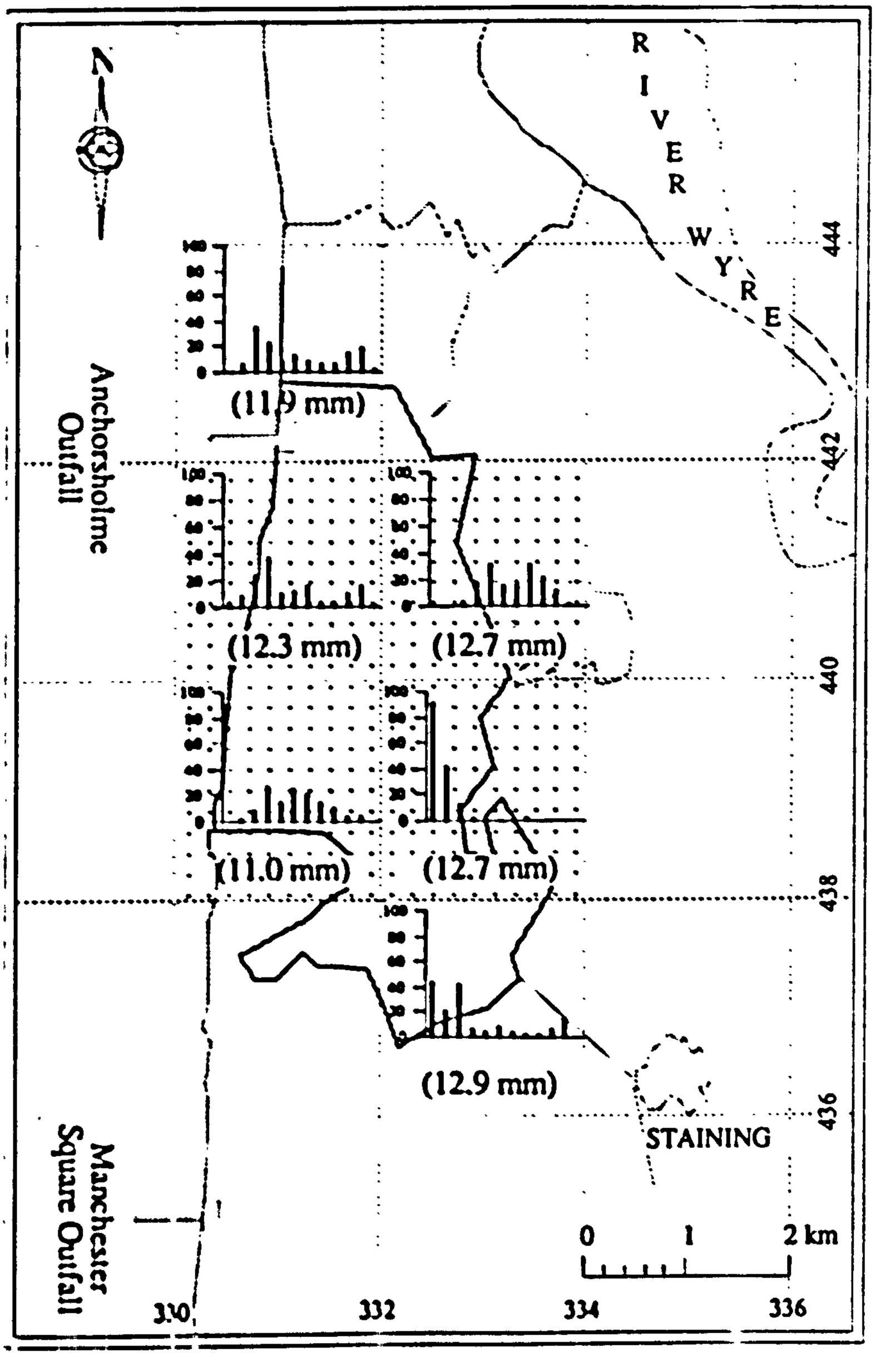

Fig.10.4 The spatial distribution pattern of storm: (D060Min.T1Year) designed for the Anchorsholme subcatchment

(Note: Data resolution: 2km in space and 5minutes in time; The accumulated rainfall depth is shown in brackets and rainfall intensity is in mm/h)

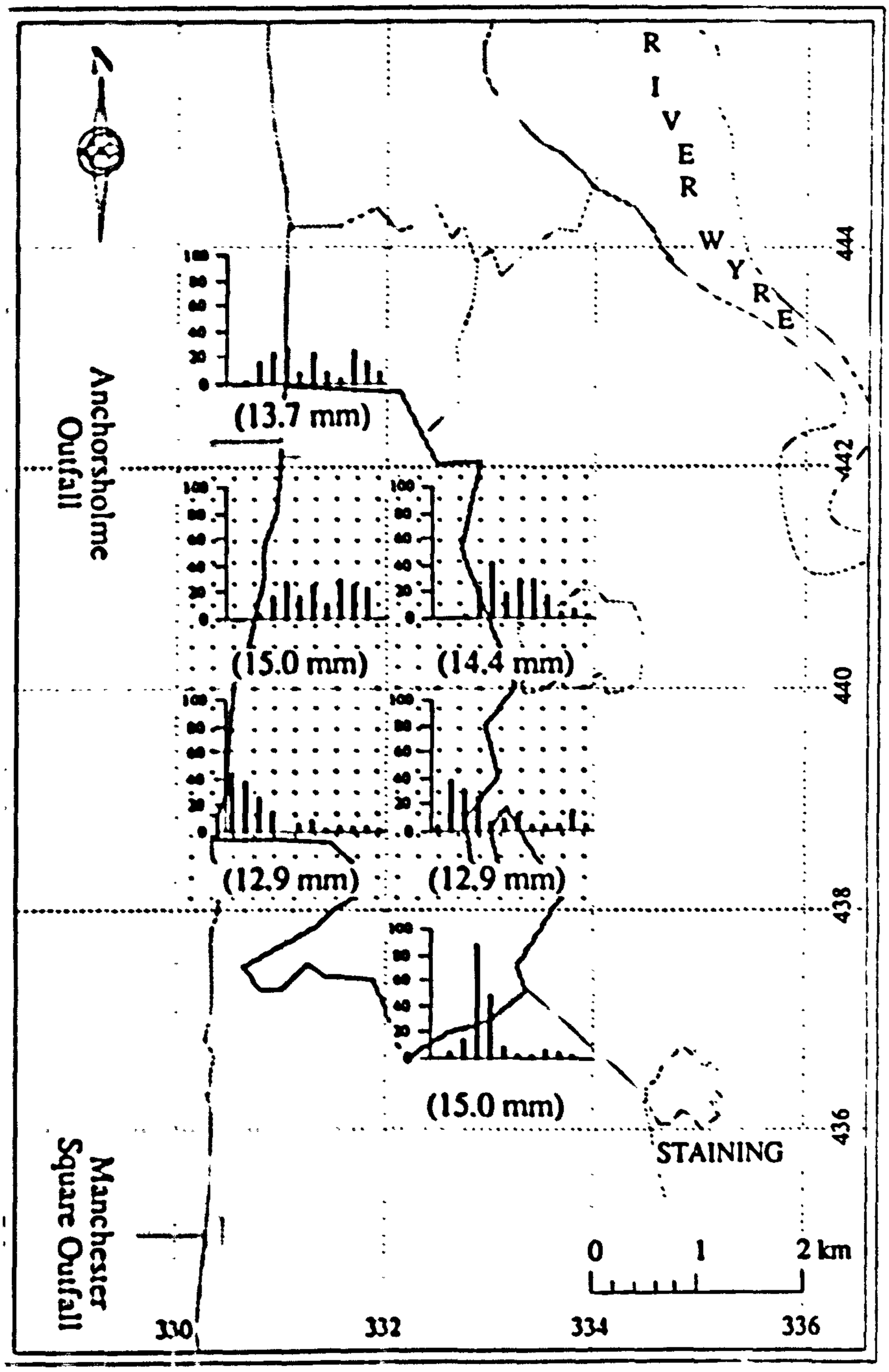

Fig.10.5 The spatial distribution pattern of storm: (D060Min.T2Year) designed for the Anchorsholme subcatchment

(Note: Data resolution: 2km in space and 5minutes in time: The accumulated rainfall depth is shown in brackets and rainfall intensity is in mm/h)

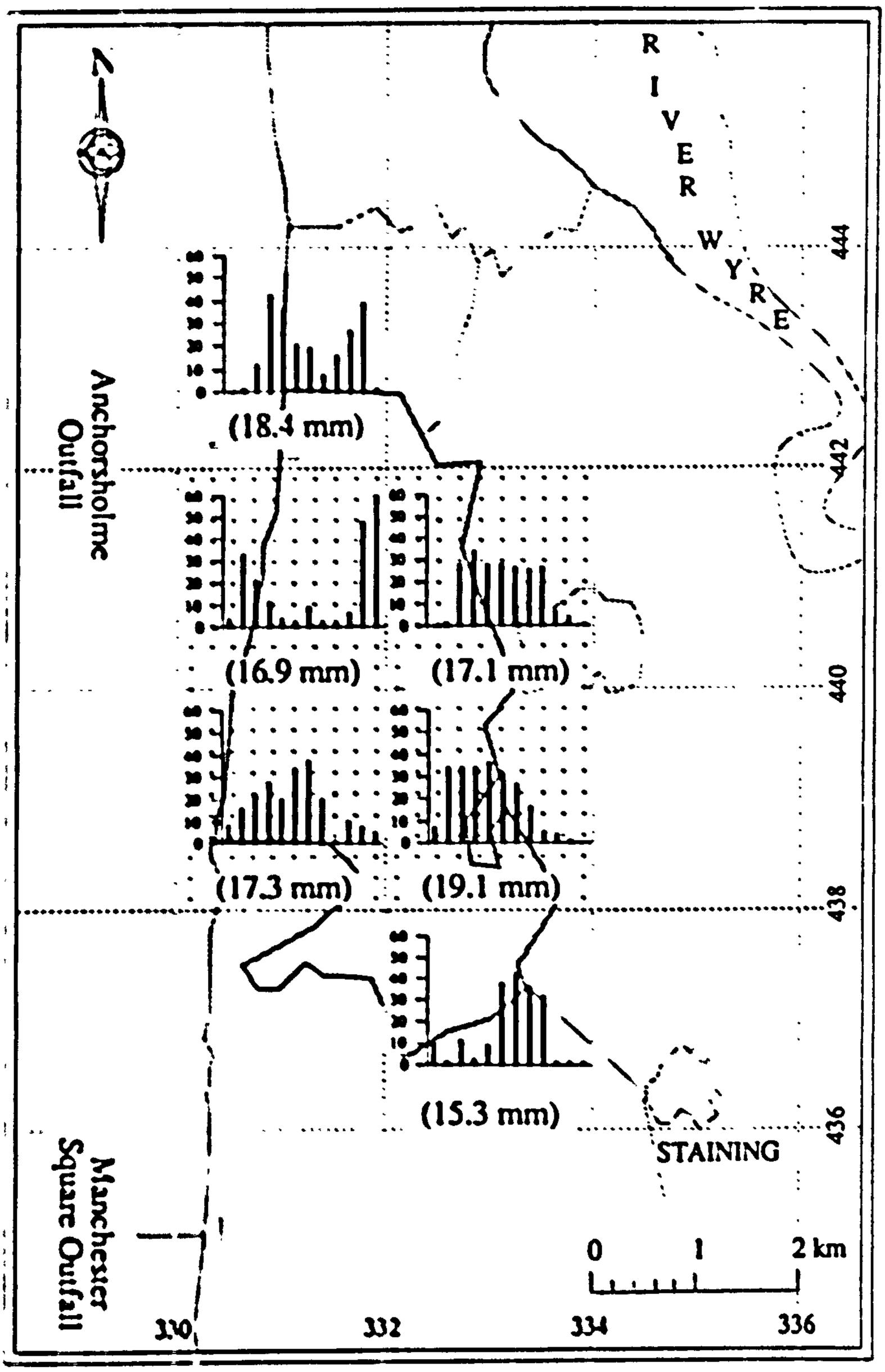

Fig.10.6 The spatial distribution pattern of storm: (D060Min.T5Year) designed for the Anchorsholme subcatchment

(Note: Data resolution: 2km in space and 5minutes in time: The accumulated rainfall depth is shown in brackets and rainfall intensity is in mm/h)

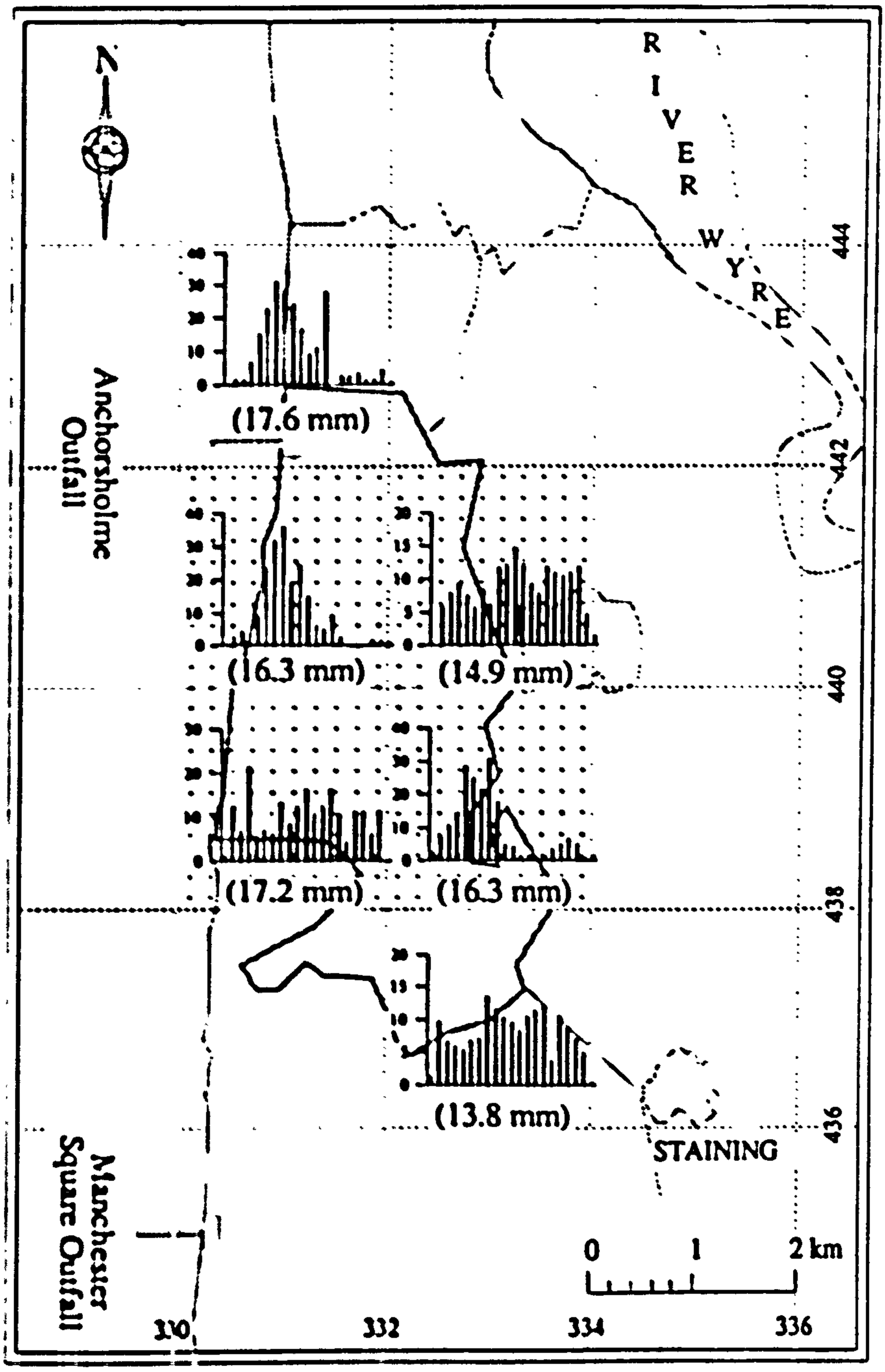

Fig.10.7 The spatial distribution pattern of storm: (D105Min.T1Year) designed for the Anchorsholme subcatchment

(Note: Data resolution: 2km in space and 5minutes in time: The accumulated rainfall depth is shown in brackets and rainfall intensity is in mm/h)

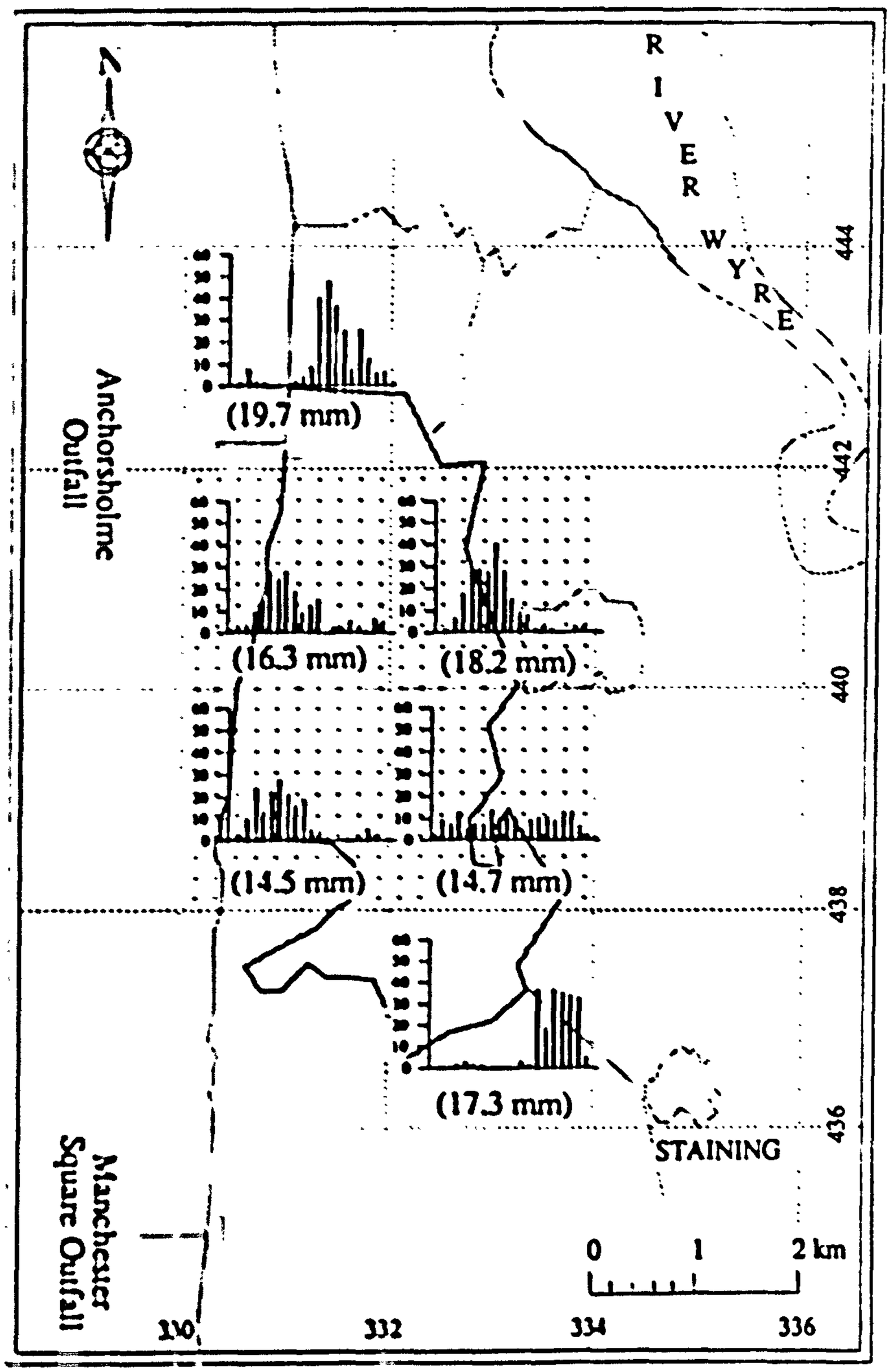

Fig.10.8 The spatial distribution pattern of storm: (D10SMin.T2Year) designed for the Anchorsholme subcatchment

(Note: Data resolution: 2km in space and 5minutes in time: The accumulated rainfall depth is shown in brackets and rainfall intensity is in mm/h)

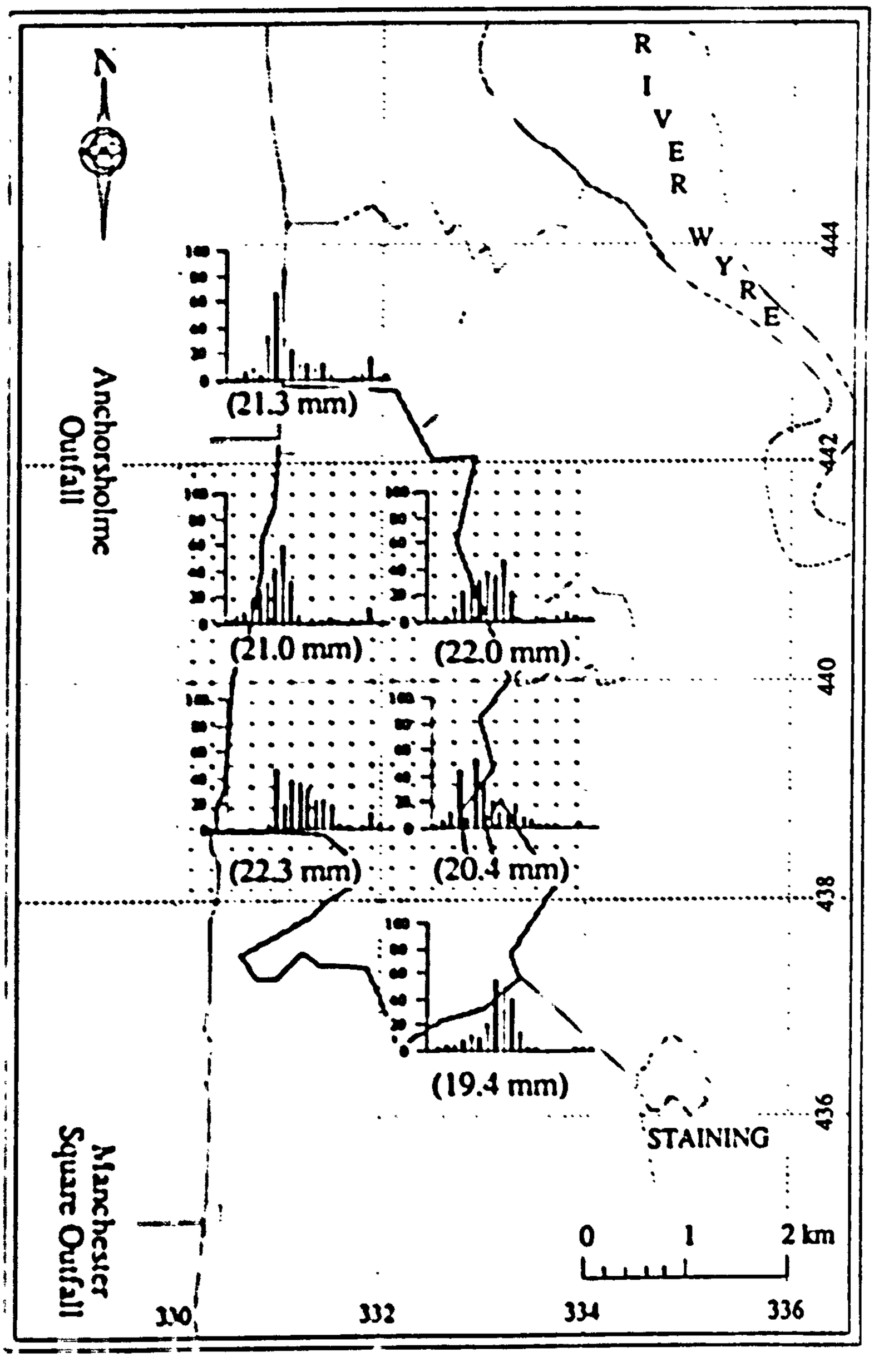

Fig.10.9 The spatial distribution pattern of storm: (D105Min.T5Year) designed for the Anchorsholme subcatchment

(Note: Data resolution: 2km in space and 5minutes in time: The accumulated rainfall depth is shown in brackets and rainfall intensity is in mm/h)

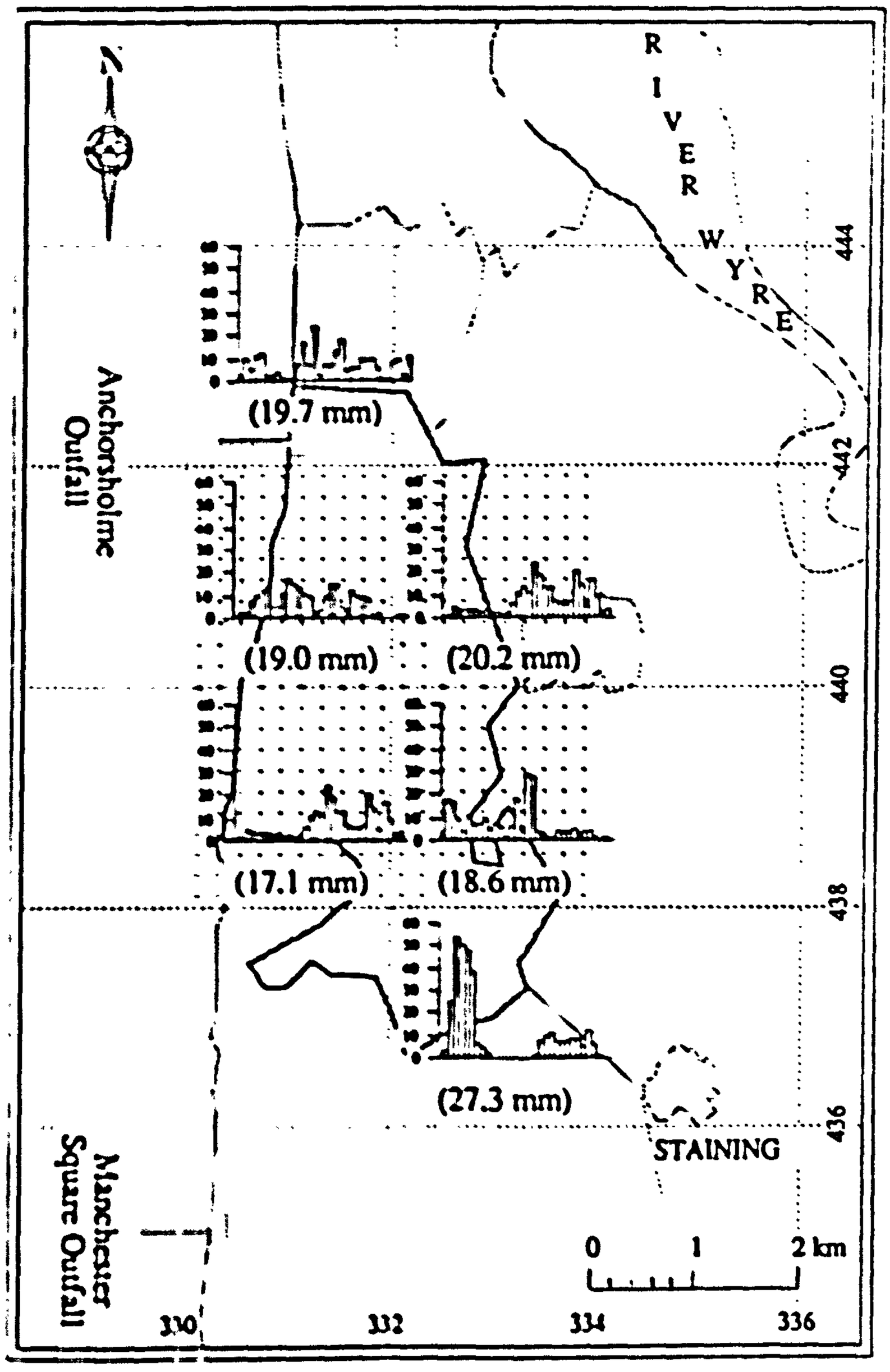

Fig.10.10 The spatial distribution pattern of storm: (D165Min.T1Year) designed for the Anchorsholme subcatchments

(Note: Data resolution: 2km in space and 5minutes in time: The accumulated rainfall depth is shown in brackets and rainfall intensity is in mm/h)

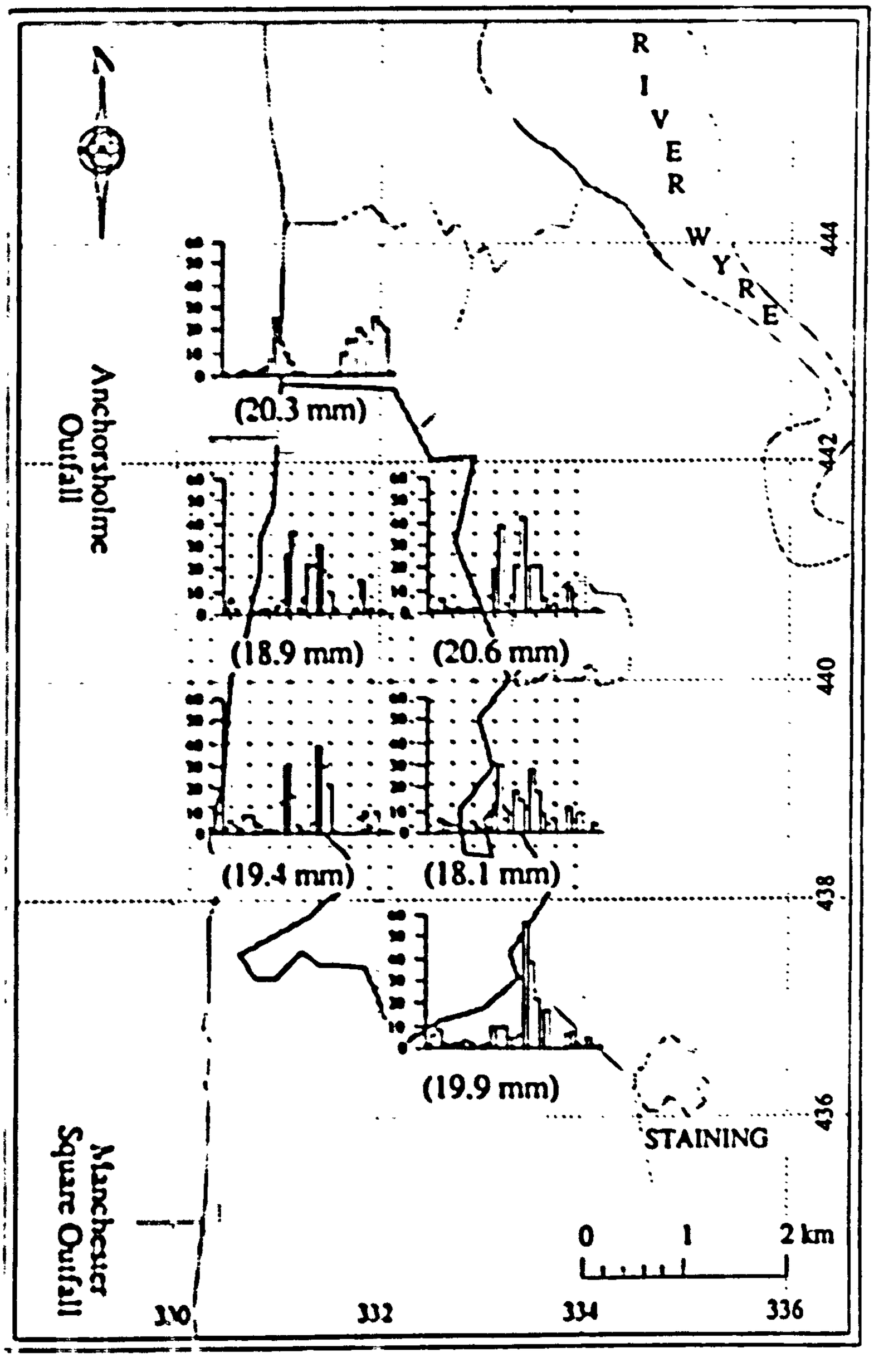

Fig.10.11 The spatial distribution pattern of storm: (D165Min.T2Year) designed for the Anchorsholme subcatchment

(Note: Data resolution: 2km in space and 5minutes in time: The accumulated rainfall depth is shown in brackets and rainfall intensity is in mm/h)

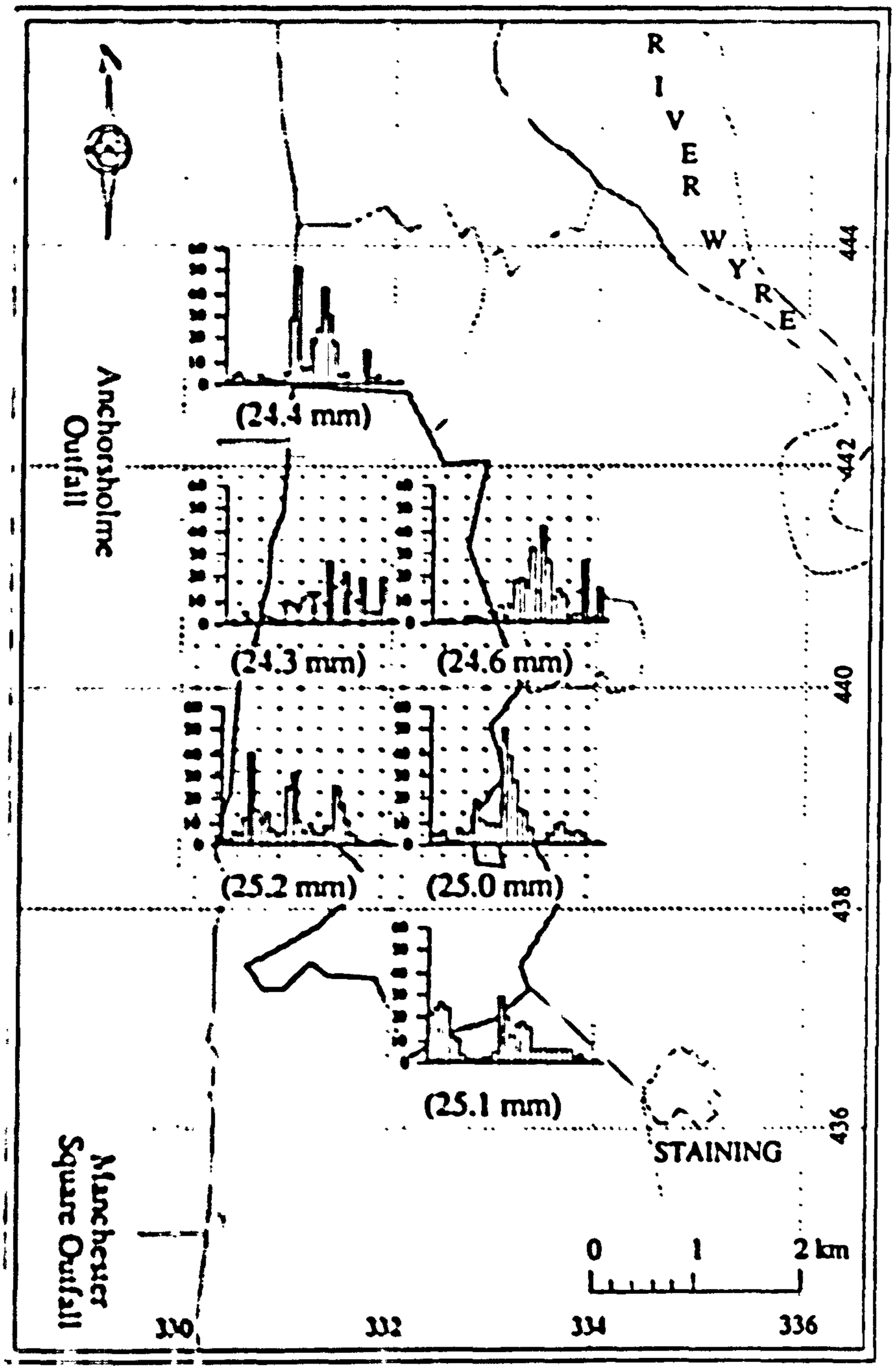

Fig.10.12 The spatial distribution pattern of storm: (D165Min.T5Year) designed for the Anchorsholme subcatchment

(Note: Data resolution: 2km in space and 5minutes in time; The accumulated rainfall depth is shown in brackets and rainfall intensity is in mm/h)

The data have a 2-km spatial resolution and 5-minute temporal resolution. It can be seen from the figures that the total rainfall volume received by any part of the catchment during a storm of the given return period is approximately the same. Such a scene is a close imitation of a widely-spread intense rainfall event. These type of events have high potential to saturate the system and result in catastrophic CSOs or flooding, therefore have greater importance to applications of stormwater management. The scene enables one to assess the impacts of spatial lumping of rainfall intensity on the total CSO volume. Since the rainfall duration, accumulative depth and temporal distribution of the storm component are intact, the assessment made will be objective. If the results indicate that the total CSO volumes produced using the lumped rainfalls are larger than that produced using distributed rainfalls then it is wise to use the distributed rainfall data for any type of storm and any modes of applications (i.e. design and RTC). This is because, during localised storms, the grid rainfall totals will be different, the spatial lumping of rainfall intensities will result in the removal of locally centred peaks and coincidence of the flow peak from each grid. Hence, the total CSO volume will be overestimated in the smaller scale catchment, and using lumped data for RTC in this case will yield an inappropriate operational control strategy.

10.5.3 Determination of RTC Strategy and Operation Strategy

Figure 10.13 shows a schematic predictive RTC control system designed for the Anchorsholme subsystem. In the system, radar rainfall and flow information may be collected and transmitted through the public and private communication channels to the control centre where flow simulation and predication would be carried out. There are two major storage facilities and a pumping station in the system: Warren Drive tank sewer has a capacity of 5420 m^3 and Moor Park tank has a capacity of 11300 m^3.

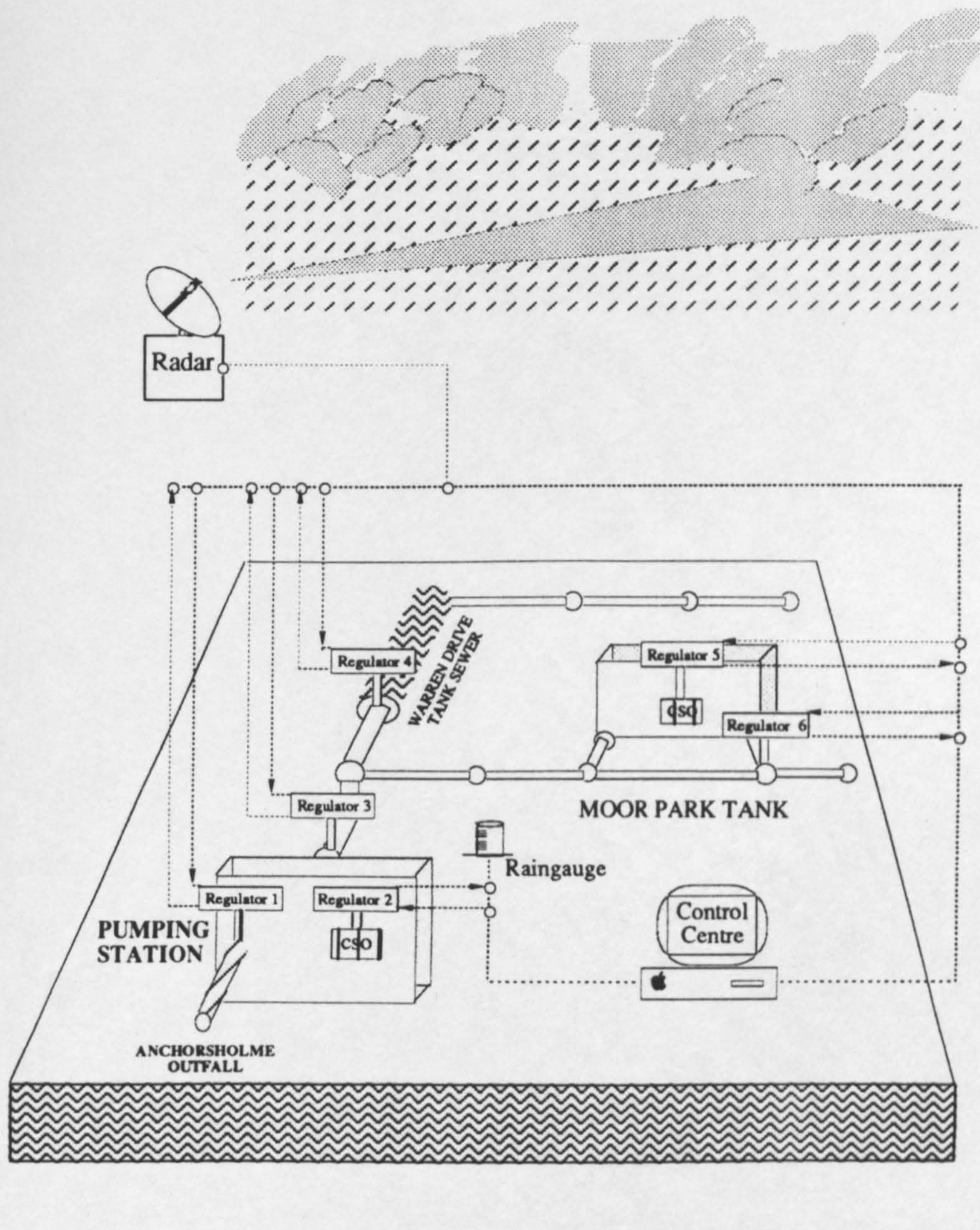

Fig. 10.13 The schematic of predictive control system designed for the Anchorsholme UDS

Regulator 1 is a set of pumps operated at constant pumping rates and Regulator 2 is an overflow weir controlling the CSO operation at the pumping station. Regulator 3 is a set of penstocks controlling the input into the pumping station. Regulator 4 controls the proportion of flow to be stored in Warren Drive sewer. Regulator 6 is used for the same purpose as Regulator 4, and Regulator 5 controls the overflow from the Moor Park tank. Radar rainfall was used as the major input data source, whilst raingauge rainfall was employed for data quality control or standby purposes.

With the above control system, an assessment of the potential benefits of RTC using radar rainfall data was made.

Since the assessment was made in simulation mode using the WASSP model, the operational control strategy had to be as simple as possible. The operation strategy was derived from the predictions of the system status at the three major control locations, where the setting alterations could potentially reduce the total CSO volume. For example, Figure 10.14 shows the predictions of the system status at the three major control sites. It was seen that a large proportion of sewer flow spilled at the Anchorsholme pumping station whilst the storage capacity at Warren Drive Tank sewer had not been activated at all due to inappropriate settings. A different situation developed at the Moor Park tank where most of the available storage capacity had been utilised. Alteration of the settings at the Moor Park tank was not likely to yield any desirable effects on the reduction of CSO volumes at the pumping station. Therefore the operational control strategy was made to only alter the settings of Regulator 2 and Regulator 4.

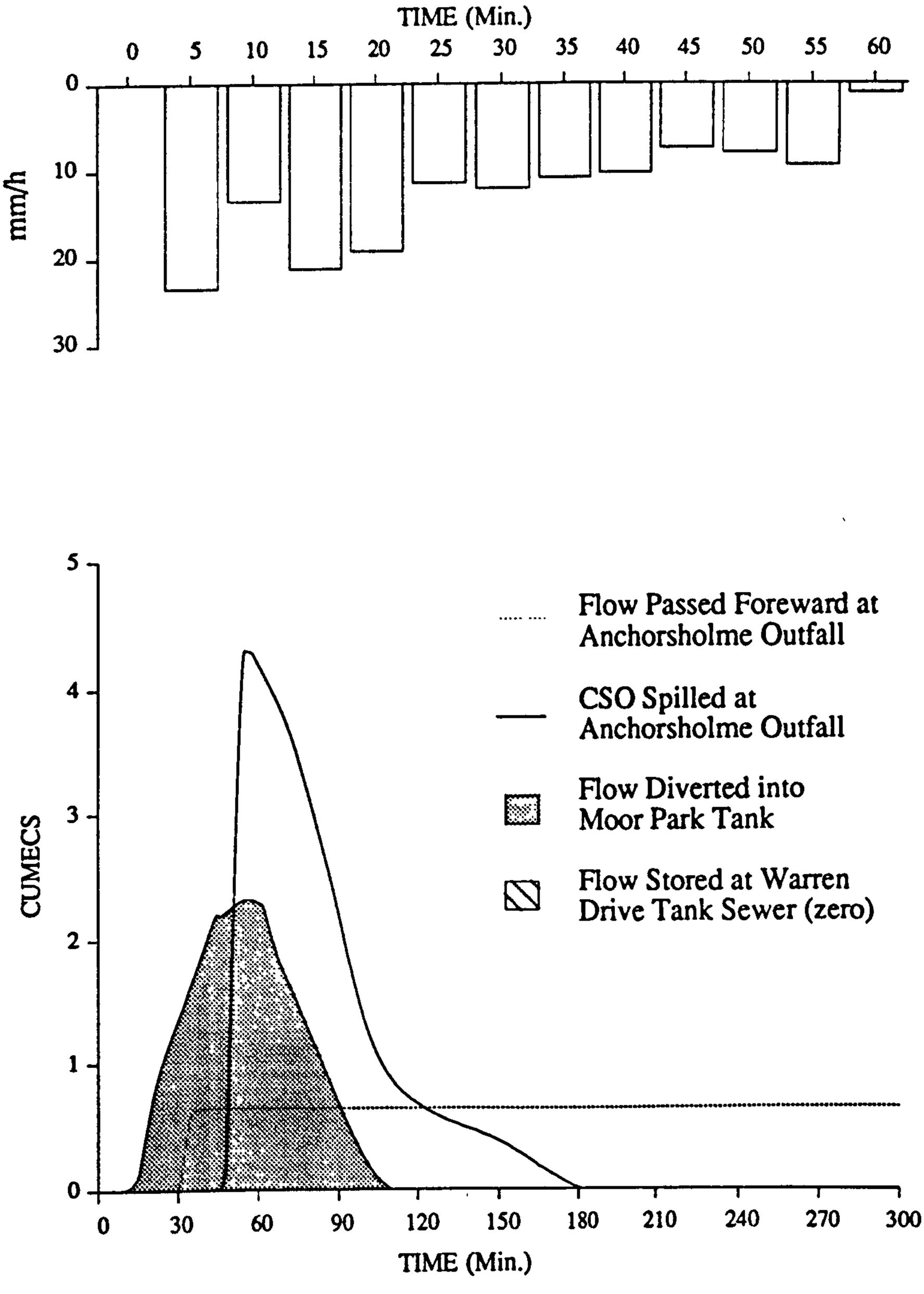

Fig. 10.14 Storage capacity at Warren Drive tank sewer left unused under passive control

The results after application of the operation strategy are shown in Figure 10.15. From the figure it can be seen that the spill at the Anchorsholme pumping station (previously shown in Figure 10.14) has been greatly reduced

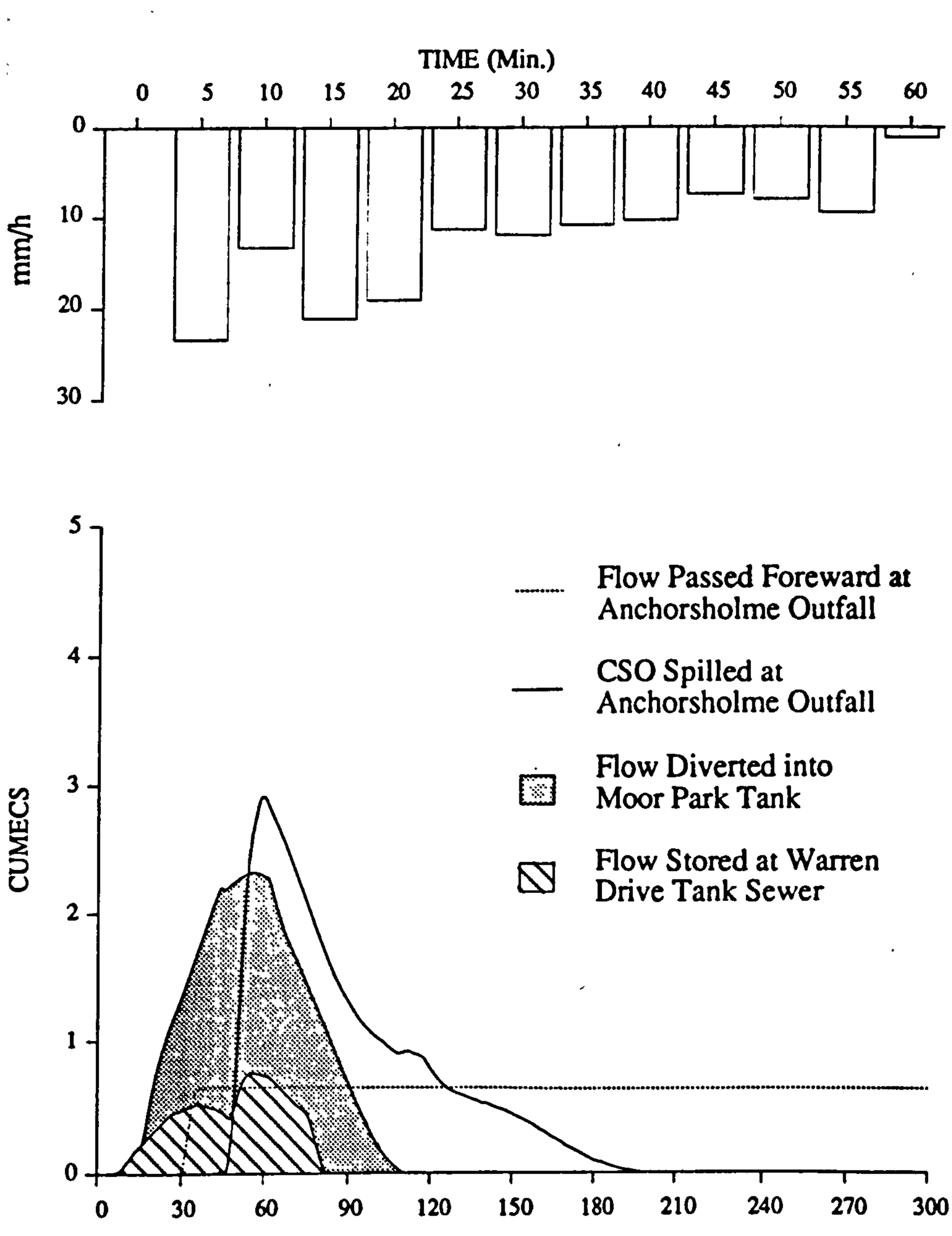

Fig. 10.15 CSO volume reduced during the same storm as shown in the Fig. 10.14 due to the application of predictive RTC

It is the alteration of the settings of the regulators based on the predicted system status that categorises the applied control strategy as a predictive strategy. Comparisons between the CSO volumes during the passive control and predictive control regimes were undertaken by applying the above operational strategy using each of the 9 distributed storms and 9 lumped storms. The lumped storm was derived from the corresponding distributed storm by averaging its 6 grid time-series rainfalls at each time step.

10.5.4 Reduction Rate in CSO Volume

The potential benefits of RTC using radar rainfall in reducing the CSO volume can be assessed using the Reduction Rate (RR), which is defined as:

$$RR = \frac{V_{pas} - V_{pre}}{V_{pas}} \times 100\% \qquad (10.1)$$

Where V_{pas} is the total CSO volume spilled during an event under the passive control and V_{pre} is the total CSO volume spilled during an event under the predictive control. In this analysis, they were respectively produced for each of the 9 distributed and lumped storms.

The results are summarised in Table 10.4. In the table, column (B) is the accumulated areal rainfall depth over the entire catchment. Column (C) and column (D) give the total CSO volumes spilled under the passive control mode for different input rainfall data resolutions. Similarly, column (E) and column (F) show the total CSO volumes spilled under predictive control mode. Column (G) is calculated as the ratio of column (C) divided by column (D), column (H) is the ratio of column (E) divided by column (F), column (I) is the ratio of column (C) over column (E) and column (J) is the ratio of column (D) over column (F).

Table 10.4 Total CSO volumes for different storms and under different control strategies

CONTROL MODE		PASSIVE (M^3)		PREDICTIVE (M^3)		INTER-COMPARISONS			
						V_{lum}/V_{2km}		RR	
⇩ STORM DATA TYPE ⇨	Depth (mm)	LUMPED	2KM	LUMPED	2KM	PASSIVE	PREDICTIVE	LUMPED	2KM
D060 Min.T1Year	12.3	12177	11991	8555	7932	1.02	1.08	29.7	33.9
D105 Min.T1Year	16.0	18369	18330	14010	14019	1.00	1.00	23.7	23.5
D165 Min.T1Year	20.3	25697	25335	22875	22507	1.01	1.02	11.0	11.2
D060 Min.T2Year	14.0	14358	13504	10073	9580	1.06	1.05	29.8	29.1
D105 Min.T2Year	16.8	19678	16269	15568	12315	1.21	1.26	20.9	24.3
D165 Min.T2Year	19.5	23417	22372	20173	18506	1.05	1.09	13.9	17.3
D060 Min.T5Year	17.4	18257	17702	13690	13122	1.03	1.04	25.0	25.9
D105 Min.T5Year	21.1	22469	22653	18209	18537	0.99	0.98	19.0	18.2
D165 Min.T5Year	24.8	31362	31087	27898	27614	1.01	1.01	11.0	11.2
(A)	(B)	(C)	(D)	(E)	(F)	(G)	(H)	(I)	(J)

The Reduction Rate in CSO volume is shown in Figure 10.16 for each storm ranked by rainfall depth. The storm duration and return period are given in brackets.

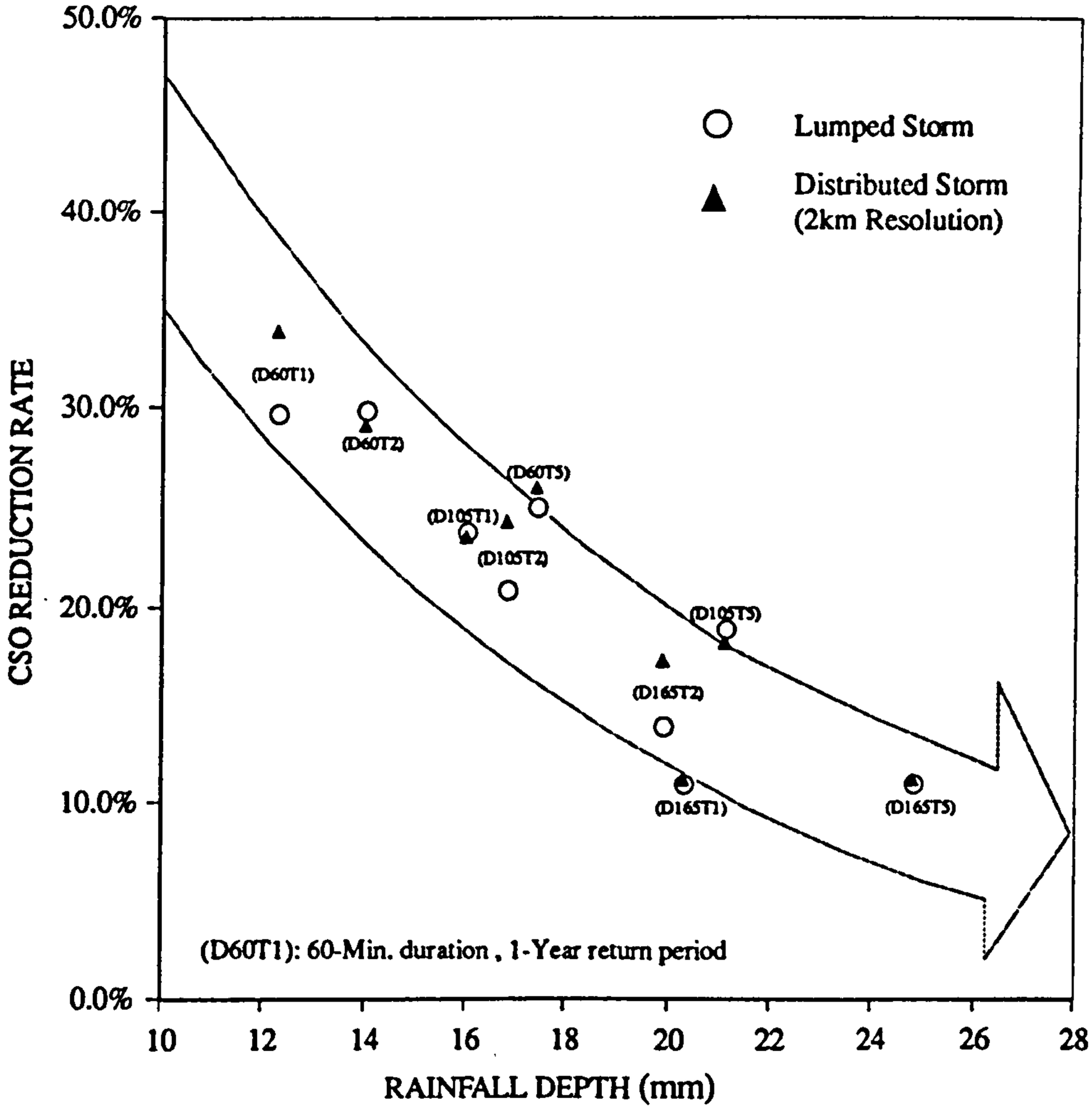

Fig. 10.16 Comparisons between the CSO volumes occurring from simulated passively and predictively controlled systems

The results indicate that: 1) Predictive control is beneficial over passive control in terms of reduction of CSO volumes; The reduction rate ranges from 10% to 30% for storms having a return period of 5 year to 1 years and duration from 1 hour to 3 hours. It is envisaged that with a multi-step forecasting and control operation the benefits could be even more substantial with the existing storage capacity;

2) The benefits gained through predictive control decreases with total rainfall depth. This conclusion should hold for any UDS. For those storms lasting longer than 3-hours and having a return period of more than 5 years, predictive RTC seems only slightly superior to passive control due to relatively early saturation of the limited storage capacity;

3) Slightly more CSO volumes were spilled when using the lumped rainfalls than that using the distributed rainfalls during most of the storms studied due to the coincidence of the local peaks resulted from the lumping of rainfall intensities. This implies that for RTC control, distributed storms should be used whenever possible, and for design purposes, using a lumped storm will result in a safer but costly solution whereas for control purposes it may result in an unnecessary operation. If design storage volume is proposed based on the results obtained using a distributed rainfall event configured using the method developed during this study, the proposal will be more objective and economic whereas the protection level will still be quantifiable and comparable to that using conventional lumped design storms of the same scale;

4) Urban Hydrological Radar has an important role to play in provision of higher resolution and more accurate estimates of precipitation in addition to an objective flow prediction in the RTC scenario!

10.6 Summary

1) Application of RTC on the Fylde UDS is beneficial in terms of operational improvements. A considerable percentage (in the present study from 10% to 30%) of the CSO volume spilled under passive control can be reduced if predictive control is employed.

2) The benefit to be gained from using RTC is determined by the total storage capacity, control strategy, operation strategy and the storm characteristics (i.e resolution and scale, especially the accumulated rainfall depth).

3) The application of radar rainfall data has considerable prospects in predictive RTC for urban drainage systems.

CHAPTER 11

CONCLUSIONS AND RECOMMENDATIONS

11.1 Conclusions

In recognising the importance and potential that weather radar may provide the required rainfall data for urban drainage system control in real-time, a number of relevant issues on the radar rainfall data quality, real-time flow prediction and application of radar rainfall data have been addressed in this thesis . The major findings and achievements are summarised as following:

11.1.1 Suitability of X-band Radars

The minimum detectable rainfall (MDR) is an objective indication of the suitability of a weather radar system, which varies with the radar range, intervening rainfall characteristics and the radar constant. Providing the target rainfall intensity is not below the MDR of an X-band radar system, the rainfall is detectable and can be corrected to a comparable accuracy of that would have been observed by a co-located C-band radar system if the amount of attenuation can be identifiable through certain reference such as the ground truth. Since at shorter ranges (<20 km) the rainfall within a uniformly scattered moderate intervening rainfall field (<36 mm/h) is detectable, X-band radars may be suitable for detecting samll to moderate rainfalls within a range of 15-20km.

11.1.2 Radar Rainfall Data Resolution

Temporal and spatial resolutions are important factors which determine the accuracy of quantitative radar rainfall data. Providing that the system's discretising resolution is adequate, the valid temporal resolutions (χ) of the input data to a hydrological model can be determined based on the rule:

$$\chi \leq \frac{U_i - (\Delta - 1)}{2} \quad ; \quad \chi = 1, 2, 3, \cdots$$

where U_i-(Δ-1) is the lag-to-inflection duration of the system's PR. The Half Of the lag-to-inflection duration (HOLTID) is a dominant factor which governs the validity of a model input data resolution and determines the model's performance level.

The present UK radar rainfall products use 5 minutes as the maximum temporal resolution and 2 km as the maximum spatial resolution. Using a lower temporal resolution than 5 minutes (i.e 10 minutes, or 15 minutes) had been found feasible providing it is shorter than the system HOLTID whereas the use of a spatial resolution lower than 2-km, say 5-km, is not recommended unless for lumped use. However, because spatial lumping of rainfall intensities will result in a similar smoothing effect to the temporal averaging, the validity of a spatial resolution should be also dependent on the system HOLTID which determines which frequency is allowed to pass the system, the longer HOLTID, the more high frequency components will be filtered. Therefore, so long as the spatial lumping will not result in a removal of the passable frequencies then it is possible to use a lower spatial resolution. Since a larger system usually has a longer HOLTID, if an RTC application is positioned at the downstream or outlet of a larger catchment then a lower resolution than 2km or even lumped data may be feasible.

11.1.3 Radar Rainfall Data Quantisation

A more efficient quantisation scheme has been developed for the radar rainfall data processing, transmission and archive purposes. The new scheme uses the inverse parabolic cosine as its compressor (β-Law):

$$y(s) = \frac{\text{Arch}(\beta s+1)}{\text{Arch}(\beta+1)} = \frac{\ln(\beta s+1+\sqrt{(\beta s+1)^2-1})}{\ln(\beta+1+\sqrt{(\beta+1)^2-1})}$$

which may be applied in either static or adaptive mode. The β-Law is able to cope with a wider dynamic range of rainfall intensities with relatively less quantising errors than many of the existing compressors.

With the adaptive quantisation, more accurate rainfall data can be obtained than using the static quantisation schemes. The adaptively quantised 3-bit data can be used to replace the statically quantised 8-bit data for urban hydrological applications.

The occurrence of radar rainfall intensities is governed by a probability density function in the form:

$$p(n,\tau,\alpha)=\frac{\alpha R^{n\alpha-1}}{\tau^n\Gamma(n)}e^{-R^\alpha/\tau}$$

where R is a rainfall intensity in mm/h;

p(•) is the PDF of R;

n, τ and α are constants.

It is also the PDF of the radar reflectivity in mm^6/mm^3. If expressed in terms of dB, the PDF of the radar reflectivity is:

$$p(Z_{dB}) = \frac{\alpha}{\tau^n \Gamma(n)} e^x, \quad \text{where } x = \alpha n Z - \frac{1}{\tau} e^{\alpha Z}$$

The true occurrence frequency of a rainfall intensity in the quantised data is magnified by a factor being equal to the quantum.

11.1.4 Dynamic Linear Reservoir and the CPTF Model

A dynamic linear reservoir (DLR) is a linear system that has a time-variant storage factor. Based on the DLR concept, three types of the general conceptual pulse response functions have been developed respectively for modelling the systems that have different dynamic characteristics (Appendix-II):

Type-1 (PR-C):

$$h(u) = \frac{\eta \alpha (u - \Delta + 1)^{n\alpha - 1}}{\tau^n \Gamma(n)} e^{-(u-\Delta+1)^\alpha / \tau}$$

Type-2:

$$h(u) = \frac{\eta}{\Gamma(n)} \left[\frac{\ln U}{\tau_0 \beta} \right]^{n-1} \frac{U^{-\frac{1}{\tau_0 \beta}}}{\tau_0 + \tau_2 e^{-\beta u}}, \quad U = \frac{\tau_0 e^{\beta u} + \tau_2}{\tau_0 + \tau_2}$$

Type-3:

$$h(u) = \frac{\eta U^{n-1}}{\tau_3^n \Gamma(n)} (1 - e^{-\theta u}) e^{-U/\tau_3}, \qquad U = u + \frac{1}{\theta} e^{-\theta u} - \frac{1}{\theta}$$

All the PR functions have a similar shape. A great number of special cases of the Type-1 PR have been developed over the last 40 years. However, the other two types

have not been seen in any publication and is considered to be a relatively novel development.

Using the Type-1 PR (i.e. PR-C), a conceptually parametrised transfer function (CPTF) model has been developed specially for real-time flow simulation and prediction purposes. The model has two forms. The Naive CPTF model is a linear filter type whereas the Advanced CPTF model is a Markov Process. The Naive CPTF model is suitable for parameter adaption and the Advanced CPTF model is ready for state updating.

Identification of CPTF model is quite straightforward and simple. Genetic algorithms are implemented as a simple but efficient tool for minimisation of the modelling errors. The PR parameters identified at the first step guarantees a physically realisable PR function to be established and using the identified PR function a Naive CPTF model can be derived. The CPTF model parameters computed at the second step enable an Advanced CPTF model to be constructed. The Naive CPTF model can be updated in real-time using the parameter updating technique and the Advanced CPTF model can be updated by state updating and/or parameter updating techniques. Before carrying out the identification procedure, base flow separation and net rainfall derivation are not required. The model is intended to be applied by feeding the 'raw' input, therefore should be identified using the raw data.

Existing UH models and NCTF models are also able to be converted into CPTF models. The performance of a CPTF model is at least as good as a NCTF model in flow simulations. However, for adaptive forecasting applications, the CPTF model is more robust and flexible than the NCTF model. UH models can be adequately replicated by the corresponding Naive CPTF models.

In broad terms, the performance of a CPTF model in simulation of a drainage system is quite satisfactory. However, in prediction mode, it is dependent on the HOLTID and

the variability of the system's PR (or IR). If the PR function is relatively stable from event to event then an average CPTF model with state updating will generally suffice. Otherwise, a parameter adaptive CPTF model should be used.

11.1.5 Radar Rainfall Data Accuracy

Radar rainfall accuracy is a time, space, rainfall type and radar device dependent issue. Hameldon Hill radar overestimated the rainfall depths within a range shorter than about 20km and underestimated the depths beyond that range. Except for some of the bright band situations, the areal radar rainfall accumulations were smaller than that estimated using the raingauge data. However, using the hourly areal radar rainfall produced a more accurate reproduction of the observed flow hydrograph than using the raingauge rainfall data. This fact proved that 1) despite the fact that the radar rainfall estimates are not perfect they do represent the major spatial distribution characteristics of a rainfall field; 2) even with a densely scattered raingauge network (1 gauge per 13 km^2), it was not possible to derive an adequate and representative areal rainfall pattern; 3) how to improve the radar performance under Bright-band conditions is a challenging task which is currently under investigation using the vertically pointing radars.

11.1.6 RTC for UDS Using Radar Rainfall Data

RTC is beneficial to the urban drainage system management in terms of operational improvements. A considerable percentage of the CSO volume spilled under passive control can be reduced if predictive control is applied. In the case of the Fylde study, upto a 10-30% reduction in the total CSO volume can be achieved with the existing storage capacity and the studied storm scales (i.e. duration ≤ 3 hours and return period ≤ 5 years). The benefit to be gained from using RTC is determined by the total storage capacity, control strategy, operation strategy and the storm characteristics (i.e resolution and scale, especially, the accumulated rainfall depth). Radar rainfall has a considerable application prospects in predictive RTC systems.

11.2 Recommendations

A. ON THE REAL-TIME SIMULATION MODEL

At the operational stage of a RTC system, simulation models are required to assist the operator to workout a control operation strategy to achieve the objectives: 1) maximisation of inflow; 2) minimisation of overflow and fully utilisation of the treatment capacity. The models should be adaptive to the system state variables.

Theoretically, given the realisation of a system defined over a short time period, the pulse response of CPTF model can be identified. As the CPTF model has excellent adaptability, therefore it can be used for operational RTC purpose. However, a CPTF model is essentially a single-input and single-output (SISO) system. Though it may be possible to decompose a system that has multiple inputs and multiple outputs (MIMO) into a number of local SISO subsystems so that each can be handled by a CPTF model, a menu detailing the decomposition procedure need to be produced, and further studies into the procedure on how to cascade and cluster the individual models are necessary.

B. ON THE PLANNING OF A RTC SYSTEM

In planning a RTC system for a UDS, the following rules may be observed:

Step 1: Modify the existing passive control devices (*basic level control*) to RTC devices by making the inflow or outflow or both settings adjustable and install flow sensors, mainly at the locations of CSOs, flow diversions and storage facilities.

Step 2: Locally operate the updated control devices reactively using the available information of the controlled local flow variables to reduce the frequency or volume of

CSO spills (*local low-level control*).

Step 3: Regionally coordinate the operation of the local reactive control devices based on their downstream available drainage capacity and the status of storage facilities to help minimise the frequency or volume of CSO spills (regional low-level control).

Step 4: Upgrade the regional reactive RTC system by using radar rainfall and a real-time network simulation model, and operate the system predictively (*regional high-level control*).

Step 5: If necessary link up all the regional predictive subsystems to form a global predictive RTC system (*global high-level control).*

C. ON THE POTENTIAL APPLICATION OF THE CPTF MODEL FOR REAL-TIME DRAUGHT MANAGEMENT

Real-time draught management requires the input-storage-output relationship of a water-resources system to be simulated and/or predicted in real-time. In the simplest case, a water-resources system is a simple reservoir. To determine the system inflow using rainfall measurements, a real-time rainfall-runoff model is needed. As the CPTF model is very flexible and easy to be used in real-time, it will have considerable potential for application on the real-time draught management. A decision support system for draught management has been developed within North West Water Limited (Walker, Jowitt and Bunch, 1993). It is high likely that its performance can be improved if the CPTF model can be integrated into the system.

REFERENCES

(A)

Amoroso, L., 1925. *'Ricerche intorno alla curva dei redditi'*. Annali di Mathematica, Serie IV, Tomo II, 123-159

Andersson, T and B. Andersson, 1992. *'Radar rain forecasts for sewage systems'*. Preprints: 2nd International Symposium on Hydrological Applications of Weather Radar, Hannover, FRG, 7th-10th September.

Atlas, D., K. R Hardy and J. Joss, 1964. *'Radar reflectivities of storms containing spongy hail'*. J. Geophysics Research., **69**, p1955-1961.

(B)

Banks, C. J. et al, 1984. *Communications and data formats. FAAG Report 108.* Meteorological Office, pp112.

Bardsley, W. E., 1983. *'An alternative distribution for describing the instantaneous unit hydrograph'*. J. Hydrol., 62: p375-378.

Battan, L. J., 1973. *Radar observations of atmosphere.* The University of Chicago Press, pp317.

Bedient, Philip B, Wayne C. Huber, 1988. *Hydrology and floodplain analysis.* Addison-Wesley Publishing Co, pp650.

Bittanti, S. and R. Scattonlini, 1982. *'Optimal stochastic control of a liquid-saturated steam heat exchange'*. in: Time series analysis-Theory and practice 2, Editor: O. D. Anderson, North Holland Publishing Co.

Blanchet, F., D. Brunelle and A. Guillon, 1992. *'Influence of the spatial heterogeneity of precipitation upon the hydrologic response of an urban watershed'*. Preprints: 2nd International Symposium on Hydrological Applications of Weather Radar, Hannover, FRG, 7th-10th September.

Blanchet, F., A. Guillon, P. Briat and P. Bourgogne, 1993. *'A reference measurement of areal rainfall allowing for control of radar, raingauge estimates'*. Sixth International Conference on Urban Storm Drainage, Proceedings Vol. I, Edited by Jiri Marsalek and Harry C. Torno, p378-384.

Bolton Metropolitan Borough Council, 1987. *Bradshaw valley study project reports*, pp45

Box. G. E. P. and G. M. Jenkins, 1976. *Time series analysis: Forecasting and control.* HoldenDay, San Francisco, CA, p337-380.

Bras, R. L., 1990. *Hydrology.* Addison-wesley Publ. Co, pp643.

(C)

Cattermole, K. W., 1962. *'Contribution to discussion of Purton (1)'*. Proc. IEE, 109B, p486

Cattermole, K. W., 1969. *Principles of pulse code modulations.* Illiffe Books Ltd., London, pp 125-152

Chatfield, C., 1984. *The analysis of time series: An introduction.* Chapman and Hall, p84-85.

Chen, S. J. and V. P. Sigh, 1986. *'Derivation of a new variable instantaneous unit hydrograph'*. J. Hydrol., 88: p25-42.

Chow, V. T., et. al., 1988. *Applied hydrology.* McGill book Co, pp273.

Cluckie, I. D., 1987. *'Real-time rainfall-runoff models and use of weather radar information'*. In: Weather Radar and Flood Forecasting, Edited by V. K. Collinge and C. Kirby, John Wiley & Sons Ltd, p171

Cluckie, I. D. et. al, 1987. *'Some hydrological aspects of weather radar research in the United Kingdom'*. Hydrological Sciences J., 32, 3, 9, p329.

Cluckie, I. D. et. al, 1989. *'Radar signal quantisation and its influence on rainfall-runoff models'*. In: Hydrological Applications of Weather Radar, Editors, I. D. Cluckie, C. G. Collier, Ellis Horwood Ltd., 1991, p440.

Collier, C. G., P. R. Larke and B. R. May, 1983. '*A weather radar correction procedure for real time estimation of surface rainfall*'. Q. J. R. Meteorol., Soc., **109**, p589-608.

Collier, C. G., 1986. '*Accuracy of real-time radar measurements*'. In: Weather Radar and Flood Forecasting, Edited by V. K. Collinge and C. Kirby, John Wiley & Sons Ltd, p71

Collier, C. G., 1989. *The applications of weather radar systems-A guide to uses of radar data in Meteorology and hydrology.* Ellis Horwood Ltd, p19.

Collinge, V. K. and C. Kirby. 1987. *Weather Radar and Flood Forecasting.* John Wiley & Sons Ltd, pp296.

Collinge, V. K., 1989. '*Weather radar calibration in real time: prospects for improvement*'. In: Hydrological Applications of Weather Radar, Editors, I. D. Cluckie, C. G. Collier, Ellis Horwood Ltd., 1991, p25-42

Council of the European Communities, 1976. *Directive Concerning the Quality of Bathing Water.* (976/160/EEC). Official J. of the European Community No. L31.

Crawford, N. H.and R. K. Lindsay, 1966. *Digital simulation in hydrology Stanford Watershed Model I'V. T.R. 39.* Department of Civil Engineering, Stanford University, Stanford, California.

Crawshaw and Head, 1988. *Fylde Coast bathing water improvements environmental investigations for the design of sea outfalls.* In: Long Seaoutfalls. Thomas Telford, London, p 53-66.

Crozier, C. L., 1986. *King weather radar operations menu and users guide.* Research Report No 1, Toronoto Weather Radar Research Station, King City, Ontario.

(D)

Department of the Environment/National Water Council, 1983. *The Wallingford Procedure.* DOE/NWC Standing Technical Committee Report No.28, Vol. 1 to 5.

Delrieu, G, J. D. Creutin and H. Andrieu, 1989. '*Validation of a short-range X-band radar system for rainfall measurement over an urban area*'. In: Hydrological Applications of Weather Radar, Editors, I. D. Cluckie, C. G. Collier, Ellis Horwood Ltd., 1991, p234.

Ding, J. Y., 1974. '*Variable unit hydrograph*'. J. of Hydrol., 22, p53-69.

Diskin, M. H., 1964. '*A basic study of the linearity of the rainfall runoff process in watersheds*'. Ph.D. Thesis. University of Illinois, Urbana, USA.

Dobson, C., 1993. '*Forecasting flows in the Severn and Trent catchments*'. Minutes of British Hydrological Society (BHS) Rainfall-Runoff Modelling Meeting, 23rd June, 1993.

Dooge, J. C. I., 1959. '*A general theory of the unit hydrograph*'. J. Geophys. Res., 64(2), p241-256.

Dooge, J. C. I., 1973. '*Linear theory of hydrologic systems*'. U.S. Dept. of Agriculture Technical Bulletin No. 1468, p232-260.

Duncan, M., R., A. Bellon, G. L. Austin and I. D.Cluckie, 1991. '*Attenuation effects in C and X-band radar data used for urban hydrology*'. Preprints: 25th conference on radar meteorology, June, 1991, Paris, France, American Meteorological Society, p 326-329.

Duncan, M. R., F. A. Fabry and I. D. Cluckie et. al., 1992. '*McGill/Salford C-band Hydrological Radar*'. Preprints: 2nd International Symposium on Hydrological Applications of Weather Radar, Hannover, FRG, 7th-10th September.

(E)

Edson, C. G., 1951. '*Parameters for relating unit hydrographs to watershed characteristics*'. Trans. A. G. U. August, 1951, Vol. 32, No. 4, p591-596.

English, E. J., 1973. '*An objective method of calculating areal rainfall*'. Meteorol. Mag., London, 103, p 275-288.

Ermolin, Y. A., 1992. *'Operational control of urban sewerage system of Moscow'*. Preprints: 2nd International Symposium on Hydrological Applications of Weather Radar, Hannover, FRG, 7th-10th September.

(F)

Fleming G., 1975. *Computer simulation techniques in hydrology.* Elesevier North-Holland, INC, pp333.

Forshaw, W. and D. Walters, 1990. *Bolton sewerage real time control case study and in-sewer telemetry.* Personal communication.

Franke, R. and G. Neilson. 1980. *'Smooth interpolation of large sets of scattered data'*. Internat. J. Numer. Methods Eng., 15, p1691-1704.

(G)

Galli, G. and J. Joss, 1989. *'Using and adjusting conventional radar reflectivity data for estimation of precipitation: past, present and future studies in Switzerland'*. In: Hydrological Applications of Weather Radar, Editors, I. D. Cluckie, C. G. Collier, Ellis Horwood Ltd., 1991 , p43-48.

Germanopoulos, G, Jowitt, P. W. and J. P. Lumbers, 1986. *'Assessing the reliability of supply and level of service for water distribution systems'*. Proc. Instn. Civ. Engrs, Part 1, 1986, 80, April, p413-428.

Granger, C. W. J. and P. Newbold, 1977. *Forecasting Economic Time series.* New York: Academic press, pp 301.

Gray, D. M., 1961. *'Synthetic unit hydrographs for small drainage areas'*. Proc., ASCE, J. Hyd. div., 87, No. Hy4 (july).

Gray, D. M., 1973. *Hand book on the principles of hydrology.* Port Washington, N. Y.: Water Information Centre, Inc.

Green, M. J., 1989. *'Real-time control for urban drainage systems: advantage or disadvantage'*. In: Hydrological Applications of Weather Radar, Editors, I. D. Cluckie, C. G. Collier, Ellis Horwood Ltd., 1991, p580-589.

Gunn, K. L. S., and T. W. R. East, 1954. *'The microwave properties of precipitation particles'*. Q. J. R. Meteorol. Soc., **80**, p522-545.

(H)

Han, D., 1991. *Weather radar information processing and real time flood forecasting.* Ph. D. Thesis. Water Resources Research Group, University of Salford, U.K., pp278.

Harpin, R., 1982. *Real-time flood routing with particular emphasis on linear methods and recursive estimation techniques.* PhD thesis. School of Civil Engineering, University of Birmingham, U.K, pp367.

Hitschfeld, W. and J. Bordan, 1954. *'Errors in the radar measurement of rainfall at attenuating wavelengths'*. Meteorology, 11, p67-68.

Hitch, T. J. and B. D. Hems, 1987. *'A comparison of radar gauge measurements of rainfall over Wales in October 1987'*. Meteo, Magzine, 117, p276-279.

Holland, J. H., 1992. *Adaptation in natural and artificial systems.* MIT press, Cambridge, Mass, pp211.

Hutchings C and P. Dempsey, 1991. *Fylde Stormwater Management Study.* Final Report, No. UC 1128, WRc, p14-17.

(I)

Isermann, R., 1980. *'Practical aspects of process identification'*. Automatica, J. of IFAC, Vol 16, p575-587.

(J)

Jäke, O. and T. Einfalt, 1992. *'Assessing the use of rainfall forecasts for urban drainage systems with FITASIM'*. Preprints: 2nd International Symposium on Hydrological Applications of Weather Radar, Hannover, FRG, 7th-10th September.

Johnson, N. L. and S. Kotz, 1970. *Continuous uunivariate distributions-1.* Houghton Mifflin Co. Boston, p199.

Jones,, D. M. A., 1956. 'Rainfall drop-size distribution and radar reflectivity'. Research Report, No. 6. Urbana: Meteor. Lab. Illinois State Water Survey.

Joss, J. K., K. Schran, J. C. Thoms and A.Waldvogel, 1970. '*On the quantitative determination of precipitation by radar*'. Wissenschaftclich Mitfeilung No. 63, Eidgenossischen Kommission Sum Studiumder Hagelgibung und der Hagelsher, p38

Joss, J. K.and A. Waldvogel, 1989. '*Precipitation measurement and hydrology - A review*'. Battan Memorial and radar Conf., American Meteorological Society, Boston, MASS.

(K)

Kaneko, H and T. Sekimoto, 1963. '*Logarithmic PCM encoding without diode compandor*'. IEEE Int. Convention Rec. Part 8. p226-281.

Karlinger, M. R., and B. M. Troutman, 1985. '*Assessment of the instantaneous unit hydrograph derived from the theory of topologically random networks*'. Water Resources Res. 21(11): 1693-1702.

Kempthorne, O. and L. Folks, 1971. Probability, statistics and data analysis. The Iowa State University Press, USA, p199-204.

Koopmans, L. H., 1974. The spectral analysis of time series. Academic Press.p266, p314.

(L)

Larson, J., 1990. '*Real time operation and off-line optimisation in the city of Malmo, Sweden*'. Fifth intern. conf. on urban storm drainage, OSAKA, p1249-1552.

Lawrence, D., 1991. *Handbook of genetic algorithms*. Van Nostrand Reinhold, New York, p5.

Lindgren, B. W., 1976. *Statistical theory*. 3rd Edition, Macmillan Publ. Co., Inc., p199.

Lienhard, J. H., 1964. '*A statistical mechanical prediction of the dimensionless unit hydrograph*'. J. Geophys. Res., 69, No. 24, p5231.

Lienhard, J. H. and P. L. Meyer, 1967. '*A physical basis for the generalised gamma distribution*'. Quarterly of Applied Mathematics, 25, p330-334.

(M)

Maddaus, W. O., and P. E. Eagleson, 1969. '*A distributed linear representation of surface runoff*'. Hydrodynamics Lab. Rept. No. 115, Dept. of Civil Eng. MIT, Cambridge, Massachusetts, June.

Mandeville A.N., P. E. O' Connel, J.V. Sutcliffe and J. E. Nash, 1970. '*River flow forecasting through conceptual models, Part III-The Ray catchment at Grendon Underwood*'. J. Hydrol., 11, p109.

Marshall, J. S. and W. Mck. Palmer, 1948. '*The distribution of raindrops with size*'. J. of Meteorology, 5, p165-166.

Marshall, J. S., and W. Hitschfield, 1953. '*Interpretation of the fluctuating echo from randomly distributed scatters. Part I*'. Canadian J. Phys. 31, p962-994.

Marshall, J. S., 1957. '*The constant-altitude presentation of radar meteorology*'. J. of Applied Meteorology. Vol. 8. February, p171-172.

McCallister, J. P. and J. L. Teague, 1968. '*Radar requirements for operational hydraulic analysis*'. Proc. Radar Meteorol. Conference 13th. Boston, USA, p416-421.

(N)

Nash, J. E., 1957. '*The form of the instantaneous Unit Hydrograph*'. In: General Assembly of Toronto, 3-14 Sept. Publication No 45.Volume III, p114-121. IASH.

Nash, J.E., and J.V. Sutcliffe, 1970. '*River flow forecasting through conceptual models, Part I-a discussion of principles*'. J. Hydrol., 10, p282-290.

Natural Environment Research Council, 1975, *The flood study report. Five volumes*. London.

New Scientist, 12 June 1993, p11.

Norreys, R., 1991. *Water quality river impact model*. PhD. Thesis. Water Resources Research Group, University of Salford, U.K, pp300.

North West Weather Radar Project, 1985. *Consortium Report*, pp73

Novotny, V., A. Capodaglio and H. Jones, 1992. '*Real time control of wastewater treatment operations*'. Wat. Sci. Tech. Vol. 25, No. 4-5, p89-101.

(O)

Osbourne, H. B. and K. G. Renard, 1969. '*Analysis of two major run-off producing south-west thunderstorms*'. J. of Hydrology, 8, pp 282-302.

O'Connel, P. E., J. E., Nash, and J. P. Farrell, 1970. '*River flow forecasting through conceptual models, Part II-The Brosna catchment at Ferbane*', J. of Hydrol., 10, p317-329.

O'Donnell, T., 1983. '*Deterministic catchment modelling*', Int. Post-graduate course in real-time river flow forecasting. Foundation for Post-graduate courses. Agricultural University, Wageningen. The Netherlands.

Orman, N. R., 1991. *Fylde Stormwater Management Study: review of sewer modelling*. Report No. UC1194. WRc, p22-24.

(P)

Papageorgiou, M., 1983. '*Automatic control strategies for combined sewer systems*'. J. of Environmental Eng., Vol. 109, No. 6, p1385-1402.

Pilgrim, D. H., 1977,. '*Isochrones of travel time and distribution of flood storage from a tracer study on a small watershed*'. Water Resources Res. 13(3), p587-595.

Powell, S. M., 1985. *River basin models for operational forecasting of flow in realtime*. PhD thesis. School of Civil Engineering, University of Birmingham, U.K, p92-100.

Powell, S. M. and I. D. Cluckie, 1985. *'On the sampling interval of discrete transfer function models of the rainfall-runoff process'.* 7th IFAC/IFORS Symposium on identification and System Parameter Estimation, York, U.K., July, p1119-1124.

(R)

Reed, D. W., 1984. *A review of British flood forecasting practice.* Report No 90. August. Institute of Hydrology, U.K.

Rosenbrock, H. H., 1960. 'An automatic method for finding the greatest or least value of a function'. The Computer Journal, Vol. 3, p175-184.

Ruck, G. T. et. al., 1970. *Radar cross section hand book.* Plenum Press, New Yrok, pp472 pp

(S)

Sarino and S. E. Serrano, 1990. *'Development of the instantaneous unit-hydrograph using stochastic differential-equations'.* Stochastic hydrol. and Hydraulics, Vol 2/4, p151-160.

Schwarts, M., 1980. *Information transmission, modulation, and noise, a unified approach to communication systems, third edition.* McGraw-Hill Book Company, p108-128.

Semke, M., 1989. *'From radar rainfall data to hydrological data'.* Hydrological Applications of Weather Radar, Editors, I. D. Cluckie, C. G. Collier, Ellis Horwood Ltd., 1991, p509-518.

Shaw, E. M., 1983. *Hydrology in Practice.* Van Nostrand Reinhold (UK) Co. Ltd, p349.

Shaw, E. M., 1988. *Hydrology in practice.* Second edition, Van Nostrand Reinhold (International).

Shearman, R. J. and P. M. Salter, 1975. *'An objective rainfall interpolation and mapping technique'.* Hydrol. Bulletin, XX, 39, p353-363.

Shepherd, D., 1968. '*A two-dimensional interpolation function for irregularly spaced data*'. Proc. 23rd Nat. Conf. ACM, Brandon/systems press Inc., Princeton, p517-523.

Shepherd, G. W., 1987. *On the utilisation of weather radar in the simulation of Urban Drainage Networks*. PhD thesis. School of Civil Engineering, University of Birmingham, U.K., pp238.

Sherman, L. K., 1932. *Stream flow from rainfall by a unit hydrograph method*, Eng. News Record, 108, p501-505.

Shilling, W., 1985. '*A survey on real time control of combined sewer systems in the United States and Canada*'. Proceeding of the 4th IAWRRC workshop Houston, Denver, USA, p595-600.

Shilling, W.and M. Semeke, 1985. '*Combined sewer system control in real time-Bremen, West Germany*'. Proceeding of the 4th IAWRRC workshop. Houston, Denver, USA, p183-189.

Shilling, W., 1987. '*Real time control of urban drainage systems-the state-of-the art*'. IAWPRC/IAHR joint committee.

Smith, B., 1957. 'Instantaneous companding of quantised signals'. BSTJ, 36, p653.

Smith, B. D., 1953. 'Coding by feedback methods'. Proc. IRE, 41, p1053-1058.

Smith, C. J., 1986. '*The reduction of errors caused by the bright-bands in quantitative rainfall measurements made using radar*'. J. of Atmospheric and Oceanic Tech. Vol. 3, p 129-131.

Snyder, F. F., 1938. '*Synthetic unit-graphs*', Trans. AGU, 19, p447-454

Snyder, W. M., W. C. Mills, and J. C. Stephens, 1970. '*A method of derivation of nonconstant watershed response functions*', WRR, 6, p261-274.

Stacy, E. W., 1962. '*A generalisation of the gamma distribution*', Annals of Mathematical Statistics, 33, p1187-1192.

(T)

Tilford, K. A., 1992. *Weather radar for operational Hydrology.* PhD thesis. Department of Civil Engineering, University of Salford.

Trodda, P. D., J. W. Labadie and N. S. Grigg, 1977. *'Automatic control strategies for urban stormwater'*. J. of the Hydraulic Division, December, 1977, p1443-1459.

(U)

Ulaby, F. T. and R. K. Moore and A. K. Fung, 1981. *Microwave remote sensing.* In 3 Volumes, Addition-Wesley Publ., Reading, Mass, pp2162

(V)

Vaye, I. N., 1985. *Time series rainfall.* MSc Thesis. School of Civil Engineering, University of Birmingham, U.K.

Verworn, H. R., 1989. *'Hydrological relevance of radar rainfall data'*. In: Hydrological Applications of Weather Radar, Editors, I. D. Cluckie, C. G. Collier, Ellis Horwood Ltd., 1991, p531-540.

(W)

Walker, S., P. W. Jowitt and A. H. Bunch, 1993. *'Development of a decision support system for drought management within North West Water'*. J. of the Institution of Water and Environmental Management, &, June, p295-303.

Wallace, P. R., 1953. *'Interpretation of the fluctuating echo from randomly distributed scatters. Part II'*, Canadian J. Phys. 31, p995-1009.

Water & Environment, July/August 1993, p8.

Weibull, W., 1939. *The phenomenon of rupture in solids.* Ingenior Vetenskaps Akademiens Handlingar, **153**, 2.

Wheater, H. S., 1993. *'What use are models?'* Minutes of BHS Rainfall-runoff Modelling Meeting, 23rd June, 1993.

Ward, R. C. and M. Robinson, 1990. *Principles of hydrology,* 3rd edition. McGill Book Co.(UK) Ltd, p286-289.

Weyand, M. and M. Dolimann, 1990. *'Experience and results of real time control within a combined sewer system'*. Fifth Intern. Conf. on urban storm drainage, 1990, OSAKA, p1237-1242.

(Y)

Yuan, J. and I. D. Cluckie, 1992. *A Comparative Study of Radar resolutions and quantisation Levels in the Context of Urban Hydrology.* North West Urban Radar Project: Report No.3, pp70.

Yuan, J. and I. D. Cluckie, 1993. *Control strategies for urban combined drainage systems'*. North West Urban Radar Project: Report No.3, pp70.

APPENDIX-I

WEIBULL PROCESS AND THE RELATED DISTRIBUTIONS

The Weibull process is named after Waloddi Weibull, a Swedish physicist, who developed the theory during the study of the breaking strength of materials (Weibull, 1939), in which the following postulates are assumed to hold:

- The probability of one failure in a small time interval (t, t+dt) is: $(\alpha t^{\alpha-1}/\tau) + O(dt)$;
- The probability of more than one failure in the time interval (t, t+dt) is negligible;
- The failure in an interval is independent of the occurrence in any other interval;
- The probability of no failure in the time interval (t, t+dt) is $1-(\alpha t^{\alpha-1}/\tau)-O(dt)$.

Where the notation that p(dt) is $O(dt)$ means the limit of p(dt)/dt as $dt \rightarrow 0$ is 0. The first three postulates can be interpreted as that the occurrence probability of a failure only depends on the length of the time interval and is the same for any set of observations.

I.1. The Generalised Weibull PDF

Under the Weibull postulates, the probability of *n* failures over the period (0, t) can be expressed as:

$$P_n(t) = \frac{t^{\alpha n}}{\tau^n \Gamma(n+1)} e^{-t^\alpha/\tau} \quad ; \qquad t \geq 0 \tag{A.1}$$

Where n (>0), τ (>0) and α (>0) are statistical constants and

$$\Gamma(n+1) = n(n-1)(n-2)\cdots 1 = n!$$

Suppose that the Weibull Process is observed at the times $T_0, T_1, T_2, \cdots T_n$, i.e. arrival times at which the failures occur and $T_0 < T_1 < T_2 < \cdots T_n$, where T_n is a random variable and is equal to the sum of the exponential variables measuring the time to the first failure from the origin, to the second failure from the first, and so forth. The probability of T_n over the period (0, t) is given by:

$$\begin{aligned} P_{T_n}(t) &= \text{Probability}(T_n \leq t) \\ &= 1 - \sum_{j=0}^{n-1} \frac{t^{\alpha j}}{\tau^j \Gamma(j+1)} e^{-t^\alpha/\tau} \end{aligned} \tag{A.2}$$

Thus the PDF of T_n is given by differentiating Eq.(A.2):

$$\begin{aligned} p(t) = \frac{dP_{T_n}(t)}{dt} &= -\sum_{j=0}^{n-1} \frac{\alpha j t^{\alpha j-1}}{\tau^j \Gamma(j+1)} e^{-t^\alpha/\tau} + \sum_{j=0}^{n-1} \frac{\alpha t^{\alpha j+\alpha-1}}{\tau^{j+1} \Gamma(j+1)} e^{-t^\alpha/\tau} \\ &= \frac{\alpha t^{\alpha n-1}}{\tau^n \Gamma(n)} e^{-t^\alpha/\tau} \end{aligned} \tag{A.3}$$

where $p(\bullet)$ is the PDF of T_n, and n (>0), τ (>0) and α (>0) are parameters. This PDF was defined by Stacy (1962) as the generalised Gamma distribution while he was working in the IBM development laboratory. Unfortunately, the definition is misleading because Gamma distribution describes the Poisson Process whereas Eq.(A.3) is derived under the Weibull postulates. Therefore, a proper name should be given as the generalised Weibull (GW) PDF since a proper name is vital to the accurate

description of the properties of the process. This PDF was first discussed as early as 1925 by Amoroso, who fitted such a distribution to an observed distribution of income rates. Later in 1967, Lienhard and Meyer found the distribution can be derived from a physical model and the distinguishable ways that the event can occur in the interval from t_i to t_{i+1} is physically proportional to t^{n-1}. For further information about the development of the GW PDF the reader may find from Johnson and Kotz (1970).

A number of very popular PDFs can be obtained as special cases of the GW PDF by making certain choices for the parameters, see Table I.1.

Table I.1 The special cases of the GW PDF

PARAMETER			PDF
n	τ	α	
1	τ	α	Weibull
n	τ	1	Gamma
1	τ	2	Rayleigh
3/2	τ	2	Maxwell molecular speed
1/2	τ	2	Maxwell molecular velocity (Normal PDF)
N/2	1/2	1	Chi-square, (N=1, 2, 3...)
1	τ	1	Exponential

It is easy to show that the mean of the GW PDF is:

$$E[t]=\int_0^\infty tp(t)dt=\tau^{1/\alpha}\frac{\Gamma(n+1/\alpha)}{\Gamma(n)}; \tag{A.4}$$

the variance is:

$$(D[t])^2=\int_0^\infty (t-E[t])^2 p(t)dt=\tau^{2/\alpha}\left[\frac{\Gamma(n+2/\alpha)}{\Gamma(n)}-\frac{\Gamma^2(n+1/\alpha)}{\Gamma^2(n)}\right]; \tag{A.5}$$

and the Λth moment around the origin is

$$\sigma_t^{\Lambda}=\int_0^{\infty} t^{\Lambda} p(t)dt=\tau^{\Lambda/\alpha}\frac{\Gamma(n+\Lambda/\alpha)}{\Gamma(n)} \qquad (A.6)$$

Replacing the random variable, *t*, in Eq.(A.3) by the rainfall intensity, R, the GW PDF can be used to satisfactorily portray the distribution of rainfall intensities. The parameters for example for the Northwest England region were identified as: $n = 2$, $\tau = 1.05$ and $\alpha = 1/2$. Therefore, the mean rainfall intensity was about 7.0 mm/h, and the variance was approximately 102.0 $(mm/h)^2$. That the occurrence of rainfall intensity appeared to follow the Weibull Process deviates from the traditional point of view in which rainfall intensity is believed to be better described by the Poisson Process. The GW PDF is suitable where the conditions of 'strict randomness' of the exponential distribution are not satisfied.

I.2 The PDF of Radar Reflectivity

In addition, knowing the relationship between rainfall intensity R and radar reflectivity Z:

$$Z = aR^b, \text{ or} \qquad (A.7)$$

$$Z_{dB}=10\log_{10}(aR^b) \qquad (A.8)$$

the PDF of radar reflectivity Z (mm^6/m^3) and Z_{dB} can be derived, where *a* and *b* are constants.

$$\text{Since } \int_0^{\infty} p(R)dR = \int_0^{\infty} \frac{\alpha R^{\alpha n-1}}{\tau^n \Gamma(n)} e^{-R^{\alpha}/\tau}\, dR = 1 \qquad (A.9)$$

By substitution of Eq.(A.7) into Eq.(A.9), we obtain:

$$\int_0^{\infty} \frac{\alpha (Z/a)^{(\alpha n-1)/b}}{\tau^n \Gamma(n)} e^{-\frac{(Z/a)^{\alpha/b}}{\tau}} d(Z/a)^{1/b} = 1 \tag{A.10}$$

which is equivalent to

$$\int_0^{\infty} \frac{\alpha (Z/a)^{\alpha n/b-1}}{ab\tau^n \Gamma(n)} e^{-\frac{(Z/a)^{\alpha/b}}{\tau}} dZ = 1 \tag{A.11}$$

Let $\alpha/b = \alpha'$ and $\tau a^{\alpha'} = \tau'$, Eq.(A.11) can be simplified into:

$$\int_0^{\infty} \frac{\alpha' Z^{\alpha' n-1}}{\tau'^n \Gamma(n)} e^{-Z^{\alpha'}/\tau'} dZ = 1 \tag{A.12}$$

Thus the PDF of radar reflectivity Z (mm^6/m^3) is

$$p(Z) = \frac{\alpha' Z^{\alpha' n-1}}{\tau'^n \Gamma(n)} e^{-Z^{\alpha'}/\tau'} \tag{A.13}$$

which is also a special case of the GW PDF. The apostrophe can be dropped without confusing α' with α and τ' with τ for the sake of neatness.

Since $Z = C'r^2 \overline{P}_r$ (see Chapter 2), where C' is a constant, the GW PDF can also be used to describe the distribution of the mean returned power $\overline{P}_r$ for any given radar range, *r*. As to the returned power P_r, Marshall and Hitschfeld (1953), and Wallace (1953) showed that the P_r is exponentially distributed which is one of the special cases of the GW PDF.

Similarly, by substitution of Eq.(A.8) into Eq.(A.9) the distribution of Z_{dB} can also be derived, which has a form of the generalised extreme value distribution:

$$p(Z_{dB}) = \frac{\alpha''}{\tau''^{n}\Gamma(n)} e^{x}, \quad \text{where } x = \alpha'' n Z_{dB} - \frac{1}{\tau''} e^{\alpha'' Z_{dB}} \tag{A.14}$$

It is easy to infer that this PDF can also be used to describe the distribution of the radar received mean power $\overline{P}_r$ in dB.

The above generalised PDFs are very useful for the statistical analysis of the meteorological, hydrological data and the other problems such as the reliability of supply and level of service for water distribution systems (Germanopoulos, Jowitt and Lumbers, 1986).

I.3 Summary

GW PDF can be used to represent the frequency distribution of rainfall intensities and radar received signals. It is suitable for use when the conditions that 'strict randomness' of the exponential distribution are not satisfied.

APPENDIX-II

DYNAMIC LINEAR RESERVOIR

Since Sherman (1932) developed the Unit Hydrograph (UH) theory and Edson (1951) derived the form of the Well-known Nash model (Nash, 1957), many conceptual linear Pulse Response (PR) functions (or Instantaneous Unit Hydrographs) have been suggested, for example, by Dooge (1959), Gray (1961, 1973), Diskin (1964), Lienhard (1964), W. O. Maddaus and P. E. Eagleston (1969), Bardsley (1983), Karlinger and Troutman (1985) and Sarino and Serrano (1990). These PRs can be broadly classified into two categories: 1) static and 2) dynamic.

As any rainfall-runoff system is essentially heterogeneous, nonlinear and dynamic, in order to accurately model the system there are three fundamental problems which need to be successfully dealt with: 1) spatial homogeneity, 2) system linearity, and 3) temporal variability. To simultaneously tackle these problems is difficult. Often a rainfall-runoff system is treated as an average or lumped linear system. Such a treatment is practically justifiable, especially when the system has been decomposed into a number of smaller and relatively homogeneous subsystems or 'grids'. The assumption that a rainfall-runoff system is linear is probably never quite true, however, it supplies a useful approximation of the actual systems. Though several nonlinear PRs have been proposed such as by Ding (1974) and Chen, et, al. (1986), the models have not gained popularity, possibly due to the involved computation complexity.

Assuming that a rainfall-runoff system behaves like a spatially homogeneous but temporally varying linear reservoir which is called dynamic linear reservoir, a number of typical PRs of the system can be derived.

II.1 Dynamic Linear Reservoir (DLR)

A dynamic linear reservoir is characterised by a time-variant storage factor. It can be defined as (see Chapter 5):

$$\begin{cases} A_1(t)\dfrac{dQ}{dt} + Q = \eta R \\ Q(t)\big|_{t=0} = 0 \end{cases} \tag{II.1}$$

Where R is the gross input, Q is the output of the reservoir and η is the percentage runoff factor. Note, $A_1(t)$ is the dynamic storage factor (>0), which is a function of time. For a constant input, R, the solution of Eq.(II.1) is:

$$Q(t)=\eta R - C_0 e^{-u}, \qquad u=\int_0^t A_1^{-1}(t)dt \tag{II.2}$$

This is the discharge from the DLR under a consistent input R, which will gradually increases with time and eventually reach an equilibrium state: ηR, where C_0 is an integration constant. For a unit pulse input which terminates immediately after being applied, the PR of the DLR represented by Eq.(II.2) is:

$$H(t) = C_1 A_1^{-1}(t)e^{-u}, \qquad u = \int_0^t A_1^{-1}(t)dt \tag{II.3}$$

By differentiating this equation, a general definition of the PR of the DLR can be given as

$$\begin{cases} \dfrac{1}{H}\dfrac{dH}{dt} = -A_1^{-1}\left(\dfrac{dA_1}{dt}+1\right) \\ H(t) \quad \geq 0 \\ \int_0^{\infty} H(t)dt = \eta \end{cases} \tag{II.4}$$

To obtain a solution for the PR, H(t), an explicit expression of $A_1(t)$ is required. In chapter 5, a conceptual definition has been given to $A_1(t)$, and has been proved as valid. However, the definition should not be unique because there are at least 6 possible ways that A_1 may vary with time, see Figure II.1:

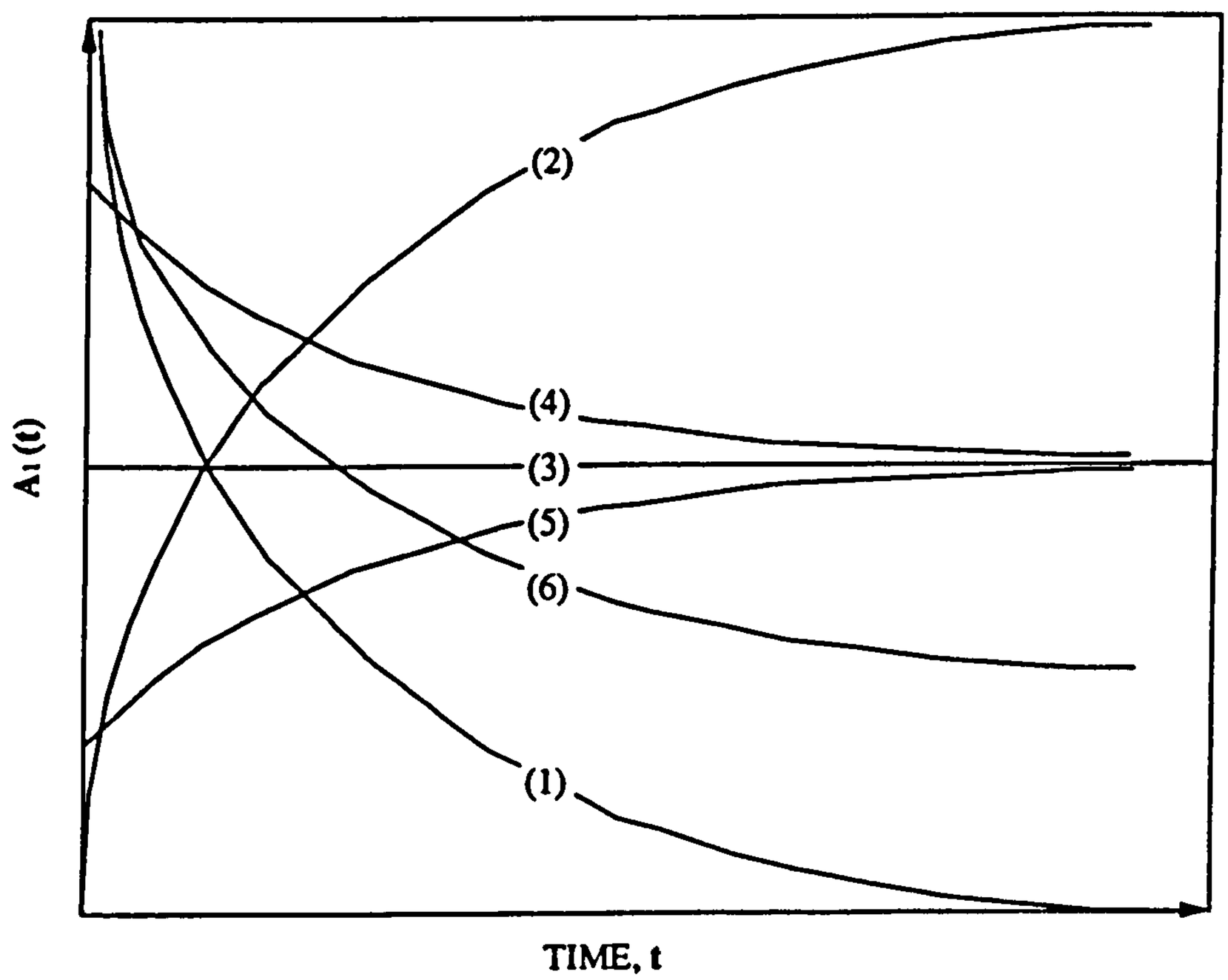

Fig.II.1 The possible variations of $A_1(t)$ with time

(1) Decreases from infinity towards zero;

(2) Increases from zero towards infinity;

(3) Stays constant;

(4) Decreases from a positive value towards another positive value;

(5) Increases from a positive value towards another positive value and

(6) Decreases from infinity towards a positive value.

Therefore, a more general definition may be given as:

$$A_1(t) = \tau_0 + \tau_1 t^{1-\alpha} + \tau_2 e^{-\beta t} + \tau_3 (1 - e^{-\theta t})^{-1} \tag{II.5}$$

Where τ_0, τ_1, τ_2 and τ_3, are the static storage factors and, α, β and θ are the stability factors (see Chapter 5) which are dimensionless and positive. A dynamic storage factor is an index of the system's impedance and is a function of the roughness factor, wetness factor, evaporation factor, soil permeability, the drainage channel geometrical characteristics (i.e. length, shape and area) and the hydraulic gradient.

By substitution of Eq.(II.5) into Eq.(II.4) the general PR of the DLR becomes,

$$\begin{cases} \dfrac{1}{H(t)}\dfrac{dH}{dt} = -\dfrac{\tau_1(1-\alpha)t^{-\alpha} - \tau_2\beta e^{-\beta t} - \tau_3\theta(1-e^{-\theta t})^{-2}e^{-\theta t} + 1}{\tau_0 + \tau_1 t^{1-\alpha} + \tau_2 e^{-\beta t} + \tau_3(1-e^{-\theta t})^{-1}} \\ H(t) \quad \geq 0 \\ \int_0^{\infty} H(t)dt = \eta \end{cases} \tag{II.6}$$

The shape of the PR function depends on the parameter values, τ_0, τ_1, τ_2, τ_3, α , β and θ. To find a general solution of Eq.(II.6) is difficult. However, if $\tau_1 = \tau_2 = \tau_3 = 0$, then $A_1(t) = \tau_0$ (>0) and Eq.(II.6) becomes

$$\begin{cases} \dfrac{1}{H(t)}\dfrac{dH}{dt} = -\dfrac{1}{\tau_0} \\ H(t) \quad \geq 0 \\ \int_0^{\infty} H(t)dt = \eta \end{cases} \tag{II.7}$$

Because $A_1(t)$ is a constant in this case, Eq.(II.7) defines a static linear reservoir which has the storage characteristic $S = \tau_0 Q$, where S is the storage (volume) of the reservoir. The solution of Eq.(II.7) is:

$$H(t)=\frac{\eta}{\tau_0}e^{-t/\tau_0} \tag{II.8}$$

This is the PR-A which has been described in Chapter 5. Recall the generalised Nash-model (i.e. PR-B):

$$h(t)=\frac{\eta t^{n-1}}{\tau_0^n\Gamma(n)}e^{-t/\tau_0} \tag{II.9}$$

It can be seen that the relationship between H(t) and h(t) is

$$h(t)=\frac{t^{n-1}}{\tau^{n-1}\Gamma(n)}H(t) \tag{II.10}$$

This relation is very useful for derivation of h(t) from H(t), where t and τ is respectively the numerator and denominator of the power of e^{-1} in the H(t).

II.2 Typical PRs of the DLR

Type-1: $\tau_0=\tau_2=\tau_3=0$. From Eq.(II.5) and Eq.(II.6), we have

$A_1(t)=\tau_1 t^{1-\alpha}$ and

$$\begin{cases}\dfrac{1}{H(t)}\dfrac{dH}{dt}=-\dfrac{\tau_1(1-\alpha)t^{-\alpha}+1}{\tau_1 t^{1-\alpha}}\\ H(t)\quad\geq 0\\ \displaystyle\int_0^{\infty}H(t)dt=\eta\end{cases} \tag{II.11}$$

Where $\tau_1>0$. This DLR has already been discussed in Chapter 5. Its PR is the PR-C. The variation range of the dynamic storage factor is from 0 to $+\infty$ or from $+\infty$ to 0. This means that, during a rainfall-runoff event, the dynamic system will transit from

one of the two extreme states to another: 1) zero impedance and 2) infinite impedance. To effectively model the systems that are dynamic within a finite range other than $[0,+\infty)$, an additional parameter need to be used:

Type-2: $\tau_1=\tau_3=0$. The dynamic storage factor and PR definition is respectively:

$$A_1(t)=\tau_0+\tau_2 e^{-\beta t} \text{ and}$$

$$\begin{cases} \dfrac{1}{H(t)}\dfrac{dH}{dt}=-\dfrac{-\tau_2\beta e^{-\beta t}+1}{\tau_0+\tau_2 e^{-\beta t}} \\ H(t) \quad \geq 0 \\ \int_0^{\infty} H(t)dt=\eta \end{cases} \tag{II.12}$$

To ensure $A_1(t)>0$, τ_0 and τ_2 should satisfy $\tau_0>0$ and $\tau_0>|\tau_2|$. The characteristics of $A_1(t)$ varying with time for different β values are shown in Figure II.2, which indicates that the dynamic storage factor either exponentially attenuates from $\tau_0+|\tau_2|$ towards the asymptote $A_1(t)=\tau_0$ when $\tau_2>0$, or rises exponentially from $\tau_0-|\tau_2|$ towards the same asymptote when $\tau_2<0$. This means, unlike the first type dynamic system, this system has a bounded dynamic range. It starts from a state defined by $\tau_0+|\tau_2|$ or $\tau_0-|\tau_2|$ and progressively settles down to a stabilised state defined by τ_0. It can be used to model the progressive increase in the discharging speed when $\tau_2>0$, or the opposite when $\tau_2<0$.

Let $u=e^{-\beta t}$, the solution of Eq.(II.12) can be found as

$$H(t)=\frac{\eta}{\tau_0+\tau_2 e^{-\beta t}} e^{-\frac{1}{\tau_0\beta}\ln\frac{\tau_0 e^{\beta t}+\tau_2}{\tau_0+\tau_2}} \tag{II.13}$$

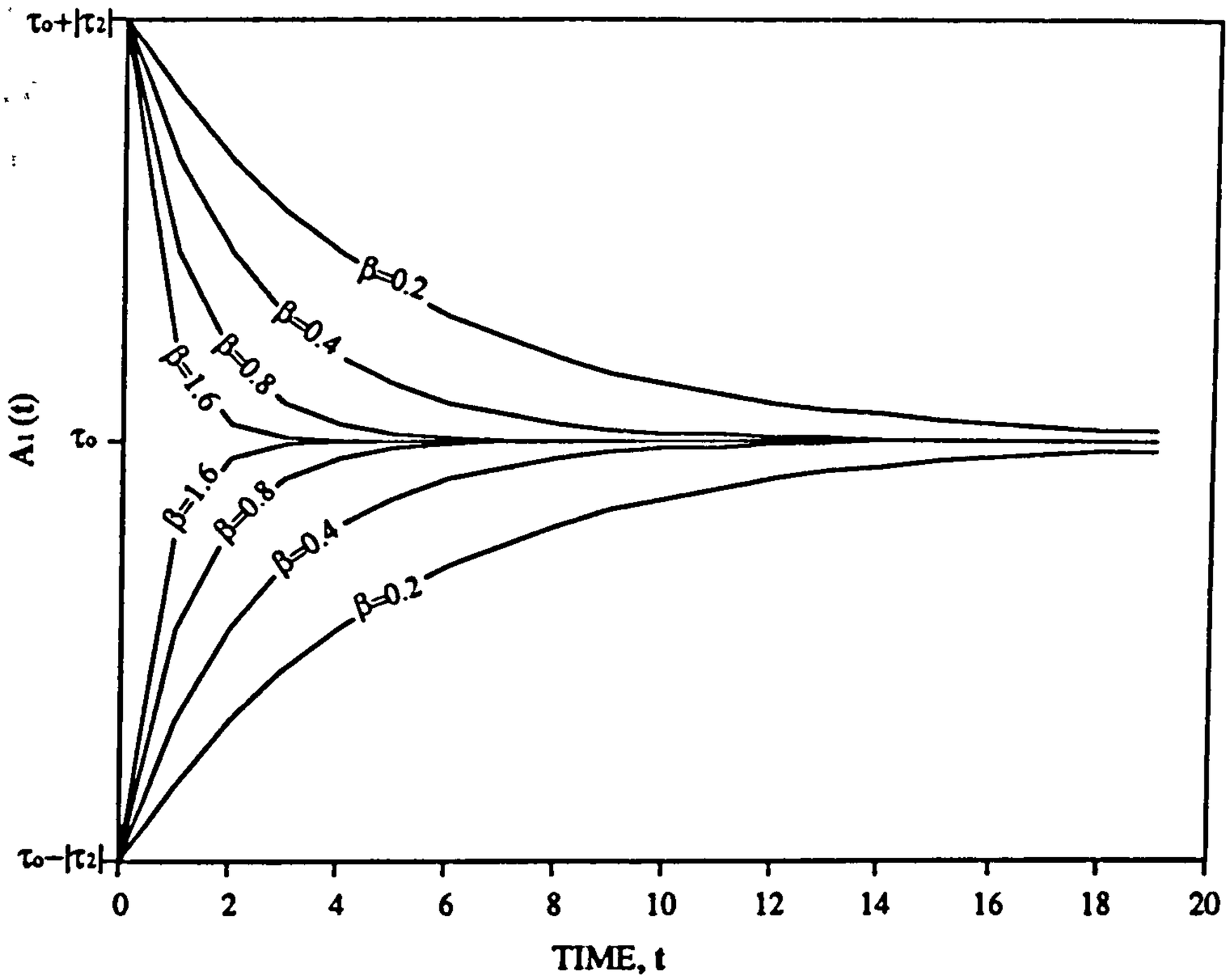

Fig.II.2 The variation of $A_1(t)$ of the Type-2 PR with time for different β values

It is analogue to a PDF when η=1. Replacing t in Eq.(II.10) by $\ln[(\tau_0 e^{\beta t}+\tau_2)/(\tau_0+\tau_2)]$ and τ by $(\beta\tau_0)$, the PR for the cascaded n-reservoir system can be derived using the h(t)~H(t) relation:

$$h(t)=\frac{t^{n-1}}{\tau^{n-1}\Gamma(n)}H(t)$$

$$=\frac{\eta}{(\tau_0\beta)^{n-1}\Gamma(n)}\frac{1}{\tau_0+\tau_2 e^{-\beta t}}\left[\ln\frac{\tau_0 e^{\beta t}+\tau_2}{\tau_0+\tau_2}\right]^{n-1} e^{-\frac{1}{\tau_0\beta}\ln\frac{\tau_0 e^{\beta t}+\tau_2}{\tau_0+\tau_2}} \qquad \text{(II.14)}$$

It can be simplified into:

$$h(t)=\frac{\eta}{\Gamma(n)}\left[\frac{\ln u}{\tau_0\beta}\right]^{n-1}\frac{u^{-\frac{1}{\tau_0\beta}}}{\tau_0+\tau_2 e^{-\beta t}},\quad \text{where}\quad u=\frac{\tau_0 e^{\beta t}+\tau_2}{\tau_0+\tau_2} \qquad \text{(II.15)}$$

It is also analogue to a PDF when η is equal to 1. There are five parameters, η, n, τ_0,

τ_2 and β in this model. To demonstrate the performances of the Type-1 and Type-2 PRs, a comparison was made with the well-known Nash-model in fitting a given PR. The result is shown in Figure II.3.

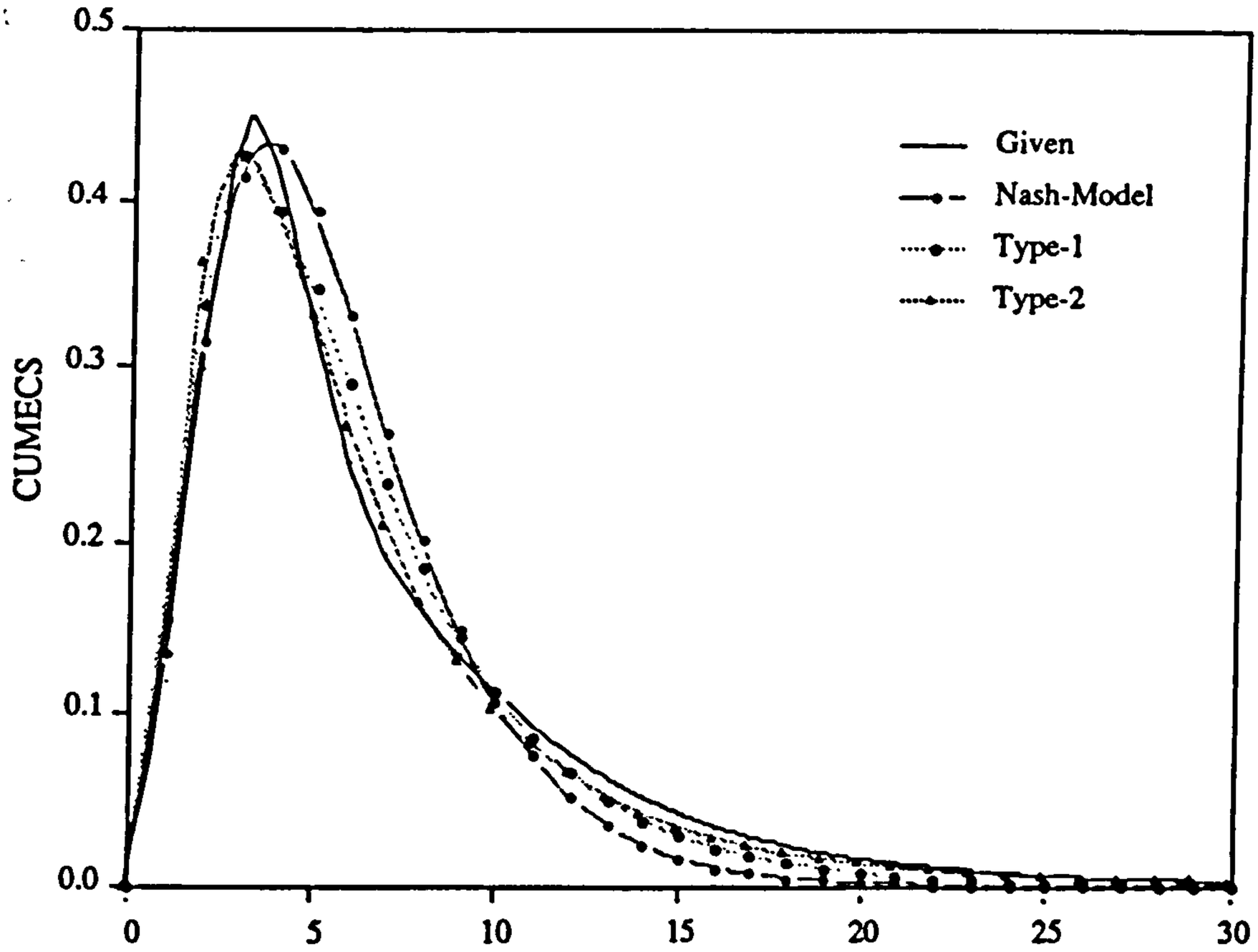

Fig. II.3 Performance of the Nash model, Type-1 and Type-2 PRs in fitting a given PR

The result indicates that, if listed in an order as Nash-model, Type-1 (i.e. PR-C) and Type-2 PRs, an increasing accuracy has been obtained in fitting the given PR which was highly peaked and slowly tailed.

Between the Type-1 and Type-2 PRs there exists another transition type:

Type-3: $\tau_0=\tau_1=\tau_2=0$. The dynamic storage factor and PR definition is respectively:

$A_1(t) = \tau_3(1-e^{-\theta t})^{-1}$ and

$$\begin{cases} \dfrac{1}{H(t)}\dfrac{dH}{dt} = -\dfrac{-\tau_3\theta(1-e^{-\theta t})^{-2}e^{-\theta t}+1}{\tau_3(1-e^{-\theta t})^{-1}} \\ H(t) \quad \geq 0 \\ \int_0^{\infty} H(t)dt = \eta \end{cases} \tag{II.16}$$

Where $\tau_3 > 0$. The variation of $A_1(t)$ with time for different θ values is shown in Figure II.4.

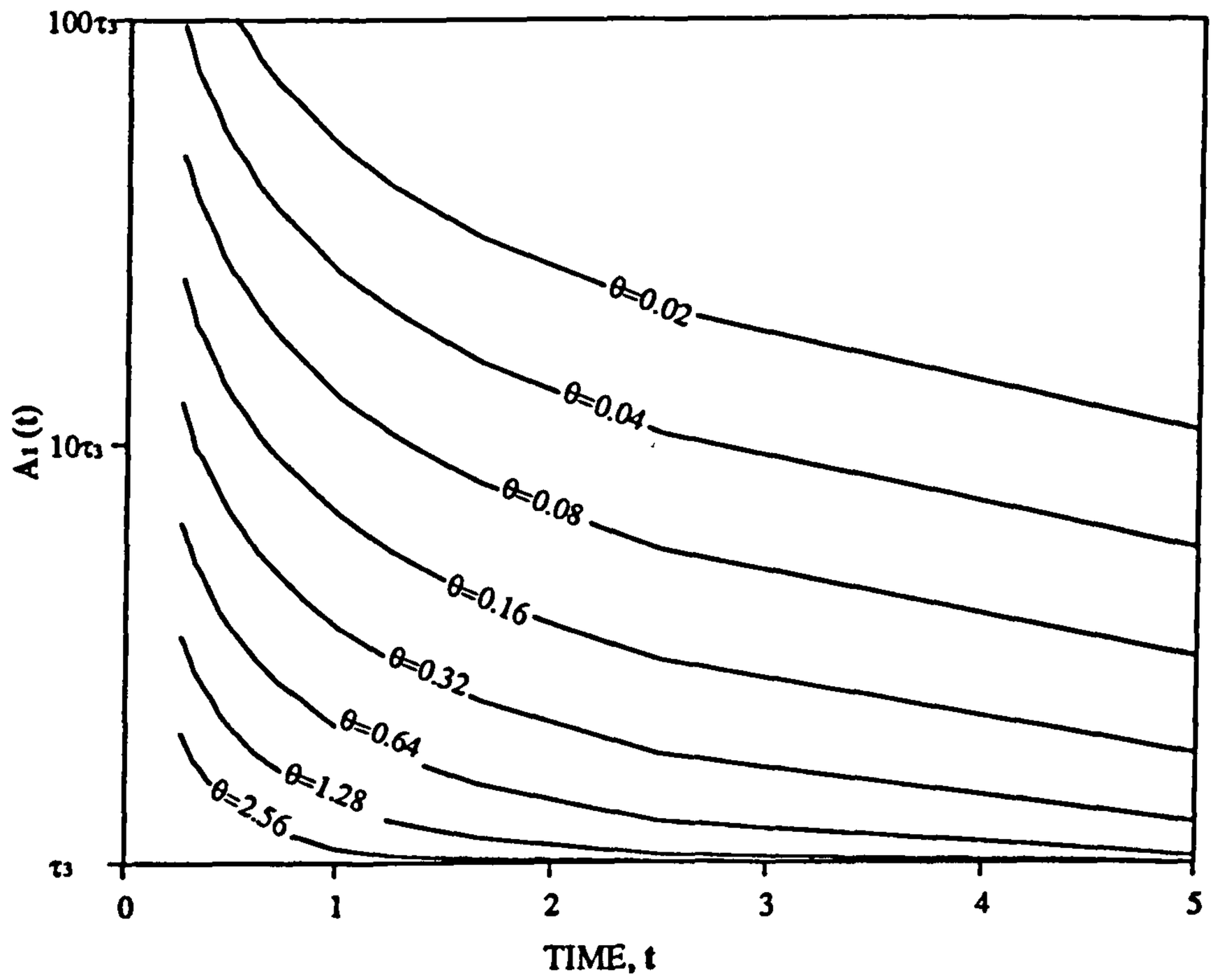

Fig.II.4 The variation of $A_1(t)$ of the Type-3 PR with time for different θ values

It is seen in the figure that the static storage factor is the asymptote of the dynamic storage factor. The speed that $A_1(t)$ approaches to τ_3 and hence the dynamic reservoir approaches to the static reservoir, is governed by the parameter θ. This model can be used to model a system which transits from dry to wet or coarse to smooth during an storm event. It is similar to the second type DLR when τ_2 is positive and approaches to infinity, and the difference between this type of DLR and the first type is that the

lower bound of its $A_1(t)$ is τ_3 (>0) rather than 0. The solution of Eq.(II.16) is:

$$H(t)=\frac{\eta}{\tau_3}(1-e^{-\theta t})e^{-\frac{1}{\tau_3}(t+\frac{1}{\theta}e^{-\theta t}-\frac{1}{\theta})} \tag{II.17}$$

The time-to-peak of this PR is at

$$t_p=\frac{1}{\theta}\ln\frac{2}{2+\theta\tau_3-\sqrt{(2+\theta\tau_3)^2-4}} \tag{II.18}$$

Clearly, t_p is more sensitive to the parameter θ than to τ_3. This is a very useful property. The PR can be effectively shaped by adjusting the parameter τ_3 alone while the time-to-peak position may be kept without being significantly altered.

Taking t in Eq.(II.10) as $t+(1/\theta)e^{-\theta t}-1/\theta$, and τ as τ_3, the PR of the cascaded n-reservoir system can be obtained as:

$$\begin{aligned} h(t)&=\frac{t^{n-1}}{\tau^{n-1}\Gamma(n)}H(t)\\ &=\frac{\eta u^{n-1}}{\tau_3^n\Gamma(n)}(1-e^{-\theta t})e^{-u/\tau_3}, \qquad u=t+\frac{1}{\theta}e^{-\theta t}-\frac{1}{\theta} \end{aligned} \tag{II.19}$$

This model has different characteristics from both of the first two types. It has four parameters, η, n, τ_3 and θ, however, a pure time lag may be also included.

The characteristics of the Type-2 and Type-3 n-reservoir PRs are shown in Figure II.5(a), Figure II.5(b) and Figure II.6, which indicate that the shape of each PR changes significantly with its parameters. A summary of the main functions of each parameter is given in Table II.1. The shape characteristics of the PR varying with the parameter τ_2 in Figure II.5(a) and Figure II.5(b) are somewhat surprising, which indicate that:

1) if τ_2 is positive and relatively large there will be a time lag, however;

2) a pure time lag does not exist (i.e. without changing the shape of an PR), any time lag will be accompanied by a more or less change in the shape of the PR and

3) when τ_2 approaches to zero or negative, the time lag is negligible or will not occur. Under this condition, any change in τ_2 will result in a parallel movement of the recession limb along the time axis, and a change in the shape of the rising limb (which will become fatter or thinner).

Throughout the above analysis, it has been implicitly assumed that with the transformation of rainfall into runoff, the impedance of the system changes in a progressive and smooth manner. This may not be entirely true. However, there is no other choices but using what seems capable of describing and explaining the major characteristics of the observed facts. The parameters of the three general n-reservoir PRs can be identified using various techniques, such as moment analysis, maximum likehood or simply by 'curve fitting'.

II.3 Summary

The first type of PR has been proved as being valid, which is a generalised Nash-model. Many existing models can be treated as its special cases. The other two types of models have the same degree of physical justification as the first one. The major difference between the three models lies within the variation range defined for the dynamic storage factors.

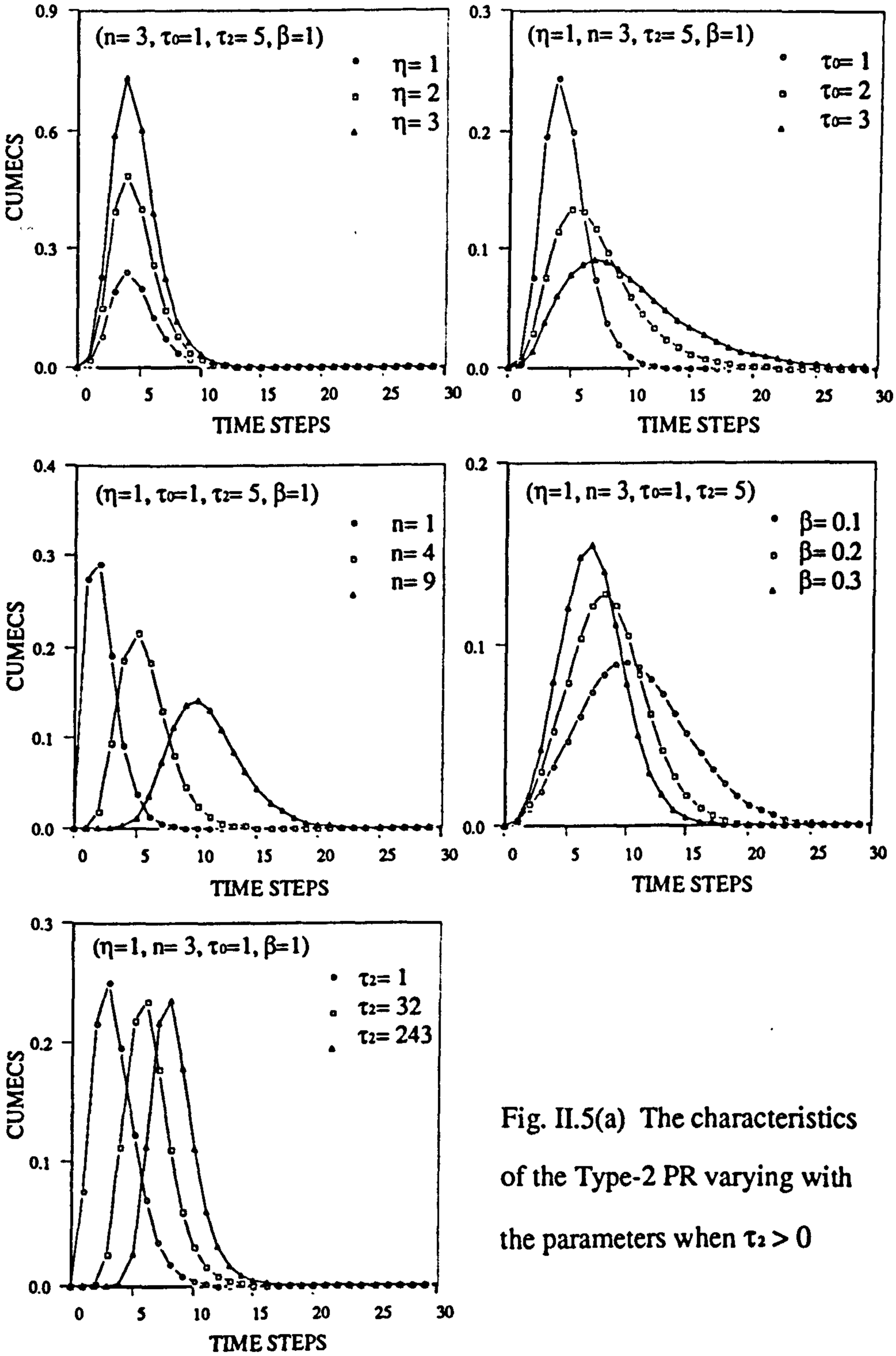

Fig. II.5(a) The characteristics of the Type-2 PR varying with the parameters when $\tau_2 > 0$

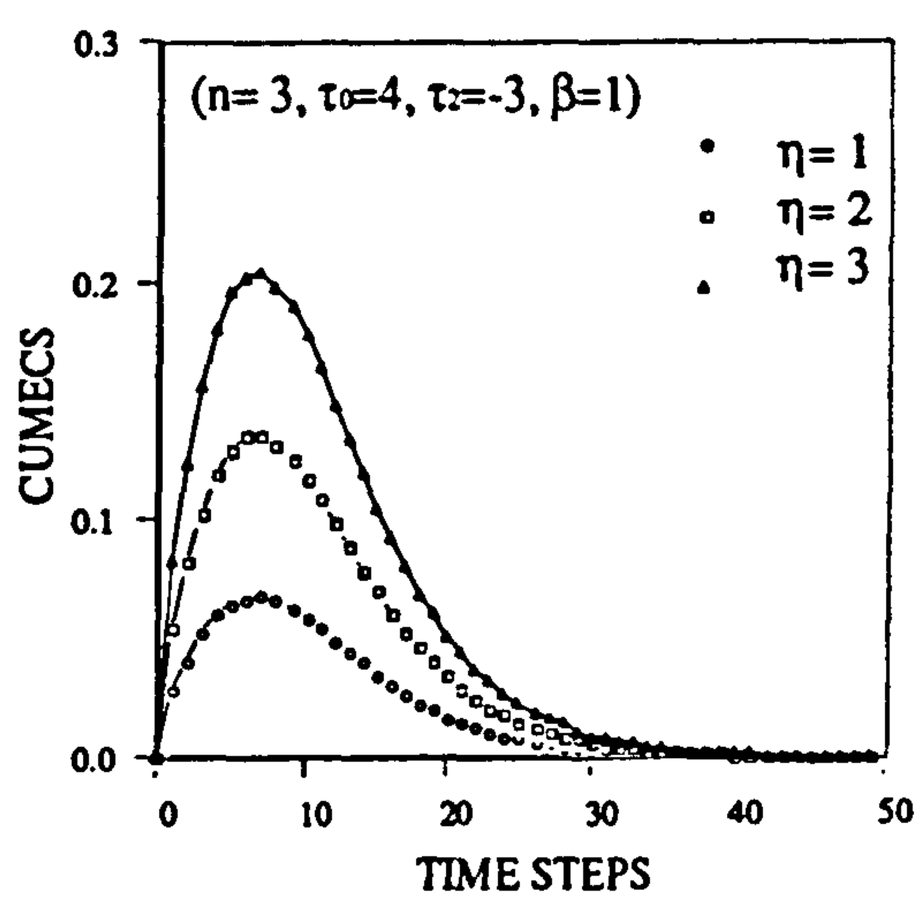

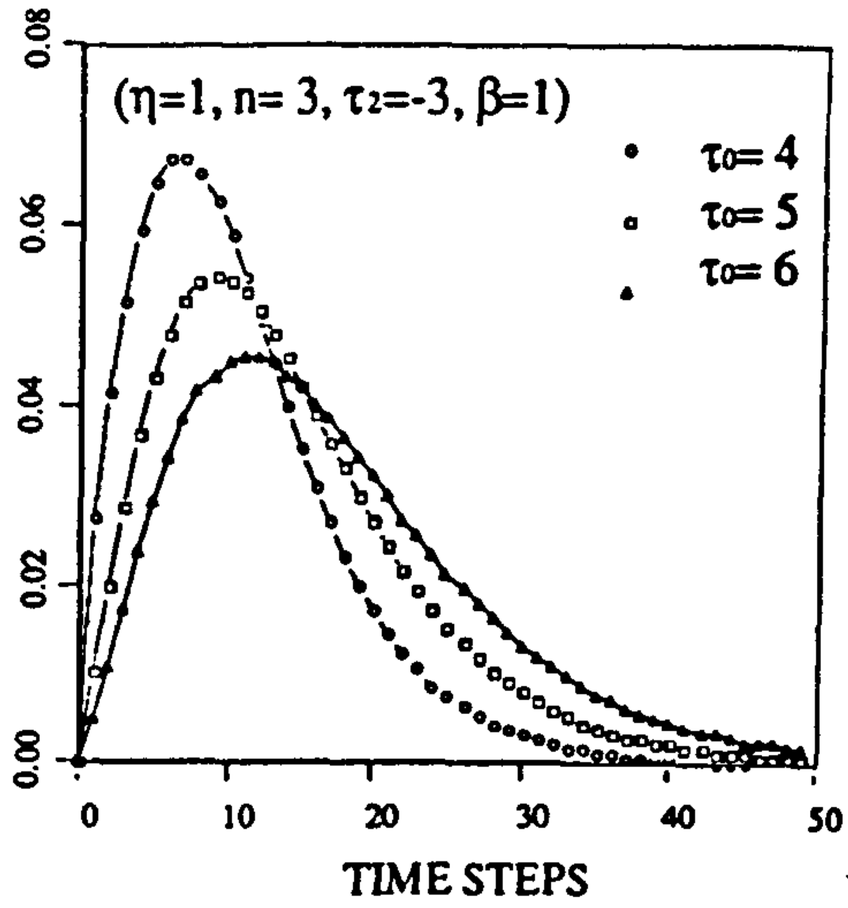

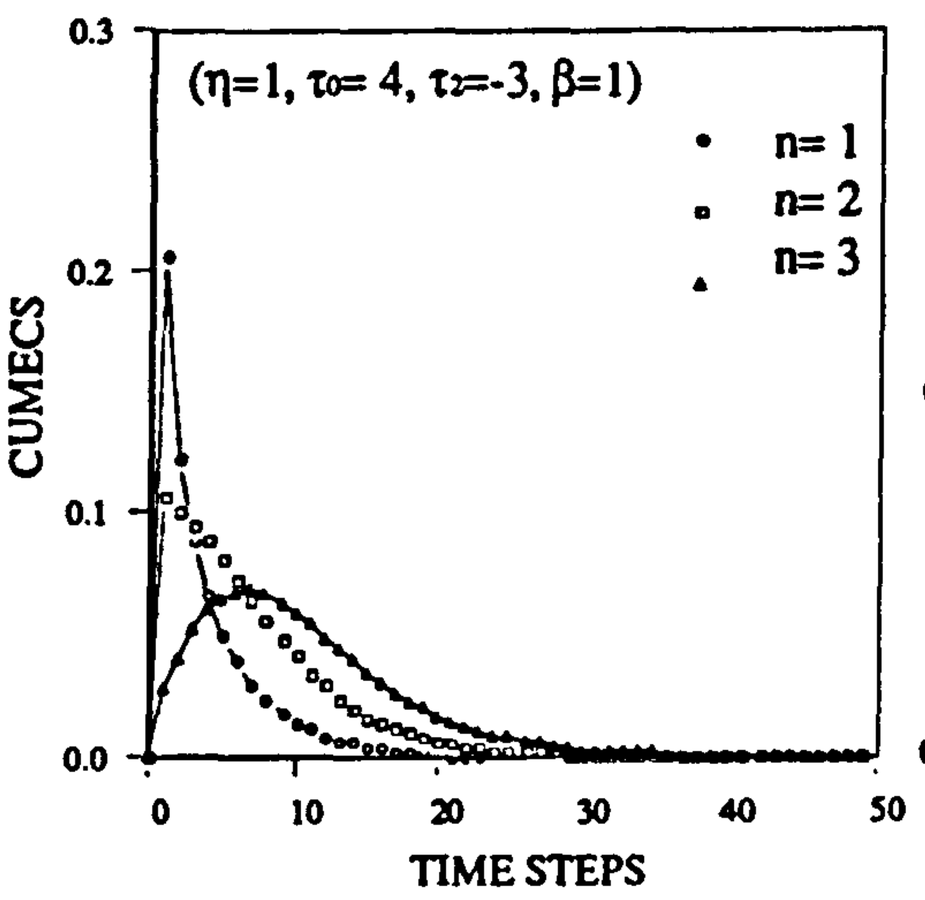

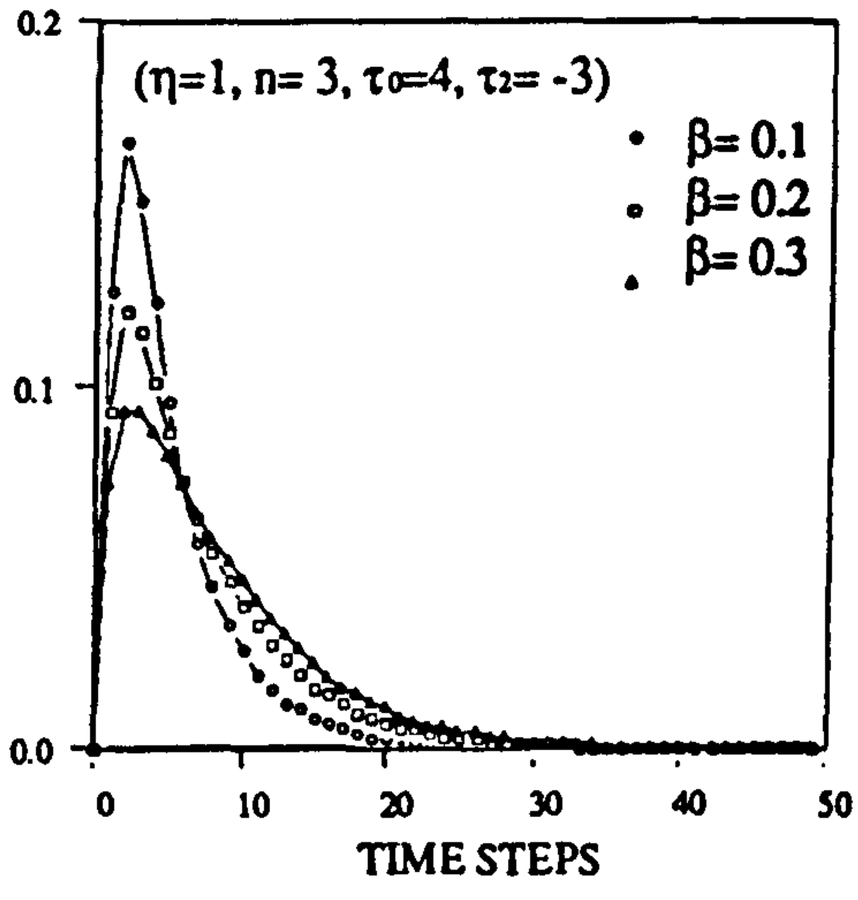

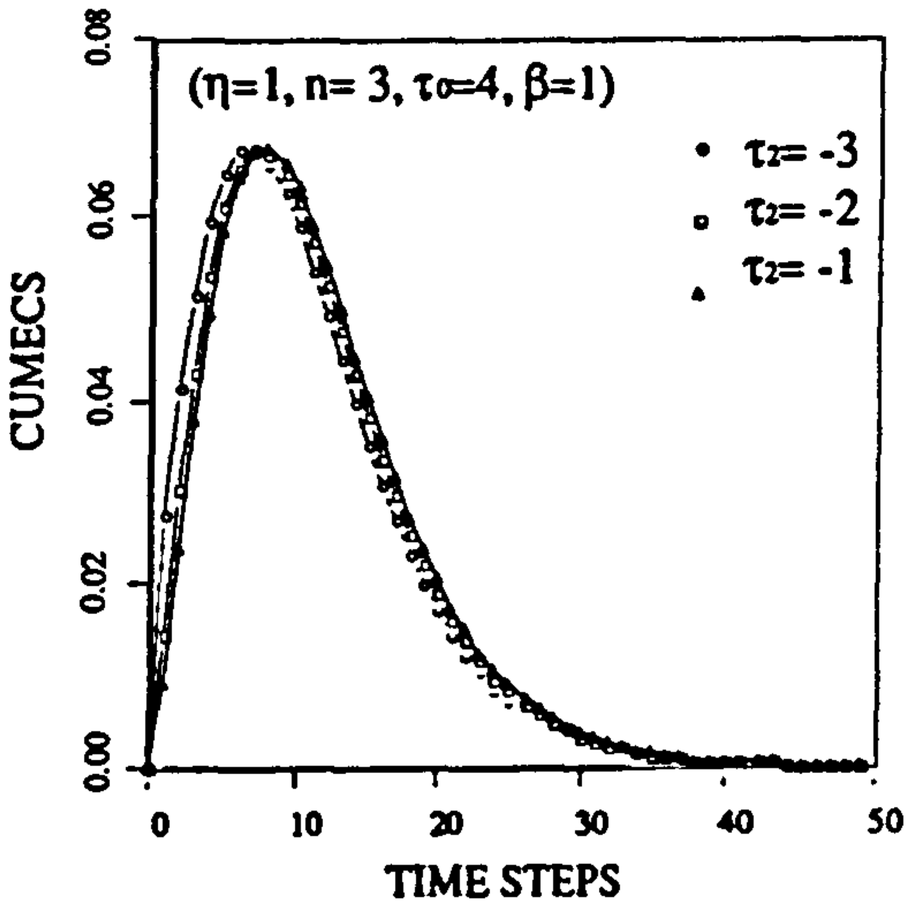

Fig. II.5(b) The characteristics of the Type-2 PR varying with the parameters when $\tau_2<0$

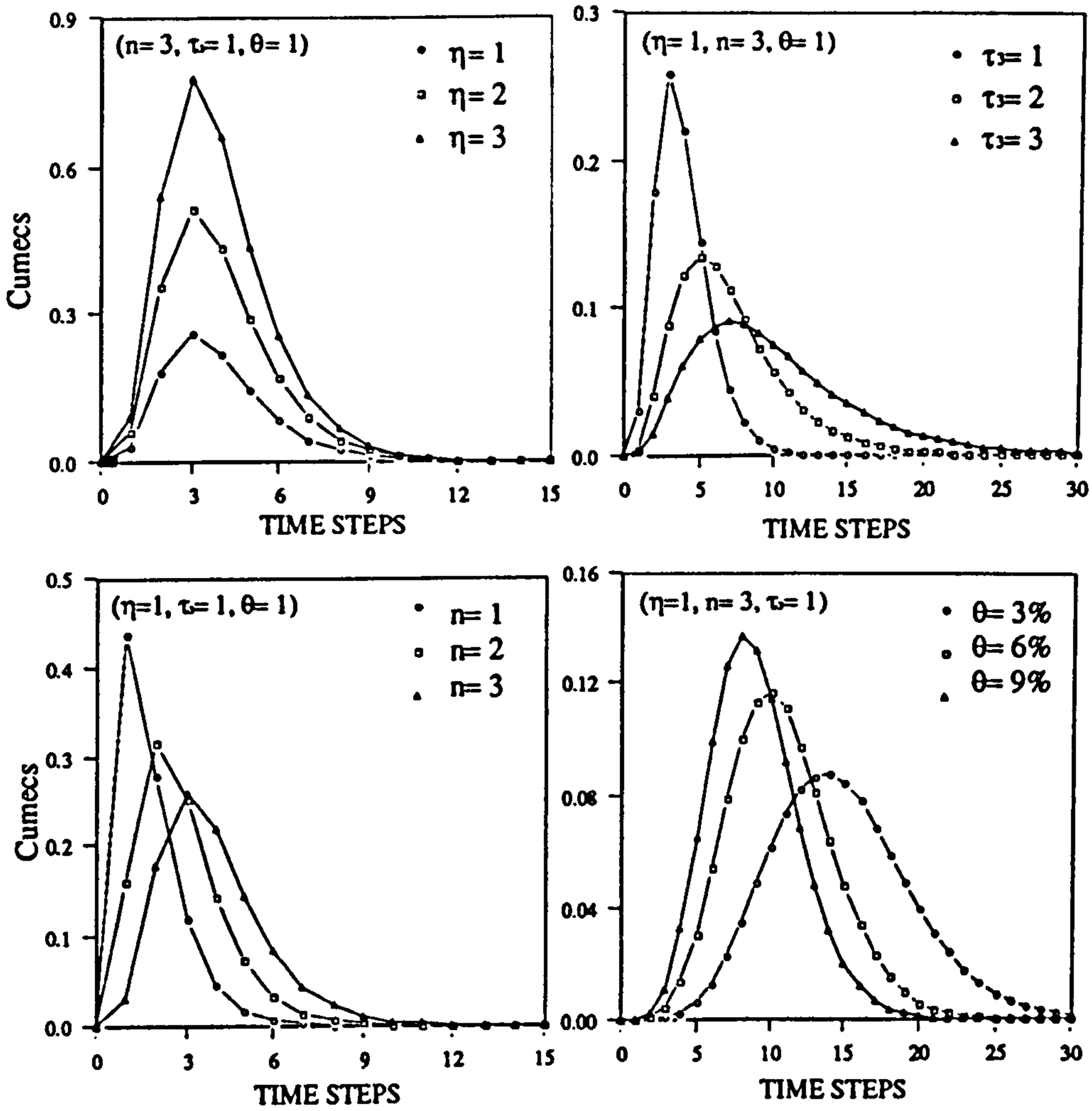

Fig.II.6 The characteristics of Type-3 PR varying with the parameters

Table II.1 Main functions of the PR parameters

PARAMETER	MAIN FUNCTIONS
η	Proportionally changes the amplitude of the PR
n	Mainly determines the peak, time to peak and the shape of the rising limb
τ_0, τ_1, τ_3	Mainly portrays the peak, time to peak and the shape of the recession limb
τ_2	Moves the PR along the time axis with very slight change in the peak and shape
α, β, θ	Has both the effects of n and τ (τ_0, or τ_1 or τ_3)

APPENDIX-III

EXAMPLES OF USING THE GENETIC ALGORITHMS

Given a randomly generated population which constitutes N members of randomly selected chromosomes, i.e PR parameter vectors: $[\eta_i, n_i, \tau_i, \Delta_i, \alpha_i]$, $i = 1, 2, 3, \cdots, N$, the desired best member can be obtained by evolving the population using a genetic Algorithm (GA). The five PR parameters, η_i, n_i, τ_i, Δ_i, α_i are the genes of a chromosome. The fitness of a chromosome is measured by the Fitness Factor (see Chapter 6 for detail).

In this Appendix two examples are presented to illustrate how the 'best' PR parameter vector which uniquely defines a PR function was found using the:

- *Random-Mutation GA*
- *Comprehensive GA*

III.1 Using the Random-Mutation Genetic Algorithm

[Problem Definition]: *Given a rainfall hyetograph and the corresponding hydrograph (or input and output), determine the CPTF PR using the Random-Mutation GA.*

This requires the five PR parameters which uniquely defines the PR to be identified. By convoluting the identified PR with the given rainfall input a simulated hydrograph

can be produced. The simulation error is indicated by the Fitness Factor (FF). A smaller FF value means a smaller simulation error. The identification procedure is illustrated in Figure III.1. The sequantial numbers of the evolution generations are shown at the top of the figure, and below which the simulated and given hydrographs are shown together with the Fitness Factor for each generation. The best chromosome of each generation is given in a table at the bottom of the figure.

Generation 1: a population containing 1 chromosome was randomly generated at the time 16:36:41, and the five genes of the chromosome were [η=3.80, n=4, τ=1.10, Δ=1, α=1.02] which formed the 1st-generation parent member of the population. Its fitness is indicated by the Fitness Factor, FF=0.510.

Generation 2: The genes of the 1st-generation chromosome were firstly copied and then randomly perturbed in order to give births to children members with different Fitness Factors from their parent (single parent!). Within less than 1 second since the begin of this evolution process, one of the child chromosome was born at the time 16:36:41, who has better fitness (FF=0.219) than its parent . Thus the parent member in the population was replaced by this child who formed the second generation of the population. The genes of the second generation chromosome were [η=2.64, n=3, τ=1.61, Δ=2, α=1.23].

Generation 3 to Generation 9: The above evolving process continued until the best (up to the 9th generation) child chromosome was born at the time: 16:37:50 with a Fitness Factor, FF=0.032, and the process was interrupted by the user who decided to use the 9th-generation chromosome as the identified PR which is defined by: [η=2.50, n=7, τ=0.60, Δ=1, α=0.85].

The computation was carried out on a VAX-4000-100 computer. It can be seen from

the figure that the evolution of the first three generations only took up 1 second CPU, and the second three completed within 11 seconds and the last three consumed 58 seconds! As the time taken for obtaining a new generation increases with the progression of the evolution, an automatic interruption can be programmed based on the time interval between the last generation and the current generation, e.g. [if CPU ≥ 30 seconds then Stop]. To speed up the evolution procedure, a suggestion is given as to use the Comprehensive GA and/or restrict the evolving space according to the magnitude and conditions of the actual system by specification of the minimum and maximum values that a PR parameter may take. For example,

η: from 10^{-2} to 10^{2}

n: from 1 to 10

τ: from 0.1 to 5

Δ: from 0 to 10

α: from 1/n to 3

The key steps for utilising the Random-Mutation Genetic Algorithm are:

- *Gene copying*
- *Random perturbation*
- *Fitness assessment*

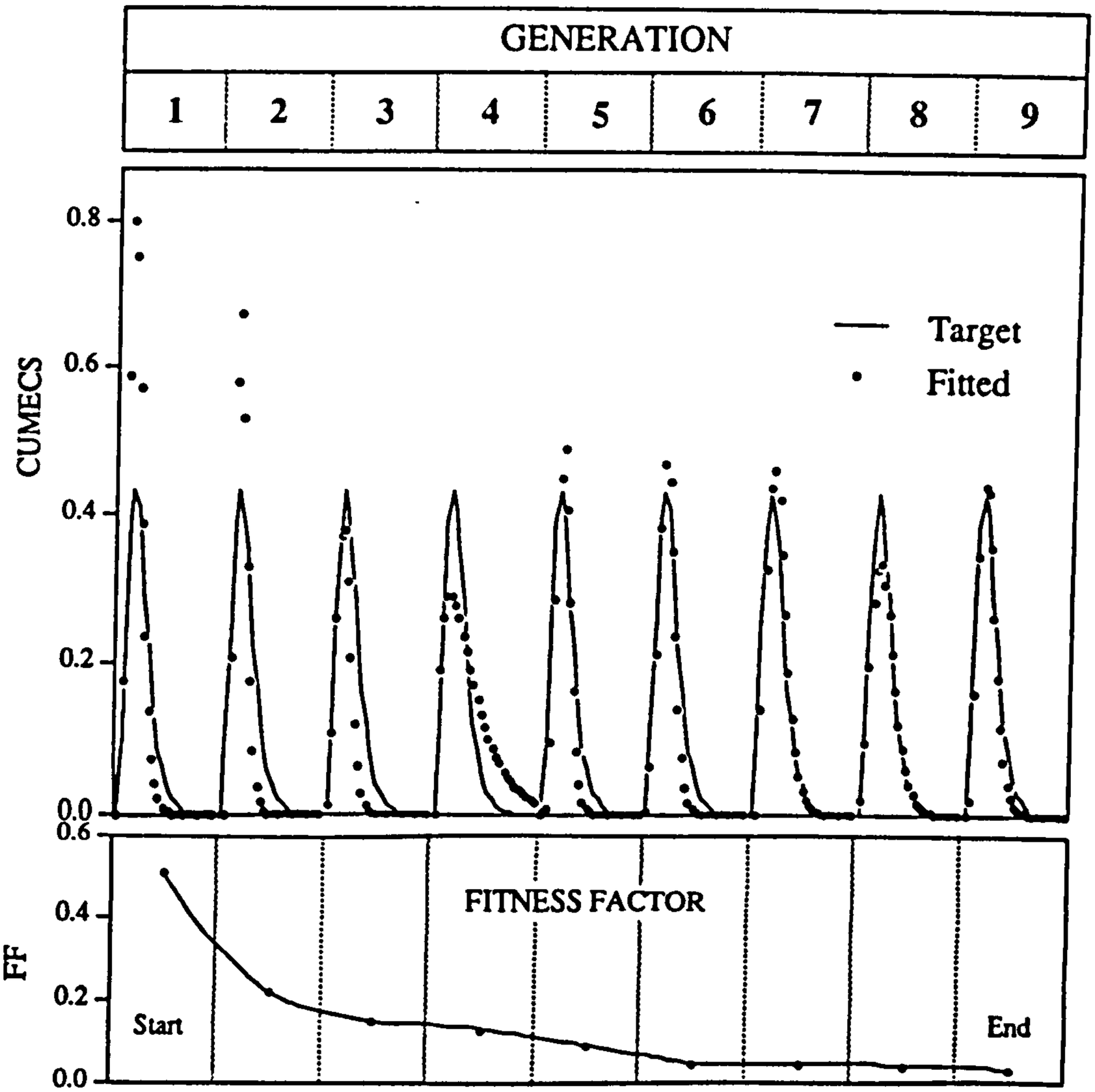

TIME (Hr.:Min.:Sec.)		16 :36:41	16 :36:41	16 :36:41	16 :36:42	16 :36:42	16 :36:52	16 :37.05	16 :37:35	16 :37.50
GENES / PR PARAMETERS	η	3.80	2.64	1.89	3.58	2.34	2.46	2.95	2.58	2.50
	n	4	3	3	2	4	4	2	3	7
	τ	1.10	1.61	4.36	3.57	2.64	3.13	4.77	3.93	0.60
	Δ	1	2	0	1	1	0	2	0	1
	α	1.02	1.23	1..53	0.90	1.39	1.41	1.34	1.24	0.85
	CHROMOSOMES / PR PARAMETER SETS									

Fig. III.1 *Parameter Identification using the Random-Mutation Genetic Algorithm*

III.2 Using the Comprehensive Genetic Algorithm

[Problem Definition]: *Given a rainfall hyetograph and the related hydrograph (or input and output), determine the CPTF PR using the Comprehensive GA*

The solution to this problem can be demonstrated using the same input and output data sets as that have been used in III.1. The details of the evolving procedure is listed as following for every two generations, i.e. 1, 3, 5,···.

<LIST OF THE POPULATION EVOLUTION>

G-1	13(Hr.)	30(Min.)	45(Sec.)	3.71(η)	1(n)	2.604(τ)	2(Δ)	0.812(α)	0.436(FF)

η	n	τ	Δ	α	FF	
3.25	2	1.22	2	0.93	0.774	Note:
1.80	1	2.83	2	2.93	2.017	(1) This is the randomly generated initial population with 9 parents Chromosomes.
4.65	3	2.60	1	0.57	0.621	(2) Each Chromosome has five Genes:η, n, τ, Δ and α.
1.78	3	0.42	3	0.78	0.705	
3.71	1	2.60	2	0.81	0.436 →	(3) The best member of this generation.
1.33	6	2.99	2	2.12	0.535	It has also bee shown in the header of this table.
1.48	5	2.02	2	2.80	1.700	
0.97	7	2.01	2	1.01	1.000	(4) This generation is labelled as G-1
3.59	3	0.65	1	1.87	9.005	(5) Evolution time: 13:30:45

G-3	13(Hr.)	30(Min.)	45(Sec.)	1.78(η)	3(n)	1.220(τ)	2(Δ)	0.930(α)	0.135(FF)

η	n	τ	Δ	α	FF	
3.25	2	1.22	2	0.93	0.774	
1.78	3	2.01	2	1.01	0.207*	(1) The last two less-fit parents members of the first generation have been replaced by the two more-fit children marked as '*' within less than 1 sec.
4.65	3	2.60	1	0.57	0.621	
1.78	3	0.42	3	0.78	0.705	
3.71	1	2.60	2	0.81	0.436	
1.33	6	2.99	2	2.12	0.535	
1.48	5	2.02	2	2.80	1.700	
0.97	7	2.01	2	1.01	1.000	
1.78	3	1.22	2	0.93	0.135*→	(3) The best member of the 3rd generation (G-3)

G-5	13(Hr.)	30(Min.)	45(Sec.)	1.78(η)	3(n)	1.220(τ)	2(Δ)	0.930(α)	0.135(FF)

η	n	τ	Δ	α	FF	
3.25	2	1.22	2	0.93	0.774	
1.78	3	2.01	2	1.01	0.207	
4.65	3	2.60	1	0.57	0.621	
1.78	3	0.42	3	0.78	0.705	
3.71	1	2.60	2	0.81	0.436	
1.33	6	2.99	2	2.12	0.535	
1.78	3	1.22	2	1.01	0.149*	
1.78	3	1.22	2	1.01	0.149*	
1.78	3	1.22	2	0.93	0.135→	The best member of this generation (G5)

G-7	13(Hr.)	30(Min.)	45(Sec.)	1.78(η)	3(n)	1.220(τ)	2(Δ)	0.930(α)	0.135(FF)

η	n	τ	Δ	α	FF	
1.78	3	1.22	2	1.01	0.149*	
1.78	3	2.01	2	1.01	0.207	
4.65	3	2.60	1	0.57	0.621	
1.78	3	1.22	2	1.01	0.149*	
3.71	1	2.60	2	0.81	0.436	
1.33	6	2.99	2	2.12	0.535	
1.78	3	1.22	2	1.01	0.149	
1.78	3	1.22	2	1.01	0.149	
1.78	3	1.22	2	0.93	0.135→	The best member of this generation

G-9	13(Hr.)	30(Min.)	46(Sec.)	1.78(η)	3(n)	1.220(τ)	2(Δ)	0.930(α)	0.135(FF)

η	n	τ	Δ	α	FF	
1.78	3	1.22	2	1.01	0.149	Up to this generation all of the parent members in
1.78	3	2.01	2	1.01	0.207	the initial population have been replaced by the
1.78	3	1.22	2	0.81	0.173*	reproduced children except the one marked by '!'
1.78	3	1.22	2	1.01	0.149	
3.71	1	2.60	2	0.81	0.436!	
1.78	3	1.22	2	0.81	0.173*	
1.78	3	1.22	2	1.01	0.149	
1.78	3	1.22	2	1.01	0.149	
1.78	3	1.22	2	0.93	0.135→	The best member of this generation

G-11	13(Hr.)	30(Min.)	46(Sec.)	1.78(η)	3(n)	1.220(τ)	2(Δ)	0.930(α)	0.135(FF)

η	n	τ	Δ	α	FF	
1.78	3	1.22	2	1.01	0.149	
1.78	3	1.22	2	0.81	0.173*	
1.78	3	1.22	2	0.81	0.173	
1.78	3	1.22	2	1.01	0.149	
1.78	3	1.22	2	0.81	0.173*	
1.78	3	1.22	2	0.81	0.173→	It became the last worst member of this generation
1.78	3	1.22	2	1.01	0.149	
1.78	3	1.22	2	1.01	0.149	
1.78	3	1.22	2	0.93	0.135→	The best member of this generation

G-13	13(Hr.)	30(Min.)	46(Sec.)	3.02(η)	8(n)	0.360(τ)	2(Δ)	0.594(α)	0.088(FF)

η	n	τ	Δ	α	FF	
1.78	3	1.22	2	1.01	0.149	
1.78	3	1.22	2	0.81	0.173	
1.78	3	1.22	2	0.81	0.173	
1.78	3	1.22	2	1.01	0.149	
3.02	8	0.36	2	0.59	0.088*→	The best member of this generation
1.78	3	1.22	2	0.93	0.135*	
1.78	3	1.22	2	1.01	0.149	
1.78	3	1.22	2	1.01	0.149	
1.78	3	1.22	2	0.93	0.135	

G-15	13(Hr.)	30	46(Sec.)	3.71(η)	3(n)	1.220(τ)	2(Δ)	0.812(α)	0.079(FF)

η	n	τ	Δ	α	FF	
1.78	3	1.22	2	1.01	0.149	
3.70	5	0.60	2	0.69	0.091*	
3.71	3	1.22	2	0.81	0.079*→	The best member of this generation
1.78	3	1.22	2	1.01	0.149	
3.02	8	0.36	2	0.59	0.088	
1.78	3	1.22	2	0.93	0.135	
1.78	3	1.22	2	1.01	0.149	
1.78	3	1.22	2	1.01	0.149	
1.78	3	1.22	2	0.93	0.135	

G-17	13(Hr.)	30(Min.)	46(Sec.)	3.71(η)	3(n)	1.220(τ)	2(Δ)	0.812(α)	0.079(FF)
η	**n**	**τ**	**Δ**	**α**	**FF**				
1.78	3	1.22	2	1.01	0.149				
3.70	5	0.60	2	0.69	0.091				
3.71	3	1.22	2	0.81	0.079→	The best member of this generation			
1.78	3	1.22	2	1.01	0.149				
3.02	8	0.36	2	0.59	0.088				
1.78	3	1.22	2	0.93	0.135				
3.71	3	1.22	2	0.81	0.079*→	The best member of this generation			
3.71	3	1.22	2	0.81	0.079*→	The best member of this generation			
1.78	3	1.22	2	0.93	0.135				

G-19	13(Hr.)	30(Min.)	46(Sec.)	3.71(η)	3(n)	1.220(τ)	2(Δ)	0.812(α)	0.079(FF)
η	**n**	**τ**	**Δ**	**α**	**FF**				
3.71	3	1.22	2	0.81	0.079*→	The best member of this generation			
3.70	5	0.60	2	0.69	0.091				
3.71	3	1.22	2	0.81	0.079→	The best member of this generation			
3.71	3	1.22	2	0.81	0.079*→	The best member of this generation			
3.02	8	0.36	2	0.59	0.088				
1.78	3	1.22	2	0.93	0.135				
3.71	3	1.22	2	0.81	0.079→	The best member of this generation			
3.71	3	1.22	2	0.81	0.079→	The best member of this generation			
1.78	3	1.22	2	0.93	0.135				

G-21	13(Hr.)	30(Min.)	47(Sec.)	3.71(η)	3(n)	1.220(τ)	2(Δ)	0.812(α)	0.079(FF)
η	**n**	**τ**	**Δ**	**α**	**FF**				
3.71	3	1.22	2	0.81	0.079→	The best member of this generation			
3.70	5	0.60	2	0.69	0.091				
3.71	3	1.22	2	0.81	0.079→	The best member of this generation			
3.71	3	1.22	2	0.81	0.079→	The best member of this generation			
3.02	8	0.36	2	0.59	0.088				
3.71	3	1.22	2	0.81	0.079*→	The best member of this generation			
3.71	3	1.22	2	0.81	0.079→	The best member of this generation			
3.71	3	1.22	2	0.81	0.079→	The best member of this generation			
3.71	3	1.22	2	0.81	0.079*→	The best member of this generation			

G-23	13(Hr.)	30(Min.)	47(Sec.)	3.55(η)	2(n)	2.936(τ)	2(Δ)	1.107(α)	0.079(FF)
η	**n**	**τ**	**Δ**	**α**	**FF**				
3.71	3	1.22	2	0.81	0.079	Up to this generation, all parents became identical to			
3.71	3	1.22	2	0.81	0.079*	each other, therefore, cross-over will not take any effect			
3.71	3	1.22	2	0.81	0.079	for further reproduction			
3.71	3	1.22	2	0.81	0.079				
3.71	3	1.22	2	0.81	0.079*				
3.71	3	1.22	2	0.81	0.079				
3.71	3	1.22	2	0.81	0.079				
3.71	3	1.22	2	0.81	0.079				
3.71	3	1.22	2	0.81	0.079				

G-25	13(Hr.)	30(Min.)	47(Sec.)	2.95(η)	3(n)	2.104(τ)	1(Δ)	1.014(α)	0.005(FF)
η	**n**	**τ**	**Δ**	**α**	**FF**				
3.71	3	1.22	2	0.81	0.079	Up to this generation, the whole evolving process			
3.71	3	1.22	2	0.81	0.079	took up 2 seconds which was mush shorter than the			
3.71	3	1.22	2	0.81	0.079	time taken for the **Random-mutation** GA to			
3.71	3	1.22	2	0.81	0.079	achieve a similar accuracy.			
3.71	3	1.22	2	0.81	0.079				
3.71	3	1.22	2	0.81	0.079				
3.71	3	1.22	2	0.81	0.079				
2.95	3	2.10	1	1.01	0.005*→	The best member of this generation			
3.55	2	2.94	2	1.11	0.069*				

Generation 1: a population containing 9 chromosomes was randomly generated (i.e. population size, N=9) at the time 13:30:45:

η	n	τ	Δ	α	F F
[3.25	2	1.22	2	$0.93]_1$	0.774
[1.80	1	2.83	2	$2.93]_2$	2.017
[4.65	3	2.60	1	$0.57]_3$	0.621
[1.78	3	0.42	3	$0.78]_4$	0.705
[3.71	1	2.60	2	$0.81]_5$	0.436
[1.33	6	2.99	2	$2.12]_6$	0.535
[1.48	5	2.02	2	$2.80]_7$	1.700
[0.97	7	2.01	2	$1.01]_8$	1.000
[3.59	3	0.65	1	$1.87]_9$	9.005

which formed the 1st-generation of the population, the subscription denotes the order of the parent members. The population size was arbitrarily chosen. The fitness of each member is indicated by the Fitness Factor (FF).

Generation 3: The third generation was produced. The reproduction techniques used were *Gene copying+One-point cross-over+Random-mutation*. Firstly, the 9 1st-generation chromosomes were copied, and then 5 of the parents copies were selected to form 10 couples which were selected using the *Roulette Wheel Parent Selection Technique* (Chapter 6). Cross-over took place when each couple exchange some of their genes. Let $[\bullet\bullet\bullet\bullet\bullet\bullet]_i$, for i=1, to 5, denote the five selected parents, the cross-over order was:

$[\bullet\bullet\bullet\bullet\bullet\bullet]_1 \Leftrightarrow [\bullet\bullet\bullet\bullet\bullet\bullet]_2$ $[\bullet\bullet\bullet\bullet\bullet\bullet]_1 \Leftrightarrow [\bullet\bullet\bullet\bullet\bullet\bullet]_3$ $[\bullet\bullet\bullet\bullet\bullet\bullet]_1 \Leftrightarrow [\bullet\bullet\bullet\bullet\bullet\bullet]_4$ $[\bullet\bullet\bullet\bullet\bullet\bullet]_1 \Leftrightarrow [\bullet\bullet\bullet\bullet\bullet\bullet]_5$

$[\bullet\bullet\bullet\bullet\bullet\bullet]_2 \Leftrightarrow [\bullet\bullet\bullet\bullet\bullet\bullet]_3$ $[\bullet\bullet\bullet\bullet\bullet\bullet]_2 \Leftrightarrow [\bullet\bullet\bullet\bullet\bullet\bullet]_4$ $[\bullet\bullet\bullet\bullet\bullet\bullet]_2 \Leftrightarrow [\bullet\bullet\bullet\bullet\bullet\bullet]_5$

$[\bullet\bullet\bullet\bullet\bullet\bullet]_3 \Leftrightarrow [\bullet\bullet\bullet\bullet\bullet\bullet]_4$ $[\bullet\bullet\bullet\bullet\bullet\bullet]_3 \Leftrightarrow [\bullet\bullet\bullet\bullet\bullet\bullet]_5$

$[\bullet\bullet\bullet\bullet\bullet\bullet]_4 \Leftrightarrow [\bullet\bullet\bullet\bullet\bullet\bullet]_5$

During each evolving cycle or generation, 20 children members were produced using the One-point cross-over technique, and the separation point was randomly generated.

Having obtained all of the children members, the fitness of each child member was assessed and the fittest one was allowed to step into the population to replace the worst parents member so that evolution of the population could be achieved. Thus, the second generation of the population was yielded (which has not been shown in the list), and from which the third generation was produced. The best chromosome of the third generation was:

η	n	τ	Δ	α	FF
[1.78	3	1.22	2	0.93]	0.135

which was produced by crossing over the two parents members of the second generation (G2) and the separation point was marked by '^':

η	n	τ	Δ	α	FF
[3.25	2^	1.22	2	$0.93]_1$	0.774
[1.78	3^	0.42	3	$0.78]_4$	0.705

These two members can also be seen in the first generation (G1). On conditions when the two crossing-over parents were identical, the random mutation technique was applied to randomly perturb all the genes (i.e. the five PR parameters) of the reproduced children.

Generation 5 to Generation 25: The above evolving procedure continued until the best (up to 25th generation) child chromosome [η=2.95, n=3, τ=2.10, Δ=1, α=1.01] was born at the time: 13:30:47 with a Fitness Factor, FF=0.0005.

Unlike the previously illustrated Random-mutation GA which always produces a new and better chromosome at every evolving cycle, the Comprehensive GA illustrated here can only ensure that the worst member in the population can be replaced by a better child so that the overall quality of the population can be improved. It does not guarantee that the best member of the population can be upgraded for every generation.

Similar to Figure III.1, the best members and their Fitness Factors for the generations: 1, 5, 9, 13, 17, 21 and 25 are shown in Figure III.2. It can be seen from the figure that 1) the evolution was much faster than that achieved using the Random-mutation GA because the best genes spread within the population were rapidly evolved into a single chromosome after only a small number of generations, and 2) to further speed up the evolution it is crucial for more new and better genes to appear in the population. This can be achieved by allowing more high-quality children members (i.e. not only the best one) to enter the population and replace an equal number (≤1/2 of the population size) of less-fit parents members. The replacement of the less-fit parents members is not likely to affect the arising of the population-best member because it is quite possible that their best genes have been already utilised by the other better members of the population, especially at the later stages of the evolution when the entire population had been dominated by a single chromosome. The key steps for using the Random-Mutation Genetic Algorithm are:

- *Gene copying*
- *Parents selection*
- *Cross-over/random perturbation*
- *Fitness assessment*
- *Replacement of the less-fit parents with the better child chromosomes*

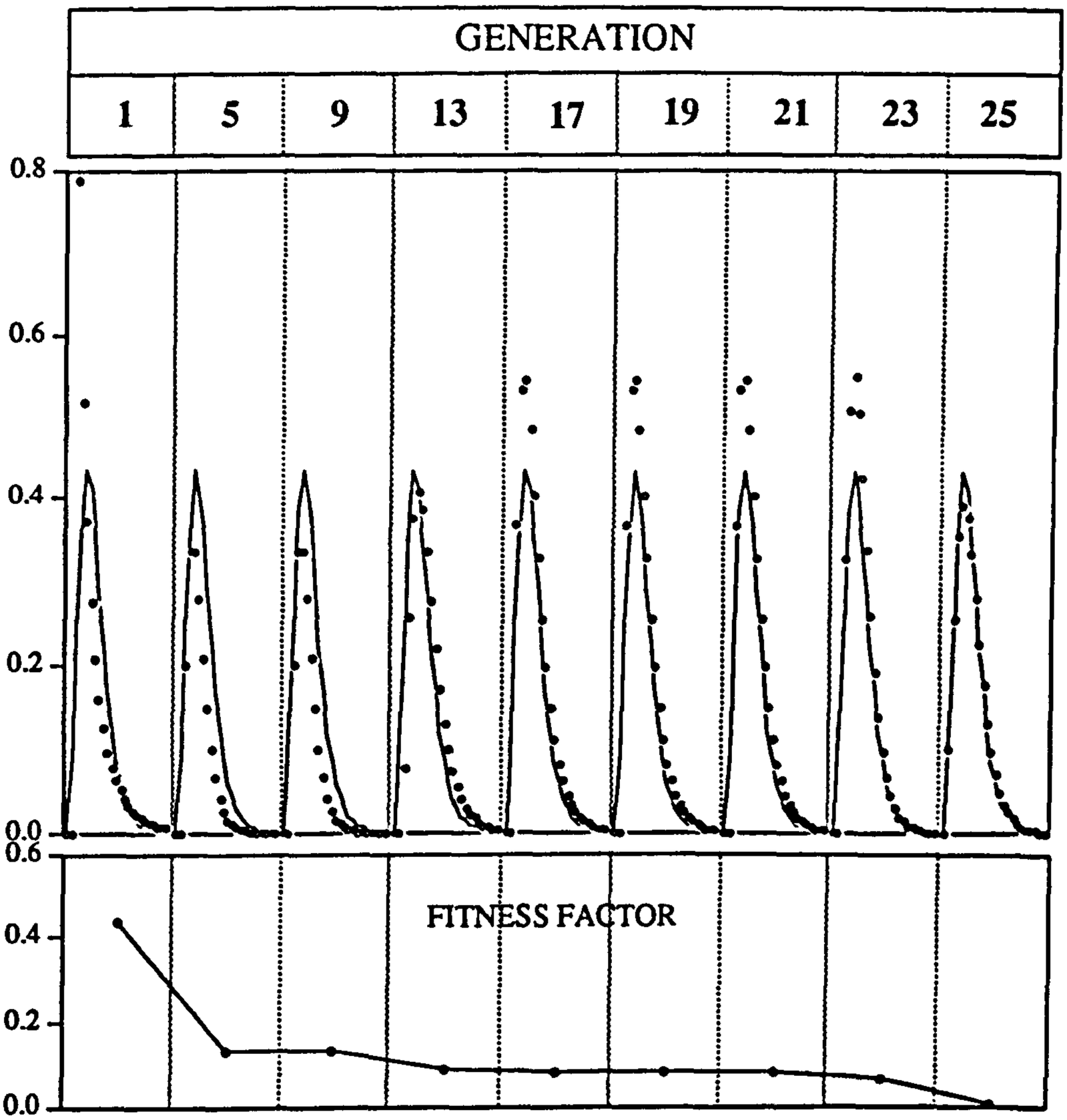

Fig. III.2 *Parameter Identification using the Comprehensive Genetic Algorithm*